

Volume 122 Numbers 1-4(1991) ^{FE}

ARS 29180-2-PH-CF

AD-A257 053



FERROELECTRICS

The International journal devoted to the theoretical, experimental,
and applied aspects of ferroelectrics and related materials.

2

PROCEEDINGS OF THE THIRD INTERNATIONAL CONFERENCE ON FERROELECTRIC LIQUID CRYSTALS

S DTIC
ELECTE
OCT 26 1992
A **D**

Part II of II Parts

June 23-28, 1991
Boulder, Colorado, USA

Guest Editors:

Noel A. Clark
David M. Walba
Mark A. Handschy
Garret Modell

088400

This document has been approved
for public release and sale; its
distribution is unlimited.

GIB
Philadelphia

GORDON AND BREACH SCIENCE PUBLISHERS
Reading Paris Montreux Tokyo Melbourne

FERROELECTRICS

and related materials

EDITOR: George W. Taylor

Princeton Resources, P.O. Box 211, Princeton, NJ 08540, USA

ASSOCIATE EDITORS

Peter Günter

Institut für Quantenelektronik
ETH,
CH 8093 Zurich, Switzerland

Sidney B. Lang

Department of Chemical Engineering
Ben Gurion University of the Negev
Beer Sheva 84120, Israel

Koichi Toyoda

Research Institute of Electronics
Shizuoka University
Hamamatsu 432, Japan

Bibliographers

Koichi Toyoda, Shizuoka (Ferroelectrics)

S. B. Lang, Beer Sheva (Pyroelectrics)

Book Review Editor

S. C. Abrahams, Ashland, OR

EDITORIAL BOARD

Ryuji Abe, Nagoya

F. Ainger, Northampton, UK

K. S. Aleksandrov, Krasnojarsk

E. F. Bertaut, Grenoble

A. S. Bhalla, State College, PA

R. Blinc, Ljubljana

L. E. Cross, State College, PA

V. Dvorak, Prague

J. Fousek, Prague

V. M. Fridkin, Moscow

A. M. Glass, Murray Hill, NJ

J. A. Gonzalo, Madrid

G. H. Haertling, Clemson, SC

W. Heywang, Munich

B. Hilezer, Poznan

Sadao Hoshino, Yokohama, Japan

V. Janovec, Prague

Jinzo Kobayashi, Tokyo

S. K. Kurtz, University Park, PA

C. E. Land, Albuquerque, NM

W. J. Lawless, Westerville, OH

V. V. Lemanov, Leningrad

M. A. Marcus, Rochester, NY

W. J. Merz, Zurich

K. A. Müller, Zurich

H. E. Müser, Saarbrücken

Terutaro Nakamura, Tokyo

C. F. Pulvar, Washington, DC

G. A. Samara, Albuquerque, NM

Shozo Sawada, Iwaki, Japan

G. Shirane, Brookhaven, NY

L. A. Shuvalov, Moscow

W. A. Smith, Arlington, VA

J. Stankowski, Poznan

E. C. Subbarao, Pune

Kenji Uchino, Tokyo

F. G. Ullman, Lincoln, NE

Yu. N. Venetsev, Moscow

Zhi-wen Yin, Shanghai

I. S. Zheludev, Moscow

GENERAL INFORMATION

Aims and Scope *Ferroelectrics* is designed to provide a forum for people working in ferroelectrics and related materials such as ferroelastics, ferroelectric-ferromagnetics, electrooptics, piezoelectrics, pyroelectrics, nonlinear dielectrics, and liquid crystals. *Ferroelectrics* publishes experimental and theoretical papers aimed at the understanding of ferroelectricity and associated phenomena and applied papers dealing with the utilization of these materials in devices and systems. An important aspect of *Ferroelectrics* is to provide a vehicle for the publication of interdisciplinary papers involving ferroelectricity.

The editor invites original papers and short communications on the theory, fabrication, properties, and applications of ferroelectrics and related materials. In addition to research papers, *Ferroelectrics* publishes appropriate and timely review articles. There are no charges to authors or to institutions.

Notes for contributors can be found at the back of the journal.

Please see inside back cover for information on subscription rates and ordering information.

© 1991 Gordon and Breach Science Publishers S.A.

All rights reserved. No part of this publication may be reproduced or utilized in any form or by any means, electronic or mechanical, including photocopying and recording, or by any information storage or retrieval system, without permission in writing from the Publisher.

LICENSE TO PHOTOCOPY This publication is registered for copyright in the United States of America and is protected under the Universal Copyright Convention and the Bern Convention. The Publisher is not a member of the Copyright Clearance Center or similar payment centers in other parts of the world. Accordingly, permission to photocopy beyond the 'fair use' provisions of the USA and most other copyright laws is available from the Publisher by license only. Please note, however, that the license does not extend to other kinds of copying, such as copying for general distribution, for advertising or promotion purposes, for creating new collective works, or for resale. It is also expressly forbidden for any individual or company to copy any article as agent, either express or implied, of another individual or company. For licensing information, please write to P.O. Box 161, 1820 Montreux 2, Switzerland.

REPRINTS OF INDIVIDUAL ARTICLES Copies of individual articles may be obtained from the Publisher's own document delivery service at the appropriate fees. Write to: Reprint Department, P.O. Box 786, Cooper Station, New York, NY 10276, USA or P.O. Box 90, Reading, Berkshire RG1 8JL, U.K.

Permission to reproduce and/or translate material contained in this journal must be obtained in writing from the Publisher. Please contact Rights and Permissions Officer, P.O. Box 161, 1820 Montreux 2, Switzerland.

FERROELECTRICS, ISSN 0015-0193, is published monthly for SFr. 521.00 per volume by Gordon and Breach Science Publishers S.A., Poststrasse 22, 7000 Chur, Switzerland. Second-class postage paid at New York, NY and additional mailing offices. POSTMASTER: Send address changes to FERROELECTRICS, c/o Gordon and Breach Science Publishers S.A., P.O. Box 786, Cooper Station, New York, NY 10276.

Distributed by STBS Ltd., P.O. Box 90, Reading, Berkshire RG1 8JL, U.K. Printed in the United States of America.

OCTOBER 1991

DISCLAIMER NOTICE



THIS DOCUMENT IS BEST QUALITY AVAILABLE. THE COPY FURNISHED TO DTIC CONTAINED A SIGNIFICANT NUMBER OF COLOR PAGES WHICH DO NOT REPRODUCE LEGIBLY ON BLACK AND WHITE MICROFICHE.

PROCEEDINGS OF
**THE THIRD INTERNATIONAL CONFERENCE
ON FERROELECTRIC LIQUID CRYSTALS**

June 23-28, 1991
Boulder, Colorado, USA

Guest Editors:

Noel A. Clark
David M. Walba
Mark A. Handschy
Garret Model

Accession For	
NTIS	CRA&I <input checked="" type="checkbox"/>
DTIC	TAB <input type="checkbox"/>
Unannounced <input type="checkbox"/>	
Justification	
By	
Distribution	
Availability	
Date	
Dist	Source
A-1	

DATE OF DEPOSIT

CONTENTS—PART II

Note on Pagination, Author Index and Table of Contents

The Proceedings of the Third International Conference on Ferroelectric Liquid Crystals are being published in two volumes of FERROELECTRICS (Volumes 121 and 122). Volume 121, Part I includes Sections A–D. Volume 122 begins with Section E and runs through Section L. To facilitate indexing and referring to these Proceedings, the page numbers of Volume 122 will run continuously from the end of Volume 121. The Table of Contents and Author Index will be repeated in full in both Volumes.

The alpha-numeric code e.g., [O-24], [P-78], given at the end of each paper in the Table of Contents, indicates the position of that paper in the Program Book of Abstracts. Papers that were not received in time to be printed in the special editions of Ferroelectrics dedicated to the 1991 Conference will appear in regular issues of Ferroelectrics with a footnote tying them into the Conference.

SPONSORS AND ORGANIZING COMMITTEES	xiii
LIST OF PARTICIPANTS	xv
PREFACE	xvii

Section E: Device Technology

FERROELECTRIC LIQUID CRYSTAL DISPLAYS FOR TELEVISION APPLICATION [O-23]

W. J. A. M. HARTMANN 1/[355]

LARGE AREA FERROELECTRIC LIQUID CRYSTAL DISPLAYS [O-24]

S. K. HEEKS, A. MOSLEY, B. M. NICHOLAS,
P. C. RUNDLE AND P. SCHLUSCHE 27/[381]

A HIGH CONTRAST AND HIGH TRANSMITTANCE MULTIPLEXING SSFLC DISPLAY UTILIZING NAPHTHALENE BASE LIQUID CRYSTAL MATERIALS [O-28]

A. MOCHIZUKI, K. MOTOYOSHI AND M. NAKATSUKA 37/[391]

ELECTRO-OPTICAL PROPERTIES OF FERROELECTRIC LIQUID CRYSTALLINE POLYMERS [O-29]

K. YUASA, S. UCHIDA, T. SEKIYA, K. HASHIMOTO
AND K. KAWASAKI 53/[407]

THE "JOERS/ALVEY" FERROELECTRIC MULTIPLEXING SCHEME [O-33]

P. W. H. SURGUY, P. J. AYLIFFE, M. J. BIRCH,
M. F. BONE, I. COULSON, W. A. CROSSLAND,
J. R. HUGHES, P. W. ROSS, F. C. SAUNDERS AND
M. J. TOWLER 63/[417]



MICRO-OPTIC SWITCH USING CHIRAL NEMATIC-SMECTIC C* PHASE TRANSITION FERROELECTRIC LIQUID CRYSTALS

[P-62]

A. M. BIRADAR, S. S. BAWA, C. P. SHARMA AND
S. CHANDRA

81/[435]

CONTROLLING THE GREY LEVEL CAPACITY OF A BISTABLE FLC SPATIAL LIGHT MODULATOR [P-66]

M. KILLINGER, J. L. DE BOUGRENET DE LA TOCNAYE
AND P. CAMBON

89/[443]

PHOTOVOLTAIC OPTICALLY ADDRESSED SPATIAL LIGHT MODULATOR [P-67]

C. C. MAO, B. LANDRETH, K. M. JOHNSON AND
G. MODEL

101/[455]

OPTICAL BISTABLE AND LIMITING BEHAVIORS IN FERROELECTRIC LIQUID CRYSTAL AND OPTICAL PROCESSING [P-69]

M. OZAKI, H. MORITAKE, A. TAGAWA, N. SHIGENO
AND K. YOSHINO

113/[467]

Section F: Polymer FLCs

ANOMALOUS CURRENT AND ELECTROOPTIC RESPONSE IN A POLYACRYLATE FERROELECTRIC LIQUID CRYSTAL WITH LARGE SPONTANEOUS POLARIZATION [O-43]

K. SKARP, G. ANDERSSON, S. T. LAGERWALL,
H. KAPITZA, H. POTHS AND R. ZENTEL

127/[481]

LINEAR ELECTROMECHANICAL EFFECT IN A POLYMERIC FERROELECTRIC LIQUID CRYSTAL [O-44]

N. ÉBER, L. BATA, G. SCHEROWSKY AND A. SCHLIWA

139/[493]

A CHIRAL SIDE-CHAIN POLYMER WITH LAYERED STRUCTURE [P-149]

L. BATA, K. FODOR-CSORBA, J. SZABON,
M. V. KOZLOVSKY AND S. HOLLY

149/[503]

INDUCED SPONTANEOUS POLARIZATION IN A SIDE CHAIN POLYMER [P-156]

G. SCHEROWSKY, K. GRÜNEBERG AND K. KÜHNPAST

159/[513]

Section G: Chiral Systems

ON THE APPEARANCE OF THE ANTIFERROELECTRIC PHASE [O-47]

H. TAKEZOE, A. FUKUDA, A. IKEDA, Y. TAKANISHI,
T. UMEMOTO, J. WATANABE, H. IWANE, M. HARA
AND K. ITOH

167/[521]

- PHASE TRANSITIONS AND SWITCHING PROPERTIES IN
ANTIFERROELECTRIC LIQUID CRYSTALS [O-48]**
H. ORIHARA AND Y. ISHIBASHI 177/[531]
- POLYMER-DISPERSED CHOLESTERIC LIQUID CRYSTALS—
CHALLENGE FOR RESEARCH AND APPLICATION [O-51]**
H.-S. KITZEROW AND P. P. CROOKER 183/[537]
- FERROELECTRIC LIQUID CRYSTALS AS FLOW-FIELD
SENSORS IN BOUNDARY LAYER INVESTIGATION [O-52]**
D. S. PARMAR 197/[551]
- DIRECTOR STRUCTURES OF A CHIRAL SMECTIC I LIQUID
CRYSTAL IN THE SURFACE STABILIZED GEOMETRY [P-61]**
R. SHAO, Z. ZHUANG AND N. A. CLARK 213/[567]

Section H: Antiferroelectrics

- LANDAU-KHALATNIKOV DYNAMICS OF HELICOIDAL
ANTIFERROELECTRIC LIQUID CRYSTALS [P-60]**
B. ŽEKŠ, R. BLINC AND M. ČEPIČ 221/[575]

Section I: Optics

- NONLINEAR OPTIC PROPERTIES OF HETEROCYCLIC
COMPOUNDS HYPERPOLARIZABILITY-STRUCTURE
CORRELATION [P-116]**
G. SUBRAMANIAM, S. POLASHENSKI AND
K. KENNEDY 229/[583]

Section J: Interfaces

- FERROELECTRIC LIQUID CRYSTAL ALIGNMENT BY OBLIQUE
EVAPORATION OF SiO₂ [P-119]**
D. ARMITAGE 239/[593]

ELECTRIC FIELD INDUCED MACROSCOPIC FLOW IN FREE-STANDING FERROELECTRIC FILMS [P-124]	
G. HAUCK AND H. D. KOSWIG	253/[607]

RELATIONS BETWEEN SURFACE PROFILE AND FREE SURFACE ENERGY OF SMECTIC C LIQUID CRYSTALS [P-130]	
P. SCHILLER	261/[615]

Section K: Theory

ON THE ELASTIC FREE ENERGY OF SMC* AND SMC₂* PHASES [P-160]	
M. NAKAGAWA	279/[633]

OPTICAL STUDIES OF SMECTIC C* DISPLAYS [P-161]	
J. M. OTÓN, J. M. S. PENA, A. SERRANO AND F. OLARTE	293/[647]

Section L: Comments after the Conference

SIMPLE PICTURE OF THE ANTIFERROELECTRIC SMECTIC C_A PHASE	
I. DAHL	311/[665]

AUTHOR INDEX	i-ii
---------------------	------

ANNOUNCEMENTS	
----------------------	--

CONTENTS—PART I

Note on Pagination, Author Index and Table of Contents

The Proceedings of the Third International Conference on Ferroelectric Liquid Crystals are being published in two volumes of FERROELECTRICS (Volumes 121 and 122). Volume 121, Part I includes Sections A–D. Volume 122 begins with Section E and runs through Section L. To facilitate indexing and referring to these Proceedings, the page numbers of Volume 122 will run continuously from the end of Volume 121. The Table of Contents and Author Index will be repeated in full in both Volumes.

The alpha-numeric code e.g., [O-24], [P-78], given at the end of each paper in the Table of Contents, indicates the position of that paper in the Program Book of Abstracts. Papers that were not received in time to be printed in the special editions of Ferroelectrics dedicated to the 1991 Conference will appear in regular issues of Ferroelectrics with a footnote tying them into the Conference.

SPONSORS AND ORGANIZING COMMITTEES	xiii
LIST OF PARTICIPANTS	xiv
PREFACE	xvii

Section A: Dynamics

**BROADBAND DIELECTRIC RELAXATION STUDY IN A
FERROELECTRIC LIQUID CRYSTAL BY TIME DOMAIN
REFLECTOMETRY [O-3]**

R. NOZAKI, T. K. BOSE AND J. THOEN 1

**THE MOLECULAR ORIGIN OF FERROELECTRICITY IN FLC: A
CHALLENGE FOR DIELECTRIC SPECTROSCOPY AT
MICROWAVE FREQUENCIES [O-4]**

F. KREMER, A. SCHÖNFELD, S. U. VALLERIEN,
A. HOFMANN AND N. SCHWENK 13

**ELECTROCLINIC EFFECT IN THE N* PHASE NEAR A N* S_A S*_C
MULTICRITICAL POINT [O-5]**

C. LEGRAND, N. ISAERT, J. HMINE, J. M. BUISINE, J. P.
PARNEIX, H. T. NGUYEN AND C. DESTRADE 21

**A NEW FLC-EO CELL SHOWING QUASI-TRISTATE
CHARACTERISTICS [P-75]**

M. KIMURA, A. MOCHIZUKI, M. ITOH AND
S. KOBAYASHI 33

**THE EFFECT OF BIASING ELECTRIC FIELD ON RELAXATIONS
IN FLC INVESTIGATED BY THE DIELECTRIC AND OPTICAL
METHODS [P-77]**

J. PAVEL AND M. GLOGAROVÁ 45

**THE STRONG TEMPERATURE DEPENDENT GOLDSTONE
MODE RELAXATION FREQUENCY IN A BROAD RANGE
SmC* PHASE [P-78]**

M. PFEIFFER, G. SOTO, S. WROBEL, W. HAASE,
R. TWIEG AND K. BETTERTON

55

**COLLECTIVE AND MOLECULAR RELAXATIONS IN
POLYMERIC FERROELECTRIC LIQUID CRYSTALS AND
EXPERIMENTAL PROOF OF PIEZOELECTRICITY IN CHIRAL
SMECTIC C-ELASTOMERS [P-80]**

A. SCHÖNFELD, F. KREMER, S. U. VALLERIEN,
H. POTHS AND R. ZENTEL

69

Section B: FLC Physics

**SMECTIC C* LOCAL LAYER STRUCTURE WITHIN TEXTURE
LINES STUDIED WITH A (SUB)MICROMETER OPTICAL
MEASURING SPOT [O-8]**

A. G. H. VERHULST AND F. J. STOMMELS

79

**THE IMPORTANCE OF DIELECTRIC BIAXIALITY FOR
FERROELECTRIC LIQUID CRYSTAL DEVICES [O-35]**

J. C. JONES, M. J. TOWLER AND E. P. RAYNES

91

ION TRANSPORT IN SSFLCD's [O-37]

B. MAXIMUS, E. DE LEY, A. DE MEYERE AND
H. PAUWELS

103

**THE SURFACE ANCHORING DEPENDENCE OF THE
DIELECTRIC CONSTANT OF AN FLC MATERIAL SHOWING
ELECTROCLINIC EFFECT [O-39]**

Y. B. YANG, T. BANG, A. MOCHIZUKI AND
S. KOBAYASHI

113

**THE FIELD INDUCED STRIPE TEXTURE IN SURFACE
STABILIZED FERROELECTRIC LIQUID CRYSTAL CELLS [P-93]**

R. F. SHAO, P. C. WILLIS AND N. A. CLARK

127

**OPTICAL STUDIES OF THIN LAYERS OF SMECTIC C
MATERIALS [P-94]**

M. J. TOWLER, M. H. ANDERSON, J. C. JONES AND
E. P. RAYNES

137

LARGE ELECTROCLINIC EFFECT IN NEW LIQUID CRYSTAL MATERIAL [P-95]

P. A. WILLIAMS, N. A. CLARK, M. B. ROS,
D. M. WALBA AND M. D. WAND

143

IONIC TRANSPORT EFFECTS IN SSFLC CELLS [P-98]]

Z. ZOU, N. A. CLARK AND M. A. HANDSCHY

147

Section C: New Materials**DESIGN, SYNTHESIS AND PROPERTIES OF NEW FERROELECTRIC LIQUID CRYSTALLINE COMPOUNDS HAVING A CHIRAL CENTER DIRECTLY CONNECTED TO THE CORE AROMATIC RING [O-14]**

T. HIYAMA, T. KUSUMOTO AND S. TAKEHARA

159

SYNTHESIS AND PHYSICAL PROPERTIES OF NOVEL PHENYLBENZOATE TYPE FERROELECTRIC LIQUID CRYSTALS [P-100]

K. FUJISAWA, C. SEKINE, Y. UEMURA, T. HIGASHII,
M. MINAI AND I. DOHGANE

167

NOVEL OPTICALLY ACTIVE COMPOUNDS HAVING 2-ALKANOYLOXYPROPYL MOIETY AS CHIRAL DOPANTS [P-104]

K. MIYAZAWA, S. SAITO, K. TERASHIMA, M. KIKUCHI
AND T. INUKAI

179

HELICAL SMECTIC A* PHASE (TGB_A PHASE) IN SOME TOLAN SERIES [P-105]

H. T. NGUYEN, R. J. TWIEG, M. F. NABOR, N. ISAERT
AND C. DESTRADE

187

CHIRAL γ -LACTONES FOR FLC. THE RELATIONSHIP BETWEEN THE MOLECULAR STRUCTURES AND THE PROPERTIES [P-109]

K. SAKAGUCHI, Y. SHIOMI, M. KODEN AND
T. KURATATE

205

SYNTHESIS, SPECTRA, AND FERROELECTRIC PROPERTIES OF A SERIES OF DIHALOGENATED DOPANTS [P-111]

W. N. THURMES, M. D. WAND, R. T. VOHRA AND
D. M. WALBA

213

PROPERTIES OF A SERIES OF PHENYLPYRIMIDINE FERROELECTRIC LIQUID CRYSTALS POSSESSING THE 2,3- DIFLUOROALKOXY TAIL [P-112]	
M. D. WAND, W. N. THURMES, R. T. VOHRA, K. MORE AND D. M. WALBA	219
NOVEL FERROELECTRIC LIQUID CRYSTALS HAVING A PLANAR CORE STRUCTURE [P-114]	
A. YOKOYAMA, A. YOSHIZAWA AND T. HIRAI	225
Section D: Phase Behavior & Microscopics	
EFFECT OF THE I* PHASE TEMPERATURE RANGE ON THE NATURE OF THE TILTED FLUID TO HEXATIC TRANSITION [O-18]	
V. N. RAJA, S. KRISHNA PRASAD, D. S. SHANKAR RAO, J. W. GOODBY AND M. E. NEUBERT	235
DESIGN AND SYNTHESIS OF FERROELECTRIC LIQUID CRYSTALS. 15.¹ FLC MATERIALS FOR NONLINEAR OPTICS APPLICATIONS [O-20]	
D. M. WALBA, M. B. ROS, T. SIERRA, J. A. REGO, N. A. CLARK, R. SHAO, M. D. WAND, R. T. VOHRA, K. ARNETT AND S. P. VELSCO	247
STATIC AND DYNAMIC PROPERTIES OF OPTICAL SECOND HARMONIC GENERATION IN FERROELECTRIC LIQUID CRYSTAL [O-21]	
M. OZAKI, M. UTSUMI, T. GOTOU, Y. MORITA, K. DAIDO, Y. SADOHARA AND K. YOSHINO	259
CHIRAL ESTERS AND THEIR MIXTURES WITH STABLE S_C[*] PHASE AT AMBIENT TEMPERATURE [P-135]	
J. SZABON, L. BATA, K. FODOR-CSORBA, N. ÉBER AND A. VAJDA	275
ELECTROCLINIC AND DIELECTRIC PROPERTIES OF CHIRAL S_mC INFLUENCED BY THE SUBSTANCE CHIRALITY [P-138]	
M. GLOGAROVÁ, CH. DESTRADE, J. P. MARCEROU, J. J. BONVENT AND H. T. NGUYEN	285
TILT ANGLE BEHAVIOR OF SMECTIC C PHASE [P-140]	
M. KODEN AND T. ANABUKI	295

**HIGH PRESSURE STUDIES ON FERROELECTRIC LIQUID
CRYSTALS [P-143]**

S. M. KHENED, S. KRISHNA PRASAD, V. N. RAJA,
S. CHANDRASEKHAR AND B. SHIVKUMAR

307

**MEASUREMENT OF ROTATIONAL VISCOSITY IN THE
SMECTIC C* PHASE [P-144]**

S. KRISHNA PRASAD, S. M. KHENED, V. N. RAJA AND
B. SHIVKUMAR

319

**THE EFFECTIVE USE OF THE PRECISE SOLUTION OF THE
VAN LAAR EQUATION FOR THE CALCULATION OF THE
BINARY PHASE DIAGRAM WITH A SMECTIC C PHASE [P-146]**

A. RABINOVICH AND A. GANELINA

335

**EXPERIMENTAL STUDIES IN THE VICINITY OF THE C*-I*
TRANSITION [P-147]**

V. N. RAJA, S. KRISHNA PRASAD, S. M. KHENED AND
D. S. SHANKAR RAO

343

AUTHOR INDEX

i-ii

ANNOUNCEMENTS

PROCEEDINGS OF THE THIRD INTERNATIONAL CONFERENCE ON FERROELECTRIC LIQUID CRYSTALS

June 23–28, 1991
Boulder, Colorado, USA

SPONSORS

The Organizing Committee gratefully acknowledges the following Organizations for their support of the Third International Conference on Ferroelectric Liquid Crystals:

Canon, Inc.
Chisso Corporation
Department of the Army, U.S. Army Research Office
F. Hoffmann-La Roche Ltd.
Ferroelectrics
Fujitsu Labs.
GEC Research
Gordon and Breach Science Publishers S.A.
Hoechst AG
IBM Corporation
Material Science and Technology
Merck, EM Industries
Monsanto
Polaroid Corporation
San Nopco Limited
Sharp Corporation
3M Information and Imaging
Toshiba
U.S. Air Force Rome Laboratory at Hanscom AFB, MA
Varitronix Limited

ORGANIZING AND SCIENTIFIC COMMITTEE

Noel A. Clark, Chairman

David Walba
Garret Moddel
Kristina Johnson

Mark Handschy
Sven Lagerwall
Christian Destrade

INTERNATIONAL ADVISORY BOARD

L. Bata (Hungary)
R. Blinc (Yugoslavia)
L. M. Blinov (Russia)
D. Demus (Germany)
G. Durand (France)
C. Escher (Germany)
A. Fukuda (Japan)
T. Geelhaar (Germany)
J. W. Goodby (UK)

G. Heppke (Germany)
C. C. Huang (USA)
T. Inukai (Japan)
V. Janovec (Czechoslovakia)
J. Kanbe (Japan)
S. Matsumoto (Japan)
J. Prost (France)
M. Schadt (Switzerland)

LIST OF PARTICIPANTS

BELGIUM

DE MEYERE, A.

CZECHOSLOVAKIA

GLOGORAVA, M.

LUBOR, L.

PAVEL, J.

FRANCE

BRUNET, M.

DESBAT, B.

DESTRADE, C.

DURAND, G.

KELLER, P.

LEGRAND, C.

MACLENNAN, J.

MALTHETE, J.

PARNEIX, J. P.

GERMANY

BARH, C.

BERESHEV, L.

ESCHER, C.

GEELHAAR, T.

GRUENEBERG, K.

GRULER, H.

HENTSCHEL, D.

JOACHIMI, D.

JUNGE, M.

KITZEROW, H.

KREMER, F.

KRESSE, H.

LOTZ, A.

MICHALSKI, B.

PFEIFFER, M.

PLEINER, H.

POLOSSAT, E.

REINHART, K.-F.

SCHEROWSKI, G.

SCHILLER, P.

SCHLOSSER, H.

SEIMENSMEYER, K.

TSCHIERSCHE, C.

WAHL, J.

ZENTEL, R.

HUNGARY

BATA, L.

ÉBER, N.

INDIA

BAWA, S. S.

CHANDRASEKHAR, B. S.

KRISHNA PRASAD, S.

RAJA, V. N.

ISRAEL

COHEN, G.

ITALY

MALTESE, P.

JAPAN

HAGIWARA, T.

HIRAOKA, K.

HIYAMA, T.

ISOZAKI, T.

KANETSUGU, T.

KAZUTOSHI, M.

KIMURA, M.

KODEN, M.

KONDO, H.

KONDO, K.

MARUYAMA, M.

MITSURI, K.

MOCHIZUKI, A.

NAGAYA, T.

NAKAGAWA, M.

NAOYA, I.

NOHIRA, H.

ONNAGAWA, H.

ORIHARA, H.

OZAKI, M.

SAKAGUCHI, K.

SAKAIGAWA, A.

SEKINE, H.

SHIROH, I.

SUMITAKA, T.

SUZUKI, Y.-I.

TAKAHASHI, K.

TAKANISHI, Y.

TAKEZOE, H.
TORIUMI, H.
TSURO, S.
YAMMOTO, S.
YANG, Y. B.
YOKOYAMA, A.
YUASA, K.

NETHERLANDS
HARTMANN, W.
VERHULST, T.

PORTUGAL
FIGEUIRINHAS, J.

SPAIN
ETXEBARRIA, J.
OLARTE, F.
OMENAT, A.
ROS, B.
SANCHEZ-PEÑA, J.
SERRANO, J.
ZUBIA, J.

SWEDEN
DAHL, I.
GOUDA, F.
KOMETOV, L.
LAGERWALL, T.
MATSZCZYK, M.
MATSZCZYK, T.
SKARP, K.

SWITZERLAND
BUHECKER, R.

UK
BONE, M. F.
COLES, H. J.
DAVEY, A.
DUNMAR, D.
JONES, C.
NICHOLAS, B.
TOWLER, M.

USA
AIHARA, Y.

ARMITAGE, D.
BRANDOW, S.
CLARK, N. A.
DOROGKI, D.
FAIR, D.
FREIDMAN, L.
FUNG, B. M.
HANDSCHY, M.
JAKLI, T.
KUDO, Y.
LIEN, S.-C.
LIU, J.-Y.
MACIRI, J.
MAHMOOD, R.
MERY, S.
MEDDEL, G.
NAKAUCHI, J.
NEUBERT, M.
OUCHI, Y.
PANG, J.
PARK, C. S.
PFEIFFER, S.
PARMAR, D.
RAPPAPORT, A.
RUTH, J.
SABOL-KEAST, S.
SHAO, R.
SUBRAMANIAM, G.
THURMES, W.
VOHRA, R.
WALBA, D.
WAND, M.
WILLIS, P. C.
YANG, K. H.
ZOU, Z.

USSR
CHIGRNOV, V.
CHILAYA, G.
GERASIMOV, A.
LOSEVAS, M.
PITKIN, S. A.
PODNEKS, V.
POZHIDAEV, E.

YUGOSLAVIA
BLINC, R.
ZEKS, B.

PREFACE

The present volumes form the proceedings of the Third International Conference on Ferroelectric Liquid Crystals, held in Boulder, Colorado, USA June 23–28, 1991. These volumes continue the publication of this conference series, the proceedings of the first conference (1987) held at Bordeaux/Arcachon appearing in Volumes 84 and 85, and the proceedings of the second conference (1989) held at Göteborg appearing in Volumes 113 and 114.

As for the two preceding conferences, FLC-91 provided a broad forum for the exchange of information on FLCs, with most of the groups working in the field well represented. Exciting developments were reported in all FLC areas. The worldwide effort at developing new FLC materials continues apace, with the report of an FLC material possessing a spontaneous polarization nearly equal to the sum of all transverse molecular dipoles, and new thrusts in polymer FLCs and FLCs for electronic nonlinear optical applications. The conference saw many new developments in FLC basic and device physics, including the use of dielectric spectroscopy as a tool for studying the molecular origins of the polarization in FLCs. Particularly exciting were the FLC device developments with the emergence of sophisticated FLC devices for opto-electronic computing, display, and other light control applications, including a demonstration of a flexible polymer FLC display!

Due to the intense interest in FLCs in Japan and the large number of Japanese FLC workers, the Fourth International Conference on Ferroelectric Liquid Crystals will be held in Japan in the summer of 1993, organized by Professor A. Fukuda of Tokyo Institute of Technology.

In preparing this proceedings it was the express intention of the Guest Editors to be as timely as possible in publishing the papers of those who submitted and/or revised manuscripts describing their most recent work in time to meet the necessarily tight deadline for 1991 publication. These volumes should thus provide a view of the state of FLC science as of the summer of 1991. It should be noted that some papers submitted for the proceedings for one reason or another could not be made ready in time for inclusion in these volumes. Such papers will be published in future issues of *Ferroelectrics* either as type-set full papers or as letters, with a footnote indicating that they are part of the proceedings of FLC-91.

The Guest Editors would like to thank the sponsors, administrative assistants, and especially all of the scientists who made the meeting such a great success.

Boulder, Colorado, USA, September 1991

Noel A. Clark
David M. Walba

SECTION E
DEVICE TECHNOLOGY

FERROELECTRIC LIQUID CRYSTAL DISPLAYS FOR TELEVISION APPLICATION

WILBERT J.A.M. HARTMANN

Philips Research Laboratories, Eindhoven, The Netherlands

Abstract The surface-stabilized ferroelectric liquid crystal (SSFLC) effect is a serious candidate for application in television displays, due to its high switching speed and viewing angle independence. For the television application, however, several severe requirements must be fulfilled, of which the demand for a large amount of gray levels is very crucial in view of the bistable character of the SSFLC effect. A review and discussion of the different approaches to realize gradation in SSFLC structures is given. The so-called dither techniques yield discrete gray levels but become complex when many levels are required. Analogue gradation methods are based on in-pixel domain switching but require an accurate control of the multidomain structures. Active-matrix addressing of the SSFLC effect enhances the reproducibility of the multidomain gray levels via the charge-control process, resulting in a fast-switching, viewing-angle-independent video display. Passive-matrix addressing (multiplexing) takes advantage of the bistability and the switching speed of the SSFLC effect. One approach to control the multidomain gray levels in passive-matrix addressing is extensively dealt with; the "texture-method". The mechanism, the addressing scheme, the obtainable contrast in the different textures and the applicability of various FLC mixtures are discussed. The resulting performance of test displays, operating at video rate and possessing full gradation, is evaluated. Finally, some indications will be given of the remaining problems, which need further improvement before FLC displays can be successfully applied for television.

INTRODUCTION

Since Meyer et al.¹ first reported the existence of ferroelectricity in liquid crystals in 1975, many researchers have committed themselves to this phenomenon. In 1980, Clark and Lagerwall described the "Surface-Stabilized Ferroelectric Liquid Crystal" (SSFLC) structure², which is characterized by a high switching speed and a non-volatile bistability. Since then, other ferroelectric liquid crystal (FLC) effects like transient scatter mode (TSM)³, deformed helix ferroelectric (DHF)⁴, short pitch ferroelectric (SPF)⁵ and electroclinic (SmA*)⁶ have been reported, but will not be discussed in this review article because, with respect to display application, they appear to be in a less-developed stage than the SSFLC effect.

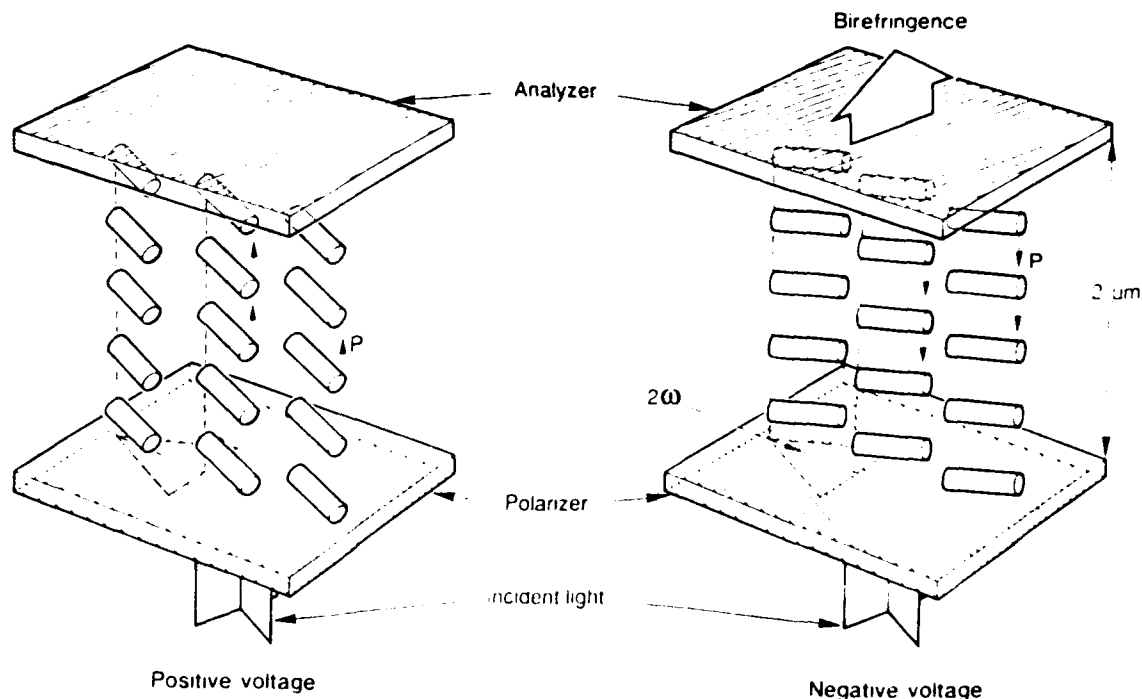


FIGURE 1 The SSFLC effect

The SSFLC effect is based on a smectic C layer configuration perpendicular to the boundary glass plates, which possess a planar-orienting alignment layer and a small distance towards each other. In this way helix formation is avoided and two bistable states exist, which possess a uniform director pattern and an UP or DOWN ferroelectric polarization (see Figure 1). A cell with $\sim 2\mu\text{m}$ thickness between crossed polarizers will exhibit a black and a birefringent bright state, which is perceived as colourless white. The advantages of the SSFLC effect are the very high switching speed ($< 100\mu\text{s}$ at room temperature), the viewing angle independence, the non-volatile bistable memory and the potential of being applied in passive-matrix-addressed (also called multiplexed) liquid crystal displays. In contrast to nematic LCDs, the number of lines of a passive-matrix-addressed SSFLC display is theoretically unlimited. Since 1988, several high-resolution displays (up to 2000 lines) have been demonstrated.^{7,8} Also video-rate ($64\mu\text{s}$ per line) is possible.⁹ The characteristic handicaps of the SSFLC structure are the required cell thickness ($\leq 2\mu\text{m}$), the fact that the materials and the SSFLC cell technology strongly deviate from that of the present LCD products, which are based on the supertwist (STN) or the twisted nematic (TN) effect.

When considering the application of the SSFLC structure for TV displays, it will be necessary to compete with the presently-available displays like the active-matrix-addressed TN LC-TV and the Cathode Ray Tube (CRT). From this

comparison, one can derive the video requirements. When applying the SSFLC effect, the most significant requirements are:

- a) colourless black and white switching, because when full colour is synthesized by combining three primary colours, well-saturated colours should be obtainable;
- b) the linenummer of a TV display is fixed (e.g. 575 for PAL) and has a tendency to increase in the near future (1150 for high-definition TV);
- c) due to the fact that all information must be refreshed with a frequency of 50 (PAL) or 60Hz (NTSC), the line-address time is fixed (e.g. $64\mu\text{s}$ for PAL);
- d) the transmission in the bright state should be maximum, especially because the use of polarized light already causes a 60% loss of intensity;
- e) the obtainable contrast ratio must be ≥ 100 ;
- f) the gradation must possess ≥ 100 gray levels.

With respect to the maximum brightness requirement, one should note that polymer-aligned SSFLC samples usually exhibit an optical switching angle between both bistable memory states of $\approx 15^\circ$ (instead of the preferred 45°) due to a tilt of the smectic layers towards the glass plates (chevron structure). The result is an additional loss in brightness of $\approx 75\%$. This can be avoided by a low-frequency electrical pre-treatment that uprightens the smectic layers^{10,11,12} or by using a high-pretilt orientation (e.g. oblique evaporated SiO_x).^{13,8}

The gradation requirement is very important when considering the SSFLC structure, as it directly contradicts the bistable character of the structure. The necessity of this large amount of gray levels is illustrated in Figure 2, where a continuous gradation image on a CRT is compared with a simulation on the same CRT in which only 16 gray levels for each colour are used (i.e. 4096 different colours).¹⁴ As can be seen, contour lines are clearly visible, especially in areas with a small colour gradient. From this kind of simulations, we concluded that ≥ 100 gray levels would be required most video test images.

This paper will focus on the possibility of meeting the gradation requirement, by discussing several approaches. Both discrete gradation techniques ("dither") and analog gradation techniques ("multidomain") will be discussed.

DISCRETE GRADATION

In the so-called "dither" techniques, the SSFLC pixels are completely switched to the black or the white state. The gradation is introduced by increasing the occurrences of the pixels in the black or white states.^{7,8,15} This can be done by dividing each pixel into many subpixels which can be switched individually to the black or the white state (Figure 3a) or by addressing each pixel more than once within the frame refresh time (Figure 3b).



FIGURE 2 Video test image with continuous anti-log gradient on (a) and with 16 gray levels per colour (b). See Color Plate I.

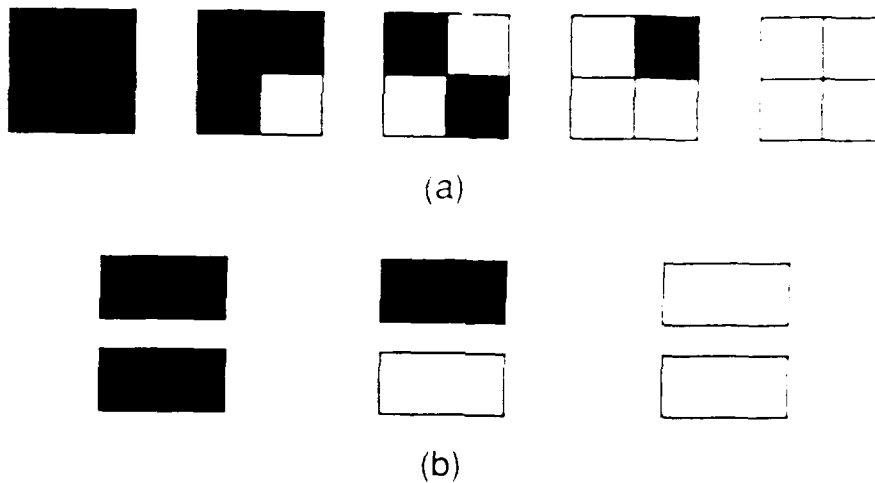


FIGURE 3 Dither techniques: (a) space integration by dividing each pixel in a number of subpixels; (b) time integration by addressing each pixel more than once within the frame refresh time.

In order to keep the complexity as low as possible one should divide the subpixels or the subframes at an unequal ratio. Also combinations of space and time integration can be made. In 1988, researchers from IFFH¹ demonstrated a 64 colour display in which a 1:3 space and a 1:1 time integration are combined to obtain 9 gray levels (see Figure 4a). In 1990, researchers from Thorn-EMI² reported that time integration with an unequal subdivision of the frame period leads to a rapid increase of the number of gray levels, without dramatically affecting the required FLC switching speed. They demonstrated an 8.5" 64 colour display in which 4

gray levels per colour are obtained by a twofold unequal time integration with $t_2 = 2t_1$ (see Figure 4b).



a



b

FIGURE 4 (a) 6-line black&white 256x320 lines FEC display with 9 gray levels (with courtesy from J.Dijon, I.E.T.D.). (b) 8.5-line 64-colour 2x240x528 lines FEC display with 4 gray levels per colour (with courtesy from P.Surguy, Thorn-EMI.).

In order to judge the feasibility of these methods for TV application, we must try to identify the optimum technique for realizing more than 100 levels. Starting from pure space integration, the most efficient way is to use subpixels with surface

ratios that follow a binary series 2^n . These subpixels can be realized by a division of both the column lines and the row lines, although the latter should be kept at a minimum, because more rows means a shorter line addressing time when the linenummer and the frame refreshing time are constant (as they are for video). Therefore the columns should be divided according to 1-2-4-8-... (i.e. 2^0-2^{i-1}) and the rows should be split into two subrows with width-ratio 1-2ⁱ. The $i=4$ case is illustrated in Figure 5, yielding 256 (2^{2i}) gray levels. The division of the rows can be replaced by a twofold time integration with an unequal division in time of 1/17th and 16/17 of the frame period. Each gray level can be realized in only one single manner. In this way the largest amount of gray levels is obtained with the smallest increase in complexity.¹⁸

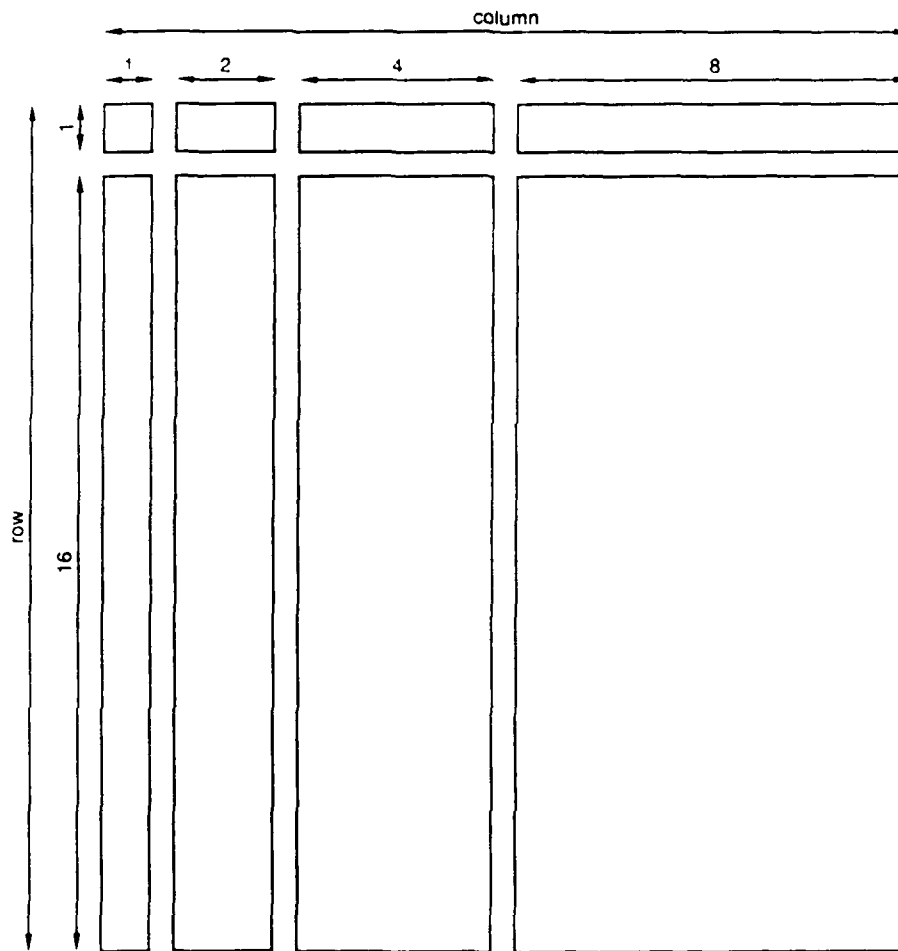


FIGURE 5 A binary subdivision is a very efficient way to achieve a large number of gray levels (256) with a small increase in complexity (number of lines).

In this binary configuration, each column is divided in 4 subcolumns and thus the column interconnection pitch increases (3" TV would require 20 μ m interconnection pitch and 10" TV 70 μ m) and the smallest ITO detail, that has to

be photolithographically made, decreases (3" TV needs a $4\mu\text{m}$ smallest subcolumn and 10" TV $15\mu\text{m}$). The number of column driver ICs increases with a factor of 4. The splitting-up of the rows requires a doubling of the SSFLC switching speed and a video frame or line storage with an increased data transfer speed.

Roughly speaking, one may conclude that the realization of a large number of gray levels using "dither" techniques in passive-matrix-addressed SSFLC displays might be possible, especially for larger-area displays, although it will require a trade-off of large technological efforts concerning: the narrow ITO line-width; the small interconnection pitch; the high number of driver ICs; the high speed data transfer or the high switching speed of the FLC. Moreover, the presence of a periodicity in the space or time integration may be expected to be noticed by the human visual system and therefore it may cause perceptive artefacts on the display. To avoid this, the complexity will have to be further increased.

ANALOG GRADATION

An analog gradation in the bistable SSFLC structure can be obtained by employing the spontaneously-present space integration: the multidomain switching behaviour. As illustrated in Figure 6, the switching from one state to the other (occurring upon voltage inversion) takes place via the nucleation and growth of domains of one of both states. In fact, it was suggested by Maltese et al.¹⁹ to modulate these multidomain structures via the pulse-width of a switching pulse. However, to realize more than 100 gray levels, each of which has to be exactly-reproducible, the nucleation and growth of the domains is not stable enough: an additional control of this process is required. To achieve this control, several ways have been suggested, of which the following will be discussed in the next sections:

- a) charge-controlled domain switching
- b) local E-field variation
- c) local FLC threshold variation.

CHARGE-CONTROLLED DOMAIN SWITCHING

In the SSFLC structure, the electrical difference between both states lies in the sign of the surface charge (the spontaneous polarization P_s). As reported earlier²⁰, an SSFLC cell can be loaded with a certain amount of charge by impressing a voltage onto it and if the cell is electrically isolated directly afterwards, the SSFLC structure can switch (partially) to the other state. This means that an amount of surface charge $\Delta Q = 2P_s\Delta A$ is transported to the other side of the sample, which results in a compensation of the surplus charge that was



FIGURE 6 The multidomain switching process

put on the sample initially. The switched area ΔA , and consequently the transmission, is thus quantitatively controlled by the initially impressed charge (see Figure 7).

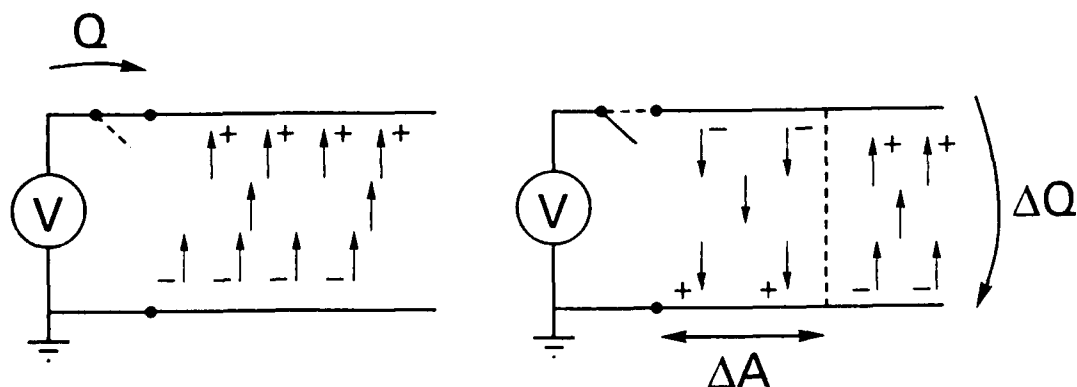


FIGURE 7 The charge-controlled FLC switching mechanism

When the addressing pulse width is significantly smaller than the FLC switching time, the gray levels are, in principle, not influenced by "kinetic" factors like domain nucleation or growth speed or by the cell thickness. The temperature

dependence is related to that of the polarization only. Figure 8 shows the microscopic appearance of the gray levels and the addressing scheme that was applied. The minimum domain diameter is $\approx 2\mu\text{m}$.

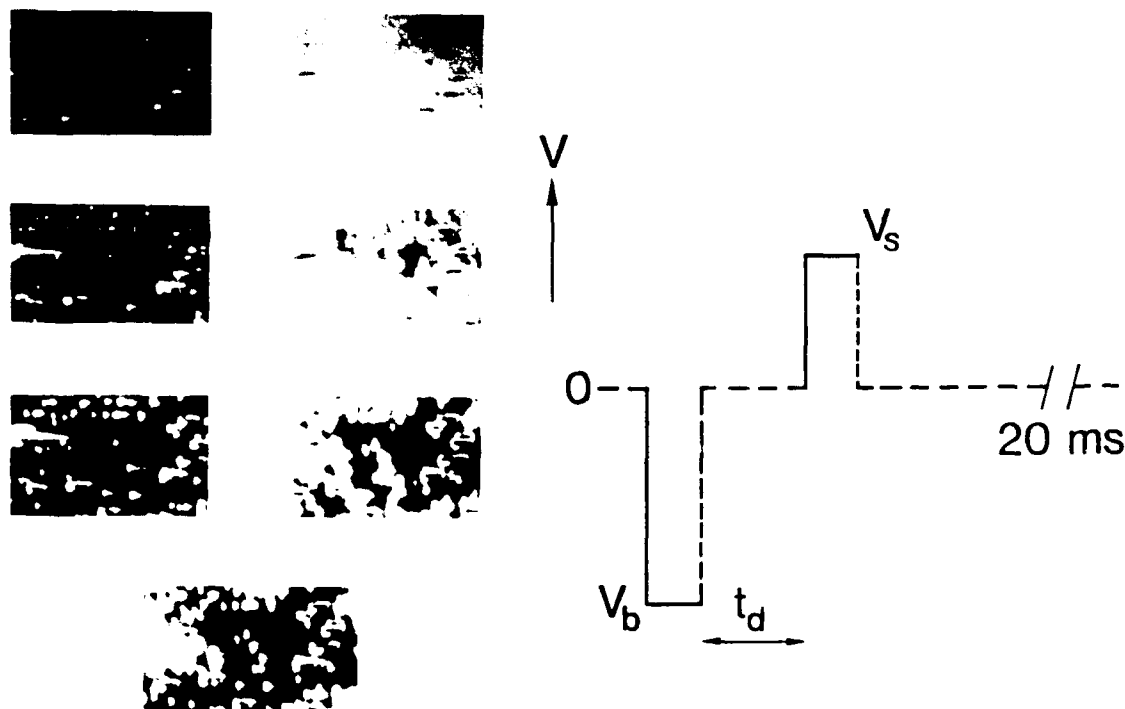


FIGURE 8 Microscopic appearance of the charge-controlled gray levels and the addressing scheme that was applied. The driving parameters are set as in Figure 9.

The addressing scheme has to consist of an invariable reset pulse to obtain an identical starting situation, shortly-afterwards followed by a variable selection pulse which determines the multidomain gray level that will be obtained. The transmission-voltage dependence is depicted in Figure 9.

In fact, we have demonstrated a video display in 1988²¹, based on an active-matrix α -Si TFT array. This active matrix is necessary because the charge-controlled mechanism requires an electrical insulation of the pixel, which cannot be obtained in passive-matrix addressing. A photograph of the display is shown in Figure 10 and some data are listed in Table I. The display is operated in the initial chevron smectic layer configuration. The optical angle between both "single-domain" memory states is $\approx 15^\circ$ (at V_s is 2 and 5.5V), but upon further increasing the selection voltage to 6V or decreasing it to 0V, a continuous (non-multidomain) director shift²² occurs, and the optical angle between these two extreme states is $\approx 40^\circ$. Therefore the brightness and contrast are relatively high. From these displays it was concluded that in principle the mechanism is able to realize a sufficient gradation and that the video requirements can be fulfilled. In

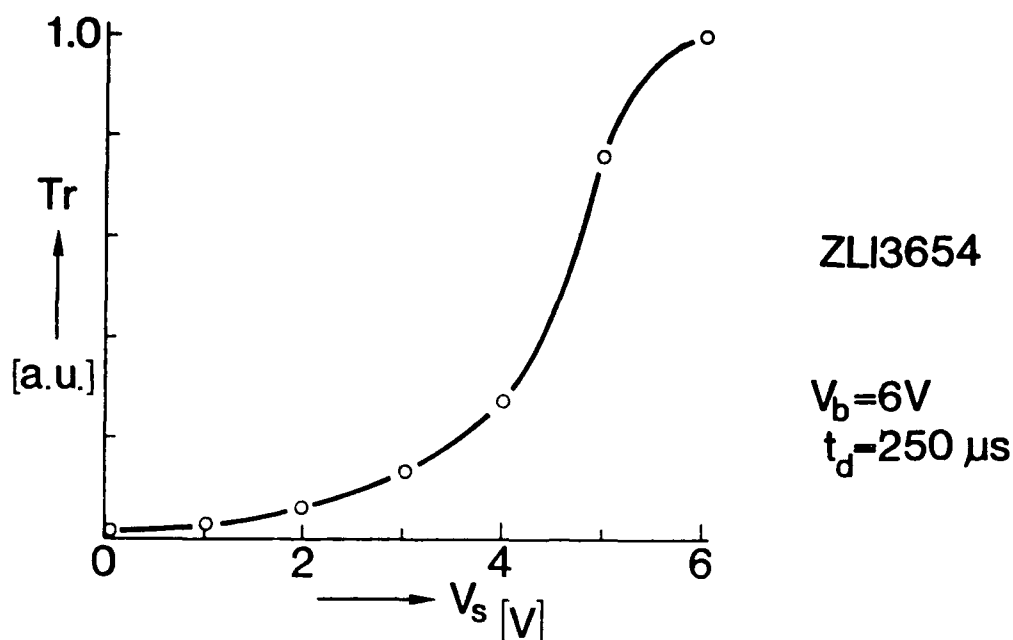


FIGURE 9 Transmission-voltage dependence of charge-controlled gradation.

comparison to active-matrix-addressed TN LC-TV significant improvements are obtained with respect to viewing angle and switching speed.

The charge-controlled mechanism can also be applied in other (non-SS) FLC effects to achieve a controlled modulation. The modulation of the "memory-capability" by means of a variable resistor or capacitor²³ is based on the same mechanism.

TABLE I Active-matrix-addressed FLC video display

array	α -Si TFT (Philips Res. Labs Redhill-UK)		
alignment	nylon6.6 one-side rubbed		
size	2" diagonal	lines	96x108
FLC	ZLI3654 (Merck)	thickness	< 2 μ m
drive frequency	50Hz	contrast ratio	100 (in pixel)
line-time	64 or 32 μ s	switching speed	< 500 μ s
drive voltages	-6/+ 6V	brightness	70%

Also optically-addressed spatial light modulators (OASLM), that can be applied in computing or image-intensifying, can use this gradation principle.²¹⁻²⁸ The principle of operation of an OASLM is illustrated in Figure 11: a low-intensity image is written onto the α -Si photoconductive layer, which transfers the information electrically to the LC layer. This image is projected using a high-intensity reflection set-up. Due to its switching speed and its high capacity, the SSFLC effect is often suggested to be used in such an OASLM structure. Charge-controlled gradation can be achieved when the activating low-intensity

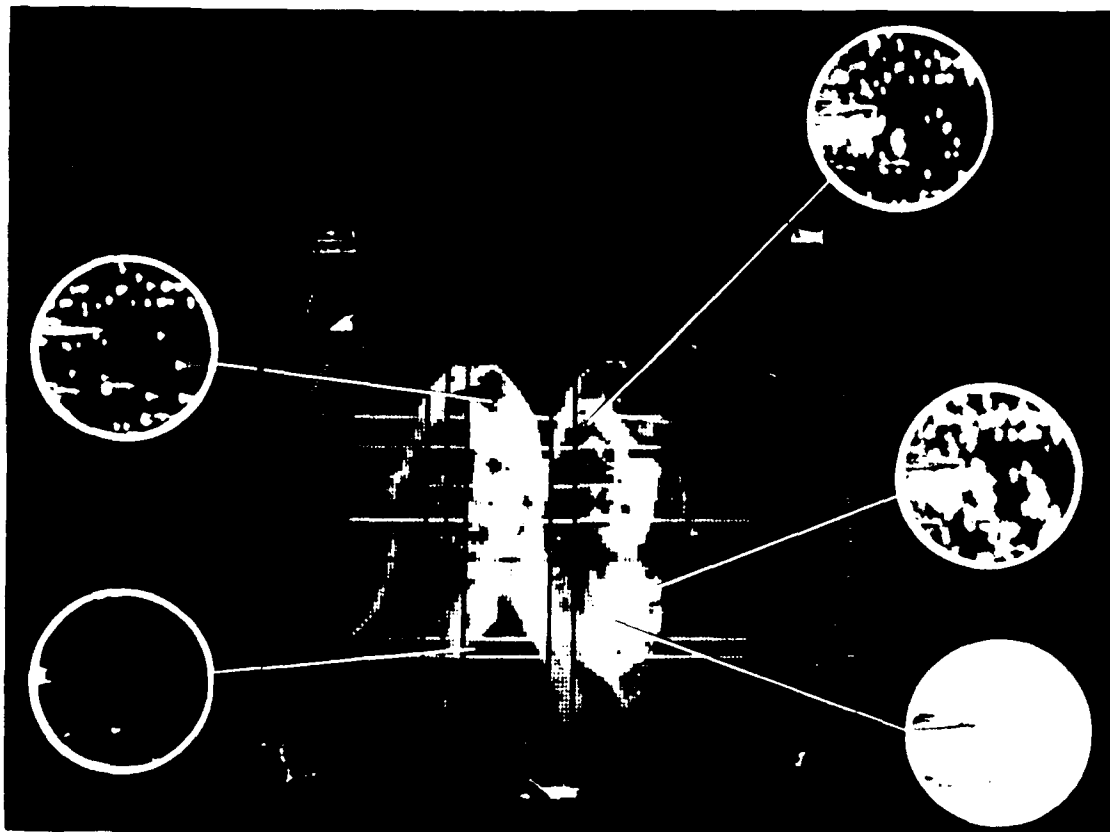


FIGURE 10 The active-matrix-addressed FLC video display, in which the charge-controlled gradation is applied.

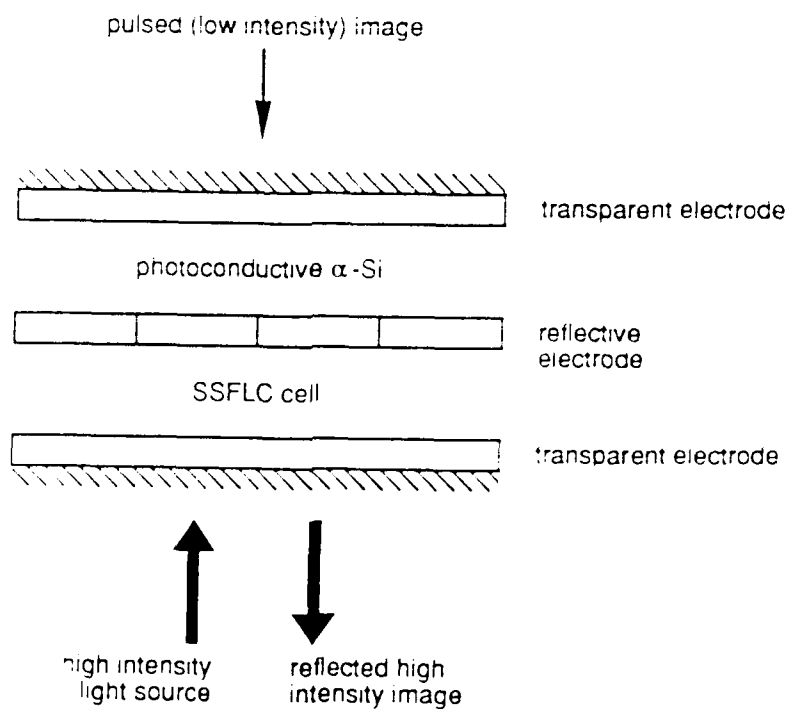


FIGURE 11 OASLM device as image intensifier

image is offered within a short time and the LC layer is electrically insulated during the rest of the time. The light-pulse then acts like the drain signal of a transistor switch.

LOCAL E-FIELD VARIATION

A uniform, bistable-switching SSFLC pixel can be provided with a controlled locally-varying electric field, by changing the thickness of the dielectric layer(s) or the electrode structure.

Varying capacitances

As illustrated in Figure 12, a controlled variation of the FLC layer thickness or a controlled variation of the dielectric layers in series with the FLC layer will result in a spatially-varying electric field on the FLC layer within a pixel. The amplitude of the applied voltage will then control which part of the pixel is provided with a field larger than the threshold for switching and thus a domain gray level will occur. These approaches have been described by researchers from Matsushita,²⁹ Canon,³⁰ Seiko³¹ and others. When considering the realization of ≥ 100 reproducible gray levels, however, the thickness control of the different layers in each pixel will have to be better than 1%.

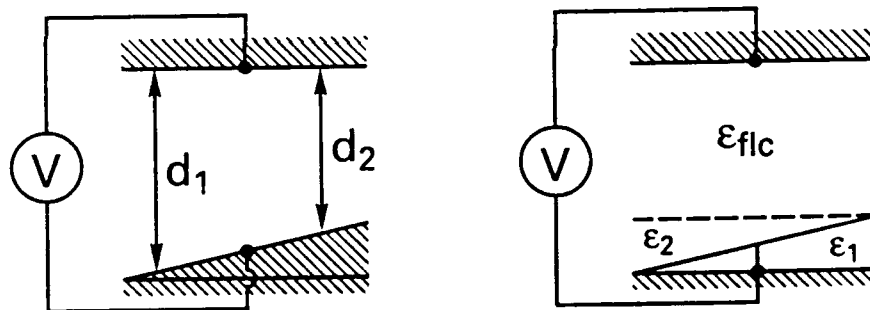


FIGURE 12 Local E-field variation by varying the thickness of the LC layer or by varying the thickness(es) of the dielectric layer(s) in series with the LC layer.

Voltage gradient over pixel electrode

As illustrated in Figure 13, a voltage gradient over a pixel area can be realized by depositing narrow metal lines at the edges of the pixel lines on top of a continuous highly-resistive ITO layer. When different voltages are applied to two adjacent metal lines, a controlled voltage gradient over the high-chmic ITO is established. When, in addition, the voltage on the counterelectrode is varied, the area of the pixel, on which a voltage is present that is larger than the SSFLC threshold changes and thus a domain gradation is realized.³² A disadvantage is

that current is running through the high-ohmic ITO continuously, which may cause power consumption and dissipation problems.

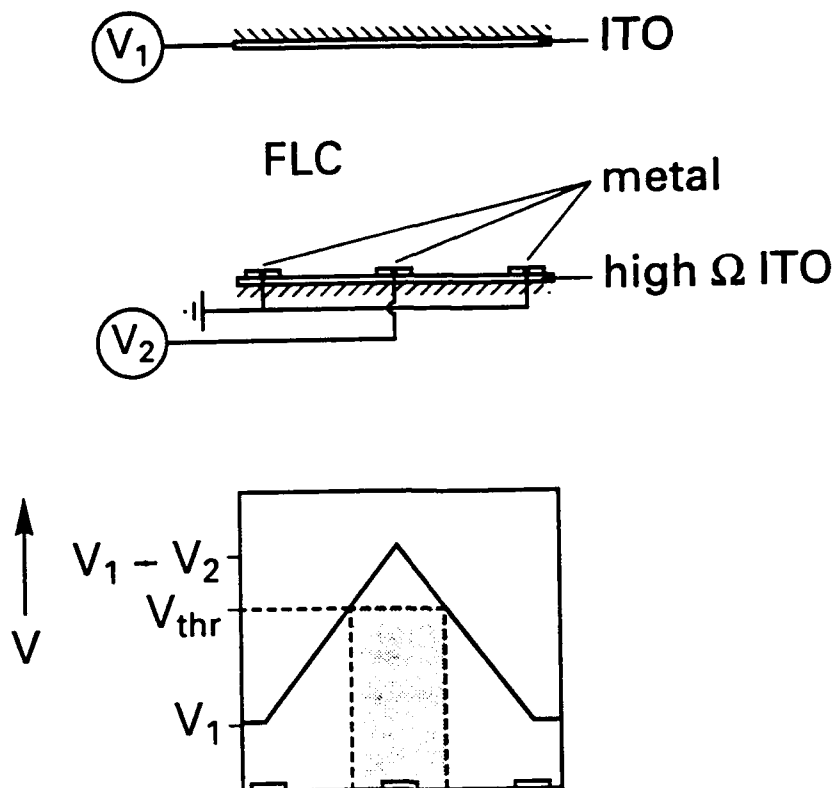


FIGURE 13 Local E-field variation by using high-ohmic ITO to obtain a controlled voltage gradient over the pixel electrode.³²

LOCAL FLC THRESHOLD VARIATION

In this approach it is not the local electric field that is varied, but it is the switching behaviour of the FLC layer itself. As was recently reported by Verhulst et al.,³³ one technique to obtain such a local variation is based on the different occurring textures in SSFLC samples: the "texture-method". In the following section the application of the "texture-method" to realize a video display is described.³⁴ Therefore, attention is paid to the choice of the texture in which the display is operated, to the addressing scheme, to the demands on the liquid crystal material and to the display configuration. As a start, a review of the "texture-method" is given.

The "texture-method"

Low-frequency electric fields applied to SSFLC samples cause an irreversible reorientation of the smectic layer structure.²² With increasing electric fields, the observed texture of the sample changes from the initial virgin texture (texture I; Figure 14a), via a rather inhomogeneous roof-type texture (texture II, Figure

14b), to a more uniform striped texture (texture III, Figure 14c).³⁵ These textures are interpreted as being the result of an uprightening of the chevron smectic layer structure to one with a smaller tilt towards the substrate normal. Theoretically, a smaller smectic layer tilt results in a larger optical angle between the planar memory states and due to the longer switching path on the smectic C cone, the threshold voltage increases.

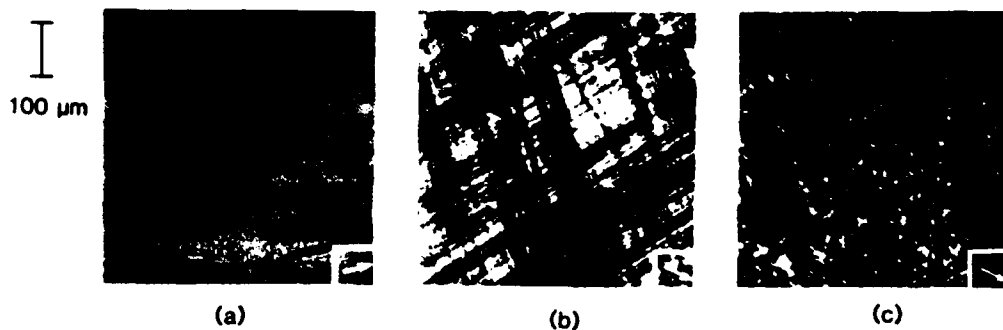


FIGURE 14 Micrographs of the various textures in an SSFLC sample: texture I (a), II (b) and III (c). The arrows indicate the rubbing direction.

It was verified by small-spot optical measurements that the uprightening of the smectic layers occurs in a locally-distributed way and thus a distribution of the threshold voltage arises.³³ Texture I possesses a uniform chevron smectic layer structure with a constant layer tilt δ_0 towards the substrate normal. Texture II comprises a broad range of smectic layer tilts varying from δ_0 to a lower value. We assume that in texture III the range of layer tilts converges again, but now towards the lower value.

The integrated transmission-voltage curve (obtained by applying an addressing scheme as described in the next paragraph), which is measured with a pixel-size spot, exhibits the familiar bistable discontinuous behaviour in texture I and changes to a slanting curve in texture II, which again becomes steeper in texture III (see Figure 15). The slanting curves in texture II and III make an analogue gradation possible. The effective switching angle between the two memory states in texture I is approximately 12° ; the averaged value in texture II usually lies between 20 and 35° and in texture III it can be 32 to 45° . This explains the difference in maximum transmission of the three curves.¹⁰

The (domain) gradation is now controlled by the texture and not by the domain nucleation and growth kinetics (as in texture I¹⁹). The uniformity of the texture can be controlled by the concentration and positioning of the cell spacers. Because both the reorientation electric field and the switching electric field depend on the thickness of the FLC layer, a compensation of thickness

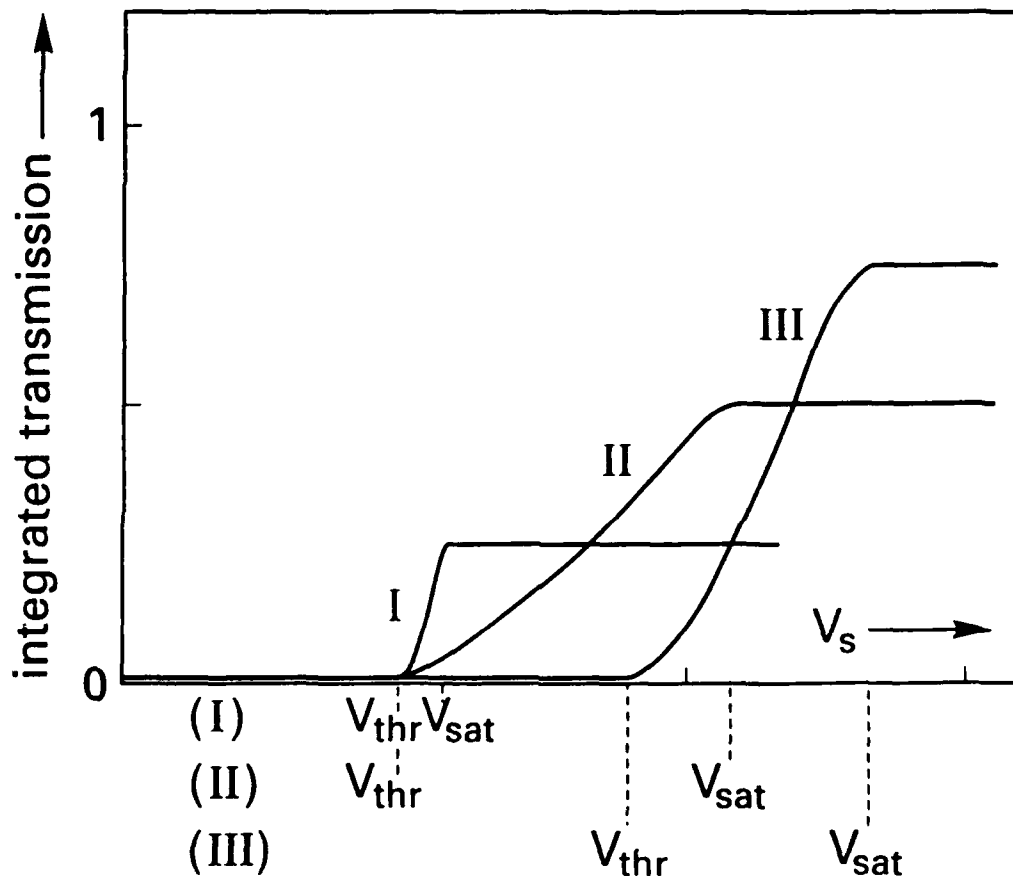


FIGURE 15 Transmission-voltage curves obtained on the different textures, measured with the addressing scheme of Figure 16.

variation occurs, giving this gradation method some tolerance to cell gap variation.³³

Addressing scheme

A preferred addressing scheme for SSFLC video displays³⁶ is depicted in Figure 16. The typical repetition rate is 50Hz (PAL-video) and the available line-time is 128 μ s (half-resolution), 64 μ s (full-resolution) or 32 μ s (high-definition). All drive voltages are bipolar to ensure that no DC electric fields occur which may degrade the liquid crystal material. Therefore, the available time for switching is only 50% of the line-time (2-slot scheme).

The rows are sequentially selected by a bipolar pulse with amplitude V_S . Immediately before selection, a reset is performed by a broad bipolar pulse with amplitude V_R . This reset assures that an identical starting situation (preferably the black state) is obtained before a gray level is written, which is necessary to obtain a reproducible gradation.^{19,21} The reset takes two line-times (or more), meaning that the row drivers have to address at least three rows simultaneously. The gray level is determined by a bipolar column pulse with a variable amplitude V_D , which modulates the effective pixel voltage during selection. The amplitude of the pixel

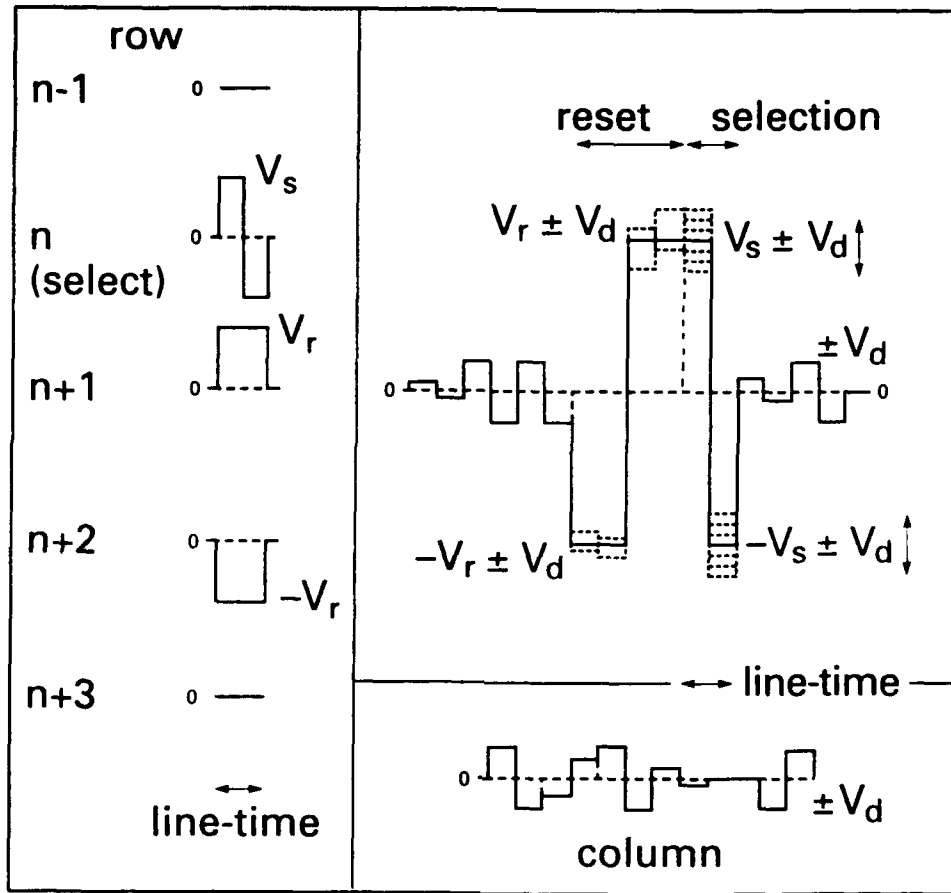


FIGURE 16 Addressing scheme to enable passive-matrix-addressed gradation in SSFLC displays by amplitude modulation: row signal, column signal and resulting pixel voltage.

voltage in the second half of the selection line-time (the switching pulse $-V_s \pm V_d$) determines the amount of switched area starting from the reset situation, thus the gray level. Electronically, it is preferred to address such a large amount of gray levels by amplitude modulation, rather than time (phase-shift) modulation. Because the reset pulses are of double width, their voltage-time product is not influenced by V_d and the reset is not affected. Due to the bipolar nature of the column signal, the response to these pulses during non-selection (i.e. crosstalk) only appears as an oscillation in transmission intensity and hardly changes the mean value of the gray level. High-frequency ac-stabilisation³⁷ is not applied, because it would bring about an unnecessary increase of the power consumption of the display driving. The settings of the drive voltages depend on the transmission-voltage curves as given in Figure 15, according to:

$$V_R \geq V_{SAT} \quad V_S = 1/2(V_{SAT} + V_{THR})$$

$$0 \leq |V_D| \leq 1/2(V_{SAT} - V_{THR})$$

and thus during selection

$$V_{THR} \leq V_{PIXEL} \leq V_{SAT}$$

Texture II or texture III

Figure 17 depicts the actual transmission vs. time recordings of an SSFLC sample to which this addressing scheme is applied ($V_D = 0$). The gray levels, obtained by varying V_S from 9 to 12V (64 μ s line-time), appear to be quite stable. The inset shows the transmission response when data pulses ($V_D = \pm 2V$) are applied during non-selection: the crosstalk. To obtain a high contrast ratio, the crosstalk (in the black state) should be as small as possible.

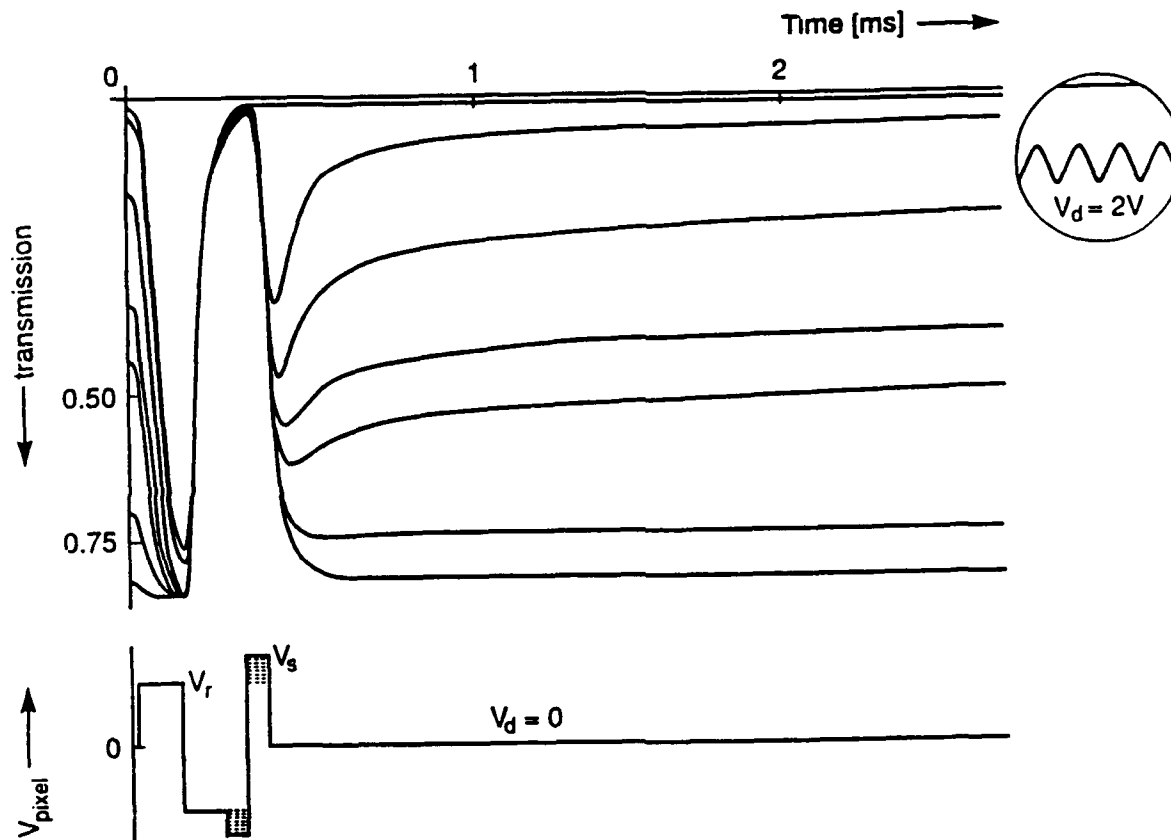


FIGURE 17 Transmission vs. time recordings of different gray levels. The inset shows the (magnified) response when data pulses are applied.

Obviously, texture III has the advantage of a steeper transmission-voltage curve (see Figure 15), thus the maximum bias V_D/V_S is lower. Additionally, texture III exhibits a smaller response to V_D than texture II, because the director position is located closer to the side of the smectic C cone.¹⁰ These two factors will lead to a much smaller crosstalk in texture III than in texture II.

In fact, Figure 18 depicts the measured contrast ratio under actual driving conditions (including the maximum-required V_D) as a function of the effective optical switching angle. It can be seen that the contrast ratio in texture II only

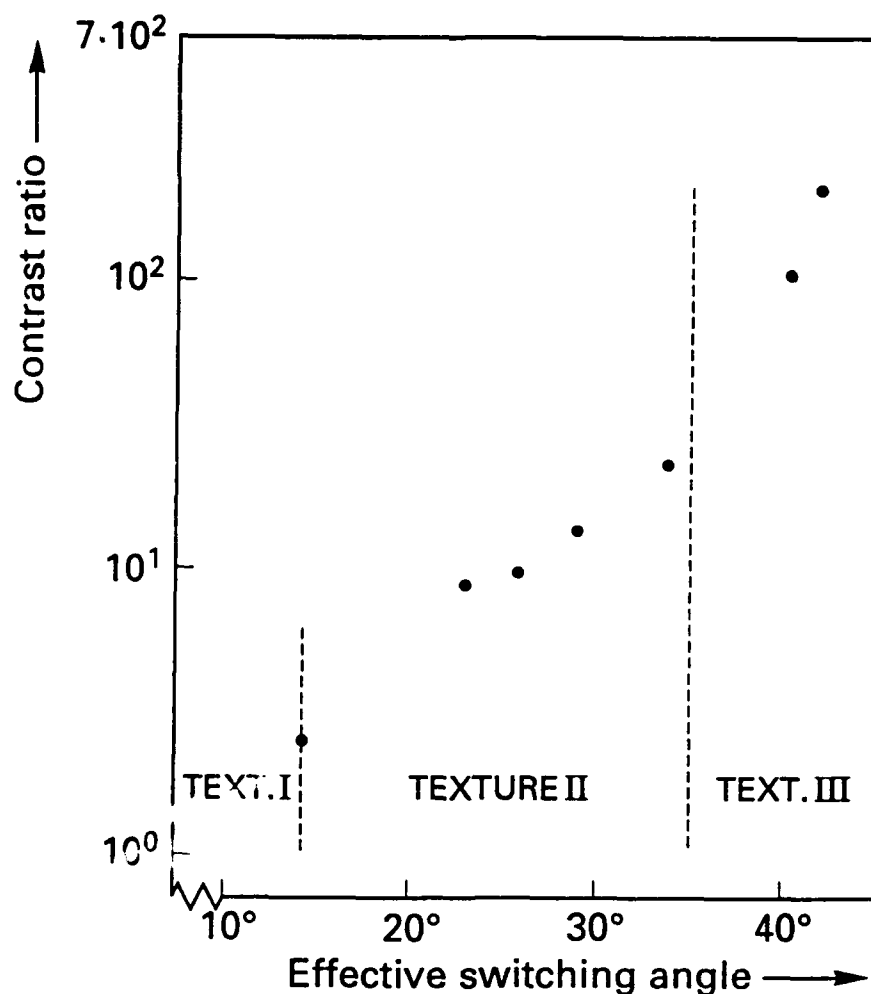


FIGURE 18 Contrast ratio under a 'worst-case' addressing condition (maximum crosstalk) vs. texture.

reaches values like 20, whereas it amounts to 200 in texture III. Therefore, texture III is strongly preferred. A disadvantage of texture III lies in the somewhat higher pulse amplitudes. Microscopically, the gray levels in texture III appear as in Figure 19.

Ferroelectric liquid crystal material

Several FLC mixtures have been tested for this application. Provided that a good orientation is obtained in texture I, most of them exhibit the abovementioned behaviour in the subsequent textures. To carry out the chevron reorientation, the value of the spontaneous polarization should not be too low.^{10,22} A high switching speed is required because the necessary pulse amplitudes increase in the subsequent textures. Table II presents some results on materials from Merck (ZLI), BDH, Hoechst (Felix) and Chisso (CS). The value V_{III} denotes the amplitude of a 25Hz square wave voltage at which the irreversible reorientation to texture III occurs¹⁰ and can therefore be used as an indication of the chevron

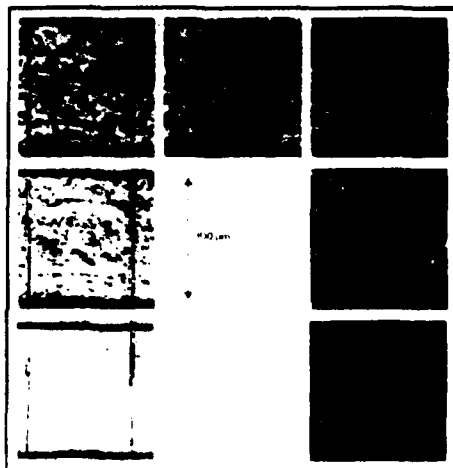


FIGURE 19 Micrographs of the gray levels in texture III

reorientability. In texture III (with an effective switching angle $\geq 35^\circ$) the values V_{THR} and V_{SAT} are obtained using the drive scheme of Figure 16. Those materials, which require the lowest V_{THR} and V_{SAT} (Felix T108 and CS1031), are preferably used. For the application, it is preferred to use C-MOS driver ICs, meaning that the required voltages should not exceed $\pm 20V$. As can be seen, mixture CS1031 can be operated in full-resolution video drive ($32\mu s$ switching-pulse width) with moderate drive voltages. At the moment, high-definition driving ($16\mu s$ pulse width) requires elevated temperatures.

TABLE II FLC mixtures in texture III

Material	P_s	V_{III}	V_{THR}	V_{SAT}
ZLI3654	29	24	25	35
ZLI4237/000	7	42	60	
ZLI4237/050	13	28	27	38
ZLI4237/100	20	23	16	25
Merck90964	38	10	12	18
BDH866	28	12	14	21
Felix T95	43	20	20	30
Felix T103	46	15	10 (17)*	15 (25)*
Felix T108	47	15	9 (17)* (32)**	14 (23)* (39)**
"	at 40°C		(16)**	(21)**
CS1026	26	22	12	17
CS1028	35	22	8 (14)*	12 (19)*
CS1031	29	50	5 (10)* (19)**	9 (16)* (25)**
"	at 30°C		(13)**	(21)**

Data taken with $1.4\mu m$ test samples with 7nm PVA alignment layers at 20°C unless otherwise stated. Switching-pulse width is $64\mu s$, (*) $32\mu s$ or (**) $16\mu s$. P_s in nC/cm^2

Display configuration

The demonstration display is 2.5" diagonal and has 140 rows and 170 columns. The alignment layer is a chemically modified polyvinylalcohol (PVA), which is moisture-resistant. The alignment layer thickness is 7nm; a thin layer is preferred, giving a large series capacitance.³⁸ Several polyimides have been tested as alignment layers but the resulting bistability is not sufficient for video-rate passive-matrix addressing. Both alignment layers are strongly rubbed in parallel directions. Weaker rubbing results in a less good performance.¹⁰ Quartz spacer beads (Shinshikyu-W) are deposited at a high concentration of 150 per pixel (1800mm^{-2}) to increase the texture uniformity. Spacer diameter and thus cell gap is $1.4\mu\text{m}$. This low value was chosen, because a thin cell requires smaller pulses. Consequently, the product $d\Delta n$ is approx. $0.21\mu\text{m}$ for most of the aforementioned materials (Δn at 560nm is mostly around 0.15). This differs considerably from the characteristic value for zero-order birefringence: $0.28\mu\text{m}$ ($\lambda = 560\text{nm}$). However, the colourless appearance and the maximum intensity of the complete spectrum, corrected for the human eye sensitivity, do not change significantly in the $d\Delta n$ range between 0.20 and $0.28\mu\text{m}$.³⁹ As a sealant Norland91 UV-curable glue is used.

The display is filled with the FLC material in the isotropic phase, cooled down to room temperature and sealed. Then the chevron reorientation treatment is performed. First a 1V, 25Hz square-wave voltage is applied for 60 s to shrink the remaining needle-like zigzag defects.¹⁰ This treatment is consecutively repeated with a stepwise-increasing amplitude from 2V to V_{III} to obtain texture III. The display, which possesses just 140 rows, is driven as if it were a half-resolution or part of a full-resolution or high-definition black&white television display with a 50Hz picture-refresh frequency.

Display performance

Figure 20 shows several photographs of the black&white display at half-resolution video driving. Table III shows some characteristics and performance data of the display. Although some less-relevant technological difficulties are still present in the display (malfunctioning external contacts and elongated bubbles), the feasibility of the principle of the "texture-method" to obtain gradation, which makes passive-matrix-addressed FLC displays for video possible, is clearly demonstrated.

The contrast ratio within a pixel is 80, but the overall contrast ratio on the display is only 30, due to the absence of a black matrix on the $10\mu\text{m}$ -wide gaps between the ITO electrodes, where the FLC is partially in the white or the black state. The image is practically viewing angle independent. In fact, Figure 21 depicts the iso-contrast curves of a similar testcell.⁴⁰ As can be seen, the contrast

TABLE III SSFLC video display based on texture-III-method

size	2.5" diagonal	material	Felix T103
lines	140x170	temperature	25°C
pixel size	260x318 μm^2	pre-treatment	1-25V
frequency	50Hz	V_R V_S V_D	17-12-3V
line-time	128 μs (half-res.)	contrast ratio	80 (in-pixel)
alignment	PVA 7nm		30 (overall)
cell thickness	1.4 μm	brightness	75%
black matrix	none	switch speed	< 500 μs



FIGURE 20 The 2.5" passive-matrix-addressed FLC video display.

ratio remains above 50% of its maximum value up to 35° inclination in all quadrants and contrast inversion does not occur. On the display, crosstalk-phenomena or flicker cannot be observed. In full-resolution video driving, the performance of the displays is unaltered, only the required drive voltages increase as indicated in Table II. The reproducibility of the transmission-voltage curve over the display area mostly lies within 40mV, which means that, in principle, 100 gray levels over a 4V range can be reproducibly addressed.

During slowly-moving scenes a faint after-image effect can be noticed, possibly due to the accumulation of ionic impurities³⁸ and the fact that a small hysteresis³³ occurs in the transmission-voltage curves (approximately 300mV). The display can be operated from 10 to 45°C, although the drive voltages have to be re-adjusted then. As is illustrated in Figure 22, the required drive voltages strongly depend on the temperature ($\approx 0.3\text{V}/^\circ\text{C}$), which means that an accurate temperature control is required. When the display has been heated above the smectic C* to smectic A transition temperature, the reorientation treatment has to be redone.

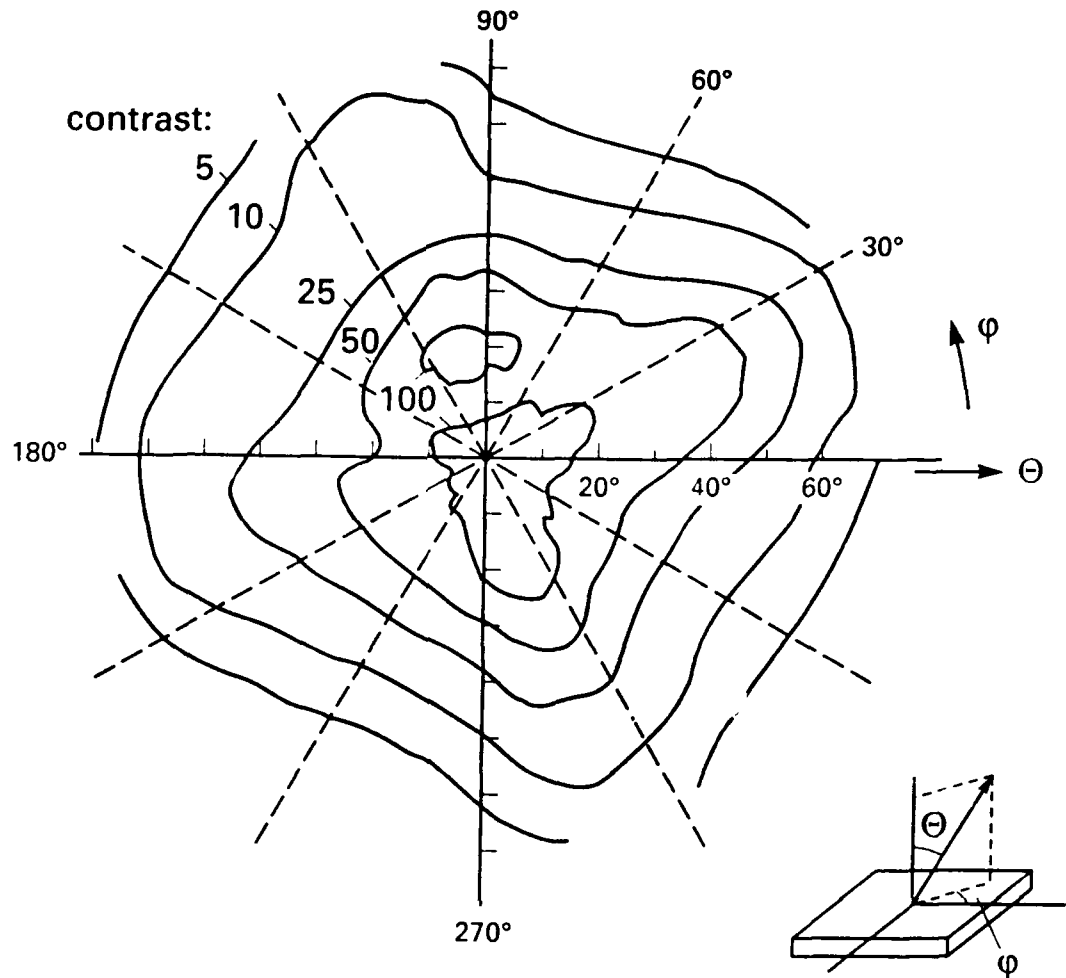


FIGURE 21 Iso-contrast curves between the memory states of an SSFLC testcell in texture III vs. viewing angle.

Evaluation of the "texture-method"

It is demonstrated that analog (continuous) gradation based on the "texture-method" can be used to realize passive-matrix-addressed FLC video displays. Technologically, it is a very simple method to introduce gradation in the bistable SSFLC effect and it possesses some tolerance to cell gap variation,³³ which is a very important technological advantage. The resulting displays possess a wide viewing angle, a high switching speed and the passive-matrix technology yields a high aperture per pixel and opens the possibility of applying an induced black matrix,⁴¹ instead of a mechanical (photolithographic) matrix. The video requirements can be fulfilled.

The remaining problems are:

- avoiding backswitching phenomena due to the high P_S of the FLC material demands that only a very thin alignment layer is used (now 70Å PVA) and that there is no barrier layer;³⁸

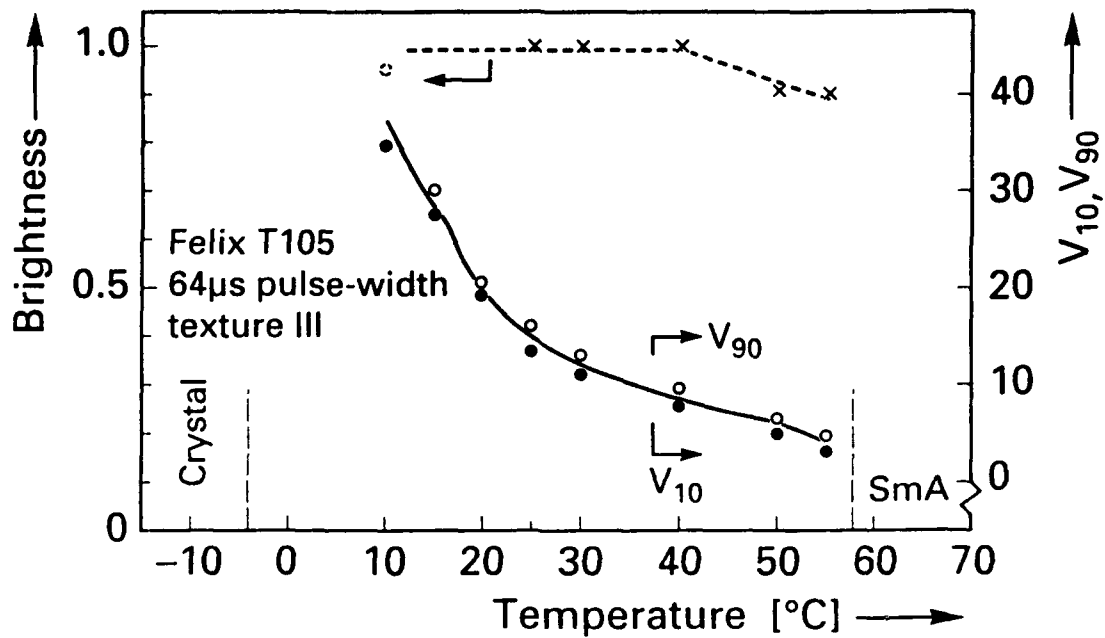


FIGURE 22 Temperature dependences of the required switching pulse amplitudes for 10 and 90% transmission (V_{10} and V_{90}) and the brightness.

- the uniformity of the texture has to be controlled over the display area, independently of alignment nonuniformities;
- the transmission-voltage curve shows a hysteresis, despite the repeated reset. This hysteresis is not fully understood yet and it should be less than the voltage difference between two adjacent gray levels to obtain a well-defined gradation;
- the temperature sensitivity of the threshold and saturation voltages is extremely high and requires a very good control and uniformity of the temperature over the display area.⁴²

CONCLUSION

When considering the application of the SSFLC structure for TV displays, the standard video requirements have to be fulfilled. The speed, the contrast and brightness, and the gradation are very important. To achieve a sufficient brightness (and contrast) when using the bistable memory states, it is necessary to use a pretilt alignment or an electrically-reoriented "quasi-bookshelf" smectic layer structure (texture III). Most eye-catching when proposing the bistable SSFLC effect for TV is the gradation requirement, of which it was shown that more than 100 levels are needed. Several ways to obtain this gradation were discussed.

- Discrete gradation ("dither"), based on space and/or time integration of completely black or white SSFLC pixels. The principle SSFLC cell structure is unaltered, but the driving and addressing methods become more complex. To realize ≥ 100 gray levels, the display complexity increases towards the borderlines of the present LCD technology.

- Analog gradation:

a) charge-controlled multidomain switching provides a well-controlled gradation, but requires the use of an active matrix for addressing;

b) local E-field variation by variable series capacitance or lateral voltage gradients have been suggested, but not yet shown in displays, possibly due to severe technological disadvantages;

c) local FLC switching threshold variation by using the "texture-III-method" is shown to be able (in principle) to meet the video requirements, but needs further optimisation with respect to reproducibility and temperature sensitivity.

Of course, one can imagine different combinations of the aforementioned techniques to get an optimum configuration. The potential of SSFLC TV displays can be derived from its superior optical performance (viewing angle, switching speed) and its simpler technology (passive-matrix). Important present handicaps are the required $\leq 2\mu\text{m}$ cell gap and the temperature sensitivity.

ACKNOWLEDGEMENT

The author wishes to thank his colleagues in the FLC team A.Verhulst, J.v.Haaren, F.Stommels, A.Luyckx-Smolders, F.Lathouwers and other fellow researchers of the Display Principles and Devices group, headed by C.Gerritsma, at the Philips Research Laboratories Eindhoven: E.Kahlman, K.Kuijk, S.Verbakel, H.Feil, E.v.d.Ven, M.Greijmans, W.Brankaert, J.Mulkens and F.Blommaert at the IPO; at the Philips Research Laboratories in Redhill-UK (M.Edwards, J.Chapman, A.Knapp, J.Shannon) and at the Philips Laboratories in Briarcliff USA (H.Sorkin, E.Stupp) for their cooperation. He is also grateful to the various suppliers of FLC mixtures: Merck, Hoechst, BDH and Chisso for their materials and discussions on the subject.

REFERENCES

1. R.Meyer, L.Liébert, L.Strzelecki and P.Keller, J.de Phys.Lett. 36, L69(1975).
2. N.Clark, S.Lagerwall, Appl.Phys.Lett. 36, 899(1980).
3. K.Yoshino, M.Ozaki, Jap.J.Appl.Phys. 2, L385(1984).
4. L.Beresnev, V.Charginov, E.Pozhidayev, D.Dergachev, M.Schadt, J.Fünfschilling, Liquid Crystals 5, 1171 (1989).
5. J.Fünfschilling, M.Schadt, SID 90 Digest p.106 (1990).
6. S.Garoff and R.Meyer, Phys.Rev.Lett. 38, 848 (1977).
7. H.Inoue, A.Mizutome, S.Yoshihara, J.Kanbe, S.Iijima, presented at Int. Display Res. Conf. 1988 San Diego, USA.
8. Y.Iwai, N.Wakita, T.Uemura, S.Fujiwara, Y.Gohara, S.Kimura, Y.Masumoto, Y.Miyatake, T.Tsuda, Y.Horio, I.Ota, Japan Display 89, Osaka, 180 (1989).
9. S.Matsumoto, A.Muruyama, H.Hatoh, Y.Kinoshita, H.Hirai, M.Ishikawa, S.Kamagami, Proc.SID 29, 255(1988).
10. W.Hartmann, A.Luyckx-Smolders, J.Appl.Phys. 67, 1253(1990).
11. Y.Sato, T.Tanaka, H.Kobayashi, K.Aoki, H.Watanabe, H.Takeshita, Y.Ouchi, H.Takezoe, A.Fukuda, Jap.J.Appl.Phys. 28, L483 (1989).
12. H.Rieger, C.Escher, G.Illian, H.Jahn, A.Kaltbeitzel, D.Ohlendorf, N.Rosch, T.Harada, A.Weippert, E.Lüder, SID 91 Digest 396 (1991).
13. T.Uemura, N.Ohba, N.Wakita, H.Ohnishi, I.Ota, Proc. of the SID 28(2), 175 (1987).
14. Simulation performed at the Institute for Perceptive Research (IPO) in Eindhoven by F.Blommaert.
15. S.Lagerwall, N.Clark, J.Dijon, J.Clerc, Ferroelectrics 94, 3(1989).
16. T.Leroux, F.Baume, J.F.Clerc, J.Dijon, C.Ebel, M.Estor, L.Mulatier, C.Vauchier, Int. Display Res. Conf. San Diego, USA. 111(1988).
17. P.Surguy, L.Banks, A.Carrington, L.Chan, M.Naylor, N.Riby, Eurodisplay 90 Amsterdam 146 (1990).
18. W.Hartmann, J.van Haaren, A.Verhulst, European Patent Application nr.9000942.
19. P.Maltese, J.Dijon, T.Leroux, D.Sarrasin, Ferroelectrics 85, 265(1988).
20. W.Hartmann, J.Appl.Phys. 66, 1132(1989).
21. W.Hartmann, IDRC 88 San Diego 191 (1988) and IEEE Trans.El.Dev. 36, 1895(1989).
22. W.Hartmann, Ferroelectrics 85, 67(1988).
23. e.g. H.Maeda, C.Gomes, M.Yoshida, B.Zhang, M.Kimura, H.Sekine, S.Kobayashi, Japan Display 89 344 (1989).
24. S.Yamamoto, T.Ebihara, N.Kato, H.Hoshi, Ferroelectrics 114, 81 (1991).
25. C.Mao, K.Johnson, G.Moddel, Ferroelectrics 114, 45 (1991).
26. M.Handschy, M.O'Callaghan, T.Drabik, SID 91 Digest 246 (1991).
27. M.Bone, D.Haven, D.Slobodin, SID 91 Digest 254 (1991).
28. D.Armitage, SPIE Vol.1257 Liquid Crystal Displays and Applications 116 (1990).
29. Y.Iwai, N.Wakita, T.Uemura, I.Ota, 13th LC meeting oct. 1987 Kyushu, Japan 138 (1987).
30. U.S.Patent no 4712877 (Canon).
31. Japan patent no 62-71929 (A) (Seiko Epson).
32. U.S.Patent no 4802744 (Canon).
33. A.Verhulst, W.Hartmann, F.Stommels, A.Luyckx-Smolders, Eurodisplay 90, Amsterdam, 150 (1990).

34. W.Hartmann, A.Verhulst, A.Luyckx-Smolders, F.Stommels, Proc. of the SID 32/2 (1991).
35. H.Dübal, C.Escher, D.Ohlendorf, proc. 6th Int.Symp. Electrets, Oxford, England, 344, sept.(1988).
36. W.Hartmann, K.Kuijk, published European Patent Application nr.322022.
37. J.Geary, SID 85 Digest 128 (1985) and J.LePesant, J.Perbet, B.Mourey, M.Hareng, G.Decobert, J.Dubois, Mol.Cryst.Liq.Cryst. 129, 61(1985).
38. Y.Inaba, K.Katagiri, H.Inoue, J.Kanbe, S.Yoshihara, S.Iijima, Ferroelectrics 85, 255(1988).
39. Calculated using dispersion data of ZLI3654 from Merck (Darmstadt) and computer programs made by F.R. Hoekstra.
40. Measured by J.C.H. Mulken.
41. N.Wakita, Y.Iwai, T.Uemura, S.Fujiwara, Y.Gohara, I. Ota, Y.Masumoto, Y.Miyatake, T.Tsuda, Y.Horio, Ferroelectrics 114, 27 (1991).
42. K.Reinhart, L.Dorfmueller, K.Marx, T.Matuszczyk, Ferroelectrics 113, 405 (1991).

LARGE AREA FERROELECTRIC LIQUID CRYSTAL DISPLAYS

S K Heeks, A Mosley, B M Nicholas, P C Rundle, P Schlusche,
GEC-Marconi Limited, Hirst Research Centre, East Lane,
Wembley, HA9 7PP

INTRODUCTION

Ferroelectric liquid crystals (FLCs) combine the established advantages of conventional liquid crystals with the additional advantages of fast switching speeds and bistable operation. This combination of properties offers the potential for producing highly multiplexed flat panel displays which have a wide angle of view, a high contrast, and are capable of showing a high information content at video rate. In addition, the fabrication of ferroelectric liquid crystal devices (FLCDs) is relatively straightforward, especially when compared with that employed for active matrix LCD technology, thus making FLCDs particularly well suited for use in large area displays operating at video frame rates.

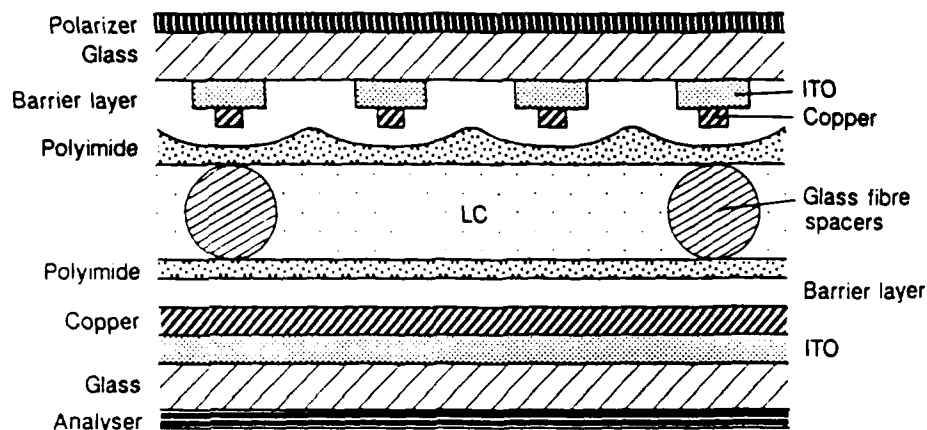
The potential of FLCs for application in passive matrix-addressed liquid crystal displays was first demonstrated by Clark and Lagerwall¹. Although this seminal work resulted in a great deal of research interest, it suffered from drawbacks in terms of device fabrication, particularly the need to shear the liquid crystal film in order to achieve the requisite planar alignment of the FLC. Relatively few large panel FLCDs have been demonstrated, and only Canon² have been able to demonstrate a 14" black and white display. The early FLCDs, for example the one described by Matsumoto et al.³, tended to incorporate ferroelectric materials with a high spontaneous polarisation (P_S) which were addressed using four slot addressing schemes. These devices suffered from vertical cross-talk which degraded the image quality.

In the present work, we report the fabrication of two large area flat panel monochrome ferroelectric displays. The two devices, a 160x125 mm² (A5 size), 400x320 pixel and a 288x192 mm² (A4 size), 640x400 pixel dot matrix display, incorporate state-of-the-art, low P_S , ferroelectric materials which have been developed by E Merck (Darmstadt) and are driven by novel drive schemes developed at GEC^{4,5}.

DEVICE CONSTRUCTION AND FABRICATION

A schematic cross-section through the FLCD is shown in Figure 1. Both the A4 and A5 displays are identical except for the absence of the copper metallisation line (used to lower the electrode track resistance) in the A5 display. The glass is sodalime, which is coated by Applied Films (USA) with 1500Å of ITO, providing ~70 ohms/square and a copper layer (2000Å) on top of this providing 250 milliohms/square. The two glass substrates which form the cell are held 1.7 µm

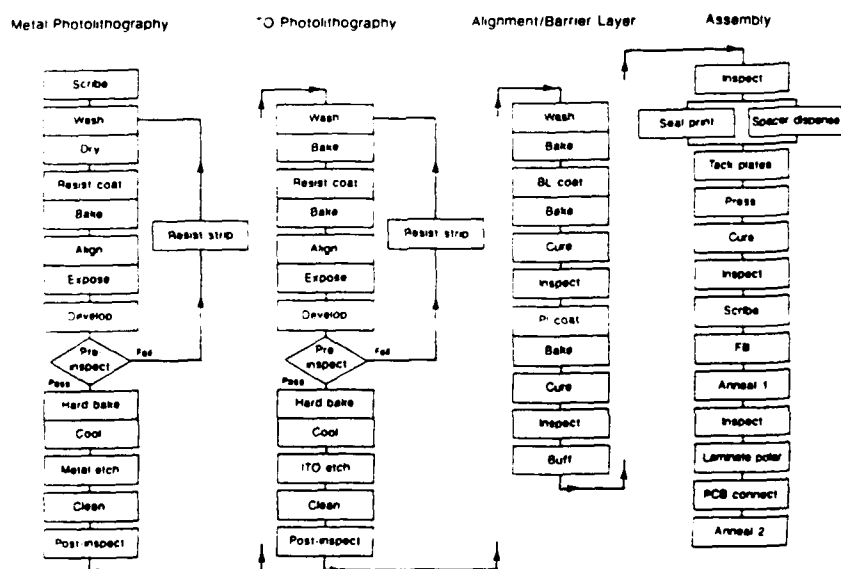
Figure 1



apart; this spacing is controlled by glass fibre spacers.

The processing involved in the fabrication of the A4 display is given in Figure 2 and broadly consists of a metal photolithography stage, an ITO photolithography stage, barrier and alignment layer deposition and assembly.

Figure 2. A4 Ferroelectric 640 x 400 Dot Matrix Fabrication Process



The metal photolithography provides a metal line of $40\text{ }\mu\text{m}$ width (pitch $400\text{ }\mu\text{m}$). These copper lines are centred on $350\text{ }\mu\text{m}$ wide ($400\text{ }\mu\text{m}$ pitch) ITO tracks. The barrier layer is based on a spun down glass material (Merck Liquicoat Si ZLI 2132) which is cured at high temperature and whose purpose is to prevent electrical shorts between top and bottom electrodes. The alignment, which shows few zigzags, and no visible macroscopic defects, is provided by a parallel-rubbed polyimide layer (Ciba Geigy Probimide 32). The assembly stage consists of randomly scattering

7 μm , glass fibre spacers on one substrate, screen-printing its corresponding partner with a thermo-setting adhesive (Mitsui XN5AC-F), hot pressing together and finally curing. The vacuum filling of the assembled cell is achieved through multiple ports along one leading edge of the cell and with the liquid crystal in the isotropic phase. Polariser are then laminated onto the surfaces of the display cell in the appropriate orientations. Finally the display cell is bonded to the drive electronics via flexible connectors.

ELECTRONICS AND DRIVING SCHEME

The contrast ratios and frame times of FLC displays are critically dependent on the addressing waveforms. Therefore, the development and cost effective implementation of these waveforms will have a great influence on the commercial exploitation of FLCs. The first published waveform, which was developed by Seiko⁶, consists of bipolar strobe pulses of amplitude V_s that are inverted every half frame, as shown in Figure 3. The data consists of a DC balanced bipolar pulse of amplitude V_d . In this scheme, because a latched state is only produced by the trailing pulses, four time slots are necessary to define the desired on and off states, consequently, the Seiko scheme is referred to as a four-slot addressing scheme. A disadvantage of this type of scheme is the long frame time,

$$\text{frame time} = \text{pulse width } (t_s) \times \text{number of slots} \times \text{number of rows.}$$

It is therefore desirable to use a two-slot addressing scheme which will reduce the frame time by half.

The original GEC two-slot addressing scheme was published in 1987⁴; however, the devices reported here employ a later and improved version of the GEC scheme⁵. In this scheme the strobe waveform takes the form of a positive pulse of amplitude V_s and duration t_s ; this is followed by a negative pulse of equal amplitude with duration t_t where $0 < t_t/t_s < 1$ (see Figure 4). There is an inversion of the strobe polarity every frame to eliminate any net DC potential across the display elements. The data waveform are of two bipolar pulses which combine with the strobe waveform to give either a normal or an inverted contrast mode. The leading pulse of the strobe waveform blanks the pixel and the trailing pulse either switches the pixel into the other state or leaves it unchanged depending on the polarity of the data pulse experienced by the pixel. Clearly, only two-slots are required to switch a pixel into its desired state and it is thus a two-slot scheme. These driving schemes are explained in more detail by T H Yeoh et al⁷.

A further reduction in the frame time, again by a half, is possible by splitting the display in half along the column electrodes and then driving the resulting two sets of row electrodes in parallel. The A4 display reported here is driven as two separate 640x200 displays.

The row (strobe) electrodes are connected and driven at both ends using high voltage drivers (Supertex HV6008). Data drive is provided by the upper and lower column drive boards. Each uses a separate 4-bit data interface which is indirectly

coupled to the 8-bit microprocessor data bus. The column drivers (Hitachi HD61104) are organised as shift and store registers, i.e. data for one line may be assembled whilst the previous line is displayed. Signal buffers are provided on board because of the relatively large number of drivers used.

Figure 3. Seiko Scheme

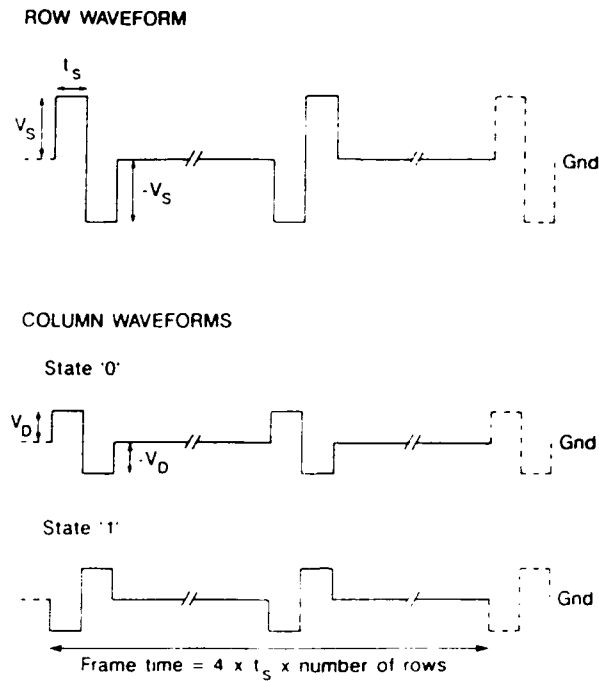
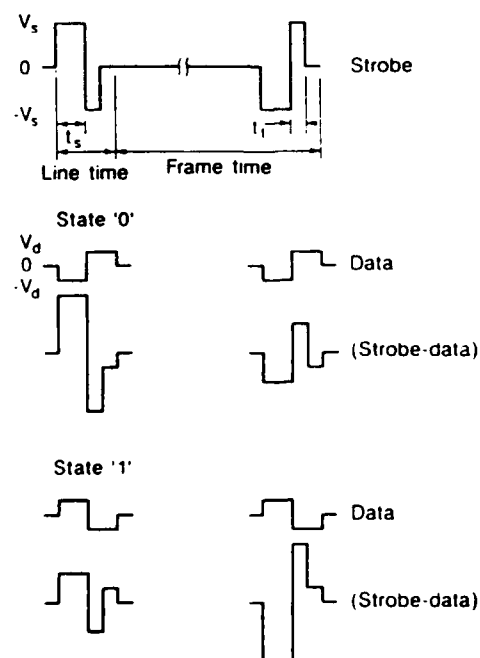


Figure 4. GEC Bipolar Addressing Scheme



RESULTS

The specifications for the A5 and A4 displays are given in the following table:

TABLE 1: Display specifications

	A5	A4
Columns x rows	400 x 320	640 x 400
Pitch	350 μm	400 μm
Interpixel gap	35 μm	40 μm
Glass area	160x125 mm ²	288x192 mm ²
Active areas	140x112 mm ²	256x160 mm ²
Duty ratio	1:320	1:200
Cell spacing	1.7 μm	1.7 μm
Alignment	polyimide	polyimide
Liquid crystals	Merck ZLI 4655-000	Merck ZLI 4655-000 and ZLI 4655-034

An A5 display is shown in Plate 1; this display is filled with Merck ZLI 4655-000 and has a uniform appearance over the entire active area. The contrast ratio of these displays varies with drive conditions but is typically $\sim 10:1$. Plate 2 shows an A4 display filled with the Merck material ZLI 4655-000. The appearance of this display is fairly uniform over the active area and has a contrast ratio of only 5:1. The latter, relatively low value of contrast ratio, leads to the conclusion that the optical performance of a ferroelectric LCD is more dependent on the area of the display than its multiplexing level. This is not surprising, since the bistable nature of ferroelectric LCDs infers that the optical performance will be independent of the multiplexing level. However, it is clear that the optimum values of the amplitudes of the data and strobe waveforms are very sensitive to the inherent variations in the cell-structure that occur across displays, especially large area displays. This high sensitivity leads to the use of voltage levels that are a compromise between the various optimum values that occur across the display, which in turn leads to a reduction in the contrast ratio of the display.

LIQUID CRYSTAL MATERIALS

Simulated multiplexing (using an arbitrary waveform generator) of single pixels of small test cells, revealed that ZLI 4655-000 was too slow to achieve video rate addressing in the A4 display when practical voltage levels were used. The minimum line time (slot time x number of slots) was found to be over 100 μs (well above the

64 μs line time required for video rate operation). Therefore mixtures of the lower P_S material, ZLI 4655-000, with the higher P_S version of this material, ZLI 4655-100, were evaluated in terms of display performance, i.e. response time, operating range and contrast ratio. These materials have the following phase sequences:

ZLI 4655-000

K < -10 S_C^* 60 S_A 69 Ch 72 I,

ZLI 4655-100

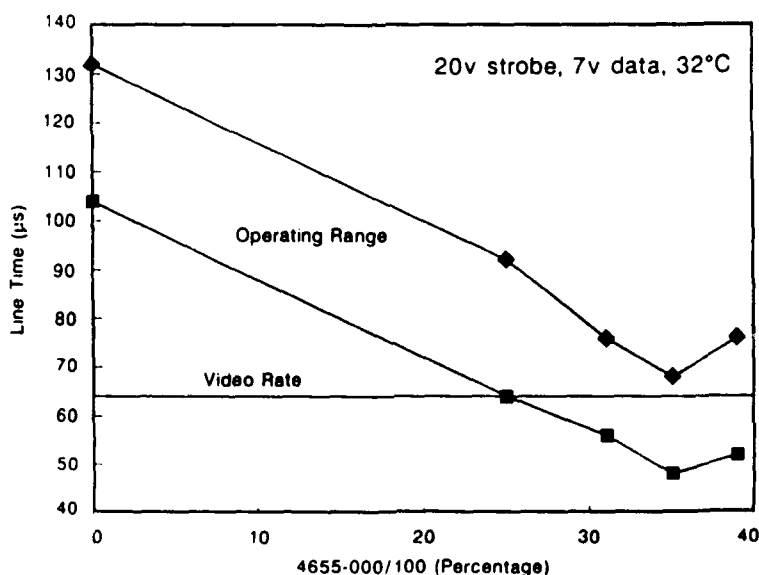
K < -10 S_C^* 61 S_A 72 Ch 76 I,

and the following properties:

	P_S (nC cm ⁻²)	Tilt angle (°)	Pitch in Ch (μm)	Pitch in S_C^* (μm)
ZLI 4655-000	+7	23.0	> +40	-
ZLI 4655-100	+22.6	25	+28	14
Temperature °C	+20	+20	+72	+20

The test cells were housed in a hot stage and all measurements were performed at $31.6 \pm 0.1^\circ\text{C}$. (This temperature was close to the typical operating temperature of large area displays placed on a light box). The contrast ratio was measured on a single pixel using a photodiode mounted on a Nikon polarising microscope. Figure 5 gives the results of one such experiment using $\pm 20\text{V}$ strobe and $\pm 7\text{V}$ data, which are practical voltage levels obtainable using Supertex HV 6008 and Hitachi HD

Figure 5. ZLI 4655 Mixtures



61104 drivers. The upper curve in this figure represents the maximum line time and the lower curve the minimum line time; areas outside the operating range produced contrast ratio of $<5:1$. It can be seen from this figure that the material which provides the optimum display performance at these voltage levels is the mixture ZLI 4655-034 (i.e. 66 parts ZLI 4655-000 and 34 parts ZLI 4655-100), which is easily capable of video rate operation.

We have subsequently made an A4 display incorporating the mixture ZLI 4655-034 (see Plate 3). This display is at present being assessed, but preliminary studies on test cells suggest that contrast ratios of about 20:1 are achievable with line times well within those required for video rate operation.

CONCLUSION

These results demonstrate that it is feasible to fabricate good quality large area, highly multiplexed dot matrix FLCs using low P_s ferroelectric materials, polyimide surface alignment layers and two slot addressing schemes. These devices give a good quality image and their ease of fabrication with relatively high yields (60% yield overall for A5 batch) demonstrate that this is a viable flat panel technology which offers advantages over the active matrix LCD technology for large area displays. Nevertheless, further improvements in the cell technology and fabrication of large area displays are required before the commercial exploitation of this technology will be realised.

ACKNOWLEDGEMENTS

The A5 and A4 displays are intermediate deliverables from the three and a half year FELICITA (ESPRIT 2360) collaborative project supported by the European Economic Community as part of the ESPRIT initiative. The aim of the project is to develop FLC technology to the point where the devices can be produced competitively within Europe.

The authors would like to acknowledge the contribution made to this work by other members of staff at the Hirst Research Centre involved in the FLC program and also our European colleagues in the ESPRIT FELICITA project, particularly E Merck (Darmstadt) for the supply of the ferroelectric liquid crystal materials. Helpful discussions with M Lewis (EEV Ltd.) are also gratefully acknowledged.

REFERENCES

1. N A Clark and S T Lagerwall, Appl. Phys. Lett. **36**, (11), 899 (1980)
2. J Kanbe, H Inoue, A Mizutome, Y Hanyuu, K Katagiri and S Yoshihara, Ferroelectrics **114**, 3 (1991)
3. S Matsumoto, A Murayama, H Hatoh, Y Kinoshita, H Hitai, M Ishikawa and S Kamagata, SID 88. DIGEST 41

4. C Bowry, A Mosley and B M Nicholas, EURODISPLAY Proceedings, 152 (1987)
5. T H Yeoh, A Mosley, M Charsley and P C Rundle, The British Liquid Crystal Society Annual Conference
6. T Harade, M Taguchi, K Iwaga and M Kai, SID 85, DIGEST 131
7. T H Yeoh, S J S Lister, A Mosley and B M Nicholas, presented at "Third International Conference on Ferroelectric Liquid Crystals", Boulder, Colorado, (1991)

Plate 1**Plate 2****Plate 3**

A HIGH CONTRAST AND HIGH TRANSMITTANCE MULTIPLEXING SSFLC DISPLAY UTILIZING NAPHTHALENE BASE LIQUID CRYSTAL MATERIALS

AKIHIRO MOCHIZUKI, KATSUSADA MOTOYOSHI and MASAKATSU
NAKATSUKA*

Fujitsu Laboratories Ltd., Atsugi, Japan

* Mitsui Toatsu Chemicals, Inc. Yokohama, Japan

Abstract

Both bookshelf and quasi-bookshelf layer structures are obtained by using naphthalene base liquid crystal mixture with a rubbed polymer orientation films panel. This panel shows a high contrast ratio reaching at 35:1 and high transmittance of 40% driven by multiplexing method.

INTRODUCTION

A surface stabilized ferroelectric liquid crystal (SSFLC) display has a great potentiality to realize a high performance information display with high information content, high contrast ratio, wide viewing angle, and fast response time.¹ Although these attractive characteristics of the SSFLC display, a practical SSFLC display is still not available. Several problems are still left to realize a practical SSFLC display. Among the problems which should be solved, a uniform liquid crystal molecular alignment is thought to be the most important to obtain a high quality screen image represented by high contrast ratio, high transmittance and wide viewing angle. In spite of much effort to obtain the uniform molecular alignment such as oblique evaporation,^{2,3} a really practical alignment method is still in the development phase.

It is well known that the phase sequence of ferroelectric liquid crystals governs the molecular alignment of the SSFLC display. Particularly for a rubbed polymer orientation films which is assumed to be the most practical for mass production, an FLC material with a phase sequence isotropic (I) - chiralnematic (N^*) - smectic A (S_A) - chiral smectic C (S_C^*), which is the most common, is generally believed to provide a clean molecular alignment. We have proposed, however, an FLC material with a phase sequence I - S_A - S_C^* and with a wide temperature range of the S_A phase can provide a better molecular alignment.⁴ This kind of material may be useful in particular case for realizing the bookshelf layer structure.

In this paper, we describe the uniform molecular alignment with rubbed polymer films panel using a particular FLC material containing a naphthalene ring in its molecular structure with a phase sequence I - S_A - S_C^* and showing a wide temperature range of S_A phase. Also we discuss the dynamic electrooptical properties of the uniformly oriented FLC panel. The results show that the uniform molecular alignment of the SSFLC display provides a high contrast ratio reaching at 35:1 and a high transmittance of 40% including two polarizers.

EXPERIMENTAL

To investigate the influence of the phase sequence on the liquid crystal molecular alignment, two types of FLC materials were used. One is Merck mixture ZLI-4139 which has the phase sequence I - N^* - S_C^* . The other is a naphthalene ring contained liquid crystal as shown in Fig. 1. This liquid crystal has the phase sequence I - N^* - S_A - S_C^* . These two FLC materials were

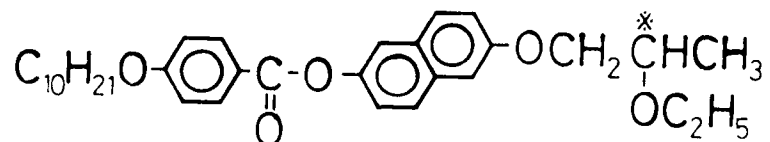


Fig. 1 The molecular structure of the naphthalene ring contained FLC. This material has the phase sequence I - N^* - S_A - S_C^* .

mixed with different ratio. The detail of these mixtures is as same as the previous papers.^{4,5}

The smectic layer structure of the SSFLC panels were investigated by X-ray diffraction measurements. The X-ray measurements were fulfilled by cooperation with Professor Fukuda's group at Tokyo Institute of Technology. To clarify the characteristic electrooptical properties of the SSFLC panel, we measured the memory stability as defined in Fig. 2. The electrooptical properties with the multiplexing drive voltage application were also investigated. We measured the electrooptical threshold properties by applying the 4-slot multiplexing method (shown in Fig. 3).⁶

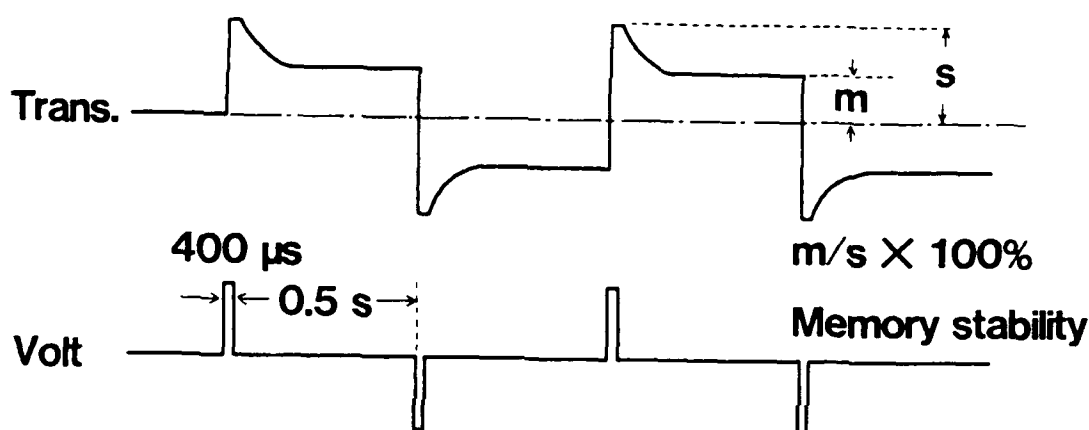


Fig. 2 The definition of the memory stability.

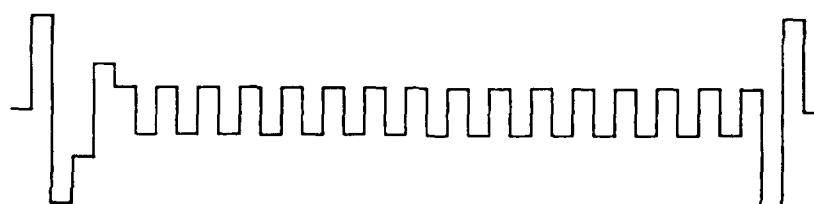


Fig. 3 The 4-slot multiplexing drive method.

RESULTS AND DISCUSSION

Molecular Alignment

We reported the relationship between the molecular alignment and the temperature range ratio of N^* and SA phases obtained by rubbed polyvinyl alcohol films panels.⁴ The phase transition temperature of each FLC mixture (ZLI-4139 and the naphthalene liquid crystal) is shown in Fig. 4. The relationship between the appearance of zigzag defects and the temperature

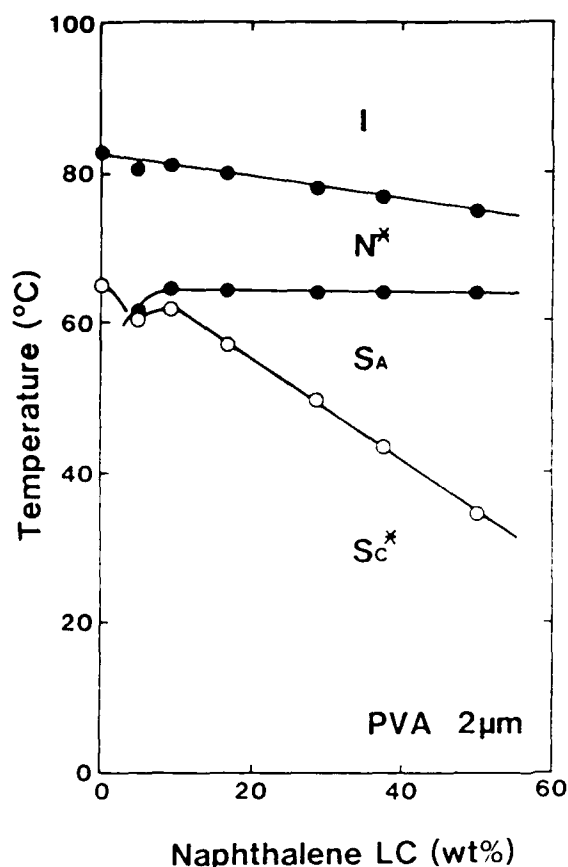


Fig. 4 The phase transition temperature of the FLC mixture. The FLC mixture consists of ZLI-4139 (Merck) and the naphthalene ring contained material as shown in Fig. 1.

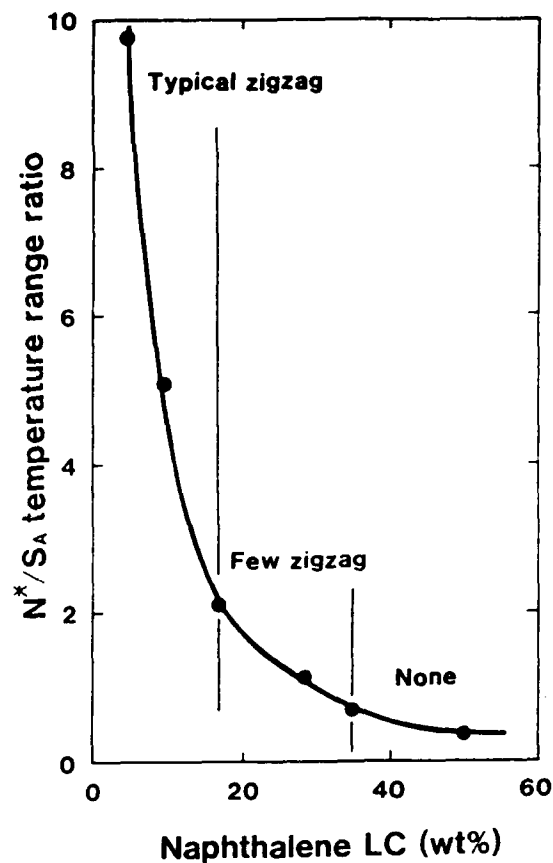


Fig. 5 The relationship between the appearance of zigzag defects and the temperature range ratio of N* and S_A phases.

range ratio of N* and S_A phases is shown in Fig. 5. Figure 5 indicates that a liquid crystal material with a wide temperature range of S_A phase provides a zigzag defect free molecular alignment. Figure 6 shows the molecular alignment of the FLC mixture which contains 40 wt% of the naphthalene material.

It is generally believed that for a rubbed polymer films panel, a chiralnematic phase is necessary to obtain a clean molecular alignment. In the chiralnematic phase, a parallel molecular alignment can be obtained. The parallel molecular alignment may lead to the formation of smectic layers. However, we have observed that several types of FLC materials such as the naphthalene ring contained FLCs which have the phase sequence I - S_A - S_C* and show a wide



Fig. 6 The molecular alignment of the naphthalene contained FLC mixture.

temperature range of S_A phase, provide a clean molecular alignment. Moreover these materials can realize the bookshelf or quasi-bookshelf smectic layer structures. In contrast, it is almost impossible to obtain the bookshelf layer structure using FLC materials with the phase sequence $I - N^* - S_A - S_C^*$ without an external treatment such as high frequency electric field applications. ⁷

We assume that the influence of the phase sequence on the smectic layer structure is based on the surface anchoring caused by rubbing treatment. It is assumed that some liquid crystal molecules are anchored on the rubbed polymer surface even in the isotropic phase as shown in Fig. 7. When the most common FLC material which has the phase sequence $I - N^* - S_A - S_C^*$ is filled in the rubbed polymer films panel, a layer structure misfit tends to happen in the cooling process from N^* to S_A phase. This layer structure misfit may produce a disordered S_A layer structure as shown in Fig. 8 (a). The FLC material which has the phase sequence $I - S_A - S_C^*$ and has a wide temperature range of S_A phase is filled in the rubbed polymer films panel, even though a layer structure misfit happens, the wide temperature range of S_A phase may relax the layer misfit, resulting in an ordered smectic layer structure as shown in Fig. 8 (b).

During the cooling process into the S_C^* phase the liquid crystal molecules tilt within the layers and the projected molecular length into the layer normal reduces. This transition induces a large amplitude of density function distribution. Due to the compensation of the density function distribution the smectic layers bend and form the so called chevron structure.^{8,9} Particularly when the smectic layer structure is disordered as shown in Fig. 8 (a), this density function distribution is so large that the smectic layer tends to turn to the chevron structure. In case the smectic layer structure is ordered as shown in Fig. 8 (b), the amplitude of density function distribution is relatively small, thus the bookshelf layer structure formed in the S_A phase has a possibility to be preserved in the S_C^* phase. Recently several papers report that the formation of quasi-bookshelf layer structure using rubbed polymer films panels.^{10,11} It is assumed that there are some reasons for the formation of the quasi-bookshelf layer structure, in some cases, however, the above mentioned reason may be applicable.

The Formation of the Layer Structure

Using the naphthalene ring contained FLC material which has a wide temperature range of S_A phase, we have obtained both the bookshelf and the quasi-bookshelf layer structure.⁵ The investigation of the relationship between the layer structure and the contents of the naphthalene ring contained FLC revealed some interesting results. One is the temperature dependence of the layer tilt angle, the other is anomalous enthalpy change in the $S_A - S_C^*$ phase transition.

Takanishi et al. showed the temperature dependence of the layer tilt angle of the naphthalene ring contained FLC (ZLI-4139 : 60 wt %, naphthalene LC : 40 wt%) which has the bookshelf layer structure (Fig. 9).¹² The $S_A - S_C^*$ phase transition temperature of this FLC material is 39.5°C. Figure 9 indicates that this material shows the bookshelf structure in the cooling process from S_A to S_C^* phases, however, it shows the slightly tilted chevron structure in the heating process. This thermal hysteresis is attributable to the disordered layer structure in the S_A phase. The residual layer misfit in the S_C^* phase is

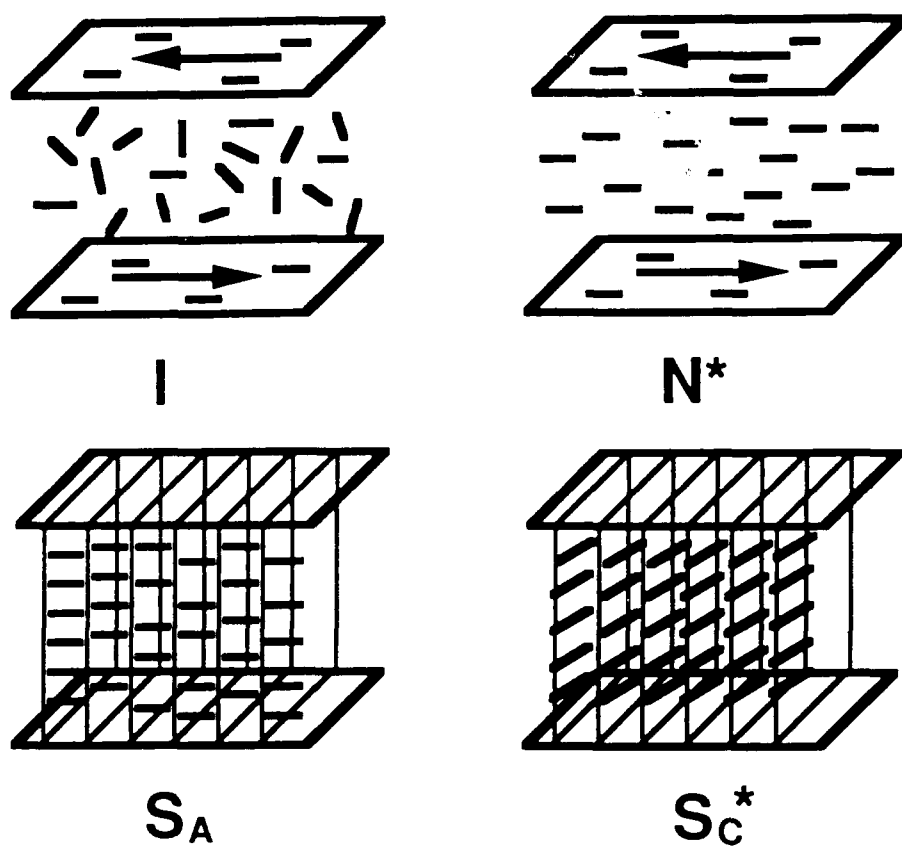


Fig. 7 The surface anchoring liquid crystals in the isotropic phase.

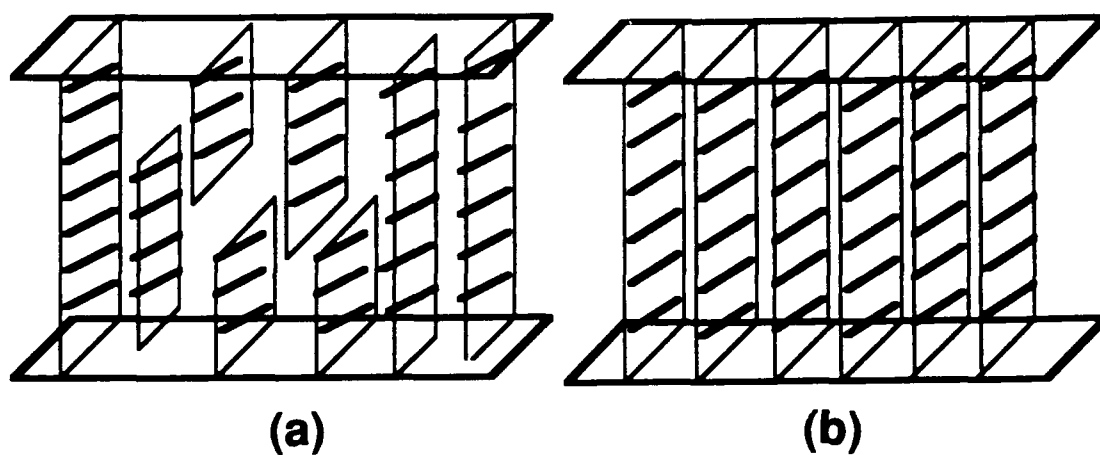


Fig. 8 The formation of the smectic layer structure in the SA phase.
(a) Disordered S_A layer structure, (b) Ordered S_A layer structure.

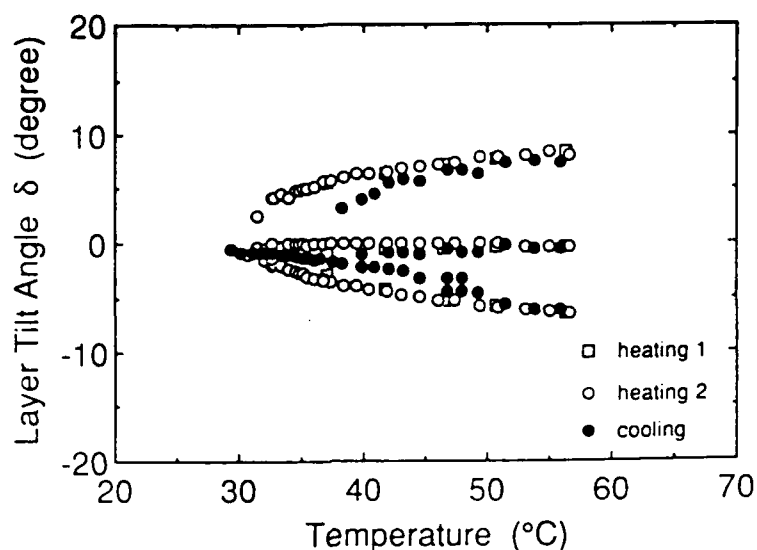


Fig. 9 The temperature dependence of the layer tilt angle of the naphthalene ring contained FLC material. This material is the mixture of ZLI-4139 (Merck) and the naphthalene material (Fig. 1).¹²

assumed to provoke the layer tilt in the heating process. In the cooling process, however, the liquid crystal molecules tilt in each layer, resulting in the bookshelf layer structure. The DSC measurement of the FLC mixtures (mixtures of ZLI-4139 and the naphthalene material shown in Fig. 1) indicate when the content of the naphthalene FLC is about 40 wt%, the enthalpy change, ΔH , becomes anomalously large in the heating process as shown in Fig. 10.⁴ Although this result is concerning with bulk FLC material, the anomalously large ΔH suggests that there is a structural phase transition between S_C^* and S_A phases in the FLC mixture.

Figure 11 is the temperature dependence of the layer tilt angle of the naphthalene base FLC mixture.⁵ The main component of this mixture is shown in Fig. 12. This mixture contains 75 wt% of the naphthalene ring contained FLC materials. The phase sequence of this mixture is I (79.3°C) - S_A (56.8°C) - S_C^* (<-5°C)K. As shown in Fig. 11, the layer tilt angle increases near the S_A to S_C^* transition temperature, then decreases with decreasing temperature. This temperature dependence of the layer tilt angle is not coincident with the temperature dependence of the molecular tilt angle which decreases monotonically with increasing temperature as same as usual FLC materials.

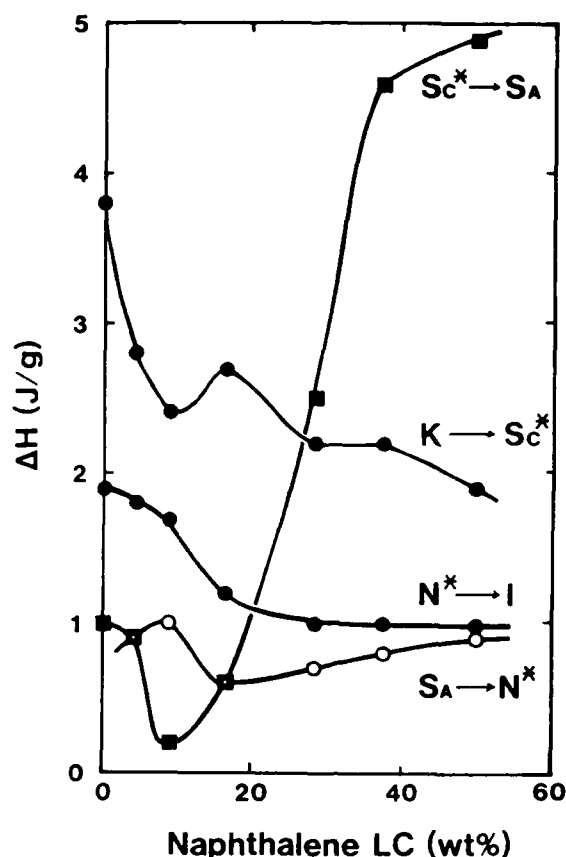


Fig. 10 The enthalpy changes of the naphthalene ring contained FLC.

The lack of coincidence is expected when the smectic layer thickness change is not caused only by the molecular tilt from the layer normal.⁵

Moreover this FLC mixture shows no thermal hysteresis unlike the material appeared in Fig. 9. Both the small layer tilt and no thermal hysteresis are assumed to be attributable to the stable smectic layer structure which may be constructed through the wide temperature range of the S_A phase.

The mechanism of realizing the bookshelf or the quasi-bookshelf layer structure by using the naphthalene base FLC mixture is now under investigation. Takanishi et al. reported that the temperature dependence of the interlayer spacing of the naphthalene base material is quite small or constant depending on the naphthalene FLC component.¹² The constant interlayer spacing of the naphthalene base material is thought to maintain the bookshelf layer structure in the SC^* phase. The constant interlayer spacing may be provided by the constant effective molecular length projected into the layer

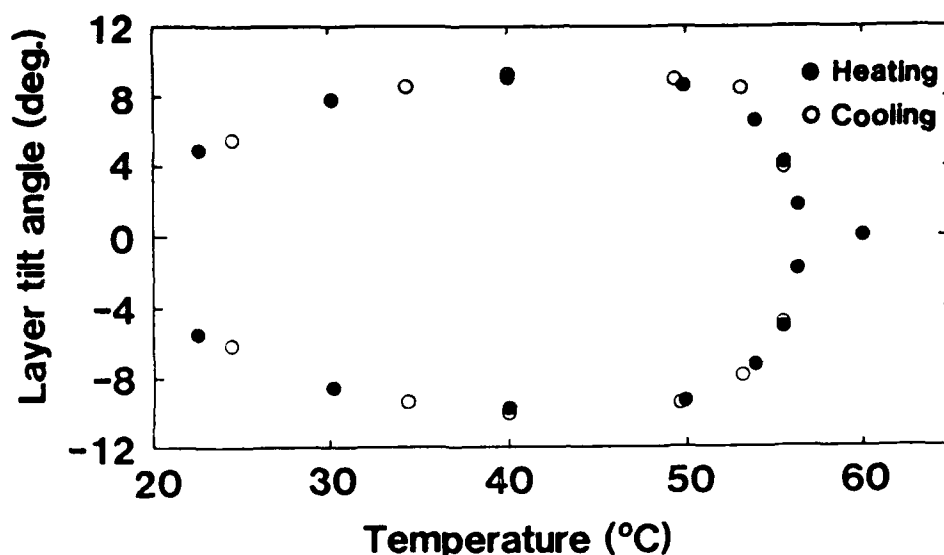


Fig. 11 The temperature dependence of the layer tilt angle of the naphthalene base FLC mixture. This mixture contains 75 wt% of the naphthalene ring contained FLC materials.

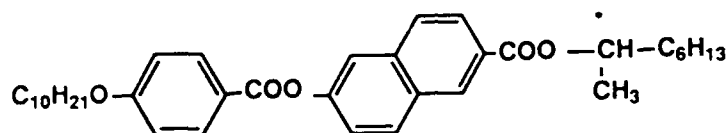


Fig. 12 The molecular structure of the naphthalene ring contained FLC. This material has the phase sequence $I - S_A - S_C^*$.

normal. To keep the molecular length constant, two liquid crystal molecules configurations indicated in Fig. 13 are possible. One is the molecular dimerization (Fig. 13 (a)). The other is the molecular stretch (Fig. 13 (b)). We need the detail investigations to clarify which molecular movement is real.

Electrooptical Performances

Memory Capability

To fabricate the practical SSFLC display, we used the naphthalene base material whose smectic layer structure (shown in Fig. 11) is stable as mentioned above. To obtain a high contrast ratio, first of all we investigated the memory capability; particularly the layer tilt angle dependence of the memory capability. Because we have obtained the stable layer structure FLC mixture

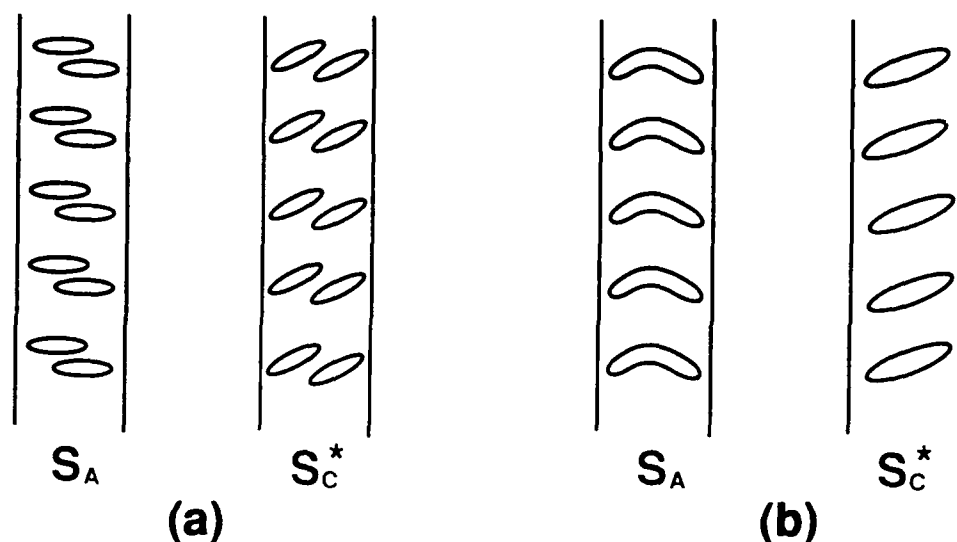


Fig. 13 Two possible liquid crystal molecules configurations in the S_A and S_C^* phases. (a) Molecular dimerization, (b) Molecular stretch.

using the naphthalene ring contained materials. This material has a small layer tilt in the S_C^* phase, namely, quasi-bookshelf layer structure. Thus we confirmed the bistability of the material. The memory stability, which is the ratio of light transmittance 0.5 seconds after removing the drive voltage, to the transmittance when drive voltage is applied, of the material is shown in Fig. 14.⁵ This figure shows that a small tilt angle produces a more stable memory effect. Several degrees of layer tilt indicate a quasi-bookshelf layer structure, providing more than 90% memory stability. This memory stability correlating to the layer tilt angle is explained as follows. It can be assumed that the director in the unperturbed state (memory state) tends to be parallel to the bounding surfaces. In a perfect bookshelf structure, the direction orientation state under an electric field is the same as in the memory state, resulting in 100% memory stability. In a shevron structure, however, the apparent tilt angle, which is the projection angle between the director and the layer normal, in the memory state is smaller than that under the field. The associated change in the transmittance by effectively terminating the field reduces the memory stability. Thus even though layer structure is not the perfect bookshelf, the effective memory stability reaching at 90% can be obtained as long as the layer tilt angle is within several degrees.

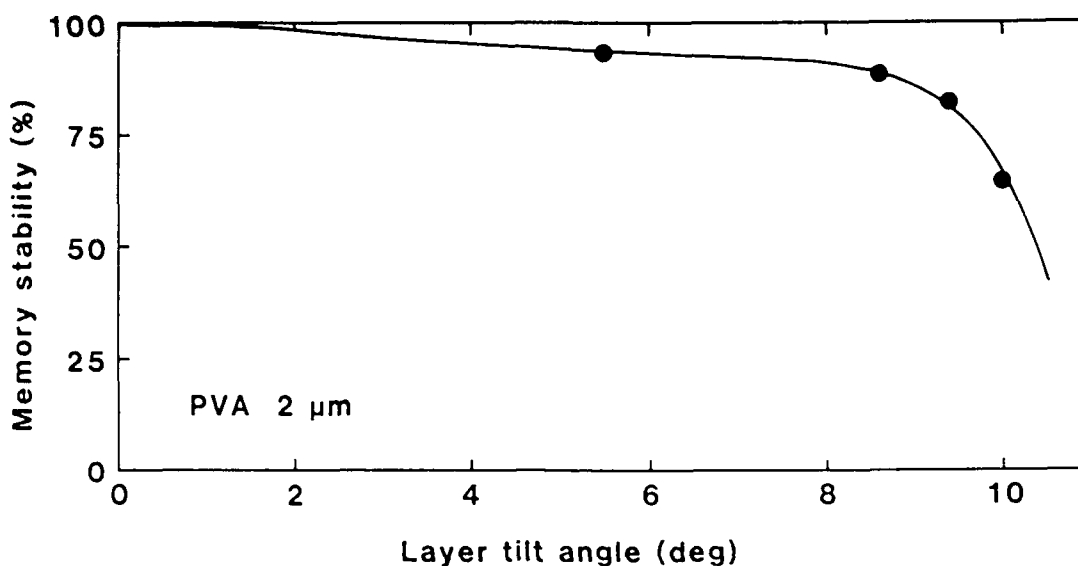


Fig. 14 The relationship between layer tilt angle and memory stability.

Dynamic Properties

In the practical multiplexed dot matrix SSFLC panel, the electrooptical threshold properties are important to obtain the high contrast display. Figure 15 shows the threshold property of the naphthalene base FLC mixture driven by 4-slot multiplexing method with 1/400 duty and 1/4 bias. In Fig. 15 the voltage represents the pulse height of the selected voltage. This figure indicates that the naphthalene base material has a wide drive voltage window. Moreover it has a high contrast ratio reaching at 40:1.

Fabrication of the Prototype

As the result of our material research, we have actually realized the SSFLC display utilizing the naphthalene base mixture as shown in Fig. 16. This display has 196 X 128 pixels, and driven by 4-slot multiplexing method. Its contrast ratio is 35:1 and the transmittance is 40% including two polarizers. The characteristics of this display are summarized in Table 1.

CONCLUSION

We have investigated the relationship between the phase sequence and the smectic layer structure, and obtained both bookshelf and quasi-bookshelf layer structure using the naphthalene base FLC mixture. The fabricated

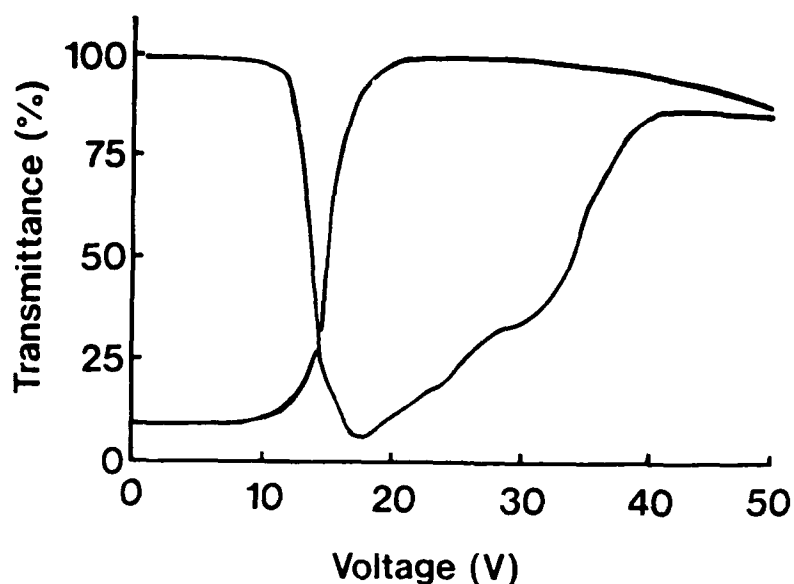


Fig. 15 The electrooptical threshold properties of the naphthalene base FLC material.

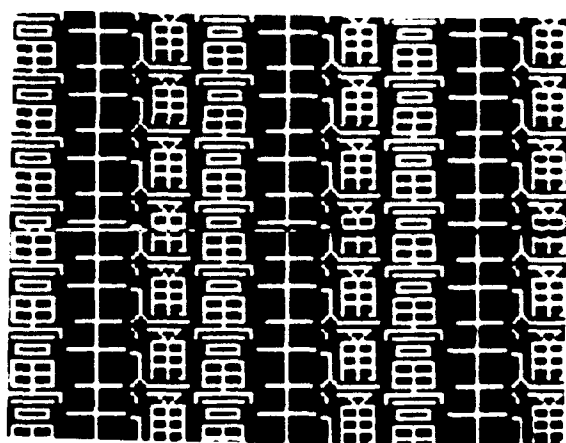


Fig. 16 The FLC prototype display using the naphthalene base FLC mixture.

SSFLC display using the naphthalene base FLC mixture shows high contrast ratio reaching at 35:1 and high transmittance of 40%. This display indicates that the ideal bookshelf structure can be prepared in the practical SSFLC display with rubbed polymer orientation films.

Table 1 The characteristics of the FLC display

Number of Pixel (dot)	196 X 128
Effective Display Area (mm ²)	70 X 50
Contrast Ratio	35 : 1
Viewing Angle (\pm degree)	70
Transmittance (%)	40
Duty Ratio	1/128
Addressing Time (μ s/line)	160
Drive Voltage (\pm V)	20

ACKNOWLEDGMENT

The authors thank Professors A. Fukuda, H. Takezoe and S. Kobayashi, Dr. Y. Ouchi and Mr. Y. Takanishi for their courteous discussions. The authors also thank Mr. H. Okuyama, T. Narusawa and Y. Yoneda for their support of this work.

REFERENCES

1. N. A. Clark and S. T. Lagerwall, Appl. Phys. Lett., **36**, 899 (1980).
2. K. Hiroshima, M. nakano and K. Shimizu, Conference record of Japan Display '89, pp. 352-355 (1989).
3. T. Uemura, N. Ohba, N. Wakita, H. Ohnishi and I. Ota, Proceedings of the SID, **28**, 175 (1987).
4. A. Mochizuki, M. Hirose and M. Nakatsuka, Ferroelectrics, **113**, 353 (1991).
5. A. Mochizuki, T. Yoshihara, M. Iwasaki, M. Nakatsuka, Y. Takanishi, Y. Ouchi, H. Takezoe and A. Fukuda, Proceedings of the SID, **31**, 123 (1990).
6. N. Wakita, T. Uemura, H. Ohnishi, N. Ohba, Y. Kobayashi and I. Ota, National Technical Report, **33**, pp. 44 (1987), in Japanese.
7. Y. Sato, T. Tanaka, H. Kobayashi, K. Aoki, H. Watanabe, Y. Ouchi, H. Takezoe and A. Fukuda, Jpn. J. Appl. Phys., **28**, L483 (1989).
8. N. A. Clark and T. P. Rieker, Phys. Review A, **37**, 1053 (1988).

9. T. P. Rieker, N. A. Clark, G. S. Smith, D. S. Parmer, E. B. Shirota and C. R. Safinya, Phys. Rev. Lett., 59, 2568 (1987).
10. H. Rieger, C. Escher, G. Illian, H. Jahn, A. Kaltbeitzel, D. Ohlendorf, N. Rosch, T. Harada, A. Weipert and E. Luder, Conference Record of The SID '91, pp. 396 (1991).
11. T. Konuma, A. Mase, S. Yamazaki, M. Yagi, H. Kondo and T. Hagiwara, Conference Record of The SID '91, pp. 400 (1991).
12. Y. Takanishi, Y. Ouchi, H. Takezoe, A. Fukuda, A. Mochizuki and M. Nakatsuka, Liquid Crystal. (Proceedings of The 13th Int'l Liquid Crystal Conference in Vancouver, 1990), in press.

ELECTRO-OPTICAL PROPERTIES OF FERROELECTRIC LIQUID CRYSTALLINE POLYMERS

KIMIHIRO YUASA, SHUNJI UCHIDA, TAKASHI SEKIYA,
KENJI HASHIMOTO AND KENJI KAWASAKI
Idemitsu Kosan Co.,Ltd. Central Research Laboratories,
1280 Kami-izumi, Sodegaura, Chiba 299-02, Japan.

Abstract Ferroelectric liquid crystalline polymers (FLCP) were synthesized. These ferroelectricities were confirmed directly by measuring the polarization reversal currents and other electro-optical properties. The smectic layer structure of FLCP was also studied. A chevron structure similar to that of low molecular FLC was observed even in FLCP cell. But the zigzag defects were not very sharp, which means that good orientation can be even in large area displays.

INTRODUCTION

Ferroelectric liquid Crystals (FLC) have attracted our interest because of its high speed response and memory effect¹. But there are still some difficulties in controlling orientation of molecules and uniform cell thickness for gaining good memory effect. We polymerized FLC in 1985 to overcome these difficulties. These polymers have side chains which consist of a flexible spacer unit, a core moiety and an optically active substituent. Similar polymers have been reported by Shibaev², Dubois³, Zentel⁴ and Kozlovsky⁵. They have reported a possibility but not confirmation of chiral smectic C (SmC*). We confirmed directly the ferroelectricity of our polymers by measuring polarization reversal currents⁶. Furthermore, other liquid crystalline properties were studied

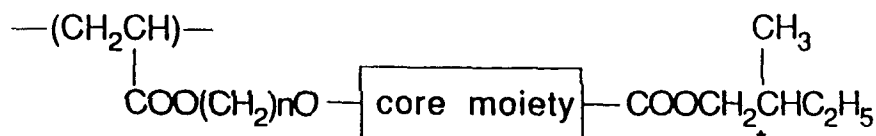
by DSC analysis, optical microscopy, X-ray diffraction and optical response time.

In the recent study, we observed the smectic layer structure of FLCP by optical microscopy and X-ray diffraction. We first observed zigzag defects in FLCP cells also. The existence of zigzag defects indicates the existence of a chevron structure similar to that of low molecular weight FLC. Although they are not very sharp compared with those of low molecular weight FLC, which means that good contrast can be realized even in large area displays.

RESULTS AND DISCUSSION

Ferroelectricity of Synthesized Polymers

The molecular structure of the polymers are given below. The synthesizing procedure was reported else⁶.



LCP	n	core moiety
p1	10	
p2	12	
p3	12	

$$M_n = 4 \times 10^3 \sim 4 \times 10^4$$

Fig. 1 shows the DSC curve of p1. The thermogram between 20°C and 60°C is magnified in the inset. A clearing point is observed around 120°C. And around 55°C, there is a transition temperature from SmA to SmC* since the transition enthalpy was 200mJ/mol as small as low molecular weight FLC and base line shifted which is characteristically seen in low molecular weight FLC. In the lower temperature region, there is a transition temperature from SmC* to higher order smectic phase around 30°C. This phase is SmI* or SmF* by existence of hexagonal intermolecular order observed by X-ray diffraction but not confirmed.

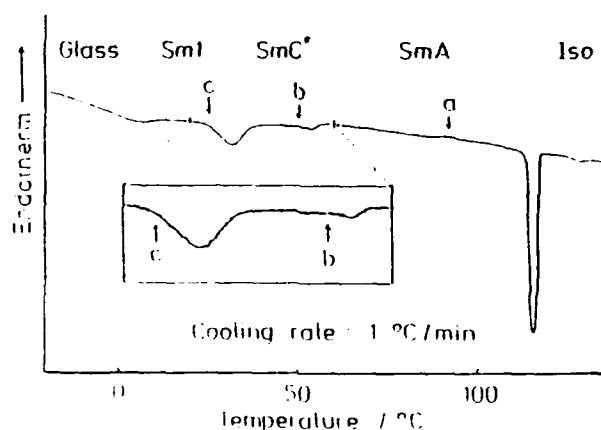
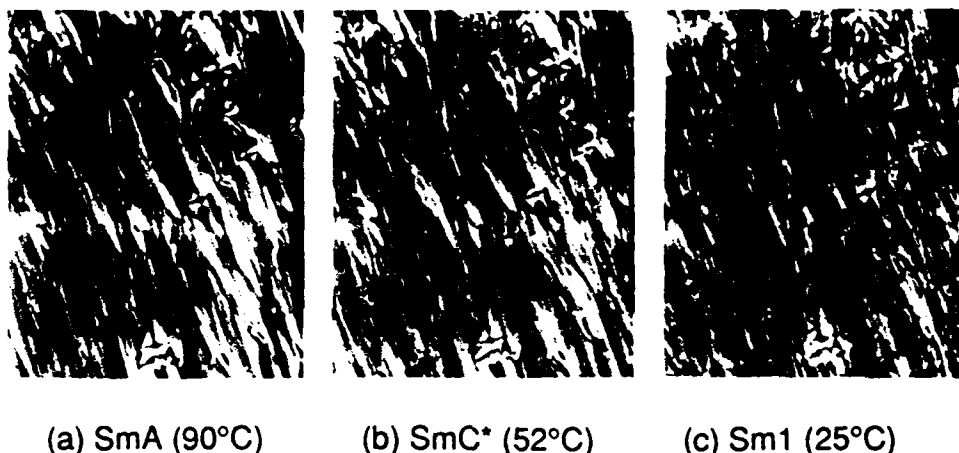


Fig. 1 DSC curve of p1 ($M_n=4 \times 10^4$).



(a) SmA (90°C) (b) SmC* (52°C) (c) SmI (25°C)

Fig. 2 Micrographs of texture of p1 at various temperatures.
See Color Plate II.

The texture of this polymer is shown in Fig. 2 at the temperatures of a, b, c indicated in Fig. 1. FLCP was laminated between a pair of glass substrates and sheared. A typical fan-shaped texture was observed at 90°C in picture (a). This texture suggests this phase is SmA. After cooling down to 52°C, equidistant lines caused by a helical structure appeared in picture (b). This proves the phase transferred to SmC*. Picture (c) is of higher order smectic phase than SmC*.

Then, we tried to measure the spontaneous polarization (P_s). Measuring P_s is a direct way to confirm the ferroelectricity. P_s was determined by measuring the polarization reversal current with triangular wave form voltages⁷. These wave forms of reversal currents measured with different frequencies are shown in Fig. 3.

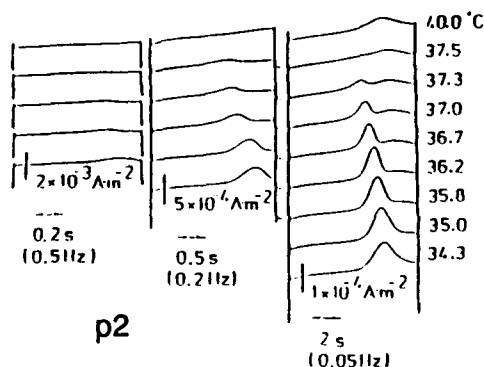
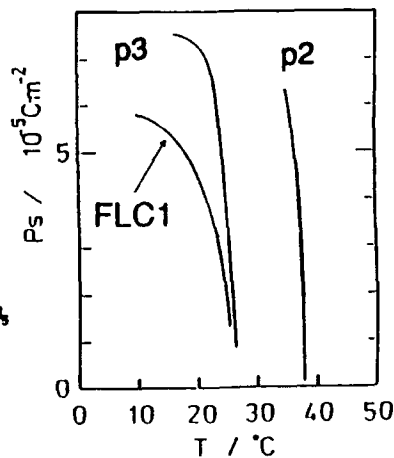


Fig. 3 Polarization reversal currents

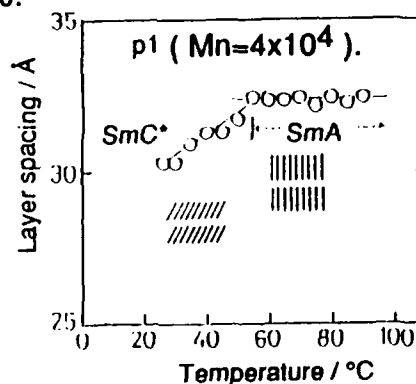
These frequencies are rather low because of slowness of response. Generally, the magnitude of observed Ps depends on the orientation of molecules, cell thickness, impurities in the liquid crystal, frequency etc. In Fig. 3, we can see a broad peak originated from ionic current particularly at high temperatures of 0.05 Hz. In case of slow response FLCP, it is difficult to distinguish the polarization reversal current from ionic current. So, the measuring conditions must be optimized. Thus, temperature dependences of Ps were determined as shown in Fig. 4. Ps of low molecular FLC corresponding to p3 is shown also in the figure. Ps of both FLCP and low molecular weight FLC rapidly rise and then level off below the transition temperature of SmA to SmC*. The magnitude of FLCP is larger than that of low molecular weight FLC. It is supposed that molecular rotation around the long axis is suppressed by bonding to the main chain to increase the magnitude of Ps.

Fig. 4 Temperature dependence of spontaneous polarization.



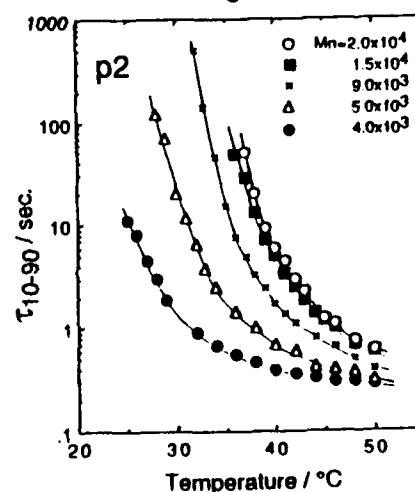
The smectic layer spacing of FLCP determined by small angle X-ray scattering is plotted against the temperature in Fig. 5. The layer spacing which was 33\AA does not change in SmA but decreases with decreasing the temperature in SmC^* . This decrease can be interpreted as a inclination of molecules by tilt angle θ .

Fig. 5 Temperature dependence of layer spacing.



The electro-optical response time was determined by measuring the transmitting light through the aligned cells placed between crossed polarizers. The response time τ_{10-90} was defined as the time required for a change of intensity from 10% to 90% on applying a square wave. $\pm 30\text{V}$ was applied across the $2\mu\text{m}$ thick cells. The response time for p2 of different molecular weight was plotted versus temperature in Fig. 6. The response time reached to sub-milli seconds in higher temperature region. It was 1 or 2 orders as fast as those of nematic liquid crystals, but still 2 to 3 orders slower than those of low molecular weight FLC. The response time became longer with molecular weight but saturated around $\text{Mn}=2 \times 10^4$.

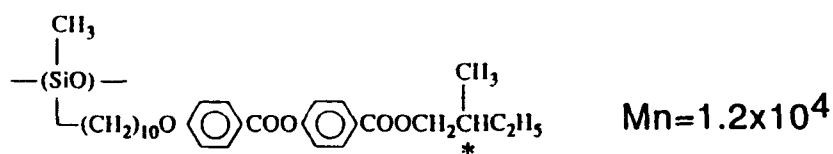
Fig. 6 Temperature dependence of optical response time.



As a result of above, our liquid crystalline polymers were confirmed to be ferroelectric.

Smectic Layer Structure of FLCP

In recent several years, it has been recognized to be very important how to control the smectic layer structure in FLC cells for realizing defect-free display devices⁸. We studied some characteristics of the smectic layer structure of FLCP. In this study, a FLCP of siloxisan type was investigated. The molecular structure and transition temperatures were given below.



Transition temperatures

glassy 15 SmC* 103 SmA 124 Iso (°C)

The transition temperatures were determined by DSC and observation of optical microscopy. This FLCP was laminated between two ITO glasses and sheared to align the molecules.

Fig. 7 Zigzag defects
in FLCP cell.
See Color Plate III.

layer normal



+2.5 V

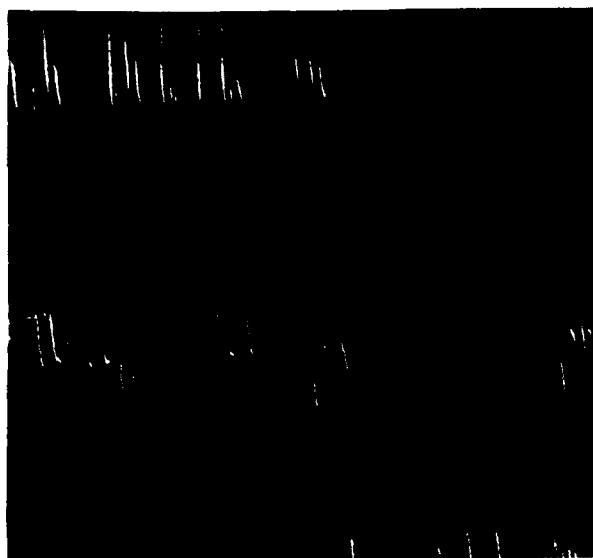


Fig. 7 shows the zigzag defects observed in this cell. DC voltage was applied to align the molecules uniformly. Two kinds of defect lines so called lightning and hairpin appeared alternately. As shown in this figure, the shape of these defect lines was not so sharp compared with those of conventional low molecular weight FLC.

Fig. 8 Asymmetrical reversal domains.
See Color Plate IV.

layer normal



-0.5 V



After decreasing the magnitude of DC voltage slowly, the direction of the voltage was changed. We can see asymmetrical reversal domains whose directions vary depending on the regions divided by zigzag defect lines in Fig. 8. This fact indicates there exists a similar chevron structure even in FLCP cell as well as low molecular weight FLC⁹. We measured X-ray diffraction to confirm this. Firstly, the Bragg angle $2\theta_B$ corresponding to smectic layer spacing was determined by measuring a small angle X-ray scattering with unaligned FLCP film. There was only one broad peak at $2\theta_B = 2.48^\circ$. By using this angle, we measured the X-ray diffraction curve of aligned cell with the geometry indicated in left side of Fig. 9.

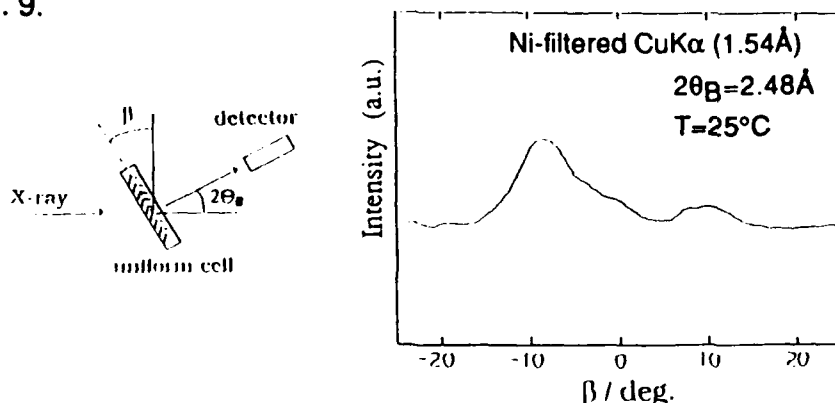


Fig. 9 X-ray diffraction curve.

The detector was fixed by $2\theta_B$ and the angle β was scanned⁸. In this measurement, the area where X-ray beam was irradiated had been determined in a defect-free area by using optical microscope preliminarily. Two large peaks were observed around $\pm 10^\circ$ in Fig. 9. This angle is rather small than the tilt angle $2\theta = 20^\circ$ determined optically. The width of these peaks is broad and the intensities does not equal each other. These suggest the chevron structure of this FLCP is not so simple as that of low molecular weight FLC. Furthermore, we made another cell to observe the chevron structure by an optical method. Similar method to low molecular weight FLC was reported by Fukuda et al.⁹

Fig. 10 Illustration of the cell structure for observing a cross section.

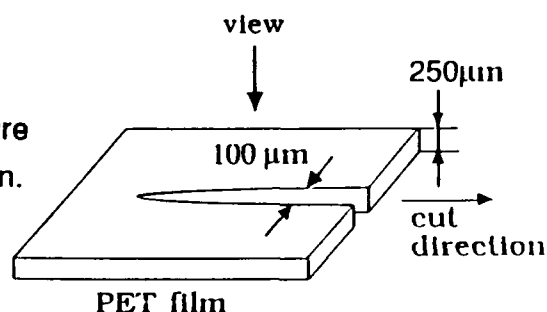


Fig. 10 shows the illustration of our cell. We used a polyethylene terephthalate film the center of which was cut by a sharp knife. The gap made by this treatment is typically about $100\ \mu\text{m}$ wide. FLCP was dropped into this gap by a capillary in isotropic phase and cooled slowly down to the temperature at which FLCP exhibit SmC^* . FLCP was aligned to both side of these edges.

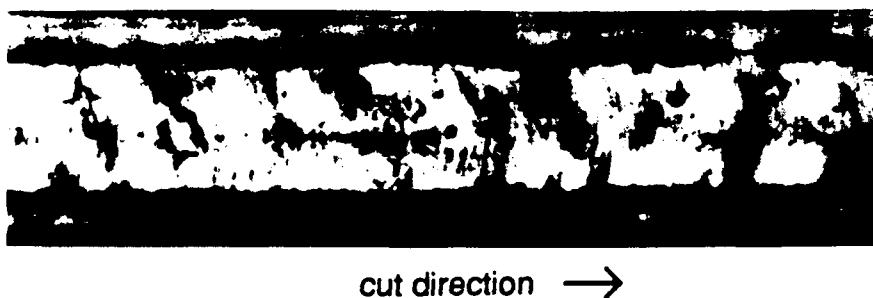


Fig. 11 Micrograph of a chevron structure of FLCP.
See Color Plate V.

We observed the texture from upside of the cell. Fig. 11 corresponds to a cross section of an usual cell. The cell gap is thick enough for this FLCP to make a helical structure. Thus many discrimination lines caused by a helical structure in SmC^* were observed. These lines bend slightly to the cut direction. This result also supports the existence of a chevron structure in FLCP cells indirectly, although this bend angle is smaller than the tilt angle determined optically.

SUMMARY

Electro-optical properties of FLCP were studied. Their ferroelectricities were confirmed by DSC, optical microscopy, measuring spontaneous polarization and X-ray diffraction.

The layer structure of FLCP was recognized to be similar to that of low molecular weight FLC. But the defect lines observed in FLCP cells are not so sharp. This fact makes it easy to align molecules and make large area displays. We have succeeded in making large area displays consisting of FLCP and plastic substrates without any alignment layers. (for example in Fig. 12)

(a) on state



(b) off state

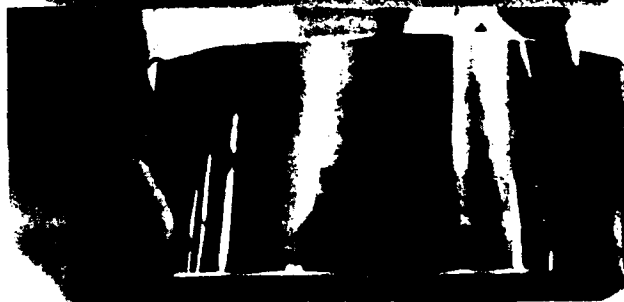


Fig. 12 FLCP display (Plastic substrates were used).
See Color Plate VI.

REFERENCES

1. Clark, N. A. and Lagerwall, S. T., *Appl. Phys. Lett.*, **1980**, 36, 899.
2. Shibaev, V. S.; Kozlovsky, M. V.; Beresnev, L. A.; Blinov, L. M. and Plate, N. A., *Polym. Bull.*, **1984**, 12, 299.
3. Dubois, J. C.; Decobert, G.; Barny, P. E.; Esselin, S.; Friedrich, C. and Noel, C., *Mol. Cryst. Liq. Cryst.*, **1986**, 137, 349.
4. Zentel, R.; Reckert, G. and Reck, B., *Liq. Cryst.*, **1987**, 2, 83.
5. Kozlovsky, M. V., *Solid State Phys.*, **1987**, 27, 98.
6. Uchida, S.; Morita, K.; Miyoshi, K.; Hashimoto, K. and Kawasaki, K., *Mol. Cryst. Liq. Cryst.*, **1988**, 155, 93.
7. Miyasato, K.; Abe, S.; Takezoe, H.; Fukuda, A. and Kuze, E., *Jpn. J. Appl. Phys.*, 22, No.10, L661.
8. Ouchi, Y.; Lee, J.; Takezoe, H.; Fukuda, A.; Kondo, K.; Kitamura, T. and Mukoh, A., *Jpn. J. Appl. Phys.*, 27, L725.
9. Fukuda, A.; Ouchi, Y.; Arai, H.; Takano, H.; Ishikawa, K. and Takezoe, H., *Liq. Cryst.*, **1989**, 5, 1055.

THE "JOERS/ALVEY" FERROELECTRIC MULTIPLEXING SCHEME

P W H SURGUY³, P J AYLIFFE², M J BIRCH², M F BONE⁴, I COULSON⁵, W A
CROSSLAND², J R HUGHES¹ P W ROSS² now ³, F C SAUNDERS¹ and M J
TOWLER¹.

1. Defence Research Agency, Electronics Division,
RSRE, Malvern, Worcestershire, WR14 3PS, UK.
2. BNR Europe Limited, London Road, Harlow, Essex,
CM17 9NA, UK.
3. THORN EMI Central Research Laboratories, Dawley Road,
Hayes, Middlesex, UB3 1HH, UK.
4. Formerly BNR Europe Limited.
5. Formerly THORN EMI.

Abstract Ferroelectric liquid crystal displays offer an attractive matrix addressed alternative for complex displays. However, their potential can only be realised by using novel addressing schemes suitable for the fast responding, DC sensitive, ferroelectric electro-optic effect.

Over a period of several years, a high performance, novel, ferroelectric drive scheme¹ has been developed in a UK, JOERS/Alvey funded, collaborative programme. The JOERS/Alvey drive scheme is based on monopulse strobe waveforms^{2,3,4} and utilises the response time - voltage minimum^{5,6} found in certain materials. Using this novel drive scheme, complex ferroelectric displays with a high contrast ratio, wide operating range and fast addressing times have been made^{7,8,9,10}.

The JOERS/Alvey drive scheme is described, compared with other published drive schemes, and the operating principles discussed.

INTRODUCTION

RMS addressed liquid crystal displays (e.g. TN, Supertwist) are restricted by a fundamental limitation in that as the number of lines is increased so the discrimination between 'on' and 'off' voltages falls thus reducing the contrast ratio, angle of view and speed. This can be overcome by the use of electro-optic effects which are fast and bistable as found in the ferroelectric smectic C device^{11,12}. Previous multiplexing schemes for the ferroelectric liquid crystal device (FLCD) have been based upon the

following premises-

i) switching is polarity dependent

ii) there should be net zero DC

iii) there is a voltage \times time ($V\tau$) product threshold for switching i.e. the switching point lies on a line of slope -1 on a $\log(V)/\log(\tau)$ plot (the τ -v characteristic).

It is this last premise which makes design of a suitable multiplexing scheme difficult since it is hard to arrange for good discrimination between switching and non-switching pulses. Schemes based upon these premises will be termed 'conventional' multiplexing schemes. We propose a novel multiplexing technique which combines the use of monopulse strobe waveforms and utilises the response time - voltage minimum found in some FLCs, to achieve good discrimination between the switching and non-switching pulses to bring a wide operating range, fast addressing time and good contrast ratio. In this new mode of operation the pulse with the highest voltage in the multiplexing scheme, which conventionally would be the switching pulse, is in fact the non-switching pulse. Schemes using the response time - voltage characteristic in this fashion will be termed ' τ -v min' schemes. A low - medium value of spontaneous polarisation (P_s) is necessary to induce the minimum in the τ -v characteristic but in spite of this, by using monopulse strobe waveforms, it is possible to achieve very fast addressing times with the added bonus that with low P_s there is less crosstalk due to the column voltages of the multiplexing waveform.

The devices used in this work were of nominal $2\mu\text{m}$ thickness and had aligning layers of rubbed polymer. Good alignment was achieved by slow cooling from the unwound cholesteric phase through an S_a phase into the Sc^* phase¹³. Among the materials used were mixtures of fluorinated biphenyl esters^{14,15}. The materials used here to illustrate the operating principles of the multiplexing schemes are typical of those used within the JOERS/Alvey programme. Recent developments have yielded superior materials with much faster operating parameters.

THE RESPONSE TIME - VOLTAGE CHARACTERISTIC

Conventionally the search for faster responding ferroelectric materials has led to the use of medium - high values of P_s . A typical response time - voltage characteristic for such a material is shown in Figure 1A. However in materials with a lower value of P_s a minimum in response time can occur. Such a characteristic is illustrated in Figure 1B.

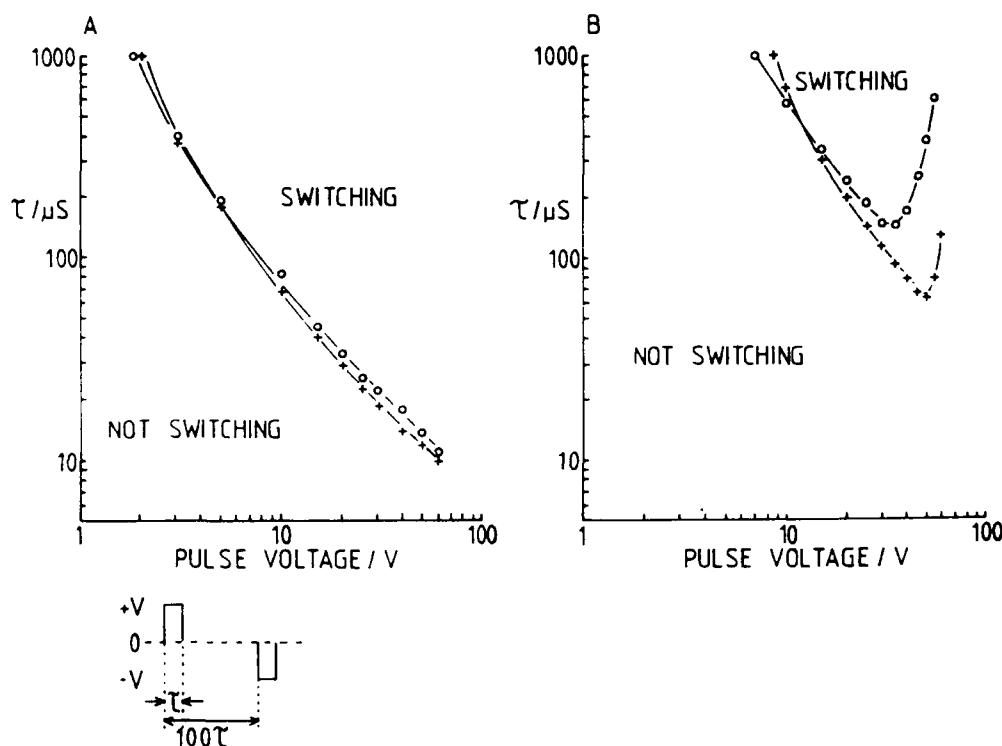


FIGURE 1. Response time as a function of voltage required to switch the device between states and showing the effect of superimposed AC bias (50kHz square wave, RMS voltage levels quoted) to simulate the effect of column (data) voltages encountered when multiplexing.

A. Material SCE 12. $P_s=16.1 \text{ nC/cm}^2$. + - 0V AC bias, o - 7.5V AC bias.

B. Material SCE 8. $P_s=5.7 \text{ nC/cm}^2$. + - 0V AC bias, o - 10V AC bias.

These characteristics were measured with a monopolar pulse of 1:100 duty cycle and alternating polarity to switch the device alternately between its two optical states. The response time is taken as the minimum pulse width at which visibly clean switching occurs with no patches or speckle visible in the cell. This is represented as a line but it must be remembered that a transient switching response occurs as the clean switching point is approached in which latching may not occur or may occur only in parts of the cell. The effect of this on the τ -v characteristic is illustrated in Figure 2, where it can be seen that the partial switching region is much broader at voltages below the minimum response time.

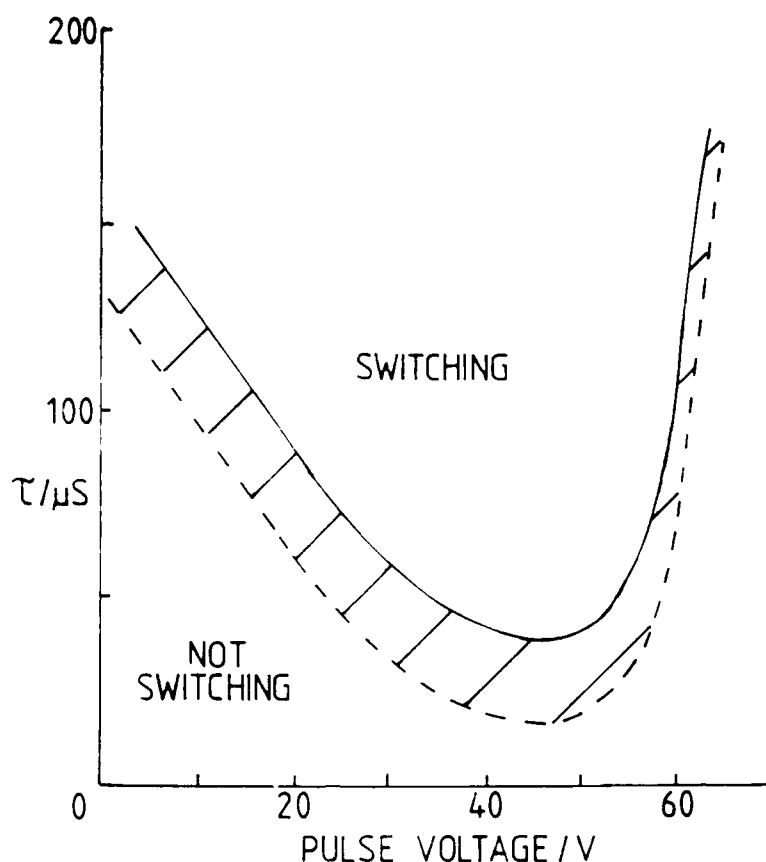


FIGURE 2. The partial switching region of the τ - v characteristic (shown shaded). Operation on the normal part of the curve is compromised by a broad partial switching region. At voltages greater than that corresponding to E_{min} the partial switching region is much reduced yielding better discrimination between switching and non-switching voltages and hence a greater operating tolerance to cell thickness variations.

In a simple system with bookshelf geometry and uniaxial dielectric anisotropy, the value of the field which gives the minimum response time is ⁶

$$E_{min} = \frac{P_s}{\sqrt{3} \cdot \epsilon_0 \cdot \Delta\epsilon \cdot \sin^2\theta}$$

where $\Delta\epsilon$ is the dielectric anisotropy, θ is the cone angle, and the minimum response time

$$t_{min} \propto 1/P_s^2.$$

It is now clear¹⁶ that within a tilted layer geometry it is the magnitude of the dielectric biaxiality that is crucial to the existence of a minimum in the τ - v characteristic. Thus while the above expression holds well for some materials it is not universally applicable.

The expression for E_{min} imposes a constraint on P_s if the minimum is to occur at a useful voltage. If this is chosen to be 40V, then for typical materials with a cone angle $\approx 20^\circ$ and $\Delta\epsilon \approx -2$ used in a $2\mu\text{m}$ cell, P_s will need to be $\approx 7 \text{ nC/cm}^2$.

Although such a modest value of P_s might be expected to restrict the switching speed, it will be shown that the minimum switching time as measured in the τ - v characteristic is not the fastest switching time that can be achieved when multiplexing with the JOERS/Alvey scheme. Furthermore the fastest switching times which can be achieved with the commonly used conventional schemes are considerably longer than would be expected from this τ - v characteristic. Thus a simple comparison of response speeds from these τ - v characteristics for low and high P_s materials does not yield a true comparison of response speeds when operated with multiplexing schemes optimised to the material characteristics.

The effect of AC bias is to stabilise the director position during the interval between the switching pulses by reducing relaxation from the switched positions. The effect of this stabilisation on the τ - v characteristic (Figure 1) is clearly more pronounced where the dielectric torque ($\propto E^2$) begins to dominate the ferroelectric torque ($\propto E$). A similar effect is obtained when switching with a bipolar pulse since the leading part of the pulse switches the director, leaving the trailing part to switch from a fully switched position. Characteristics measured using a superimposed AC bias, or with a bipolar pulse, therefore often show a minimum even if the monopolar characteristic does not.

'CONVENTIONAL' MULTIPLEXING SCHEMES

Typical of the conventional multiplexing schemes that are in widespread use e.g. 17,18,19 are the Seiko scheme²⁰, the GEC scheme²¹ and the Leti-Bari scheme¹⁸. These employ a strobe voltage, V_s , which is applied to rows and a data voltage, V_d , which is applied to columns (Figure 3) such that good discrimination needs to be achieved between a switching pulse of resultant amplitude (V_s+V_d) and a non-switching pulse of resultant amplitude (V_s-V_d). This is more fully illustrated in Figure 4. All of these schemes use a bipolar strobe pulse which differs in the width or amplitude of the leading part. The leading part in two cases (GEC and Leti-Bari) is designed to effect switching, acting as a blanking pulse in that it sets all pixels to one optical state, while the trailing part selectively switches pixels to the other optical state. In the other case (Seiko) the leading pulse will effect

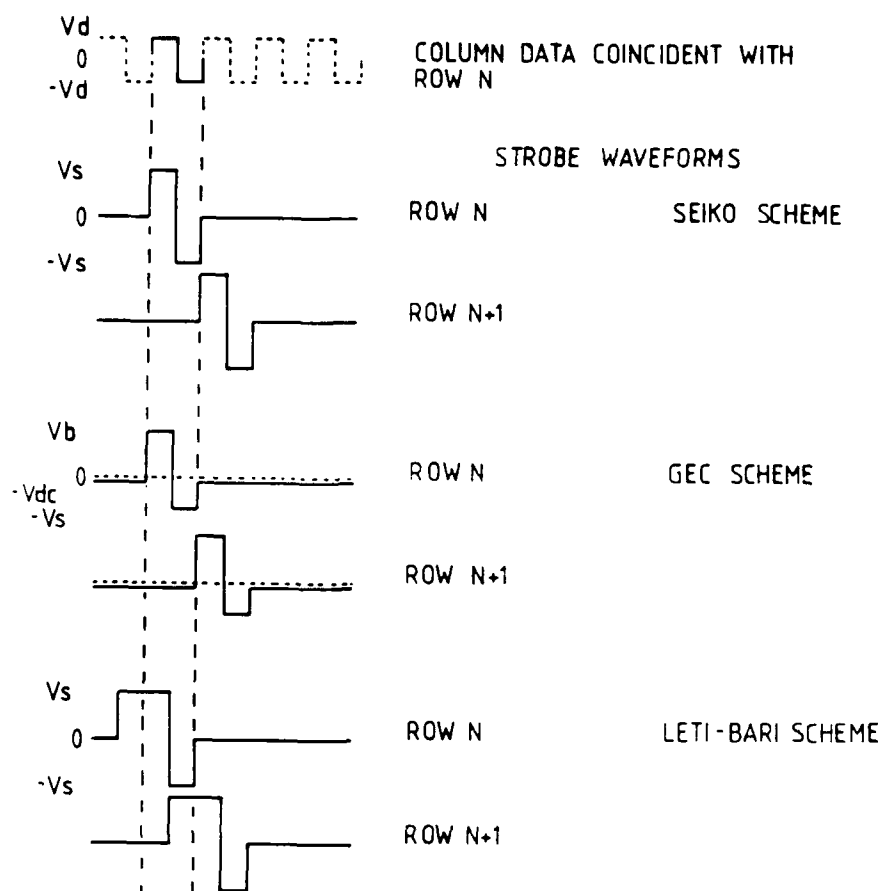


FIGURE 3. Strobe (row) waveforms for three 'conventional' multiplexing schemes showing the relationship of adjacent rows and of row and column waveforms. The Seiko scheme is DC balanced in one scan but requires two scans to switch all pixels. The GEC scheme is DC balanced in one scan, the imbalance between V_b and V_s ($V_b > V_s$) is compensated by V_{dc} ; one scan is required to switch all pixels. The Leti-Bari scheme switches all pixels in one scan but requires reversal of the strobe polarities in alternate scans to achieve DC balance.

switching when the trailing part does. Thus in all three cases the trailing part of the pulse must switch from a fully switched position of the director and it is the trailing part of the pulse which determines the state of the pixel. The switching characteristic can thus be fairly represented by a bipolar pulse measurement and such a characteristic is shown in Figure 5. This characteristic yields response times much greater than those of Figure 1A and also shows a minimum at high voltage. From this characteristic it can be seen that an

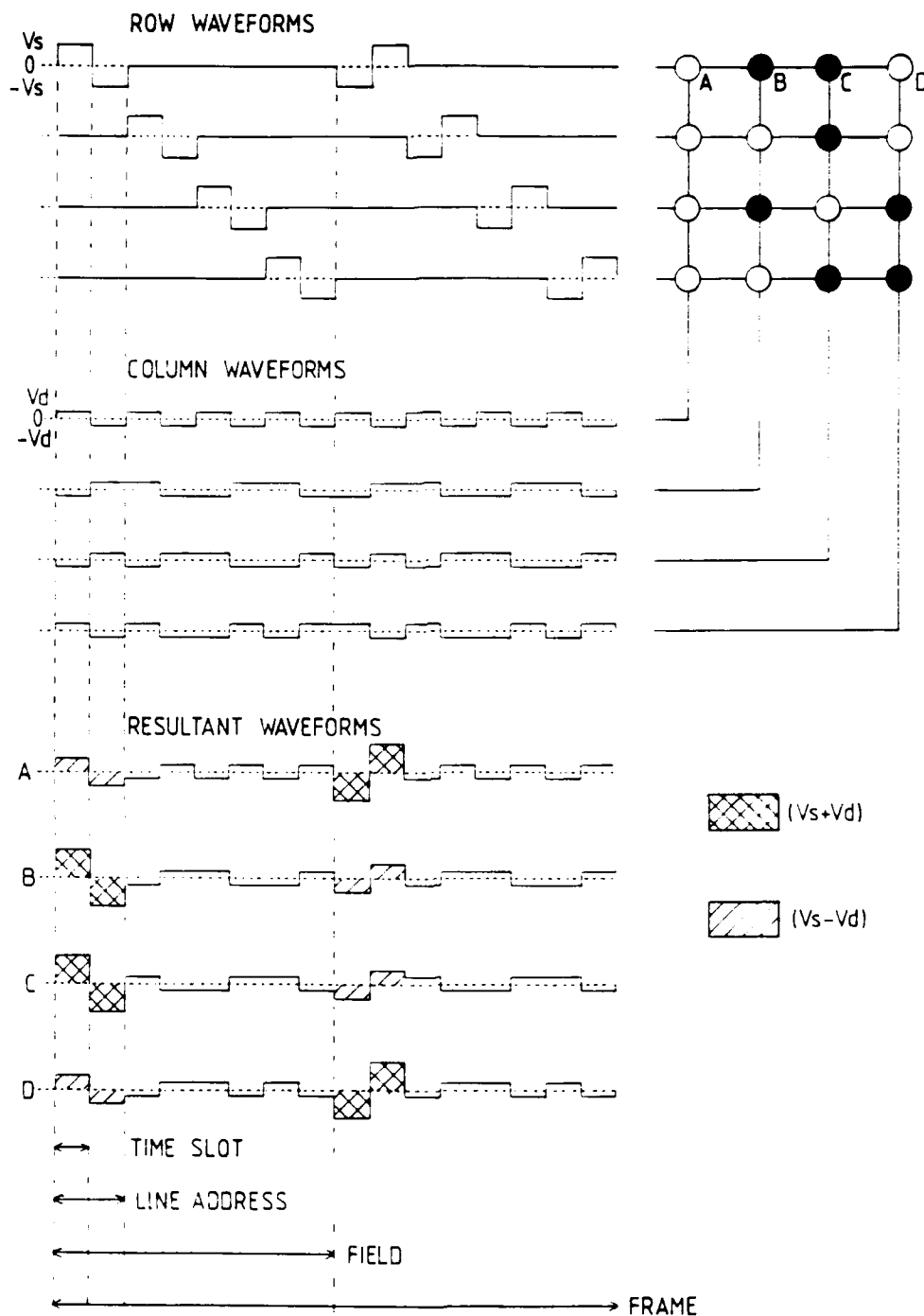


FIGURE 4. Typical example of the Seiko multiplexing scheme for the case of four way multiplexing. Pixel A is arbitrarily defined to be 'on' in response to $+(Vs+Vd)$ pulse. Pulses of amplitude $(Vs-Vd)$ and V_d are intended not to switch.

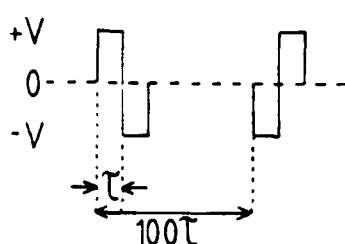
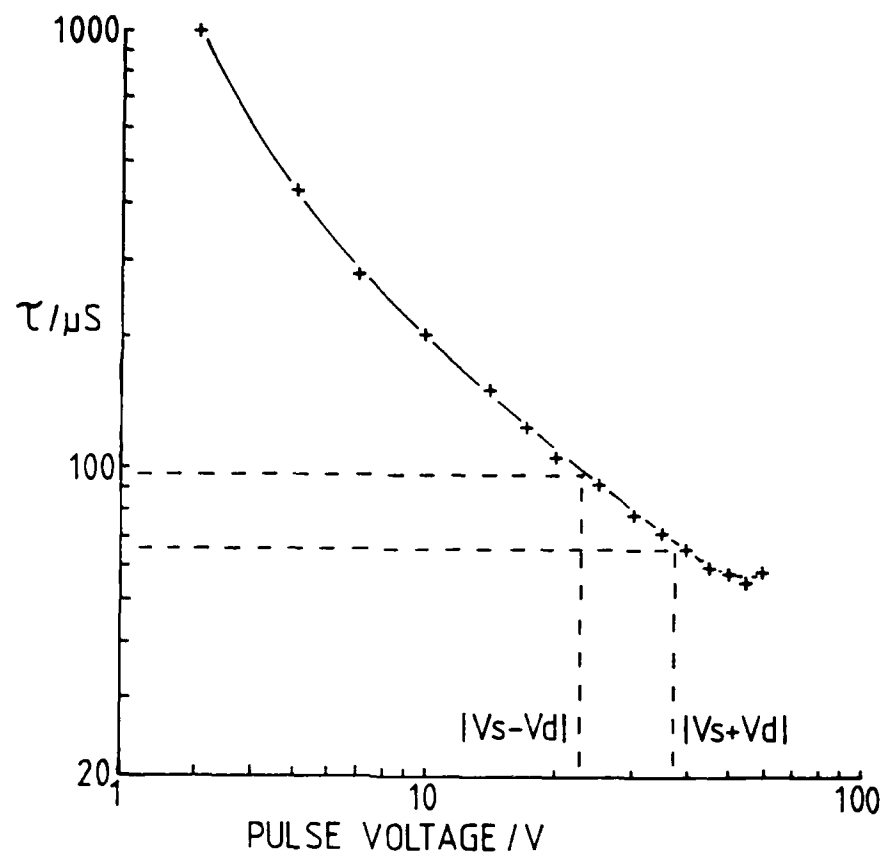


FIGURE 5. Response time as a function of voltage for material SCE 12 measured with a bipolar pulse and superimposed A.C. bias of 7.5V RMS, 50kHz square wave. The vertical lines denote the multiplexing conditions $V_s=30V$, $V_d=7.5V$ and the operating range in time is denoted by horizontal lines. The apparent discrepancy in the upper operating point between the figure and Table 1 is explained by the partial switching region as shown in Figure 2.

operating range in time can be deduced from the V_s and V_d values, the greater is the value of V_d the greater will be this range. Nevertheless the operating range is inherently narrow. There is a further inherent limitation - the non-switching pulse is never very far from the switching line and a transient effect will be associated with it which has the

effect of disturbing the director and making it more susceptible to fluctuations from the column voltage V_d , hence the contrast is poor.

A typical set of operating parameters for the SEIKO scheme are given in Table 1.

TABLE 1. Multiplexing parameters with the Seiko drive scheme. Material BDH SCE 12. $P_s = 16.1 \text{ nC/cm}^2 @ 25^\circ\text{C}$		
$V_s = 30\text{V}$ V_d	Operating Range (time slot / μs)	Contrast Ratio
5V	70 (minimum)	3.5:1
	76 (maximum)	1.8:1
7.5V	65 (minimum)	3.2:1
	85 (maximum)	2.0:1

THE JOERS/ALVEY MULTIPLEXING SCHEME

The JOERS/Alvey drive scheme uses a monopulse strobe addressing scheme. In such a scheme the strobe voltage is zero in one of the two time slots of the line address time and the voltage excursion occurs in the other slot; either slot may be chosen for the voltage excursion. The monopolar strobe pulse introduces a DC imbalance that must be compensated to avoid electrochemical degradation of the liquid crystal. Since this DC imbalance arises from the strobe waveform, it is applied equally to all pixels and can be easily compensated by writing a second field with the strobe voltages inverted, or by applying blanking pulses on a line by line basis or simultaneously to all pixels. The novel mode of operation which is described here, the JOERS/Alvey drive scheme, occurs only when the voltage excursion is applied in the trailing slot and is used with a material which shows a minimum in its τ -v characteristic. The scheme is illustrated in Figure 6 and differs fundamentally from the conventional schemes in that the resultant pulse combinations for the switching and non-switching pulses are different, not only in amplitude but in pulse shape within the two slot strobe. In the conventional schemes the pulse which switches the pixel is preceded by a pulse of the opposite polarity which has also switched the pixel; the non-switching pulse is also preceded by a pulse of opposite

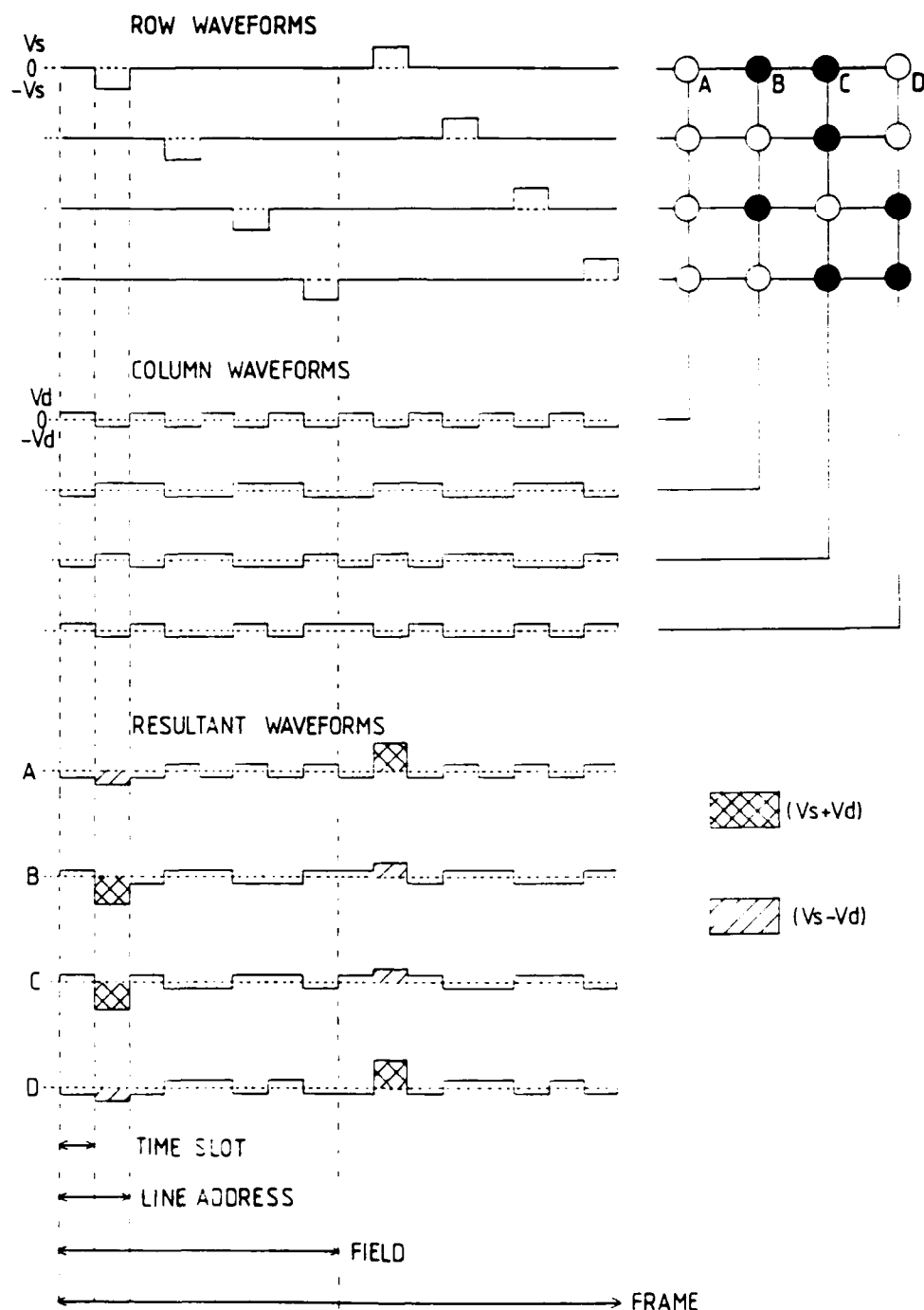


FIGURE 6. Typical example of the 'JOERS/Alvey' drive scheme waveforms showing four way multiplexing with a two-field frame. When utilising the minimum in the τ - v characteristic ($V_s - V_d$) will be the switching pulse and pulses of amplitude ($V_s + V_d$) and V_d will be intended not to switch. Thus pixel A, for example, will be switched by $-(V_s - V_d)$.

polarity. In the JOERS/Alvey scheme the resultant strobe pulse combination containing $(V_s + V_d)$ in the trailing slot always has V_d of opposite polarity in the leading slot while the resultant strobe pulse combination containing $(V_s - V_d)$ always has V_d of the same polarity in the leading slot. These differently shaped switching pulse combinations produce very different switching characteristics, illustrated in Figure 7, which permit good discrimination between switching and non-switching pulses over a wide range of pulse widths. Note that it is the low voltage pulse $(V_s - V_d)$ which effects switching at the shorter time slot and the $(V_s + V_d)$ pulse which is non-switching. Several benefits accrue from this mode of operation -

- i) the actual switching speed is greater than would be expected from the simple monopulse τ -v characteristic
- ii) the partial switching region is much reduced for voltages beyond the minimum, leading to better discrimination (Figure 2)
- iii) the non-switching pulse is situated well away from its characteristic in the non-switching region and consequently does not give rise to a transient response
- iv) the fast operation (short time slots) with the low P_s materials used with this mode of operation means less disturbance of the director from the column voltage waveform, i.e. less crosstalk and better contrast than would be encountered with the higher P_s materials at similar time slots under conventional operation.

Notice that in order to switch all of the pixels with this scheme it is necessary to either

- i) repeat the row waveform scan with the row waveform voltages inverted⁴, this is called a two field frame and is illustrated in Figure 6, or
- ii) switch all of the pixels (row at a time or page at a time) to one optical state^{2,3} with a blanking pulse of sufficient voltage x time product to ensure that, when combined with the data waveform, switching is effected, and then selectively switch pixels with the strobe pulse to the other optical state.

Certain constraints are placed on the position of the blanking pulse with respect to the strobe pulse. If the blanking pulse is too close to the switching pulse it leads to increased switching times. If the blanking pulse is too far ahead of the strobe pulse then the blanked interval may become visible as a block of scanning lines while contrast is reduced by the pixel being in the 'wrong' optical state for part of a frame. There is thus an optimum position, dependent upon liquid crystal material parameters, which is typically five - ten lines ahead of the strobe.

Monopulse strobe schemes, when used with a material which does not show a

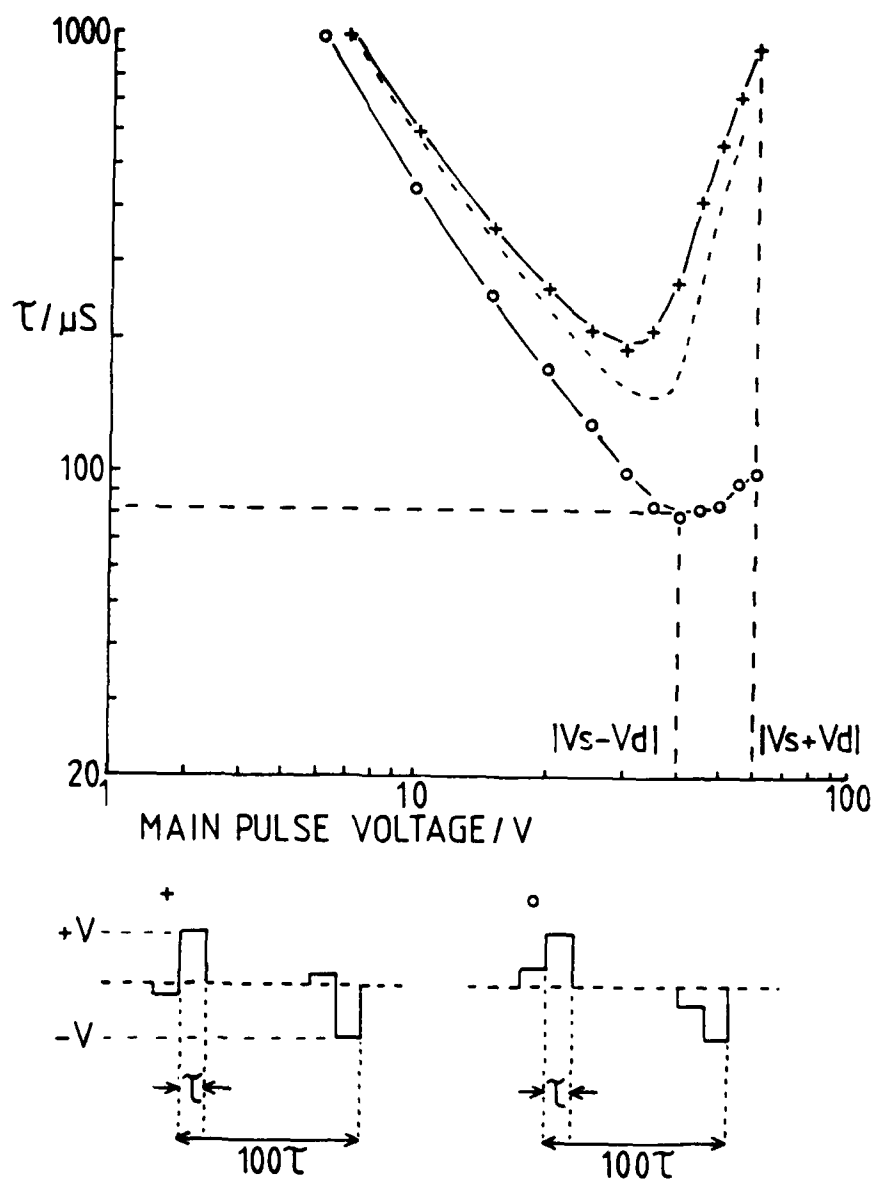


FIGURE 7. Response time as a function of voltage for the material SCE 8 for the pulse shapes shown, simulating the multiplexing conditions of $V_s=50\text{V}$, $V_d=10\text{V}$. The curves relate to the (V_s+V_d) pulse (+) which has a leading part of opposite polarity and amplitude 0.166 of the main pulse, and the (V_s-V_d) pulse (o) which has a leading pulse of the same polarity and amplitude 0.25 of the main pulse. The broken line shows the response measured with a monopolar pulse as in Figure 1B. The operating voltages are denoted by vertical lines and the fastest operating point by a horizontal line. The upper operating point is defined by the column voltage beginning to cause switching ($\approx 350\mu\text{s}$) and not by (V_s+V_d) beginning to switch.

minimum in its τ -v characteristic, work slightly quicker, but in other respects similarly to, the conventional schemes using a bipolar strobe pulse. In this mode of operation it is the resultant strobe pulse combination that contains (V_s+V_d) that effects switching, the pulse containing (V_s-V_d) does not cause switching. The voltage excursion may occur in either the leading or trailing portion of the two-slot strobe.

A typical set of operating parameters for the JOERS/Alvey scheme are given in Table 2.

TABLE 2. Multiplexing parameters with the JOERS/Alvey drive scheme.
Material BDH SCE 8.
 $P_s = 5.7 \text{ nC/cm}^2$ @ 25°C

$V_s=50\text{V}$ V_d	Operating Range (time slot/ μs)	Contrast Ratio
7.5V	58 (minimum) 75 (clean switching) 265 operates with reducing contrast to $\approx 500\mu\text{s}$.	80:1 65:1 5:1
10V	62 (minimum) 83 (clean switching) 200 operates with reducing contrast to $\approx 350\mu\text{s}$.	100:1 63:1 5:1

The minimum time slot is that at which an image takes several frames to build up, the clean switching time slot is that at which switching occurs within one frame.

COMPARISON WITH OTHER PUBLISHED DRIVE SCHEMES

Table 3 compares known published drive schemes. The devices using the JOERS/Alvey drive scheme combine the attributes of fast switching time giving video frame rates at high levels of multiplexing and high contrast ratios. These features are best achieved with materials having a relatively high value of operating voltage. While the operating voltage can be lowered by reducing P_s , this will be at the expense of speed. Other published τ -v min schemes^{24,25} have not used a monopulse strobe addressing scheme and have not succeeded in combining these benefits in one device.

TABLE 3. Comparison of Published Ferroelectric LCD Performance.

Author	Year	Pixels	Level of Multiplexing	Speed	Contrast Ratio	Voltage
Geary et.al. ²²	1985	95 x 95	512	1ms switching		Vs=+/-18V Vd=+/-18V
Matsumoto et. al. ¹⁷	1988	639 x 400	400	33µs switching time	7:1	30V
Inoue et. al. ²³	1988	1280 x 1120	-	150µs line address time	>5:1	-
Leroux et. al. ²⁶	1988	256x320	-	80µs line address	10:1 [▽]	Vs=+/-40V Vd=+/-8V
Yamamoto et. al. ^{24,+}	1989	32 x 64	32	4 Hz frame rate	40:1	+/- 30V
Reinhart et. al. ¹⁹	1989	68 x 80	64	92µs line address	2.6:1	Vs=25V Vd=25V
"		68 x 80	64	50µs line address	4.2:1	Vs=77V Vd=15V
Wakita et. al. ^{25,+}	1990	128 x 128	1000	600µs line address	≈10:1	+/-25V
Devices using JOERS/Alvey Drive Scheme.						
Bone et.al. ⁷	1987	64 x 64	1000	64µs line address time	35:1	60V peak
Ross ⁸	1988	720 x 400	625	64µs line address time	>10:1 ^Δ	-
Sparks et. al. ¹⁰	1988	128 x 128	128	100 - 160 Hz frame rate	>100:1 ^o	Vs=35V Vd=8V
Surguy et. al. ⁹	1990	288 x 528	144	50Hz frame rate 57µs line address	10:1 [*] 64 colours.	Vs=55V Vd=8V

+ Other "τ-v min" schemes.

▽ 9 grey levels.

Δ Contrast ratio in this display was low due to alignment damage, other laboratory demonstrators had shown contrast ratios ≈ 50:1.

o SLM device.

* Contrast ratio reduced by use of colour filters.

The JOERS/Alvey programme reported a 720 x 400 matrix of 240 x 180 mm showing video images in 1988⁸. This had a wide operating temperature range (25 - 35°C), a wide viewing angle and a contrast ratio greater than 10:1. A more recently developed colour display⁹ using the JOERS/Alvey drive scheme is illustrated in Figure 8.



FIGURE 8. Display multiplexed with JOERS/Alvey drive scheme using conditions given in Table 3 - Surguy et. al.

The "JOERS/Alvey" scheme brings speed advantages that are not immediately apparent from a simple comparison of operating parameters shown in Figure 1. This could suggest that material SCE 12 would multiplex much more quickly than SCE 8; this would be the case if both materials were operated on the normal part of their τ -v characteristic with one of the conventional drive schemes. When material SCE 8 is operated so as to take

advantage of its minimum with the 'JOERS/Alvey' scheme the operating speeds of the two materials with the different schemes are in fact similar, showing there is no speed penalty in using the lower Ps necessary for the JOERS/Alvey scheme.

CONCLUSIONS

We have shown that by combining the use of ferroelectric liquid crystal materials which show a minimum in their τ -v characteristic with a suitable monopulse strobe multiplexing scheme that a highly effective ferroelectric liquid crystal multiplexing scheme can be produced. The 'JOERS/Alvey' drive scheme enables highly complex ferroelectric displays with high contrast ratio, wide operating range and fast addressing times to be made.

ACKNOWLEDGEMENTS

The work reported here formed part of a programme sponsored by the UK Department of Trade and Industry under the JOERS/Alvey scheme. The collaborators were - School of Chemistry, Hull University, BDH Ltd. (now Merck Ltd.), THORN EMI Central Research Laboratories, STC Technology Ltd. (now BNR Europe Limited.), Royal Signals and Radar Establishment (now Defence Research Agency, Electronics Division) and Department of Chemistry, Bristol University.

The work owes much to many but the contributions of H. A. Pedlingham and E. P. Raynes in particular are gratefully acknowledged.

REFERENCES

1. F C Saunders, J R Hughes, P W Ross, M F Bone, P W H Surguy and I Coulson, "A method of addressing a ferroelectric LC matrix", European Patent Publication EP0306203A (4th September 1987).
2. P J Ayliffe, "Addressing liquid crystal displays", Great Britain Patent Publication GB2146473B (10th September 1983).
3. P J Ayliffe, A B Davey, "Addressing Liquid Crystal Cells", Great Britain Patent Publication GB217336B (3rd April 1985).
4. P W Ross, "Addressing Liquid Crystal Cells", Great Britain Patent Publication GB 2173629A (1st April 1986).
5. H Orihara, K Nakamura, Y Ishibashi, Y Yamada, N Yamamoto and M Yamawaki, Jap. J.

- Appl. Phys., **25**, No. 10, 839-840 (1986).
6. F C Saunders, J R Hughes, H A Pedlingham and M J Towler, Liquid Crystals, **6**, No. 3, 341-347 (1989).
 7. M F Bone, D Coates, W A Crossland, P Gunn and P W Ross, Displays Tech. Appl., **8**, No 3, 115-118 (July 1987).
 8. P W Ross, Proc. 1988 IDRC, 185-190, (October 1988).
 9. P W H Surguy, L G Banks, A N Carrington, L K M Chan, M J Naylor and N E Riby, Proc. Eurodisplay '90, 146-149, (1990).
 10. A P Sparks, R C Chittick, W A Crossland and J R Brocklehurst, IEE Colloquium Digest 1988/21, 15/1, (1988).
 11. R B Meyer, Mol. Cryst. Liq. Cryst., **40**, 33, (1977).
 12. N A Clark & S T Lagerwall, Appl. Phys. Lett., **36**, 89, (1980)
 13. M J Bradshaw, V Brimmell and E P Raynes, Proc. 6th IDRC, PD-5 (1986), published in Liquid Crystals, **21**, 107, (1987)
 14. M J Bradshaw, V Brimmell, J Constant, J R Hughes, E P Raynes, A K Samra, L K M Chan, G W Gray, D Lacey, R M Scrowston, I G Shenouda, K J Toyne, J A Jenner and I C Sage, Proc. SID Vol 29/3, 245-248, (1988).
 15. D Bishop, J Jenner and I C Sage, 11th Int. LC Conf. (1986).
 16. M J Towler, J C Jones and E P Raynes, personal communication, to be published.
 17. S Matsumoto, A Murayama, H Hatoh, Y Kinoshita, H Hirai, M Ishikawa and S Kamagami, Proc. SID Dig., **41**, (1988).
 18. P Maltese, J Dijon and T Leroux, Proc. IDRC, 98-101, (1988)
 19. K-F Reinhart, L Dorfmueller, K Marx and T Matuszczyk, 2nd Int. Symp. on Ferroelectric Liquid Crystals, 1989, published in Ferroelectrics, **113**, 405-417 (1991).
 20. T Harada, M Taguchi, K Iwasa and M Kai, Proc. SID Int. Symp. Dig., 131-134, (1985).
 21. C Bowry, A Mosley and B M Nicholas, Proc. Eurodisplay, 152-155, (1987)
 22. J M Geary, Proc. SID Dig., 128, (1985).
 23. H Inoue, A Mizutome, S Yoshihara, J Kanbe and S Iijima, Proc. 1988 IDRC, (October 1988)
 24. N Yamamoto, Y Yamada, K Mori, H Orihara and Y Ishibashi, Jap. J. Appl. Phys., **28**, No. 3, 524-529 (1989)
 25. N Wakita, T Uemura, H Ohnishi and I Ohta, Displays, 30-35, January 1990.
 26. T Leroux, F Baume, J F Clerc, J Dijon, C Ebel, M Estor, L Mulatier and C Vauchier, Proc. IDRC, 111-113, (1988)

MICRO-OPTIC SWITCH USING CHIRAL NEMATIC-SMECTIC C* PHASE TRANSITION FERROELECTRIC LIQUID CRYSTALS

A.M. BIRADAR, S.S. BAWA, C.P. SHARMA AND
SUBHAS CHANDRA

National Physical Laboratory, New Delhi 110012, INDIA.

Abstract A micro-optic switch based on total-internal reflection using ferroelectric liquid crystal is described. It uses a chiral nematic (N*)-smectic C* phase transition ferroelectric liquid crystal (FLC) in which the optic axis rotates by 90° during switching. The device exploits the maximum of birefringence in minimizing its size. The material inherent advantage of tilt angle stability with temperature provides the switching characteristics which are more stable over a wide range of temperature. An exceptionally high attenuation of 5×10^7 in the off state has been demonstrated.

INTRODUCTION

Fiber optics is of great importance for high bandwidth data transfer in multigigabit point-to-point long distance links in telecommunication. The optical routing switches reported recently^{1,2} make use of a low electric field realignment of ferroelectric liquid crystal (FLC) molecules to control total internal reflection (TIR) at a glass prism liquid crystal interface. These switches tend to have low cross talk,¹ low insertion loss, low power consumption, fast switching and exceptionally high extinction² at visible and infrared wavelengths.

In the most common configuration, liquid crystals^{3,4} and FLC's are ensembled as a thin optically uniaxial film between two dove shaped prisms. Optical routing switches¹ made with FLC's are too big to use because the critical angle of the prism for TIR is relatively large (72°). This is because of partially utilizing the

birefringence value of FLCs in defining the angle of the prism due to their selective design configuration (i.e., the rotation of optic axis by 45° for 22.5° tilt angle materials). The critical angle for TIR is also strongly temperature dependent because of the large variation of tilt angle with temperature.⁵

This letter reports a significant step forward in making a miniaturized optical routing switch using FLCs with much more temperature stable characteristic. The first step is to use a chiral nematic (N*) to smectic C* phase transition FLC mixture with a 45° tilt angle allowing the molecular and therefore the optic axis, to rotate electrically through 90° . The second is the inherent advantage of tilt angle stability with temperature thus providing the switching characteristics which are more stable over the wide range of temperature. These changes result in lower critical angle values and hence a smaller prism base angle which reduces the size of the switch. The third step is to use defect free FLC layer obtained by ordering the molecules by using only one buffed surface and applying an ac electric field.

Switch Operation

Figure 1 illustrates the basic structure of the TIR switch made using FLC material possessing chiral nematic to smectic C* phase transition. One of the indium-tin-oxide electrodes^{6,7} is coated with a nylon polymer and uniaxially buffed. the FLC material possessing the Iso-N*-SmC* phase sequence is ordered such that the optic axis is aligned along the Y-direction in one orientation and along the X-direction in the other.

Let us first consider the case in which the FLC tilt angle is 45° and n_e (extraordinary refractive index of FLC) matches with n_g (refractive index of glass). Suppose that the applied field selects the optic axis along the Y direction. When \hat{s} linearly polarized light falls on the film, its electric field is parallel to the optic axis, so the light becomes an extraordinary ray which sees the principal refractive index n_e of the FLC.

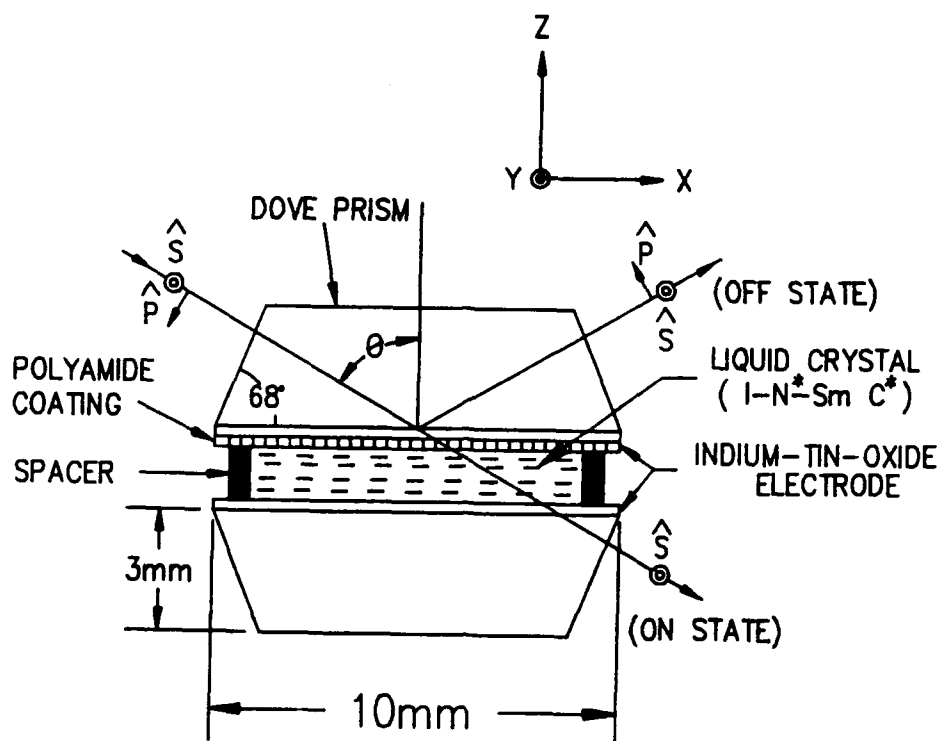


FIGURE 1 Side view of Chiral nematic-Smectic C* FLC switch, showing details of construction.

If the prism has its refractive index $n_g = n_e$, then the light will pass through the FLC prism. This is the ON state of the cell. Thus the light decomposed into ordinary \hat{p} and extraordinary \hat{s} rays sees the refractive indices given by

$$n'_p = n_0 \quad (1)$$

and

$$n'_s = n_e = n_g \quad (2)$$

For the other optic axis orientation (X-axis) the refractive indices n''_s and n''_p are given by:

$$n''_s = n_0 \quad (3)$$

and

$$\frac{1}{n_p'^2} = \frac{\cos^2\theta}{n_e^2} + \frac{\sin^2\theta}{n_o^2} \quad (4)$$

where n_o , n_e are the ordinary and extraordinary indices of FLCs. The angle θ is the angle between the direction of incidence and the Z-axis in the X-Z plane and is selected so as to give TIR for \hat{p} polarized light i.e.,

$$\theta > \arcsin \left(\frac{n_p''}{n_g} \right) \quad (5)$$

This is the OFF state of the cell.

The incident angle θ is beyond the critical angle for \hat{p} ray and is thus totally reflected. The resulting device thus switches the \hat{s} component of the incident light between transmission and reflection and always giving TIR for \hat{p} component of the incident light.

EXPERIMENTAL

The uniform alignment is obtained by treating one of the glass plates first with silane and then with a thin polyamide coating of nylon⁸ and finally buffing the prism surface. The FLC material used is CS-2004 (Chisso Corp. Japan) which is ferroelectric at room temperature having the response time around 300 μ sec at 25°C and at an applied voltage of 5V/ μ m. The material has the following phase sequence;

$$\text{Cr} \xrightarrow{-9^\circ\text{C}} \text{SmC}^* \xrightarrow{-62^\circ\text{C}} \text{N}^* \xrightarrow{-71^\circ} \text{I}.$$

The FLC material is filled between the prisms by capillary action at its isotropic temperature and then cooled slowly to smectic C* phase. An ac field of 50Hz frequency and 60 V_{pp} is applied to the cell at 61°C (1° below N*---SmC* phase transition) and is observed under a polarizing microscope (Olympus BH2). Figure 2 shows a

series of microphotographs of a $6\mu\text{m}$ thick sample of FLC. Initially the large number of focal conic domains are

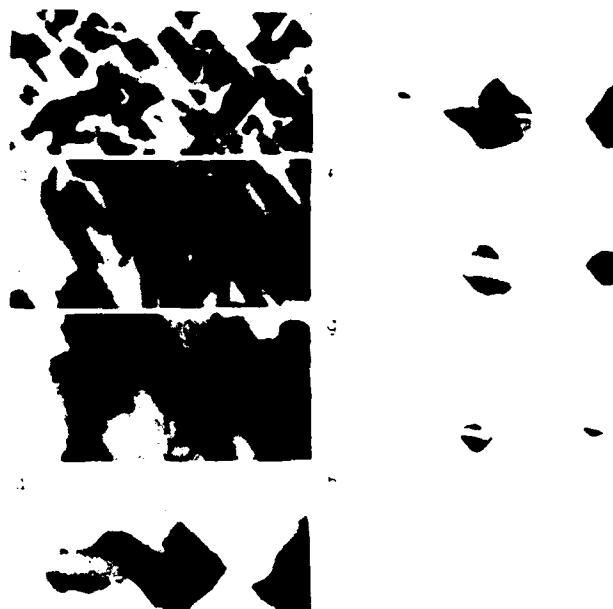


FIGURE 2 Microphotograph of a $6\mu\text{m}$ thick sample at various stages of alignment. Applied ac field is $60 V_{pp}$ at 50Hz.

formed [Figure 2(a)]. On applying ac field, the randomly aligned focal conic domains combine and reorient into a single domain as is seen through the series of micrographs [Figure 2(b-h)]. The buffing direction defines the molecular alignment direction and the smectic layers are formed at an angle 45° to this direction which is equal to the tilt angle of the smectic C* phase.

The material has a room temperature tilt angle of 44° and the optic axis moves through 88° for the two field selected states. The material has a moderate birefringence (i.e., $\Delta n = n_e - n_o = 0.15$) with $n_e = 1.65$. This value of n_e is almost equal to $n_g (=1.653)$, the refractive index of glass prisms. The optic axis orientations are chosen at an angle of 1° and 89° from the Y-axis. These directions

provide most appropriate matching of this FLC material refractive indices with that of glass. The calculated values of n_p' , n_s'' and n_p'' are 1.50, 1.50 and 1.519 respectively. The values of θ is taken as 68° (angle of prism), which is more than the critical angle for total internal reflection (66.77°), calculated for the greatest values of the n_p' , n_s'' and n_p'' with respect to n_g . The assembled aligned cell when viewed under the polarizing microscope (polarizers along X-Y directions) showed extinction in both the states irrespective of the polarity of the field. Transient light transmission is however seen during switching.

The switching was finally inspected for its operation with linearly polarized beam for a He-Ne 633 laser with 1mm collimated diameter. The incident light polarized by using Glan-Thomson prism has its polarization direction perpendicular (\hat{s}) to the plane of incidence. The cross sectional intersection of the FLC layer with the beam is an ellipse with the axes measuring ~ 1 and 2.7 mm. If the incident light is polarized in the plane of incidence (\hat{p}) the refractive indices experienced for two orientations are $n_p'(1.50)$ and $n_p''(1.519)$. The plane polarized light (\hat{p}) will thus be totally reflected in these cases. The transmitted and reflected light beams for \hat{s} polarized light for two cases of orientations do not show any apparent loss of beam quality.

The static measurements for \hat{s} polarized light show an extremely high contrast ratio of 5×10^7 in the transmitted light. The complete extinction in the off state replicate the true situation of the switching cell as there are no visible disclinations in the FLC film (Figure 2h). It has been clearly observed that the transmitted power shows no traces of leakage of the incident light. The static measurements of the switch confirm a similar behavior as observed for a 22.5° tilt angle FLC material².

RESULTS AND DISCUSSIONS

The dynamic measurements, which characterize the switching response of the switch is shown in Figure 3. The switching rise and decay behavior showed no beam interference pattern as observed by Meadows *et al.*¹ The superior switching performance of the device can be described as follow. The birefringence of the material makes its maximum contribution in defining the size and critical angle of the switch. The extraordinary refractive index (n_e) value changes from 1.65 to 1.5 in the case of 45° tilt angle FLC material whereas these values would change from 1.626 to 1.518 for nematic liquid crystal (NLC)⁴ and from 1.65 to 1.575 for 22.5° tilt angle FLC¹ material for the same n_e , n_0 and Δn value materials. The advantage of choosing a 45° tilt angle FLC material is to provide maximum permissible changes of n_s value for two optic axis orientations and thus to make smaller angle dove prisms thereby reducing the size of prisms. These advantages can be effectively

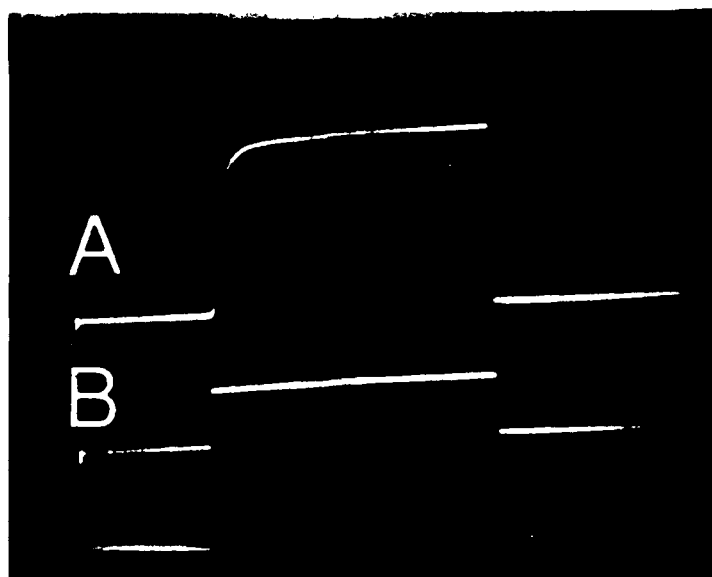


FIGURE 3: Oscillograph of the transmitted optical signal for the switch at 5Hz square wave. Applied field is $1.5\text{V}/\mu\text{m}$ (A) Optical transmission response, (B) Applied square pulse.

exploited in making large versions ($1 \times N$ and $N \times N$) non-blocking switching arrays. The 45° tilt angle FLC materials have also an inherent advantage of tilt angle stability with temperature thus providing the switching characteristics which are much more stable.

To summarize, we have proposed a miniaturized electro-optic switching cell using TIR by a chiral nematic to smectic C^* phase transition ferroelectric liquid crystal. The selection of a material with 45° tilt angle exploits fully its birefringence value and the device size could be much further reduced. This provides a large change in effective refractive indices for s component of the incident light resulting in a low value of the critical angle for TIR and thus to make a miniaturized switch. The excellent alignment of the FLC film by post treating the sample with ac field in which only one bounding surface is buffed enhances the performance on the optical switching device configuration.

ACKNOWLEDGEMENT

The authors sincerely thank Professor S.K. Joshi, Director, National Physical Laboratory, for continuous encouragement and interest in this work.

REFERENCES

1. M.R. Meadows, M.A. Handschy and N.A. Clark, Appl. Phys. Lett. **54**, 1394 (1989).
2. S.S. Bawa, A.M. Biradar, K. Saxena and S. Chandra, Appl. Phys. Letts. **57**, 1479 (1990).
3. J. Skinner and C.H.R. Lane, IEEE J. Selected Areas Commun. **6**, 1178 (1988).
4. R.A. Soref, Appl. Opt. **21**, 1386 (1982).
5. C. Oldano, Phys. Rev. Letts. **53**, 2413 (1984).
6. J.S. Patel and J.W. Goodby, J. Appl. Phys. **59**, 2355 (1986).
7. S.S. Bawa, A.M. Biradar and Subhas Chandra, Jpn. J. Appl. Phys. **25**, L446 (1986).
8. J.S. Patel, T.M. Leslie and J.W. Goodby, Ferroelectrics **59**, 137 (1984).

CONTROLLING THE GREY LEVEL CAPACITY OF A BISTABLE FLC SPATIAL LIGHT MODULATOR

M. KILLINGER, J.L. DE BOUGRENET DE LA TOCNAÏE AND P. CAMBON

Groupe Optique et Systèmes de Communications

E.N.S.T. de Bretagne, BP 832, 29285 Brest Cédex, France

Abstract Due to their memory, non-linear response and threshold, as well as their grey level capacity, ferroelectric liquid crystal spatial light modulators are useful devices for optical implementations of neural networks. We propose a phenomenological explanation of the roles, the different driving parameters like the voltage, the current and the length of the addressing pulse play in achieving and controlling these grey levels. Finally we discuss a possible optical implementation of a self organizing memory based on the model of the Kohonen map, using optically addressed SLMs.

INTRODUCTION

Although SSFLC devices are basically bistable devices, it is possible to obtain grey levels under certain driving conditions^{1,2}. The cell does then not switch uniformly, but shows a grained structure which stems from the appearance of black and white domains. Averaging the optical response over a given area results in the impression of grey. The memorized grey level is determined by the ratio of black and white domains which can be influenced by the driving conditions. This property can be utilized for analog optical computing applications, such as neural networks. One advantage of using a bistable device to produce grey levels with regard to other materials like nematics is the memory of the device. The grey levels can be stored and in the case of an optically addressed SLM the read and write operation can be carried out with light of the same wavelength. This reduces considerably the architectural complexity in cascaded architectures and allows optical feedback.

One possible application concerns the representation of the synaptic weights in neural networks. In order to enable learning these weights have to be updated. Since the device can memorize the grey level the weight updating is simply achieved by applying

an additional electrical pulse, whose polarity determines if a previously memorized grey level is reduced or increased.

Our experiments have been carried out on an electrically addressed SLM but the observations apply also to optically addressed devices³.

MULTI-DOMAIN SWITCHING

Applying an electric field to an FLC device leads to reorientation of the molecules due to interaction between the external field and the spontaneous polarization of the molecules. Two distinct orientations, UP and DOWN, are stabilized by surface interactions and the molecules maintain these orientations even in the absence of an external field. The switching is accompanied by the flow of charge which compensates the spontaneous polarization of the FLC molecules at the surface of the cell. The surface charge and the area of the cell which is in the UP and DOWN state, respectively are proportional.

Inversely, the amount of charge that is applied to a cell controls, under certain driving conditions, the area of the cell that is switched because the molecules reorient so that their spontaneous polarization compensates this surface charge. This behavior is called charge controlled switching².

To switch the whole surface A_{\max} of a cell from one bistable state to the other, a charge $Q_{\max} = 2P_s A_{\max}$ has to be applied, with P_s being the spontaneous polarization of the liquid crystal. Applying a charge $Q < Q_{\max}$ will consequently only suffice to switch an area $A < A_{\max}$, leading to the formation of black and white domains. The spatial distribution of these domains is determined by the more or less random distribution of defects in the smectic layer structure which act as nucleation sites for the domains.

Since the observation of grey levels is a spatial phenomenon, the size of the observed spot will be one of the parameters which determine the characteristic of the optical response curve. This spot cannot be made arbitrarily small without affecting the grey level behavior. In order to obtain a uniform optical response over the whole surface of the cell, this spot size is also determined by the uniformity of the spatial distribution of nucleation centers. Since our cells have not been optimized with regard to this point, the minimum spot size is relatively large (several 100 μm).

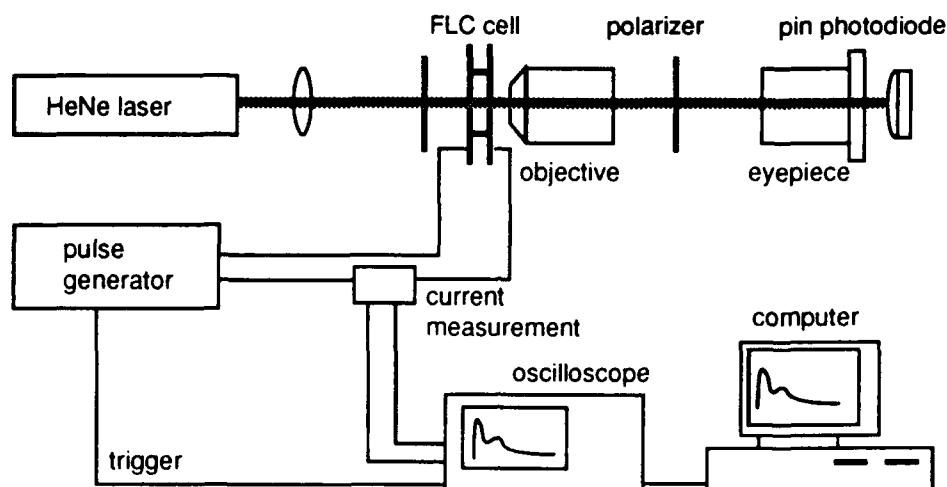
EXPERIMENTAL SETUP

FIGURE 1 Schematic of the experimental set-up. The pulse generator is either a voltage pulse generator (short circuiting the cell between the pulses) or a current pulse generator (leaving the cell electrically isolated between the pulses).

The measurements have been carried out on a test cell manufactured by STC Technology. The active area of the cell is 4 mm^2 . The two glass plates are covered with a conducting ITO layer, the spacing of the cell which is controlled by polystyrene spheres is $1.5 \mu\text{m}$. The FLC used in this cell was the SCE 13 mixture from BDH Ltd. The orientation of the FLC is obtained with alignment layers made up of obliquely evaporated SiO. The quasi bookshelf geometry is obtained by applying a 35 volts square wave, 20 Hz for about 1 minute. The cell is then truly bistable, the switching angle between both bistable states is twice the smectic cone angle and no relaxation can be observed.

The cell was set up between two crossed polarizers. The measurements of the optical response were made by illuminating the cell from behind with the collimated beam of a 633 nm HeNe Laser. A pin-photodiode placed behind the eyepiece allowed to measure the optical response. Simultaneously the current through the cell was measured. When using the voltage pulse generator in form of the voltage across a 50Ω resistance in series with the cell and when using the current pulse generator directly with a current probe (Tektronix A6302). A MacintoshII computer allowed via a HP-IB interface the acquisition of the waveform and a visualization and postprocessing of the signal.

The output voltage of the photodiode was a measure for the optical response. The applied charge can be deduced by integrating the current over the time. In order to determine the charge that leads to the switching of a given area the electrical response when switching the cell was compared with the response when no switching occurred. The difference of the charge corresponds to the charge that accompanies the switching and is a direct measure of the switched area.

EXPERIMENTAL RESULTS

Unless otherwise stated, the experiments have been carried out on the above described test cell. The driving conditions were as follows: First a negative pulse ($V=-30$ volts, $T=1$ ms) was applied to reset the total area. Then the electro-optic response to a positive pulse set pulse was observed, varying the pulse width and amplitude. Between the pulses the device was short circuited.

Measurements of the electro-optic response

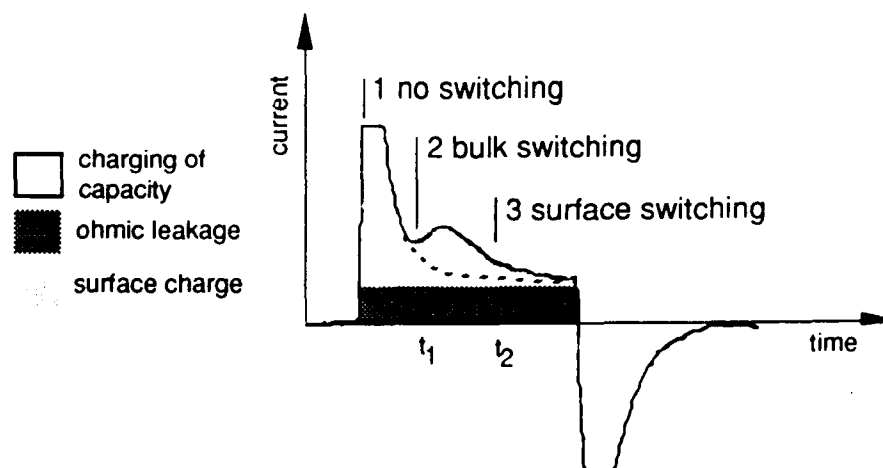


FIGURE 2(a) Current through the cell when applying a voltage pulse.

Figure 2 shows a typical response. The current through the cell, when a switching pulse is applied is the result of different contributions. The cell is basically a transparent capacitor whose dielectric consists of the FLC filling. The major contribution to the current stems from the charging of this capacity, and is of the form of a decreasing exponential function. A second contribution is due to ohmic leakage and ionic conductivity of the cell. This current depends linearly on the applied voltage. The third

contribution stems from the the reorientation of the molecule director \mathbf{n} and the macroscopic polarization \mathbf{P} which induces a transport of surface charges.

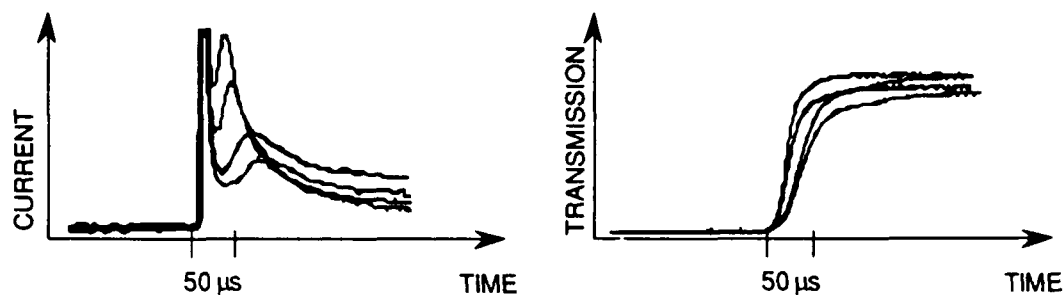


FIGURE 2 (b) Electro-optical response for voltages between 7.5 and 20 volts.

The optical response time is the time during which the optical response increases from 10% to 90% of the final value. After applying a voltage pulse the molecules begin to reorient after a time that corresponds to the end of the first peak. This time t_1 , as well as the optical response time, depend on the applied voltage. The optical response coincides with the second peak of the current. Applying a higher voltage moves the peak to the left and makes it smaller and higher, an indication that the molecules are reorienting faster.

Transient and memorized states

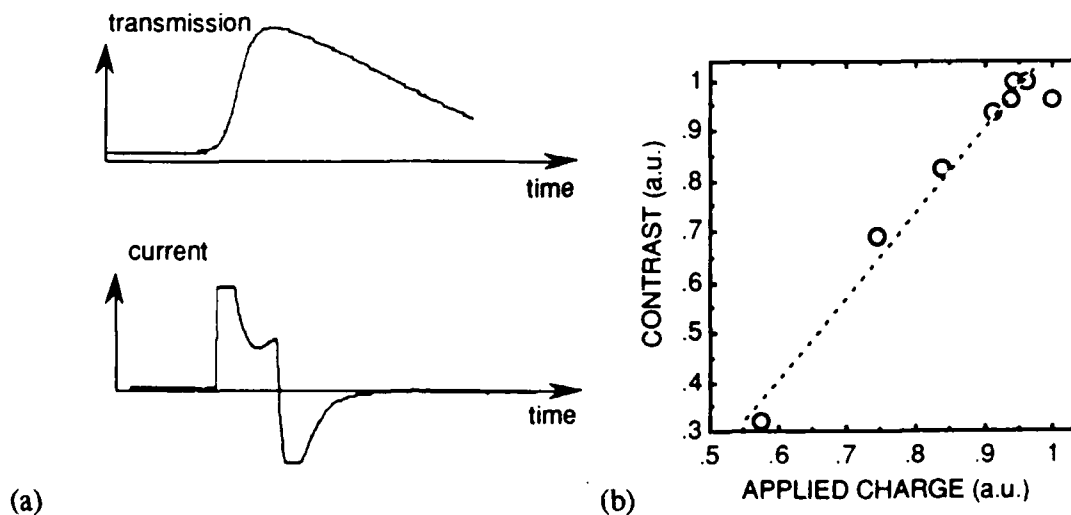


FIGURE 3 Applying a pulse which is too short to permanently reorient the molecules. The curve 3(b) shows the relation between applied charge and optical response. It can be seen that a minimum charge has to be applied to obtain a memorized optical response.

A permanent change of the optical response can only be observed if the switching pulse has been applied long enough. This minimum time t_2 coincides approximately with the "end" of the second peak. Three regimes can be distinguished. For $t < t_1$ no optical response is observable, for $t_1 < t < t_2$ a transient optical response can be observed, and only when a pulse is applied for $t > t_2$ can a memorized optical response be obtained.

A possible explanation would be the different behavior of the molecules in the bulk and near the surface. The molecules in the bulk switch faster and more easily than the ones near the surface. In order to form memorized domains which do not relax after the pulse, these domains have to grow to the surface where they can be stabilized by surface forces. If this is not the case, the bulk domains relax after the pulse back to their initial orientation^{2,4}.

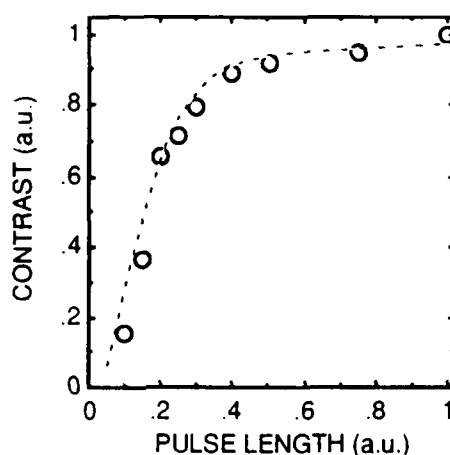


FIGURE 4 Variation of the length and amplitude of the applied pulse at the same time. Although the Vt area has been kept constant at $10^{-2}Vs$, varying the applied voltage results in a different optical response. The voltage was between 4 and 20 volts, the pulse length between 2.5 ms and 500 μ s.

Figure 4 shows the response that has been obtained by keeping the product Vt constant. It can be seen that keeping the Vt -area constant is not sufficient to obtain always the same optical response. This observation may be explained as follows. Firstly, there is a threshold voltage to switch the domains. A visual observation of the switching shows that domains switch at different voltages. Repeated switching at a given voltage forces always the same domains to switch. A visual inspection of the cell under a polarizing microscope reveals a correlation between the appearance of domains and defects.

Some domains do not switch at a given voltage, even if the pulse was applied for a very long time. This explains why below a minimum voltage a decrease of the pulse height can not be compensated by increasing the pulse length. An additional explanation

can be given with help of Figure 2. It can be seen that varying the pulse height not only shifts the second peak to the left, but also changes the shape of the curve. In order to compensate for a decreasing pulse height, the pulse length has therefore to be increased more than proportionally.

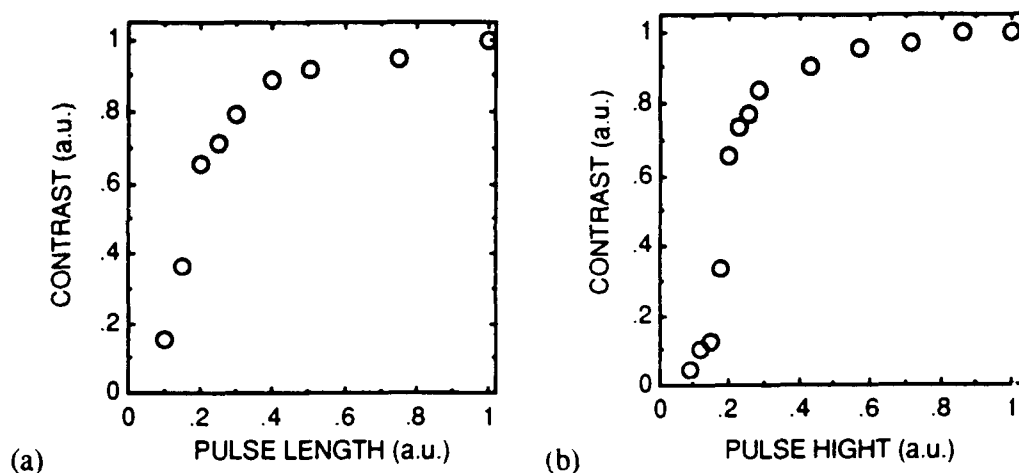


FIGURE 5 (a) The electro-optic response of the cell when varying the pulse length (200 μ s-2ms) at a constant voltage(10volts). (b) when varying the voltage (4-35volts) and keeping the pulse length constant (1ms).

Figure 5 show the optical response as a function of the pulse length and the pulse height, respectively, with one of the parameters held constant. One can see that the variation of either one of these parameters yields basically the same result, with the distinction that varying the pulse height has a stronger impact which can be explained with the same arguments as above.

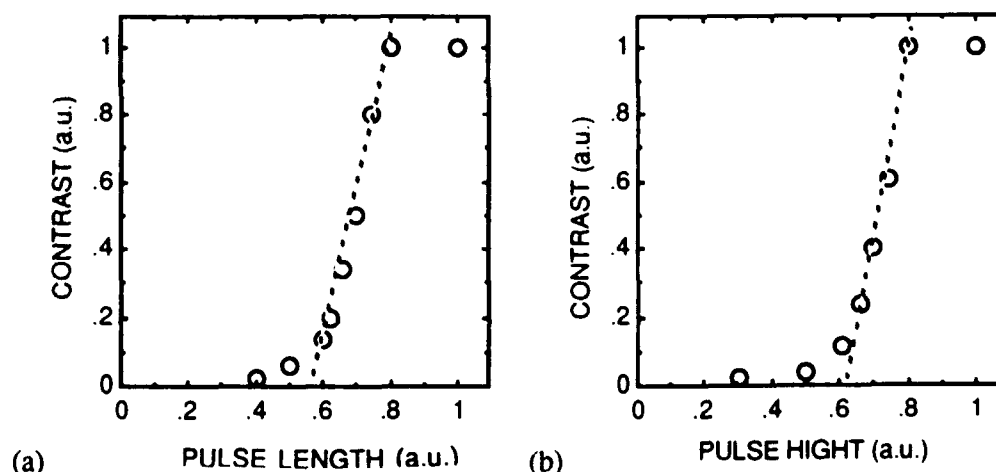


FIGURE 6 (a) The electro-optic response of the cell when varying the pulse length (20-40 μ s) at a constant current (100 μ A), (b) when varying the current (150-370 μ A) at constant pulse length (10 μ s). Here current pulses were applied instead of voltage pulses.

Figure 6 shows the addressing with current pulses. In this case the addressing scheme was different from the above mentioned in that the device was electrically isolated between the pulses. In this case the dynamical behavior of the FLC played a less important role since the switching itself was not directly influenced by the time the pulse was applied. In this case the variation of height and length of the pulses have exactly the same effect. Applying current pulses allows a direct control of the charge. The optical response as a function of these parameters shows a significantly different form than in the case of voltage addressing. This is a result of the fact that between the pulses the device was isolated and the charge controlled behavior of the cell becomes evident.

In another experiment we measured the optical response when applying subsequent pulses without intermediate reset pulses. This would correspond, for example, to a weight updating in a neural network. Figure 7 shows the result for the two modes of addressing. It is evident, that the electrical isolation between the pulses in the case of the current pulses leads, because of the charge controlled behavior of the cell, to a linear relation between the number of pulses and the obtained grey level. In the case of the voltage addressing, where the cell is only short circuited between the pulses, the switching dynamic of the liquid crystal plays an important role and the charge controlled behavior is much less important, leading to a non-linear dependency of the grey level and the number of applied pulses.

The same device can therefore exhibit linear as well as non-linear behavior, depending on the way it is operated. This results in a multiple choice for the grey level storage function which gives a large field of possible optical implementations of complex algorithms for unsupervised learning^{7,8}.

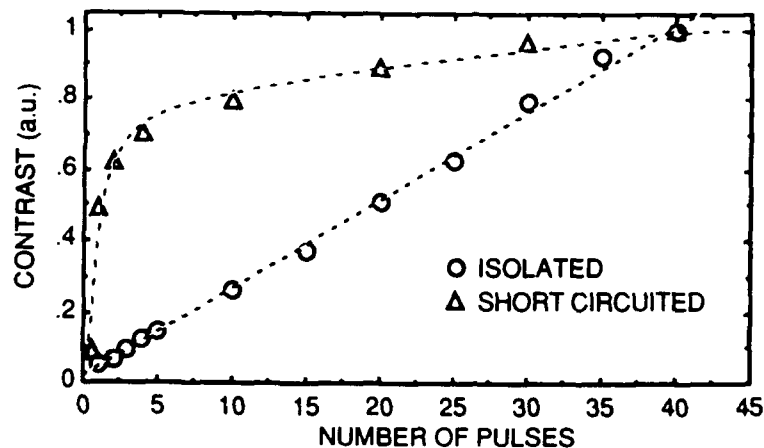


FIGURE 7 Applying subsequent pulses without intermediate reset. The electrical isolation of the cell in the case of the current pulses leads to a control of the switching by the applied charge and consequently to a linear behavior.

DISCUSSION

An SSFLC cell is bistable due to surface interaction between the molecules and the alignment layer. Applying an electric field across the cell forces the molecules in the bulk to switch faster than the molecules near the surface where they have to compete against the mechanical surface forces. When the pulse is not applied long enough to allow these bulk domains to grow to the surfaces, where they are stabilized, they switch back after the pulse has ended.

When using the voltage pulse generator (where the device is short circuited between the pulses) the switching has to occur during the time the pulse is applied. The length of the pulse affects directly the size of the permanently switched area and a charge controlled behavior is not observable. This kind of control of the grey level is nonlinear.

In the case of the current pulses (the device is electrically isolated between the pulses) the charge controlled behavior is the primary cause for obtaining the grey levels. Above a certain threshold the switched surface depends linearly on the pulse length and pulse height.

Optically addressed devices based on the modulation of the conductivity of a photosensitive layer introduce an additional nonlinearity, since the voltage that drops across the FLC layer depends nonlinearly on the applied light. This kind of device is therefore well suited for non linear applications.

Photodiode devices, especially the one presented in ⁶ (nipin photodiode structure), have already intrinsically the capacity of a charge controlled operation. The photodiode acts as current generator whose current depends linearly on the applied light and pulselength. Furthermore, the FLC is isolated when no light is applied. These devices seem suited to applications in which a precise control of the grey level behavior of a bistable FLC light modulator is necessary.

POSSIBLE APPLICATION IN NEUROCOMPUTING

The main limitation of optical implementations of neural architectures lies generally in the inadequacy of optics when it comes to implementing complex learning procedures. This is the reason why the optical loop is often opened up and a digital computer is employed to implement this crucial stage^{1,9}. The previously described observations can be used

advantageously to propose an original optical solution in the simple case of unsupervised learning⁸. This, however, requires the use of optically addressed SLMs¹⁰.

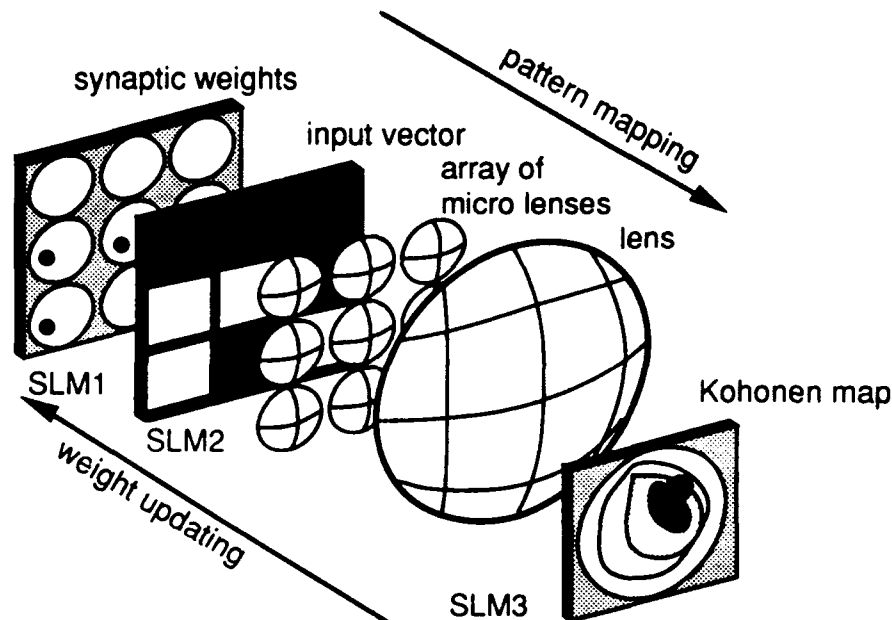


FIGURE 8 Schematic of an all-optical implementation of a self organizing memory based on the Kohonen map. Depicted is the learning stage.

The basic setup is made up of three interconnected planes, represented by three SLMs (Figure 8). The first (optically addressed) SLM contains the synaptic weights, SLM2 (addressed optically or electrically) contains the input vector and SLM3 (optically addressed) represents the neural plane. The function of this third plane is to threshold and store the result of the vector-matrix product of plane 1 and plane 2 which is obtained by a simple crossbar system⁹.

The principle of the weight updating is the following. The grey level is spatially encoded, as explained earlier, and it can be updated by spatial accumulation, obtained by successive illuminations. The information that has been thresholded and stored in SLM3 (neural plane) is fed back into the system. Only those weight areas whose contribution to the formation of the neural map has been decisive are optically addressed and their grey level is then updated by spatial accumulation. This process can be seen as an optical implementation of the "winner-take-all" algorithm, based on adjustable thresholding. It is repeated until stable areas appear on the neural map. The dynamic behavior and convergence are governed by the choice of both the threshold level and the linear or non linear function which has been chosen for the grey level encoding.

REFERENCES

1. K.M. Johnson, G. Modell, Applied Optics, Vol. 28, No. 22, pp4888-4899, (1990).
2. W.J.A.M. Hartmann, J.Appl.Phys., 66, pp1132-1136, (1989).
3. J.-L. de Bougrenet de la Tocnaye, J.R. Brocklehurst, Applied Optics, Vol. 30, No 2, pp179-180, (1991).
4. M.A. Handschy, N.A. Clark, Ferroelectrics, Vol.59, pp69-116, (1984).
5. C. Latouche, De quelques aspects fondamentaux et appliqués de cristaux liquides ferroélectriques, doctoral dissertation, Université Bordeaux, (1991).
6. P. Cambon, M. Killinger, J.L. de Bougrenet de la Tocnaye, SPIE 1991 Symposium Optical Applied Science and Engineering, San Diego, to be published.
7. T. Kohonen, IEEE Proceedings, Vol. 78, No 9, pp1464-1480, September(1990).
8. J. Duvillier, J.L.de Bougrenet de la Tocnaye, submitted to Proc.Neural networks and their applications, Neuro-Nîmes (1991)
9. P.J. de Groot, R.J. Noll, Applied Optics, Vol. 28, pp3852-3859, (1989).
10. M. Killinger, J.L. de Bougrenet de la Tocnaye, P.Cambon, R.C. Chittick, submitted to Applied Optics.
11. M.G. Robinson, K.M. Johnson et al., Proc.Optical.Computing, Salt Lake City, pp84-87, (1990).

PHOTOVOLTAIC OPTICALLY ADDRESSED SPATIAL LIGHT MODULATOR

C. C. MAO, B. LANDRETH, K. M. JOHNSON, and G. MODEL

Department of Electrical and Computer Engineering

University of Colorado at Boulder, Boulder, U. S. A.

Abstract We present the physical structure of and experimental results on a photovoltaic optically addressed spatial light modulator. The device is composed of a photosensor with a stack of four $p-i-n$ photodiodes and a ferroelectric liquid crystal light modulator. The spatial resolution is 20 lp/mm^2 and the *ON/OFF* contrast ratio is 10:1. An optical novelty filtering system using this device is also presented.

INTRODUCTION

Optically addressed spatial light modulators (OASLMs) have been used in performing real-time incoherent to coherent light conversion,¹ joint transform correlation,^{2,3} optical phase conjugation⁴⁻⁷, real-time holography⁸, and the optoelectronic implementation of neural networks.⁹⁻¹¹ Most OASLMs are hybrid electro-optic devices, which operate with an externally applied ac electric field.¹²⁻¹⁸ Writing and reading an optical pattern is usually performed during the negative cycle of an applied ac electric field. The device is refreshed during the positive cycle of the electric field, unless the device operates in an integration mode.¹⁹ The periodic refreshing may be undesirable or inconvenient for some applications. In this paper, we describe a new photovoltaic OASLM that does not require an externally applied ac electric field. It utilizes a stack of four hydrogenated amorphous silicon (a-Si:H) photodiodes operating in the photovoltaic mode, powered only by the photogenerated charge from the incident write-light illumination. In section II, we describe the physical structure of the device and in section III, present the experimental results characterizing the photovoltaic OASLM. In section IV, we demonstrate novelty filtering of images using this device. Finally, the key points of this paper are summarized in section V.

DEVICE DESCRIPTION

The novel photovoltaic OASLM, shown in Fig. 1, consists of a stack of four amorphous silicon (a-Si:H) photodiodes and a ferroelectric liquid crystal (FLC)

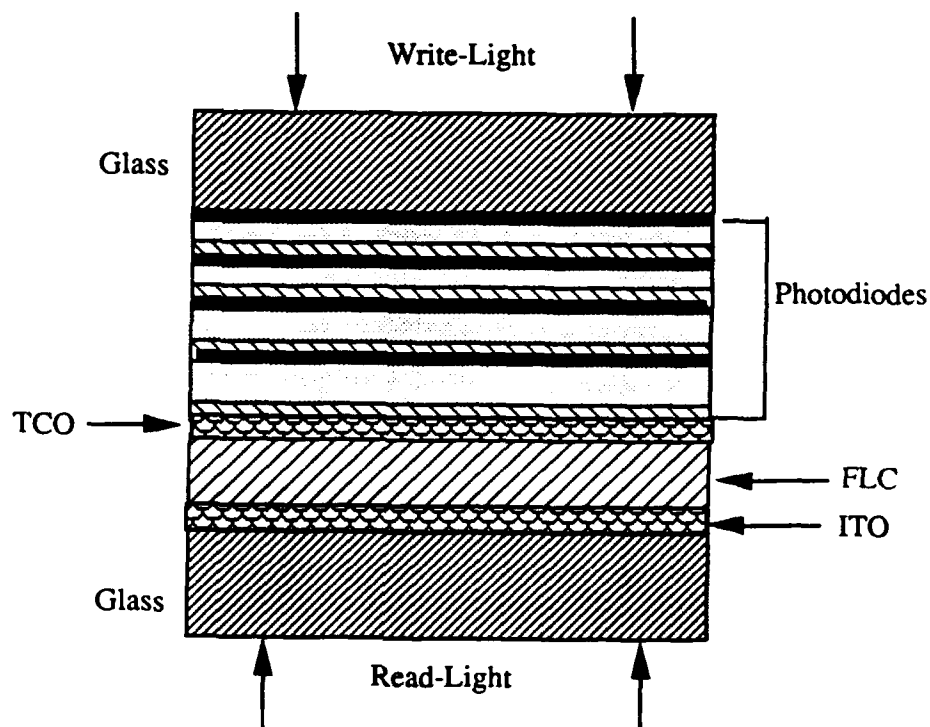


FIGURE 1. Photovoltaic optically addressed spatial light modulator comprising a stack of four hydrogenated amorphous silicon $p-i-n$ photodiodes and a ferroelectric liquid crystal light modulator.

modulator. The $p-i-n$ photodiodes are deposited onto a glass substrate coated with a transparent conducting oxide (TCO). The diode structure consists of a $\sim 100 \text{ \AA}$ boron-doped p -layer, an intrinsic layer, and a $\sim 100 \text{ \AA}$ phosphorous-doped n -layer. The thickness of each intrinsic layer is optimized such that it absorbs the same fraction (20%) of incident He-Ne laser light ($\lambda = 632.8 \text{ nm}$). The four intrinsic layers have thicknesses of $0.18 \text{ }\mu\text{m}$, $0.23 \text{ }\mu\text{m}$, $0.32 \text{ }\mu\text{m}$, and $0.50 \text{ }\mu\text{m}$, respectively. The other glass substrate is coated with an indium-tin oxide (ITO) transparent electrode. A $1 \text{ }\mu\text{m}$ gap between the a-Si:H photodiode stack and the ITO coated glass substrate is maintained for a liquid crystal modulator. The liquid crystal material used in this device is a SCE-13 FLC mixture.²⁰ Alignment was achieved with a rubbed polymer layer. The active area of the device is 13 mm in diameter.

A simple equivalent circuit for the photovoltaic OASLM is shown in Fig. 2. The incident He-Ne write beam is absorbed in the four photodiode intrinsic layers, generating electron-hole pairs. The photodiode internal electric field²¹ causes the electrons to drift towards the n -layer and the holes towards the

p-layer. Under constant illumination, this process continues until the voltage across the junction balances the internal electric field. Connecting the two electrodes (TCO and ITO) produces approximately 3 V across the liquid crystal layer, when the device is illuminated with a He-Ne laser beam. Therefore, a spatially varying write-light beam will be replicated in the form of a spatially varying voltage across the FLC modulator. When the voltage in the illuminated areas is high enough to locally switch the liquid crystal, the FLC optic axes in these areas are rotated by 45° .²² This corresponds to the *ON* state of the device. When the light is removed, the liquid crystal switches back to the *OFF* state by discharging the field through the resistors, R_{LC} or R_{sh} . In the non-illuminated regions, the FLC optic axes maintain their original orientation. We refer to this state as the *OFF* state of the device. By illuminating the device with a uniform read-light beam from FLC side, the incident optical intensity pattern is displayed, through an output analyzer.

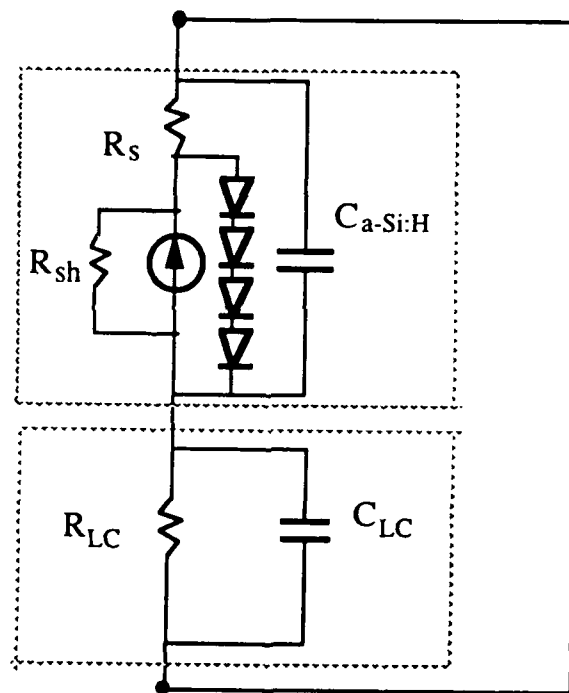


FIGURE 2. Equivalent circuit of the photovoltaic optically addressed spatial light modulator, in which the upper block represents the photodiodes and the lower block the liquid crystal light modulator.

EXPERIMENTAL RESULTS

The experimental apparatus used to measure the spatial resolution of the photovoltaic OASLM is shown in Fig. 3. A collimated He-Ne laser beam ($\lambda = 632.8 \text{ nm}$) illuminates a US Air Force (USAF) resolution test chart. Lens L_1 images the resolution test chart onto the a-Si:H photodiodes. A horizontally polarized, collimated He-Ne laser beam is incident upon the FLC side of the OASLM through a polarizing beam splitter PBS . The read-beam is partially reflected ($\sim 20\%$) at the FLC/a-Si:H interface, and analyzed by PBS . The OASLM is oriented such that the optic axis of the FLC in the *OFF* state is parallel to the polarization of the incident read light. Therefore, in the non-illuminated regions, the reflected read-beam remains horizontally polarized and is transmitted through the PBS . The reflected read-light beam, corresponding to the illuminated regions, undergoes a 90° polarization rotation and is reflected by the PBS . Lens L_2 collects the reflected light and images the pattern on the OASLM into the CCD camera. The image of the resolution test chart imaged by the CCD camera is displayed on a TV monitor. A photograph of the output pattern is shown in Fig. 4. This USAF resolution test chart image shows that the device is capable of resolving 20 lp/mm at a write-light intensity of 0.6 mW/cm^2 . In this experiment, a $+1.5 \text{ V}$ dc bias was applied across the device to help the device fully switching off. Without this dc bias, the turn-off time is longer than 1 s . The dc bias may reduce the discharging time, which is a function of the liquid crystal resistance, and produce a -1.5 V *OFF* state voltage, which also affects the turn-off time. With a bias, the turn-off time is reduced to 5 ms so that the device works better than without a dc bias.

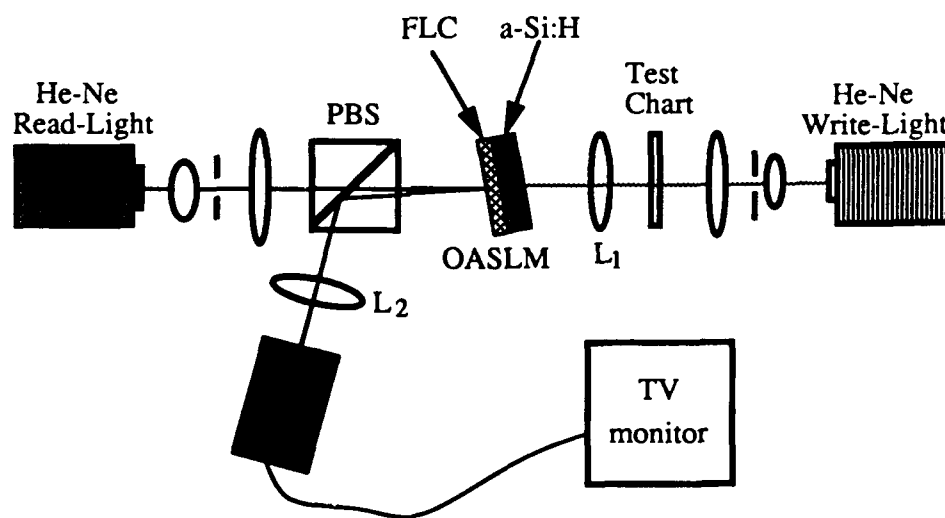


FIGURE 3. Experimental apparatus for measuring the spatial resolution of the photovoltaic optically addressed spatial light modulator.

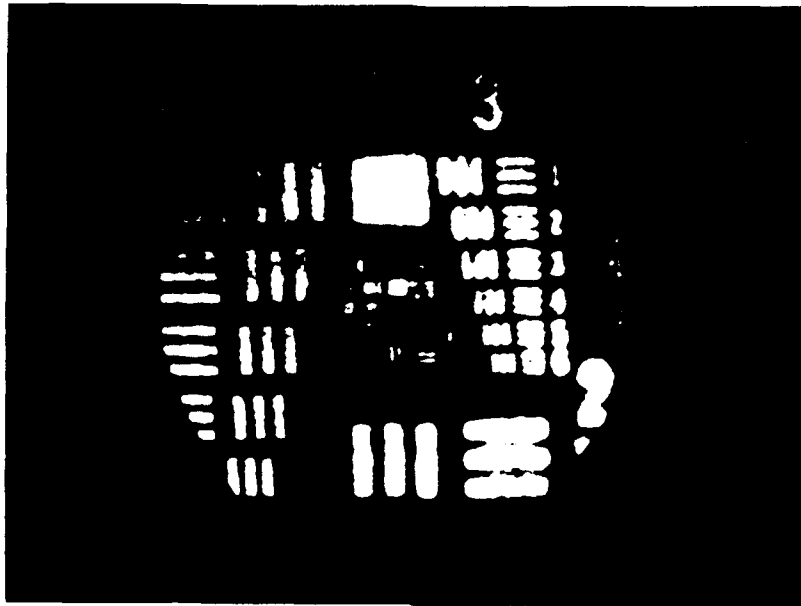


FIGURE 4. Photograph of a US Air Force resolution test chart reproduced by the photovoltaic optically addressed spatial light modulator, showing a resolution of 20 lp/mm.

The *ON/OFF* contrast ratio was measured by using an experimental arrangement similar to that shown in Fig. 3. Here, the *CCD* camera was connected to an oscilloscope and three pairs of straight lines on the USAF resolution test chart were imaged onto the a-Si:H photodiodes by lens L_1 . The spatially varying image intensity is shown in Fig. 5. This oscilloscope trace shows that the device has an *ON/OFF* contrast ratio of 10:1 and the response to the write-light is fairly uniform. To test the average contrast across the entire OASLM area, we placed a mechanical chopper (Stanford Research Systems Model SRS40) in front of the He-Ne laser used in producing the write light, removed the resolution test chart, and used a single photodetector to detect the read-out signal. The oscilloscope trace is shown in Fig. 6. The horizontal line represents the reference voltage when the read-light is blocked. The average contrast ratio shown in Fig. 6 is approximately 10:1. The response time of the device was measured by monitoring the chopped write-light and the modulated read-out-light beams using two photodetectors. Fig. 7 shows the oscilloscope traces, in which the upper trace represents the write-light intensity and the lower trace the read-out intensity. The rise time (10% - 90%) is approximately 3 ms and the fall time (90% - 10%) is approximately 5 ms.

OPTICAL NOVELTY AND MONOTONY FILTERING

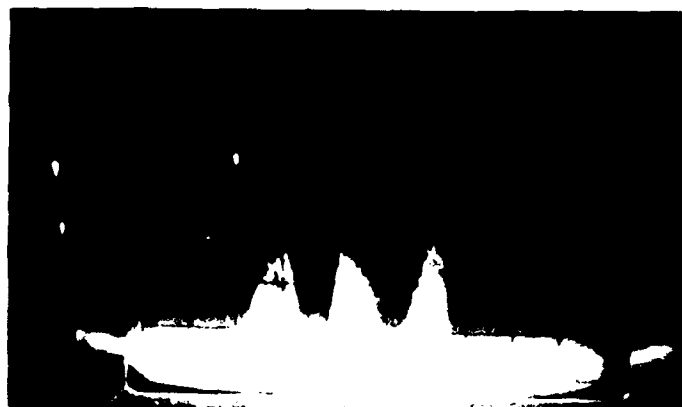


FIGURE 5. Oscilloscope trace of the read-out image of a three-line object, showing a contrast ratio of 10:1.

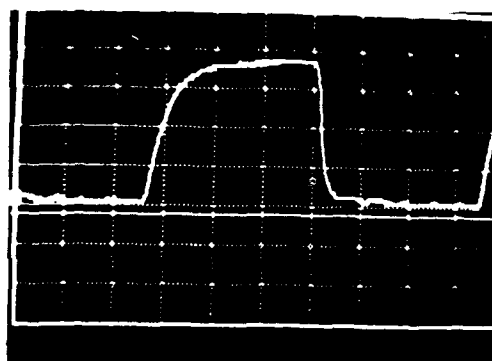


FIGURE 6. Oscilloscope trace showing the average contrast ratio of the photovoltaic optically addressed spatial light modulator. The horizontal line represents the reference voltage obtained by blocking the read-out light beam and the upper curve the read-out intensity when the write-light beam is chopped by a mechanical copper.

A novelty filter draws our attention to what is new or novel in a scene of interest. On the other hand, a monotony filter selectively displays only the stationary objects in a scene. Novelty and monotony filters have been demonstrated using real-time materials such as photorefractive crystals.²³⁻²⁹ In this section, we describe optical novelty and monotony filtering using the photovoltaic OASLM. This OASLM-based filter has the following advantages over photorefractive crystal based systems: (1) Incoherent light can be used; (2) The operating optical power is less than 2 mW/cm^2 ; (3) It has higher temporal

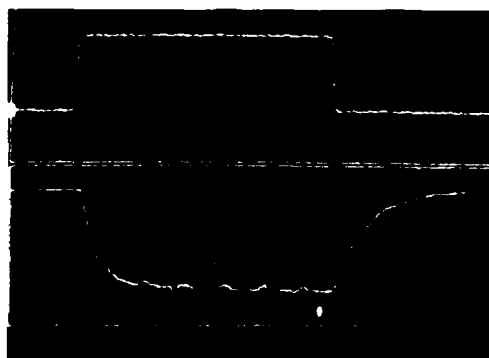


FIGURE 7. Oscilloscope traces showing the optical response of the optically addressed spatial light modulator. The upper trace shows write-light modulation, and the lower trace the read-light response. Horizontal scale: 5 ms/div.

resolution; (4) The response time of the OASLM is less dependent on the input scene intensity; (5) It is very easy to change the system from the novelty filtering mode to the monotony filtering mode to implement an optical tracking system. The disadvantages compared to photorefractive crystal based systems include: (1) The system has a smaller dynamic range of the detectable speeds of moving objects; (2) It has a lower contrast ratio; (3) It cannot amplify the images of moving objects surrounded by a uniformly bright background when operated in the novelty filtering mode.

The optical novelty and monotony filtering system using the photovoltaic OASLM is shown in Fig. 8. A He-Ne laser beam ($\lambda = 632.8 \text{ nm}$) is transmitted through polarizer P_1 and incident upon the a-Si:H photodiode side of the OASLM. The OASLM is oriented such that the optic axis of the FLC in the *OFF* state is parallel to the transmission axis of the entrance polarizer. Part of the incident He-Ne laser light is absorbed by the a-Si:H layer of the OASLM. The remainder of the light is transmitted through the device. An FLC cell is positioned behind the OASLM, whose optic-axis in one state is parallel to the transmission axis of P_1 . A second polarizer, P_2 , oriented parallel to the entrance polarizer, is positioned behind the FLC cell. When light suddenly illuminates the OASLM, it initially maintains its original polarization and is transmitted by P_2 . After the OASLM has time to respond to the incident optical signal, the polarization of the light transmitted through the OASLM is rotated by 90° , and blocked by P_2 . Therefore, P_2 transmits time varying incident light and blocks constant illumination, thus performing image novelty filtering. Fig. 9 shows the oscilloscope trace of the output optical signal, which is triggered only at the rising edge of the chopped incident optical signal. Switching the optic axis of the FLC cell by 45° changes the system to a monotony filter. When the light continuously illuminates the OASLM, the light transmitted through

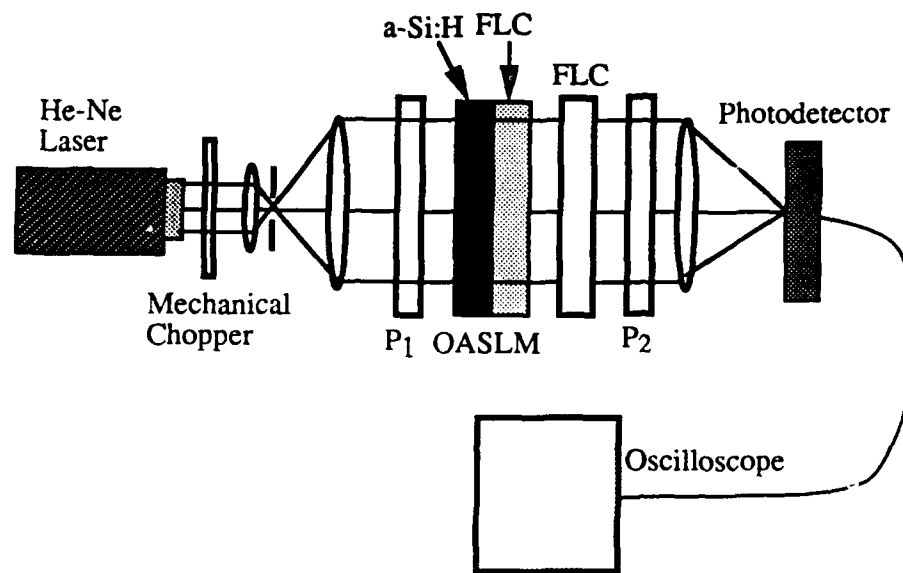


FIGURE 8. The diagram of the optical tracking system. P - polarizer.

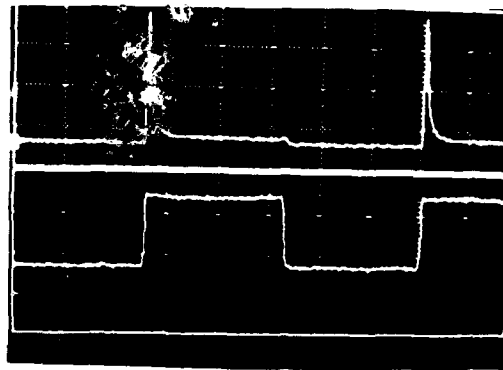


FIGURE 9. Oscilloscope traces showing the novelty filtering. The upper one represents output optical signal and the lower one the input optical signal.

the OASLM undergoes a 90° polarization rotation. Since the FLC optic-axis has an angle of 45° with the polarization of the transmitted light, it rotates the light polarization back to the original orientation. Hence, the light is transmitted through P_2 . If the incident light changes faster than the response time of the OASLM, the transmitted light through the OASLM and FLC cell has a

90° polarization rotation and hence is blocked by P_2 .

The experimental apparatus for demonstrating image optical novelty and monotony filtering is shown in Fig. 10. A collimated He-Ne laser beam is horizontally polarized and illuminates a SEIKO liquid crystal TV (Model Number LVD-012). The object displayed on the LCTV is controlled by an IBM PC computer. The transmission axes of the two polarizers, P_1 and P_2 , are aligned with the polarization of the incident light. Lens L_1 images LCTV display onto the a-Si:H photodiode stack of the photovoltaic OASLM. The transmitted light ($\sim 20\%$) through the OASLM propagates through the FLC cell and then is analyzed by polarizer P_3 , which has a parallel transmission axis to the other two polarizers. A CCD camera detects the output optical signal. For these experiments, we used a square object displayed on the LCTV. We first demonstrated novelty filtering with the optic-axis of the FLC cell parallel to the transmission axes of the polarizers. When the object was moving around the LCTV screen, the CCD camera detected the image. When the object stopped moving, the image of the object disappeared. The monotony filtering was performed by rotating the optic-axis of the FLC cell by 45° . Here, the CCD camera only detects the image when the object stops moving. In the novelty filtering mode, the image contrast ratio between a moving object and a stationary object is approximately 3:1. In the monotony filtering mode, the image contrast ratio between a stationary object and a moving object with a speed faster than the response time of the OASLM is approximately 8:1.

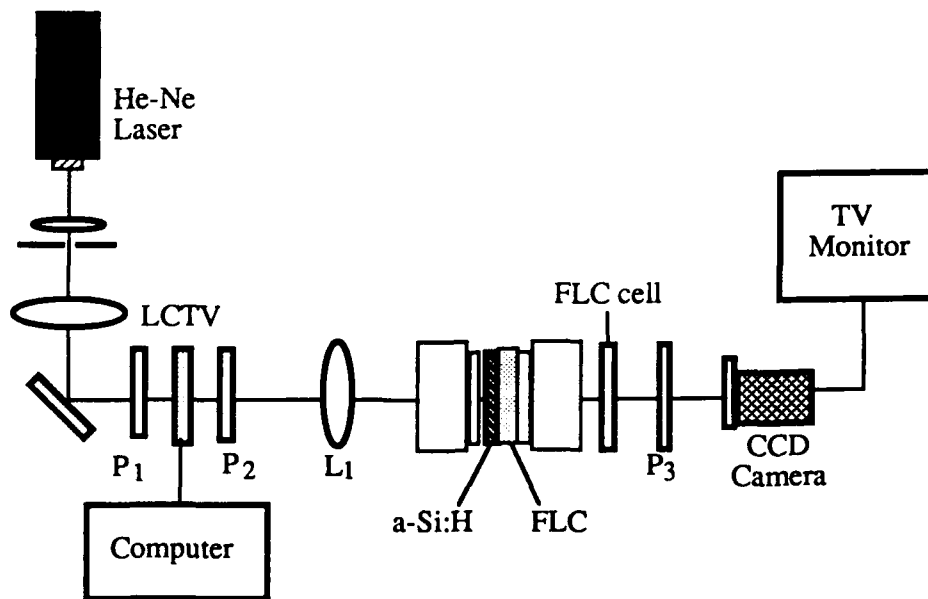


FIGURE 10. The experimental apparatus for demonstrating optical tracking.
P - polarizer, LCTV - liquid crystal TV.

These experimental results show that the system has a lower contrast ratio for novelty filtering than for monotony filtering. This is due to the slow modulation time of the LCTV. The rise time of the modulated light intensity is greater than 10 ms, which is much longer than the response time of the photovoltaic OASLM (3 ms). Hence, the OASLM has responded to the incident optical signal before the LCTV has the highest output intensity. Therefore, the light intensity transmitted by the OASLM is lower for a moving object displayed by a slow modulating device than it would be with a faster modulating device. The slow modulation time of the LCTV does not affect the contrast ratio of the monotony filtering, because the system amplifies the images for stationary objects.

CONCLUSIONS

In this paper, we present a new type of spatial light modulator, the photovoltaic OASLM. The device has an *ON/OFF* contrast ratio of 10:1, a 10% - 90% rise time of 3 ms, and a 90% - 10% fall time of 5 ms, and the device is capable of resolving 20 lp/mm².

The spatial resolution and the *ON/OFF* contrast ratio of the photovoltaic OASLM are lower than that of other a-Si:H/FLC OASLMs¹² operated with an externally applied ac field. This may be improved with a better FLC alignment. The operation of a photovoltaic OASLM is more dependent on the quality of the alignment than a common OASLM, because it operates at a much lower voltage.

The photovoltaic OASLM was used to perform image novelty and monotony filtering. The fast response time of the device produces a higher temporal resolution in the novelty filtering mode and a faster response time in the monotony mode than similar systems based on photorefractive crystals. On the other hand, the OASLM-based optical novelty system has a smaller dynamic range of the detectable speeds for moving objects than the photorefractive based novelty filtering systems for similar input intensities.

When the system works in the novelty filtering mode, it cannot display the image of a moving object surrounded by a high intensity background. In this case, the optic-axis of the FLC always has an angle of 45° to the analyzer P_3 (see Fig. 8). Hence, the output image of the moving object is always suppressed. Some of the photorefractive crystal based novelty filters have a similar problem.^{21,22} However, the background of a moving object usually has a large intensity variation. Therefore, the OASLM based novelty filter will be effective for many object tracking applications.

The novelty filter system with the LCTV has an image contrast ratio of 3:1 between the moving and stationary objects. This is much lower than that shown in Fig. 9 (10:1). The low contrast ratio is due to the slow modulation time of the LCTV as compared to the photovoltaic OASLM. The contrast ratio can be increased by using a light modulator with a faster frame rate.

ACKNOWLEDGEMENT

We gratefully acknowledge the support of the National Science Foundation through the Optoelectronic Computing Systems Center CDR8622236 (KMJ,GM). We would also like to thank S. Wichart for preparing the thin amorphous silicon film substrates and D. Doroski for fabricating the photovoltaic OASLM.

REFERENCES

1. J. Grinberg, A. Jacobson, W. Bleha, L. Miller, L. Fraas, D. Boswell, and G. Meyer, *Opt. Eng.* **14**, 217 (1975).
2. D. Jared, K. M. Johnson, and G. Moddel, *Opt. Comm.* **76**, 97 (1190).
3. T. Iwaki and Y. Mitsuoka, *Opt. Lett.* **15**, 1218 (1990).
4. O. V. Garibyan, I. N. Kompanets, A. V. Parfyonov, N. F. Pilipetsky, V. V. Shkunov, A. N. Sudarkin, A. V. Sukhov, N. V. Tabiryan, A. A. Vasiliev, and B. Ya. Zel'dovich, *Opt. Commun.* **38**, 67 (1981).
5. E. Maron and U. Efron, *Opt. Lett.* **12**, 504 (1987).
6. K. M. Johnson, C. C. Mao, G. Moddel, M. A. Handschy, and K. Arnett, *Opt. Lett.* **15**, 1114 (1990).
7. C. C. Mao, K. M. Johnson, and G. Moddel, *Ferroelectrics* **114**, 45 (1991).
8. S. Fukushima, T. Kurokawa, and M. Ohno, *Appl. Phys. Lett.* **58**, 787 (1991).
9. A. D. Fisher, W. L. Lippincott, and J. N. Lee, *Appl. Opt.* **26**, 5039 (1987).
10. M. Ishikawa, N. Mukohzaka, H. Toyoda, and Y. Suzuki, *SPIE* **963**, 527-536 (1988).
11. M. G. Robinson, K. M. Johnson, D. Jared, D. Doroski, S. Wichart, and G. Moddel, in *Optical Computing Technical Digest Series 6*, (Optical Society of America, Washington, DC), pp. 84-87, (1991).
12. G. Moddel, K. M. Johnson, W. Li, R. A. Rice, L. A. Pagano-Stauffer, and M. A. Handschy, *Appl. Phys. Lett.* **55**, 537 (1989).
13. I. Abdulhalim, G. Moddel, and K. M. Johnson, *Appl. Phys. Lett.* **55**, 1603 (1989).
14. B. Landreth, C. C. Mao, and G. Moddel, accepted by *Japanese J. of Appl. Phys.*, 1991.
15. U. Efron, P. O. Braatz, M. J. Little, R. N. Schwartz, and J. Grinberg, *Opt. Eng.* **22**, 682 (1983).
16. D. Williams *et al.*, *J. Phys. D* **21**, S156(1988).
17. P. R. Ashley and J. H. Davis, *Appl. Opt.* **26**, 241 (1987).
18. S. Fukushima, T. Kurokawa, and S. Matsuo, *Opt. Lett.* **15**, 285 (1990).
19. I. D. Hudson, R. K. Worcester, and D. A. Gregory, *Applied Optics* **30**, 2867(1991).
20. BDH-British Drug House, Broom RD., Poole, BH12 4NN England.
21. J. I. Pankove, *Optical Processing in Semiconductors*, Dover, New York, pp.302, 1971.

22. N. Clark and S. T. Lagerwall, *Appl. Phys. Lett.* **36**, 899 (1980).
23. F. C. Jahoda, B. T. Anderson, P. R. Forman, and P. G. Weber, *Rev. Sci. Instrum.* **56**, 953 (1985).
24. D. Anderson, D. M. Lininger, and J. Feinberg, *Opt. Lett.* **12**, 123 (1987).
25. M. Cronin-Golomb, A. M. Biernacki, H. Kong, *Opt. Lett.* **12**, 1029 (1987).
28. N. S.-K. Kwong, Y. Tamita, and A. Yariv, *J. Opt. Soc. Amer. B* **5**, 1788 (1988).
29. A. Marrakchi, J.-P. Huinard, and J. P. Herriau, *Opt. Commun.* **34**, 15 (1980).

OPTICAL BISTABLE AND LIMITING BEHAVIORS IN FERROELECTRIC LIQUID CRYSTAL AND OPTICAL PROCESSING

MASANORI OZAKI, HIROSHI MORITAKE, AKIRA TAGAWA,
NOBUYUKI SHIGENO AND KATSUMI YOSHINO

Department of Electronic Engineering, Faculty of Engineering, Osaka University,
2-1 Yamada-Oka, Suita, Osaka JAPAN

ABSTRACT Optical bistability and limiting have been studied in surface stabilized ferroelectric liquid crystal (SSFLC) with electrical feedback. Optical bistability and limiting are observed for the cases of positive and negative feedback gains, respectively. The hysteresis in the voltage-transmission curve which is characteristic of the SSFLC is found to contribute to the expansion of the optical bistable region in the positive feedback and to the appearance of the bistability in the negative feedback. Dynamic characteristics of switching between optical bistable states by an incident light pulse have also been studied. A new multi-logic element with both OR and AND functions which can be selected by controlling the duration of the reset light pulse can be realized. Besides of dc voltage operation, the ac operation of the feedback without dc bias voltage is also realized in the liquid crystal which shows antiferroelectric behavior and a symmetrical voltage-transmission curve.

INTRODUCTION

Optical bistability and limiting have attracted much attention from practical point of view as the optical processing. For the optical bistability, nonlinear medium and feedback are required. The device whose feedback can be optically achieved by mirrors is named as all-optical bistability,^{1,2} whereas one which requires external feedback such as an electrical circuit is known as hybrid optical bistability.^{3,4}

In liquid crystals, mainly in nematic liquid crystals, the nonlinear optical response has also been studied.⁵⁻⁸ On the other hand, the ferroelectric liquid crystal (FLC) has recently been developed as a material for high-speed display devices. In this compound, several types of electro-optical effects have been reported.⁹⁻¹² Among them the electro-optic effect with the homogeneously aligned thin (less than several μm in thickness) FLC cell between two polarizers was confirmed to exhibit short response time.¹⁰ This

type of thin cell device was systematically studied by Clark and Lagerwall and was named a surface stabilized ferroelectric liquid crystal (SSFLC), which has attracted much interest because of the potential application to fast electro-optic switching devices.¹¹

In this paper, a hybrid optical bistability and limiting in FLC utilizing a SSFLC cell with an electrical linear feedback are reported. The optical switching between two stable states using a very short light pulse is demonstrated. A new multi-logic element with sequential OR and AND functions can be realized by the control of the bias light. In addition, the hybrid bistability which is operated using ac driving voltage is also realized in the liquid crystal which shows antiferroelectric behavior.

EXPERIMENTAL

Three types of samples were used in this study. That is a mixed liquid crystal based on (2S,3S)-3-methyl-2-chloropentanoic acid 4',4''-alkoxybiphenyl ester (3M2CPAOB) which shows the Sm C* phase at room temperature and (R)-4'-(3-methoxycarbonyl-2-propoxycarbonyl)phenyl 4-[4-(n-octyl)phenyl (3MC2PCPOPB) which shows anomalous optical and electrical behavior were used.¹³ The sample was sandwiched between two In-Sn oxide (ITO)

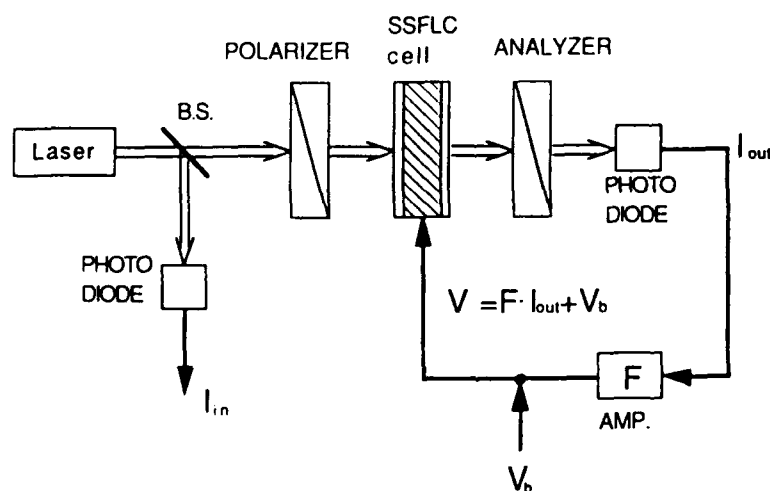


FIGURE 1 Experimental setup for the measurement of the transmission intensity I_{out} through a FLC cell with linear feedback as a function of input light intensity I_{in} . F denotes the feedback gain ($V = V_b + F I_{out}$).

coated conducting glass plates. A homogeneously aligned cell was prepared by rubbing the surfaces after coating with polyvinyl alcohol or by the oblique evaporation. The cell thickness was 2 μm .

The experimental setup for the measurement of the nonlinear response is shown in Figure 1. The light source was a He-Ne laser (632.8nm) or an AlGaAs laser diode (780 nm). The transmitted light intensity through the cell was monitored with a photodiode. The output voltage was amplified, summed with a bias voltage and fed back to the sample cell. The response time of the amplifier used in this system is less than 1 μs , which is shorter than that of liquid crystal.

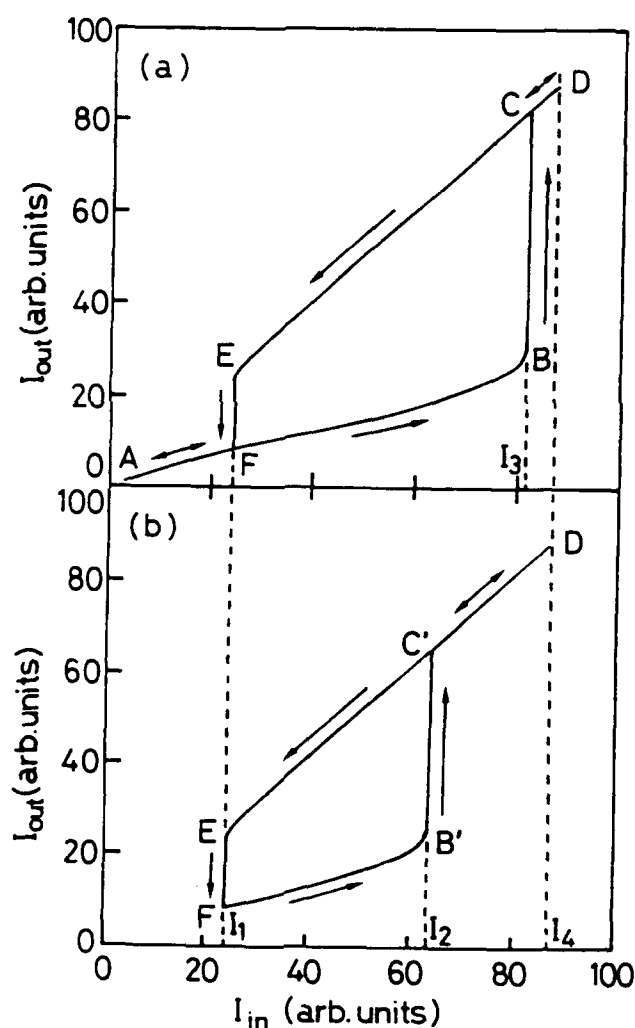


FIGURE 2 I_{in} - I_{out} curves in a SSFLC cell with positive feedback gain ($F=400$, $V_b=-7\text{V}$). (a) I_{in} changes between 0 and I_4 . (b) I_{in} changes between I_1 and I_4 .

RESULTS AND DISCUSSION

Optical bistability and limiting in SSFLC with feedback

The output light intensity I_{out} through the SSFLC with a positive feedback gain ($F=400$) and a negative bias voltage ($V_b=-7\text{V}$) is shown in Figure 2(a) as a function of input light intensity I_{in} . The SSFLC cell was placed between crossed polarizers to obtain the extinction at negative voltage application. The bias voltage V_b is lower than the threshold voltage in the V - T curve. In this case, the transmittance is low in the absence of I_{in} . With increasing I_{in} , the applied voltage increases and, then, its polarity changes to positive. The further increase of I_{in} realizes a high transmission state, resulting in the abrupt change in I_{out} at a threshold intensity I_3 . When I_{in} is decreased, the applied voltage is reduced and its polarity changes. Then, the transmittance is lowered, resulting in the further reduction of the voltage. At the threshold input light intensity I_1 ($<I_3$) I_{out} decreases abruptly. Therefore, optical bistability is realized in the SSFLC with the positive feedback.

The higher threshold light intensity in the bistable loop depends on the range of the variation of I_{in} . When I_{in} changes in the range of $I_1 \sim I_4$, the higher threshold of the optical bistable loop is lower than that of the loop whose I_{in} changes between 0 and I_4 . That is, when I_{in} increases from I_1 , I_{out} jumps from B' to C' at the threshold light intensity I_2 which is lower than I_3 as shown in Figure 2.

Figure 3 shows voltage dependences of the transmittance through the SSFLC cell (V - $T(V)$ curve), which correspond to I_{in} - I_{out} loops shown in Figure 2. When I_{in} is varied the range of $0 \sim I_4$ as shown in Figure 2(a), I_{out} changes from A to D and the lowest applied voltage is -7V . In this case, the voltage dependence of the transmittance is observed as denoted by a dashed line in Figure 3. However, when I_{in} is varied in the range between I_1 and I_4 as shown in Figure 2(b), F is the lowest state of I_{out} and the lower limit of V is -5V . This causes to observe the V - $T(V)$ curve denoted by a solid line in Figure 3. It should be noted that the profile of the $T(V)$ hysteresis changes by the range of the variation of the applied voltage. When V increases before the complete extinction is established, the threshold voltage shifts toward the negative voltage.

In the linear feedback system, the applied voltage V is expressed by

$$V = V_b + F T(V) I_{\text{in}}, \quad (1)$$

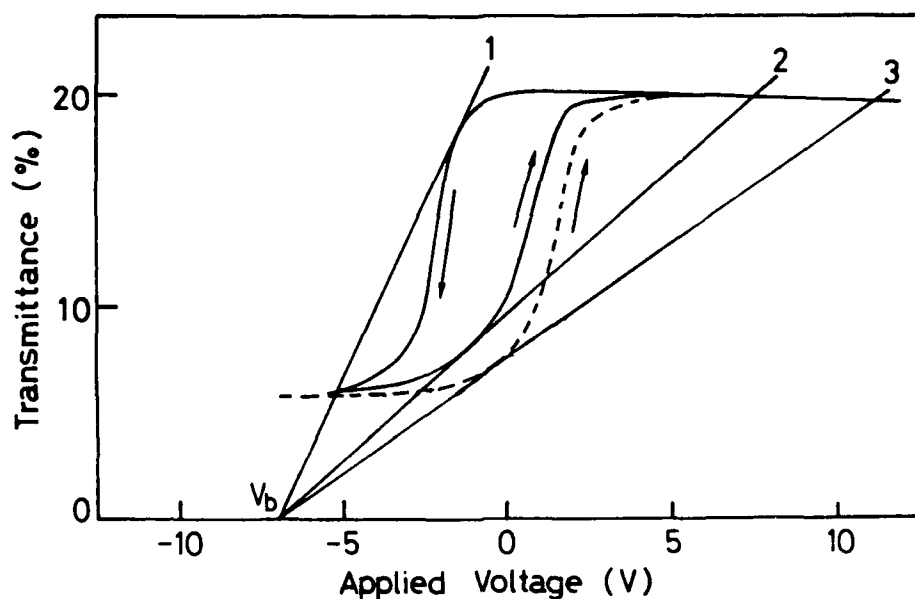


FIGURE 3 Voltage dependences of the transmittance in SSFLC cell. Dashed and solid lines correspond to I_{in} - I_{out} curves shown in Figure 2 (a) and (b), respectively.

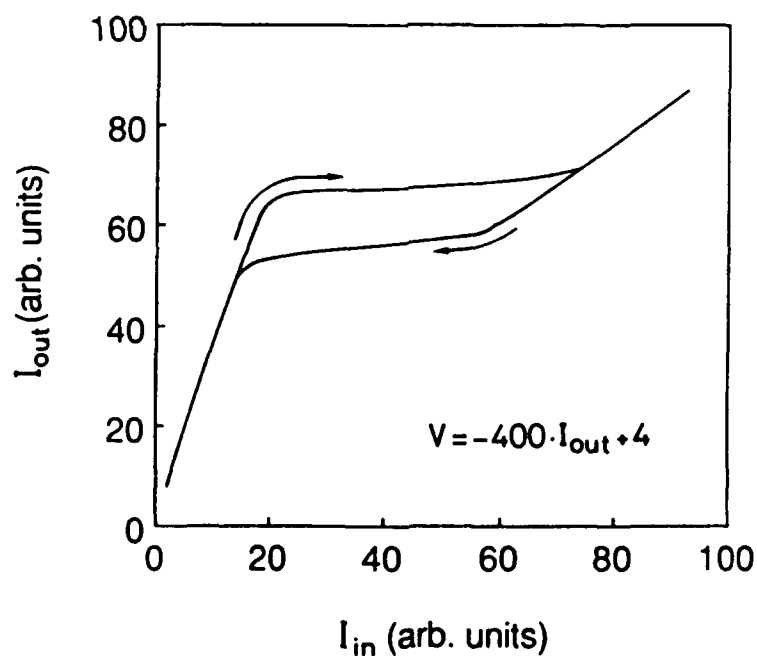


FIGURE 4 Typical I_{in} - I_{out} curve in SSFLC cell with negative feedback gain ($F=-400$, $V_b=4V$).

where F is feedback gain and $T(V)$ is the transmittance which is a function of V . One can rewrite Eq.(1) as

$$T(V) = (V - V_b) / F I_{in}. \quad (2)$$

When the input intensity I_{in} is given, the steady-state operating point with a linear feedback is determined by one of the intersections of the $T(V)$ curve and the straight line given by Eq.(2). The straight line given by Eq.(2) is also shown in Figure 3. The slope of the straight line is infinity in the absence of I_{in} and decreases with increasing I_{in} . The lines 1, 2 and 3 correspond to I_1 , I_2 and I_3 , respectively. Therefore, the difference between threshold intensities I_2 and I_3 shown in Figure 2 is attributed to the deformation of the V - $T(V)$ curve due to the incomplete reorientation of the polarization.

Figure 4 shows I_{out} through the SSFLC cell with a negative feedback gain as a function of I_{in} . The optical limiting was observed in the SSFLC cell. It should be noted that the optical bistability can also be realized even with a negative feedback gain due to the hysteresis in $T(V)$ curve.

Dynamic properties of optical bistability in SSFLC with feedback

The dynamic switching between two stable states shown in Figure 2 can be realized by the control of the incident light. The schematic explanation of the operation by the incident light pulse is shown in Figure 5(a). The off-state [L] is turned into the on-state [H] by superimposing the light pulse I_p on the bias light I_b . On the other hand, the on-state [H] is switched into the off-state [L] by shutting off the bias light instantaneously.

Figure 5(b) shows the typical switching waveform between on- and off-states. It is found that the switching can be realized with a short pulse width of the incident light pulse. The minimum pulse width T_m which is required for the complete bistable switching depends on the magnitude of I_p or the bias light intensity I_b . When $I_p/I_b=2$, T_m is 100-150 μ s.

As discussed previously, the threshold light intensity in the optical bistable loop shifts by the range of the variation of I_{in} in the static operation of the optical bistability. Also in the dynamic operation, the threshold intensity can be controlled as shown in Figure 6. When I_{in} increases from state [L] after the switching from [H] to [L] by shutting off the bias light I_b during the period T_s , the threshold light intensity depends on the pulse duration T_s . That is, the threshold intensity I_{th1} for shorter T_s is lower than I_{th2} for longer T_s .

Figure 7(a) shows V - $T(V)$ curves in the dynamic operation as shown in Figure 6. The waveform of the driving voltage is shown in Figure 7(b).

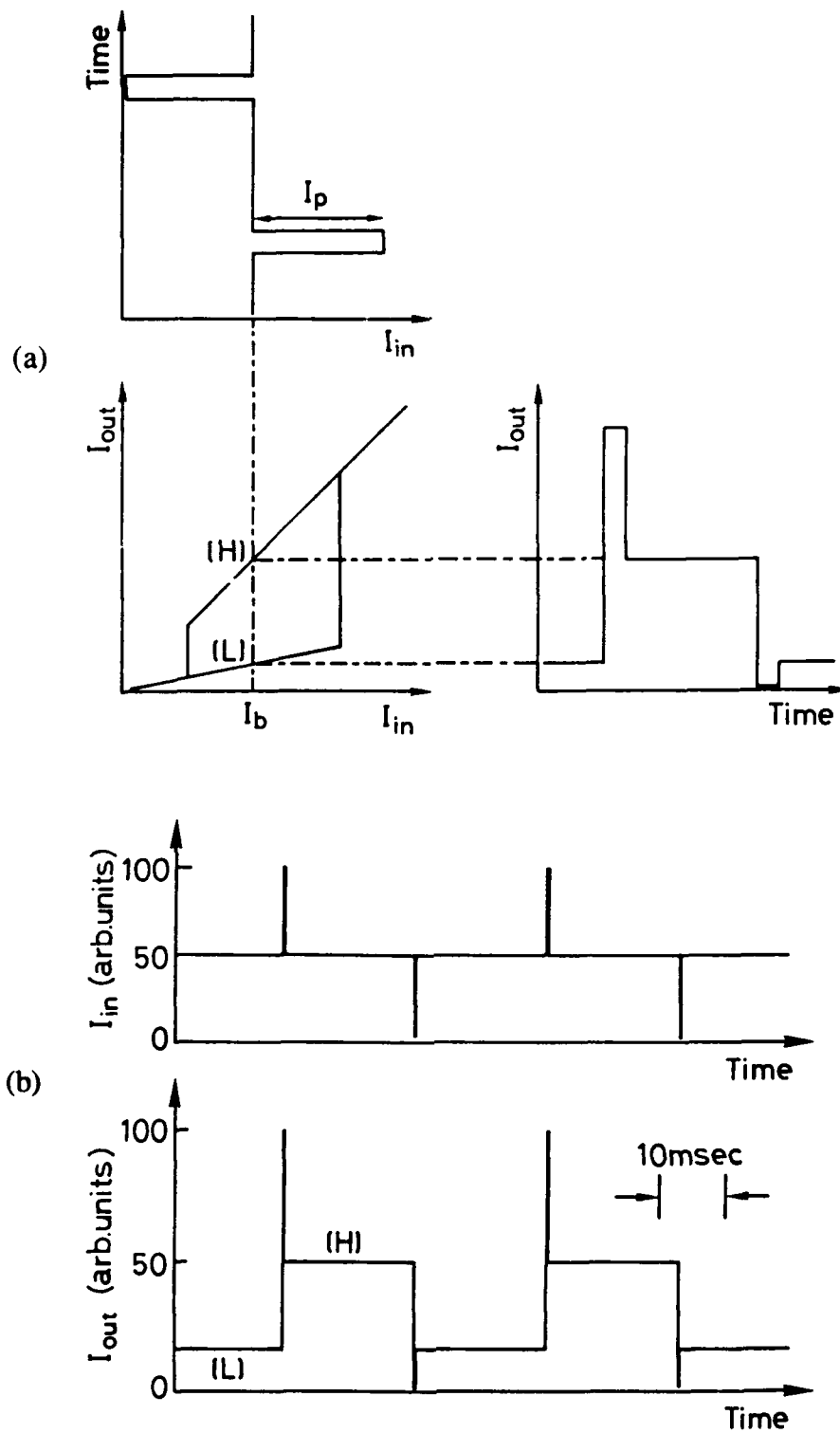


FIGURE 5 (a) Schematic explanation on the switching between optical bistable states ((H) and (L)). (b) Typical waveform of the switching between optical bistable states.

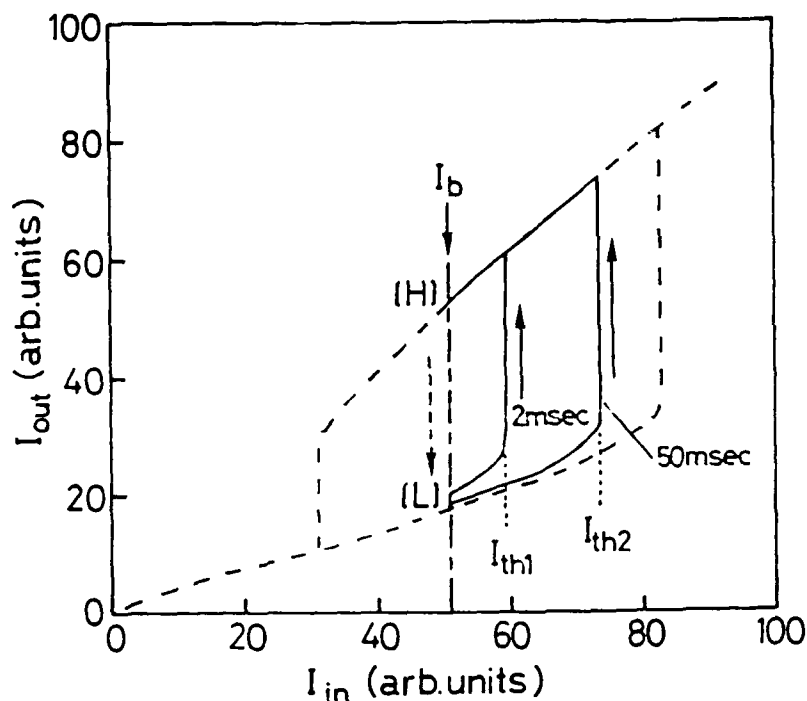


FIGURE 6 I_{in} - I_{out} curves. Dashed line denotes the static optical bistable loop with changing I_{in} between 0 and 92. Solid lines denote I_{out} with increasing I_{in} from I_b (state [L]) after the [H] -[L] switching by shutting off I_b during T_s .

According to Eq. (2), the straight lines are also shown in Figure 7(a) to obtain operating points for the bias light I_b and threshold light intensity of the bistable loop. It should be noted that the profile of the V - $T(V)$ curve depends on T_s . In other words, the length of time for which the voltage is held at -7V influences the profile of the V - $T(V)$ curve. Therefore, the operating point for the threshold intensity depends on the T_s .

The sequential selection of the logic elements (OR-gate or AND-gate) can be realized using the optical bistable loop whose threshold intensity is controllable by the duration of the momentary cut of I_b (reset pulse), as shown in Figure 6. The schematic explanation of the operation is shown in Figure 8. The intensities of input signal pulses A and B are set to be between I_{th1} and I_{th2} . As is evident from Figure 6, the threshold intensity depends on the width T_s of the reset pulse which is required to switch from [H] to [L] states. That is, I_{th1} and I_{th2} corresponds to $T_s=2ms$ and 50ms, respectively.

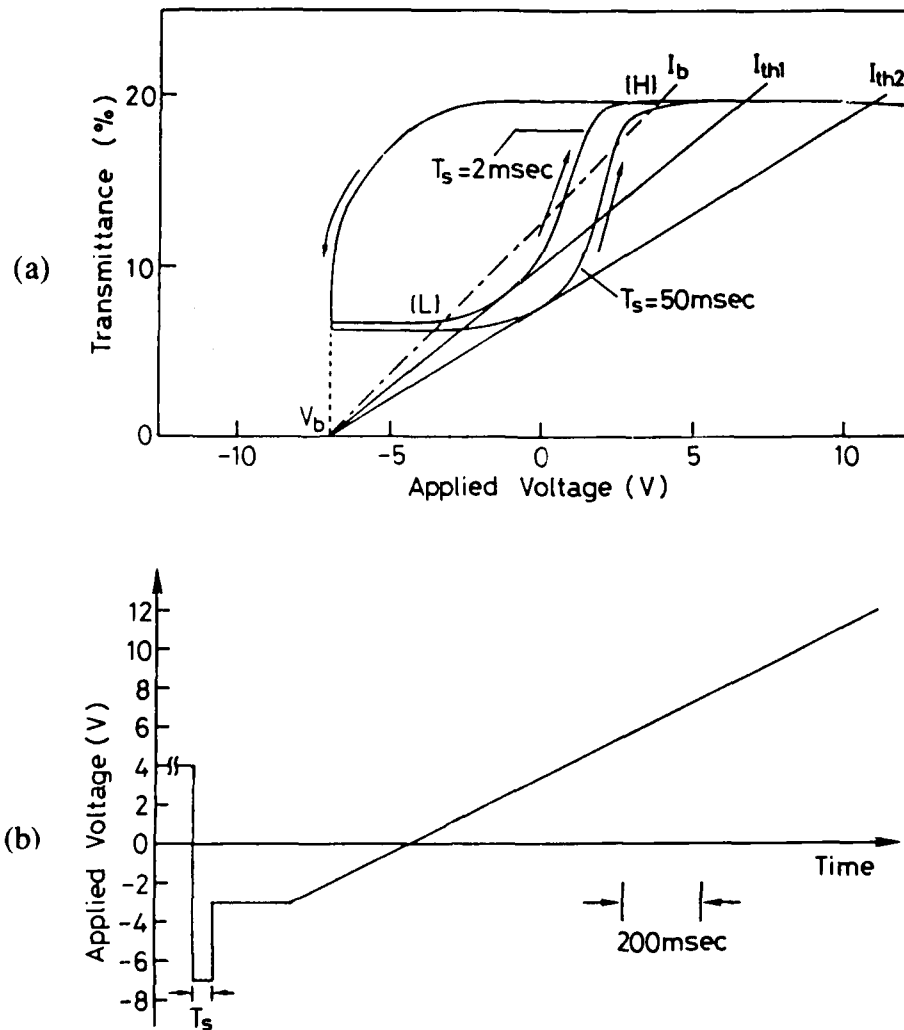


FIGURE 7 Voltage dependences of the transmittance of the SSFLC cell with positive feedback with applying the driving voltage as shown in (b). The profile depends on the reset pulse width T_s .

In order to realize the switching from [L] to [H] states, it is necessary for the input light intensity to exceed the threshold intensity. For the bistable loop with I_{th1} ($T_s = 2 \text{ ms}$), state [L] is switched into state [H] by applying a single input signal (A or B). This operation corresponds to the OR function of the logical operation. On the other hand, for the loop with I_{th2} ($T_s = 50 \text{ ms}$), [L]-[H] switching can be realized by the application of both input signals (A and B). This corresponds to the AND function. Consequently, the OR and AND functions can be sequentially selected by the reset pulse width of I_b .

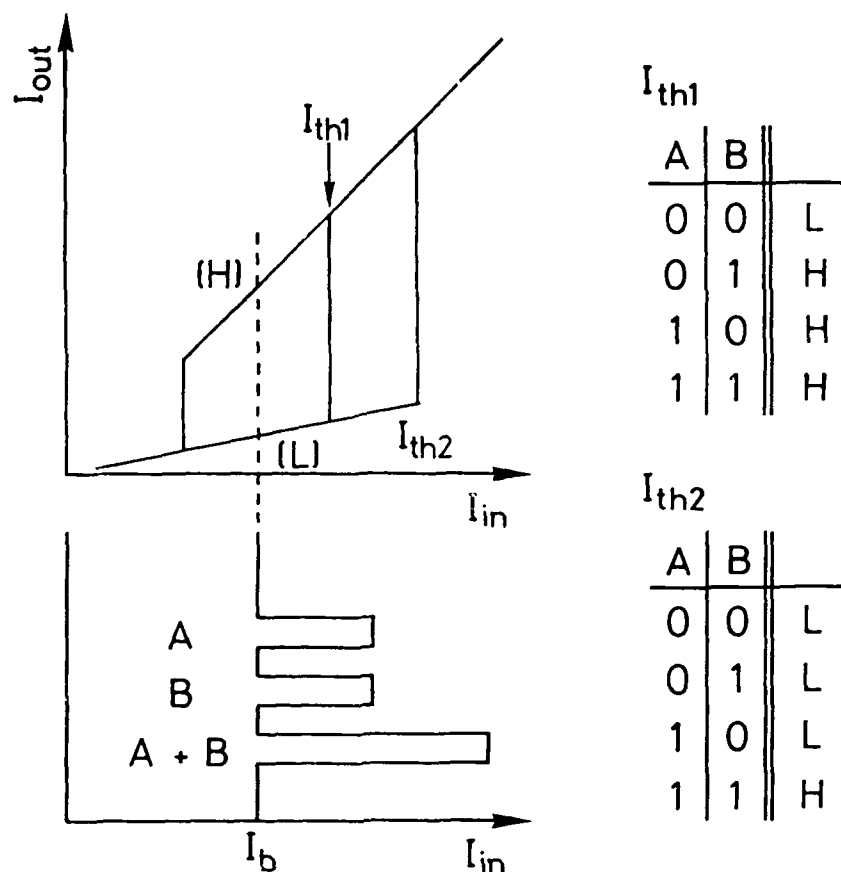


FIGURE 8 Schematic explanation on the multi-logic element using the optical bistable loop whose threshold intensity is controllable by the reset pulse width.

Figure 9 shows typical waveform of the sequential operation of OR and AND functions selected by the width of the reset pulse. The reset pulse, single input pulse (A or B) and double input pulses (A+B) are sequentially applied for the input light. The reset pulses of 2ms and 50ms in duration are alternately applied. For the short reset pulse (2ms), [L]-[H] switching is realized by the application of a single input signal (A or B), which corresponds to the OR-gate operation. On the other hand, for the long reset pulse (50ms), two simultaneous input signals (A+B) are required to realize the [L]-[H] switching, which corresponds to the AND-gate operation. Therefore, multi-logic operation can be obtained by the control of the duration of the reset pulse in the SSFLC with the positive feedback.

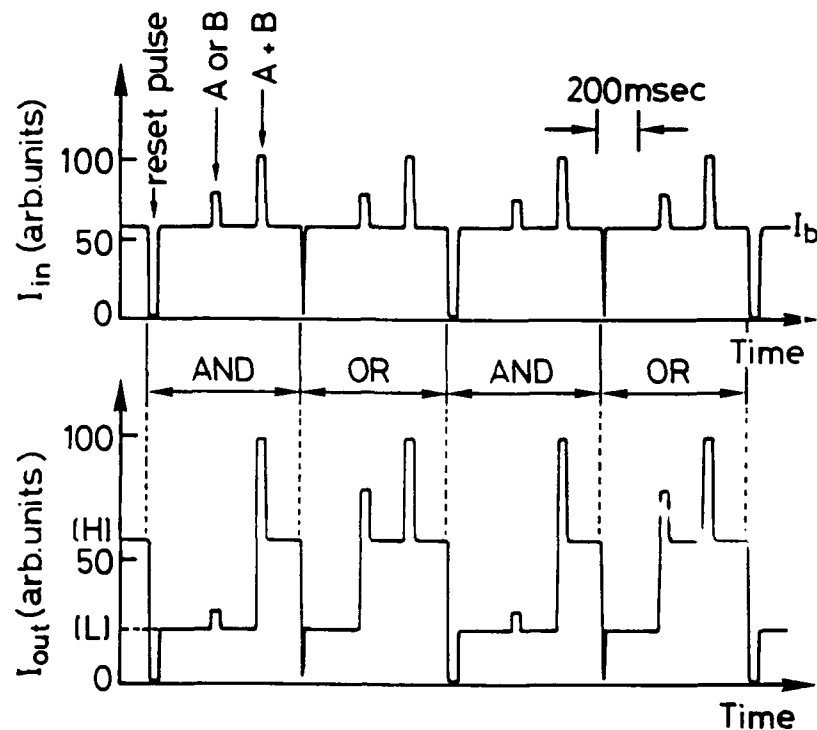


FIGURE 9 Typical waveforms of I_{in} and I_{out} in the multi-logic operation.

Optical bistability in 3MC2PCPOPB with feedback

In the system as described above, the application of dc bias and driving voltage is required. However, the dc voltage causes the storage of the polarization charge, which is disadvantageous for the SSFLC device. Recently, an anomalous optical behavior which shows three stable states in the optical transmission has been observed in 3MC2PCPOPB. This material shows the symmetrical voltage dependence of the transmission intensity as shown in Figure 10, which enables operation using ac voltage. Then the optical bistable behavior in SSFLC cell of 3MC2PCPOPB with linear feedback is studied using ac operation.

The output light intensity I_{out} through the 3MC2PCPOPB cell with a positive feedback is shown in Figure 11 as a function of the incident light intensity I_{in} . It should be mentioned that in this case the dc bias voltage is not used. The optical bistability is observed also in the 3MC2PCPOPB cell with the positive feedback.

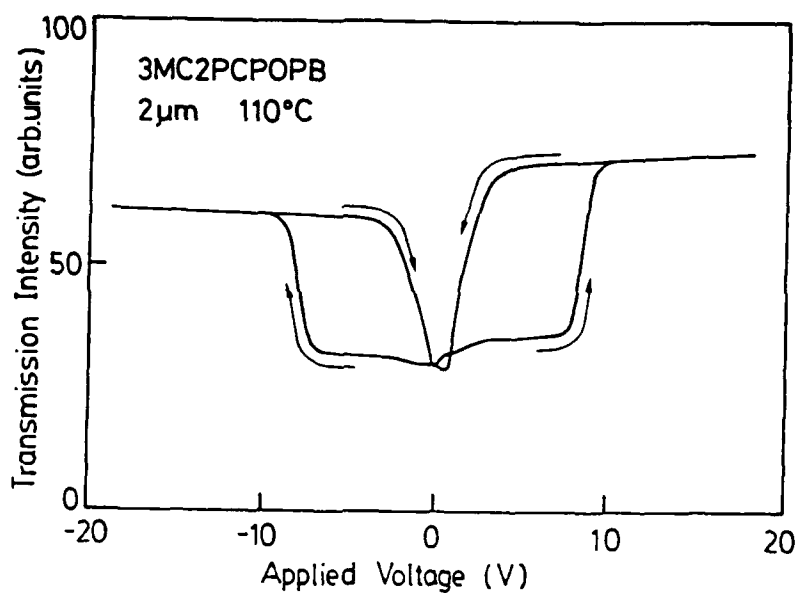


FIGURE 10 Typical voltage dependence of the transmission intensity in a SSFLC cell using 3MC2PCPOPB.

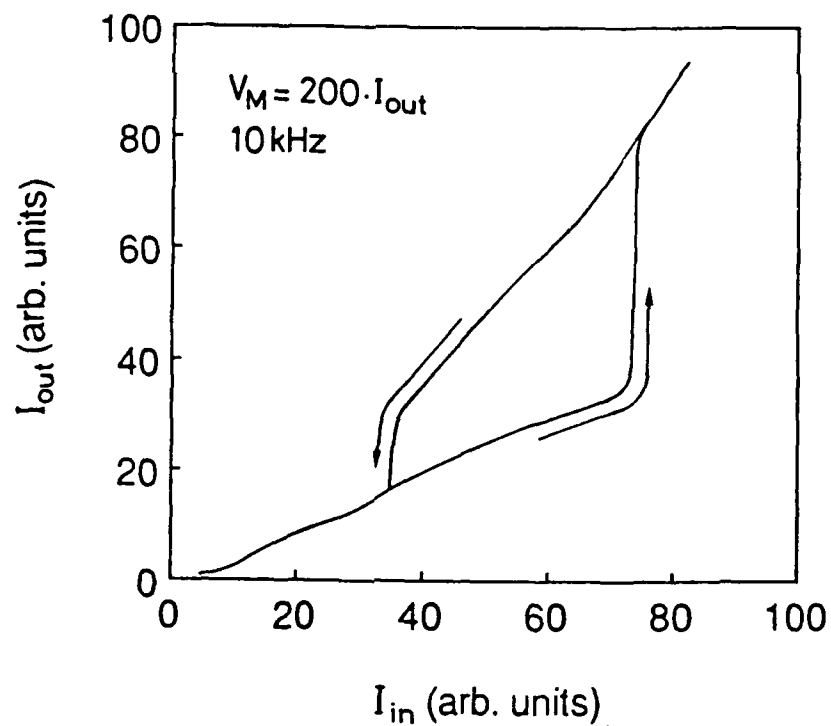


FIGURE 11 Typical I_{in} - I_{out} curve in a SSFLC cell using 3MC2PCPOPB with positive feedback gain.

CONCLUSIONS

Hybrid optical bistability and limiting in smectic ferroelectric liquid crystal using the SSFLC electro-optic effect with linear electrical feedback were demonstrated. Optical limiting and bistability were observed for the cases of negative and positive feedback parameters, respectively. It was also found that the transmission hysteresis characteristic to the ferroelectric liquid crystal resulted in the expansion of the bistable region and in the realization of the bistability with a negative feedback gain. In the SSFLC cell with feedback, the dynamic switching between bistable states was observed at a short pulse width of the incident light. A multi-logic element with sequential OR and AND functions was realized by the control of the reset pulse width. The optical bistability with an ac driving feedback was also realized using 3MC2PCPOPB which showed the antiferroelectric behavior.

REFERENCES

1. A.Szöke, V.Daneu, J.Goldhar and N.A.Kurnit, Appl.Phys.Lett., **15**, 376 (1969).
2. H.M.Gibbs, S.L.McCall and T.N.C.Venkatesant, Phys.Rev.Lett., **36**, 1135 (1976).
3. P.W.Smith and E.H.Turner, Appl.Phys.Lett., **30**, 280 (1977).
4. P.W.Smith, E.H.Turner and P.J.Maloney, IEEE J.Quantum Electron., **OE-14**, 207 (1978).
5. I.C.Khoo, Appl.Phys.Lett., **41**, 909 (1982).
6. M.M.Cheung, S.D.Durbin and Y.R.Shen, Opt.Lett., **8**, 39 (1983).
7. K.Takizawa, M.Okada, H.Kikuchi and T.Aida, Appl.Phys.Lett., **53**, 2359 (1988).
8. J.Y.Kim and P.Palffy-Muhoray, J.Appl.Phys., **66**, 362 (1989).
9. K.Yoshino, K.G.Balakrishnan, T.Uemoto, Y.Iwasaki and Y.Inuishi, Jpn.J.Appl.Phys., **17**, 597 (1978).
10. Y.Iwasaki, K.Yoshino, T.Uemoto and Y.Inuishi, Jpn.J.Appl.Phys., **18**, 2323 (1979).
11. N.A.Clark and S.T.Lagerwall, Appl.Phys.Lett., **36**, 899 (1980).
12. K.Yoshino and M.Ozaki, Jpn.J.Appl.Phys., **23**, L385 (1984).
13. K.Yoshino, H.Taniguchi and M.Ozaki, Ferroelectrics, **21**, 267 (1989).

SECTION F
POLYMER FLCs

Anomalous Current and Electrooptic Response in a Polyacrylate Ferroelectric Liquid Crystal with Large Spontaneous Polarization

**K. Skarp, G. Andersson, S.T. Lagerwall,
H. Kapitza*, H. Poths*, R. Zentel⁺**

Physics Department, Chalmers University of Technology, S-412 96 Göteborg, Sweden

*Institut für Organische Chemie der Universität, J.J. Becherweg 18-20,
D-6500 Mainz, FRG

⁺Institut. für Organische Chemie und Makromolekulare Chemie, Universitätsstr. 1,
D-4000 Düsseldorf, FRG

A side-chain polymer exhibiting a chiral smectic phase was investigated. Due to its anomalous current and electrooptic responses, we discuss the possibility of antiferroelectric order in the polymer, and compare its behaviour with a low-molar mass antiferroelectric substance. In particular, we study the birefringence modulation resulting from the field induced antiferroelectric-to-ferroelectric transition, and determine the induced polarization by the field reversal method.

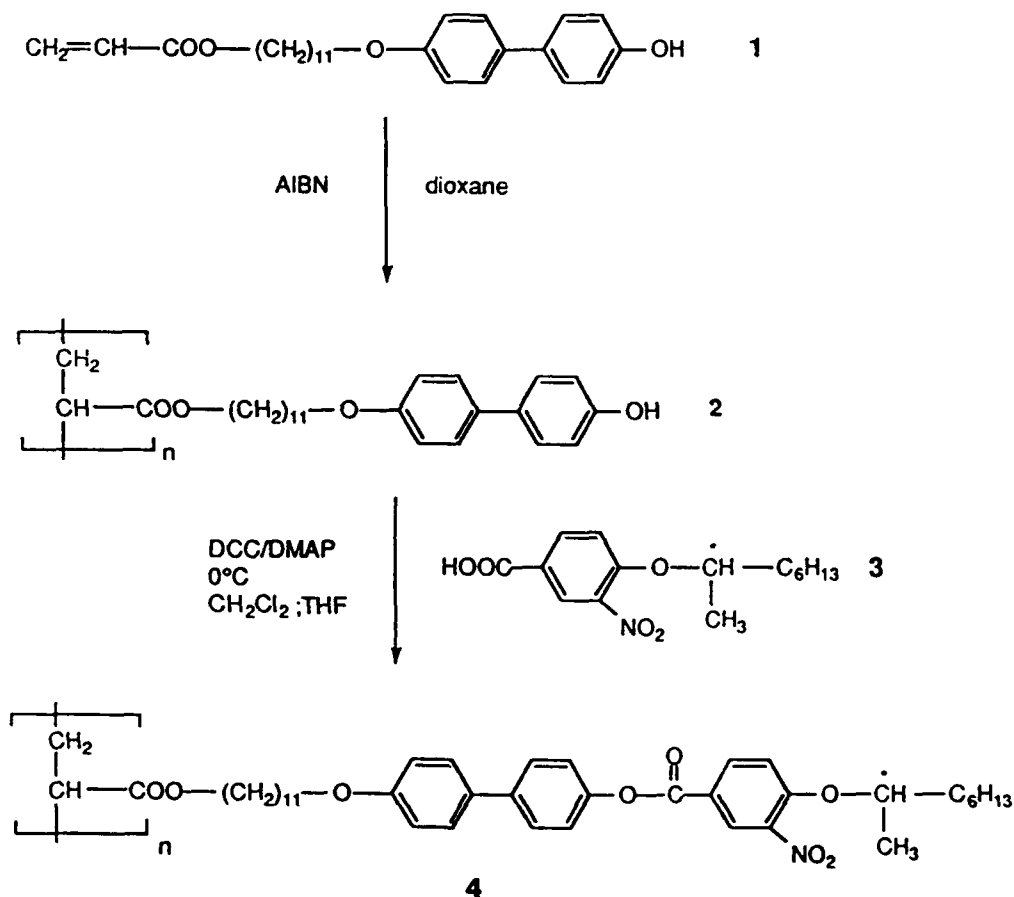
INTRODUCTION

After the first report of a polymer FLC by Shibaev et al ¹, several other such materials have been synthesized and investigated². Alignment of polymer FLCs, as compared to low-molar mass FLCs, is more difficult. This is probably due to the higher viscosity and lower mobility in the polymers. Consequently, textures are less clear and physical measurements often more obscured and difficult to interpret than in low molar mass liquid crystals. However, because of the obvious importance of these materials, deriving not only from their electrooptical but also their piezoelectric and nonlinear optical properties, they have recently become the topic of intensified investigations.

The first ferroelectric polymers were not electrooptically active, but later also switchable polymers were reported^{3,4}. In their switching properties, the ferroelectric polymers showed similar behaviour to low molar mass systems, only with longer response times and lower contrast. Recently, however, an interesting anomalous switching behaviour was observed in two different side-chain polymers^{5,6}. In the present paper we present results for a chiral polyacrylate showing three switching states and optical properties such as birefringence modulation that are characteristic of an antiferroelectric state⁷ in a low molar mass substance.

SYNTHESIS OF THE CHIRAL SIDE-CHAIN POLYACRYLATE

In preparing the chiral polyarylate **4** we used a synthetic route (see reaction scheme in figure 1), which introduces the chiral group into a preformed polymer as the last step of the synthesis. This method has already been applied for the synthesis of ferroelectric polysiloxanes and polyesters⁸⁻¹⁰.



$s_x 56$ s_c 158 i

(s_x not further identified smectic phase)

$M_{\text{GPC}} = 25.000$

Figure 1. Reaction scheme for preparing polymer **4**.

Free radical polymerization of the monomeric acrylate **1** with 2,2'-azoisobutyronitrile (AIBN) in dioxane⁹ gave the pure polyacrylate **2** (yield: 89%). Polymer analogous esterification of the polymeric alcohol **2** and the chiral ether of 3-Nitro-4-hydroxybenzoic acid **3** was done with the help of dicyclohexylcarbodiimide (DCC) and 4-dimethylaminopyridine (DMAP) at 0 °C in order to prevent racemization and gave the chiral polyacrylate **4** in good yields (90%). ¹H-NMR proved that the degree of esterification is 100% within the limits of accuracy^{9,10} The molecular weight was determined by GPC in THF against polystyrene standards. The phase transition temperatures were determined by DSC and polarizing microscopy.

LINEAR ELECTRO-OPTIC EFFECTS IN POLYMER LIQUID CRYSTALS

The observation of an electro-optic effect linear in the applied electric field might have several different physical origins, e.g. ferroelectric, electroclinic or flexoelectric effects. It might further be associated with conductive currents in the cell, or with surface induced polar ordering. Field-induced phase transitions, such as the antiferroelectric-to-ferroelectric transition, or field effects near e.g. a first-order smectic A-C transition also exhibit some linear characteristics. Thus, the observation of a linear response has to be interpreted with some care. In the case of side-chain polymers, it is helpful to compare in detail the observed behaviour with the corresponding phenomena in low molar mass liquid crystals. This is the method we will use when investigating polymer **4**.

In ferroelectric polymers, electro-optic effects with characteristics similar to the electroclinic effect have been reported¹¹. As noted above, recently also a behaviour characteristic of antiferroelectric liquid crystals was found in some polymers. Let us compare the field dependence of these two effects, cf. figure 2.

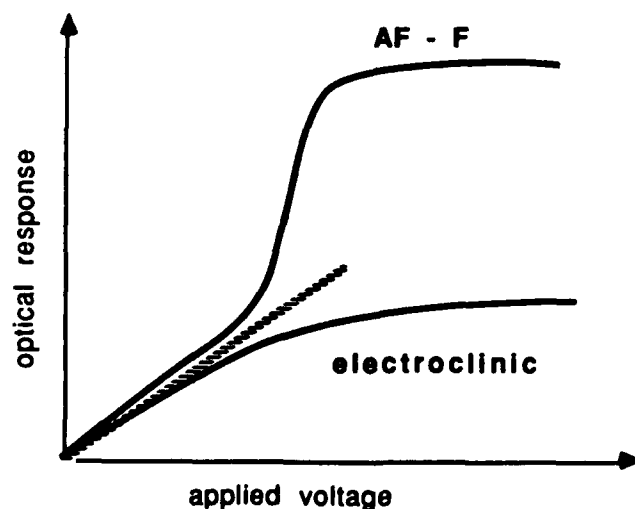


Figure 2. Schematic comparison between electroclinic and antiferroelectric-to-ferroelectric (AF-F) electro-optic characteristics.

The electroclinic effect is monotonic in the field and saturates at high fields, while the antiferroelectric-to-ferroelectric (AF-F) transition at first shows a superlinear behaviour which finally saturates at high fields. The initial slope of the AF-F curve, which is very small in the low molar mass substance MHPOBC, is exaggerated in figure 2.

ELECTRO-OPTIC AND CURRENT RESPONSE OF POLYMER 4.

One obvious requirement for studying FLC polymers is the achievement of well aligned samples. Our standard shear cell¹², built for measurements on low molar mass FLCs, has proven very useful for obtaining aligned polymer samples, having an active area of 16.8 mm² and a film thickness of 0.5-4 μm . The cell is temperature controlled in a Mettler hot-stage, and the electro-optic and current responses are measured using standard optic and electric components.

Electro-optic characterization

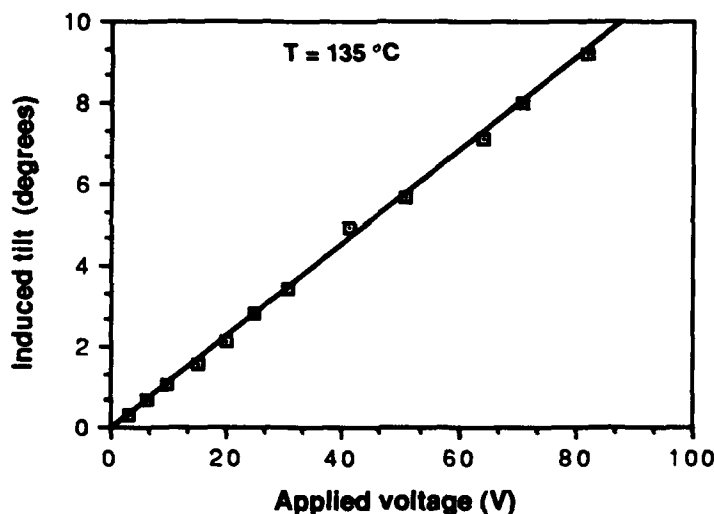


Figure 3. Induced tilt angle versus applied voltage in a 3 μm thick sample of polymer 4. (Both tilt angle and applied voltage are given as peak-to-peak values).

In order to illustrate the electro-optic response, in figure 3 is shown the induced tilt versus applied electric field at $T=135\text{ }^{\circ}\text{C}$. It is a linear response, and can be interpreted as a fairly large electroclinic effect, with an induced tilt of about 10° . However, if the frequency characteristics (shown in figure 4) are compared with that of a pure soft-mode response underlying the electroclinic effect in e.g. the smectic A phase, we find in polymer 4 a difference: The high-frequency fall-off slope is -0.3, which is very different from the value -1 that is expected for a pure soft-mode described as a Debye relaxation with one relaxation frequency. For a low molar mass smectic A*, one often finds a slope close to -1 for the electroclinic effect¹³. We have here a first indication that the observed linear effect could have another physical basis.

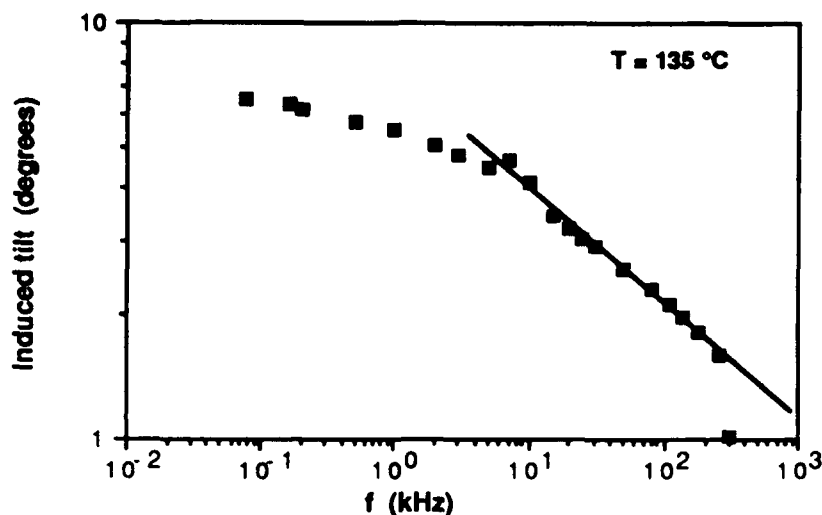


Figure 4. Induced tilt angle versus frequency, at an applied voltage of 100 V amplitude over a $3\text{ }\mu\text{m}$ cell.

Next, let us look at the temperature dependence of the induced tilt, shown in figure 5. The apparent tilt angle shows the anomaly, as compared to the electroclinic effect in the smectic A phase, of increasing with temperature, when measured at constant field.

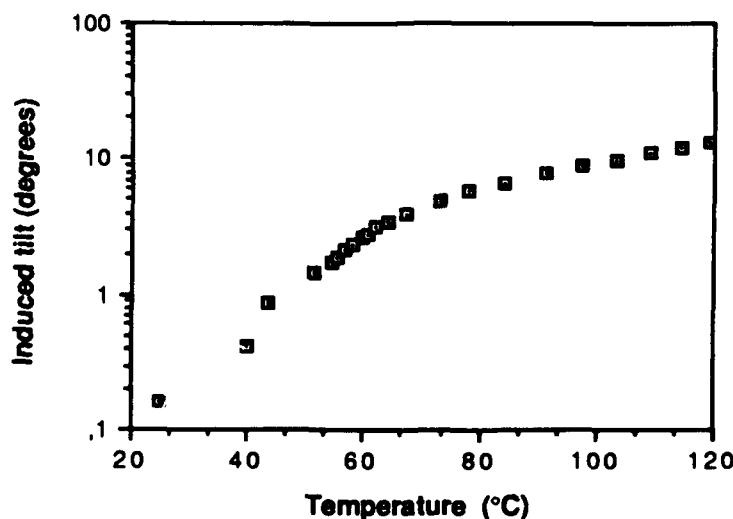


Figure 5. Induced tilt versus temperature measured with an ac voltage of 190 V peak-to-peak and 10 Hz frequency.

It is observed in figure 5 that there is a clear change in the slope of the curve around $T = 60\text{ }^{\circ}\text{C}$, coinciding with a phase transformation, probably to a higher order smectic phase, observed on a DSC recording of polymer 4. A small linear response is observed deep into this low-temperature phase. As noted in the last section, for the electroclinic effect one would expect a monotonous field-dependence of the induced tilt, that eventually would

saturate at high fields. In figure 6 we show the field-induced tilt at $T=135\text{ }^{\circ}\text{C}$. As can be seen, the behaviour is different from the electroclinic response, in that an increased slope is observed at high fields.

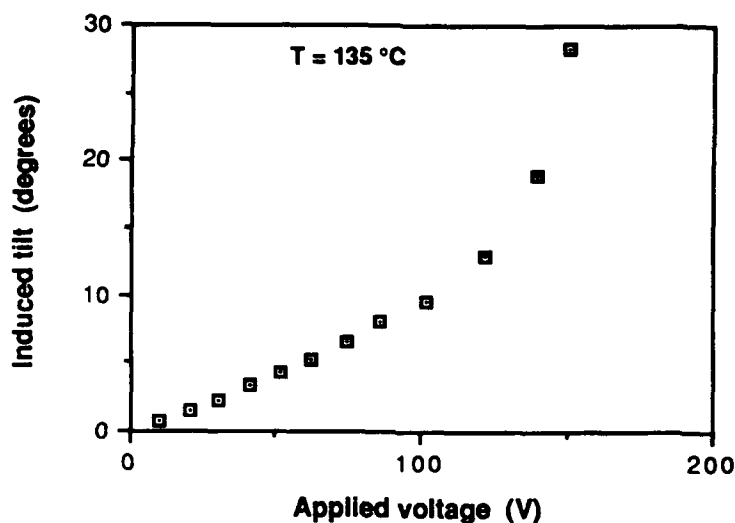


Figure 6. Induced tilt angle versus applied voltage in a 3 μm cell of polymer 4.

In figure 7a the same response is shown with both polarities of the field, and in figure 7b the oscilloscope trace of the optical versus field curve is shown. It clearly shows the existence of three optical states in the polymer at high negative, zero and high positive voltages, respectively.

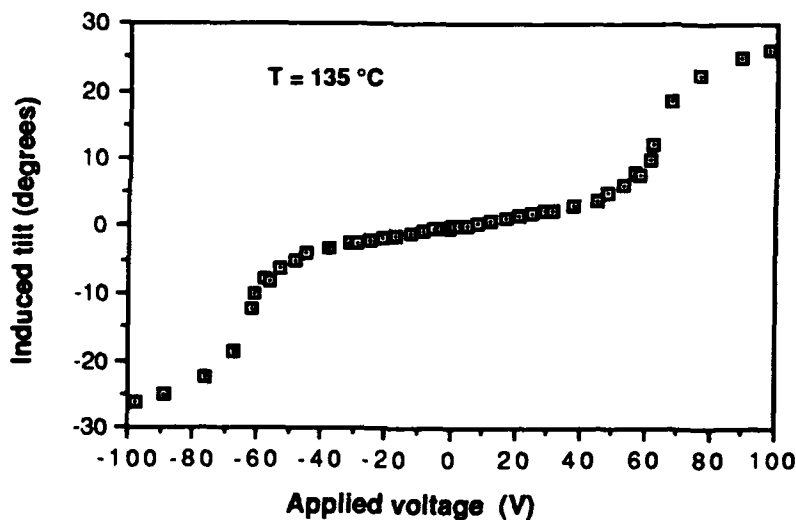


Figure 7a. Induced tilt versus amplitude of applied voltage for polymer 4.



Figure 7b. Oscilloscope trace of the optical response (vertical axis) versus applied voltage (horizontal axis). Polymer 4 in a $3.5 \mu\text{m}$ cell at $T = 136.4^\circ\text{C}$.

These observations were compared with recordings for the low molar mass antiferroelectric MHPOBC⁷, which aligned extremely well in the shear cells. All three characteristics: increase of the induced tilt with temperature, the S-shaped induced tilt-versus-field curve, and the anomalous frequency characteristics, were confirmed. In particular, the double optical hysteresis curve was found in both polymer 4 and MHPOBC. Below in figure 7c is shown the three optical states in a shear aligned cell of polymer 4.

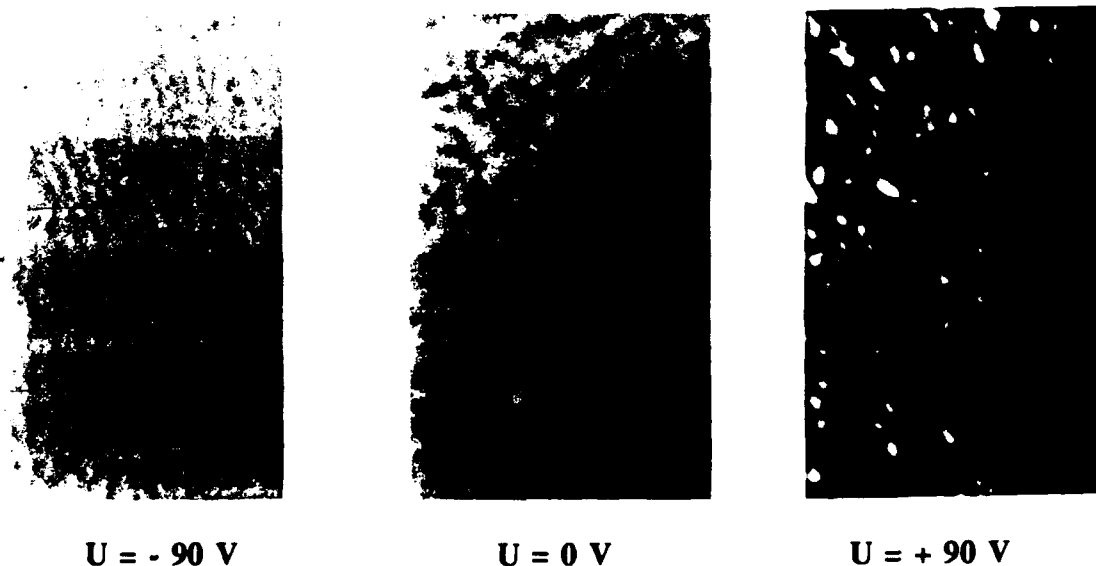


Figure 7c. Microscope pictures of the three states observed in a shear aligned cell of polymer 4 at negative, zero and positive voltages. Applied voltage = $\pm 90 \text{ V}$.
See Color Plate VII.

Optical behaviour of unoriented samples

In samples of polymer 4, one observes that the birefringence colour changes abruptly when the applied field is high enough. Typically, in our samples there is a change from grey to yellow, corresponding optically to a shift from slightly more than a lambda quarter plate to slightly more than a lambda half plate. Such behaviour is in line with the increase

in birefringence occurring at an antiferroelectric-ferroelectric transition. In order to study this effect, it turns out that it is favourable to have completely un-oriented samples, in the sense that the director is in the plane of the cell, but randomly distributed in this plane, cf. figure 8. A comparison is made with MHPOBC, which shows a larger change in birefringence at the transition, taking the cell from approximately a $\lambda/2$ to a λ -plate.



antiferro (0 V)
low birefringence



ferro (20 V)
high birefringence

See Color Plate VIII.

Figure 8a. A cell with randomly distributed director orientations. MHPOBC at $T=90^\circ\text{C}$.



applied voltage = 0 V
low birefringence



applied voltage = 180 V
high birefringence

See Color Plate VIII.

Figure 8b. A cell with randomly distributed director orientations. Polymer 4 at $T=135^\circ\text{C}$.

Applying the standard expression for the transmitted light intensity of a birefringent plate between crossed polarizers

$$I = I_0 \sin^2 2\psi \sin^2 \delta \quad \text{where} \quad \delta = \frac{\pi d}{\lambda} \Delta n$$

we can in the present case of an un-oriented sample integrate the first factor containing the local optic axis orientation ψ with respect to one polarizer axis, obtaining

$$\langle \sin^2 2\psi \rangle = \frac{1}{2\pi} \int_0^{2\pi} \sin^2 2\psi \, d\psi = \frac{1}{2}$$

thus obtaining the expression valid for a sample of randomly oriented domains

$$I = \frac{I_0}{2} \sin^2 \delta(E)$$

When an unoriented sample exhibiting an antiferroelectric to ferroelectric transition is subjected to e.g. a triangular field, one would thus expect an optical transmission variation solely caused by the field-induced change in the birefringence, $\delta(E)$. Further, the optical response should be independent of the orientation of the sample with respect to the polarizers. This is also what is observed. We show below in figure 9 the response in MHPOBC and in polymer 4. We also show the textures in the two cases. The current response shown together with the optical response will be discussed below.



Figure 9. (a) optical response for MHPOBC. (b) for polymer 4.

Current response

Associated with the observation of three optical states described above is the occurrence of two current peaks instead of one in the polarization reversal current. In figure 10 below is shown a recording of the reversal current and the optical response simultaneously. The first current peak can be interpreted as a ferroelectric to antiferroelectric transition, while the second peak is associated with the anti-erro to ferro transition occurring at higher applied fields. Thus, the antiferroelectric state exists between the two peaks, coinciding with the transmission step in the optical response. By evaluating the area of the peaks one can estimate the polarization of the substance, cf. figure 11. It is found that the polymer is light-sensitive, so that the measured polarization after exposure to the microscope lamp is lower than for a fresh sample.

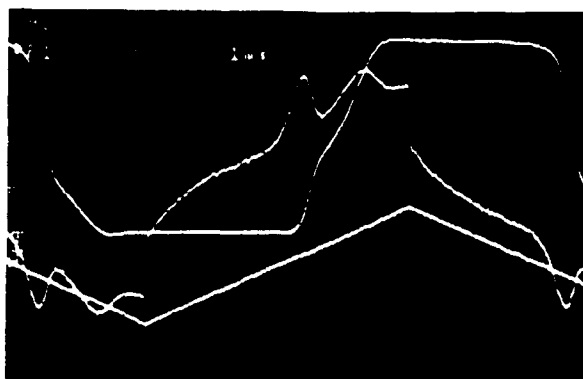


Figure 10. Oscilloscope trace of current and optical responses in polymer 4.

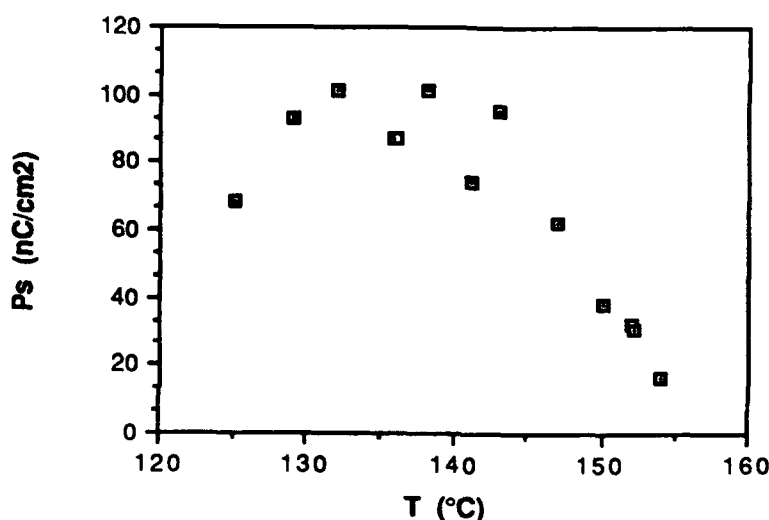


Figure 11. Spontaneous polarization P_s in polymer 4 evaluated from the area of the peaks in figure 10.

DISCUSSION

By comparing measurements on a low molar mass antiferroelectric material (MHPOBC) with the investigated polymer 4, we are able to find several similarities in their electro-optical and current responses. In particular, the fact that the field-induced change of birefringence in unoriented samples correlates with the two polarization reversal current peaks, supports an antiferroelectric model for polymer 4. Further evidence comes from the fact that one does not observe a Goldstone mode in the dielectric spectrum (which was measured above 1 Hz). This is similar to the dielectric behaviour of MHPOBC, which is essentially flat up to 1 MHz.

There is the possibility that the electro-optical response in polymer 4 could be related to a very short helical pitch. In order to investigate this point, we studied the switching in the low molar mass ferroelectric substance CE-3, which has a pitch less than 0.5 μm . Indeed, in "unoriented" samples an optical response of the birefringence modulation type discussed above could be observed. However, the characteristic current response for

MHPOBC with two peaks could not be found. In order to develop the investigations further, it would be desirable to observe the polymer in a homeotropically aligned sample in order to observe conoscopically the transition. Additional questions are raised by recent reports of similar switching behaviour in polymers with other side-group structures. One could speculate about the possibility that in a side-chain polymer there is a mechanism favouring antiferroelectric ordering.

ACKNOWLEDGEMENTS

Work supported by the National Swedish Board for Technical Development and the Swedish Natural Science Research Council.

REFERENCES

1. V.P. Shibaev, M.V. Kozlowskii, L.A. Beresnev, L.M. Blinov, and N.A. Plate, *Polym. Bull.* **12**, 299 (1984).
2. For a review, see e.g. P. Le Barny and J.C. Dubois, in *Side Chain Liquid Crystal Polymers*, C.B. McArdle, ed., (Blackie and Son, Glasgow, 1989), p. 130.
3. S. Uchida, K. Morita, K. Miyoshi, K. Hashimoto, and K. Kawasaki, *Mol.Cryst.Liq.Cryst.* **155**, 93 (1988).
4. G. Scherowsky, A. Schliwa, J. Springer, K. Kühnpast, and W. Trapp, *Liq.Cryst.* **5**, 1281 (1989).
5. J. Bömelburg, G. Heppke, and J. Hollidt, Proceedings, 20. Freiburger Arbeitstagung Flüssigkristalle, 20-22/3 1991, P 25.
6. K. Kühnpast, J. Springer, and G. Scherowsky, Proceedings, 20. Freiburger Arbeitstagung Flüssigkristalle, 20-22/3 1991, P 26.
7. A.D.L. Chandani, E. Gorecka, Y. Ouchi, H. Takezoe, A. Fukuda, *Jap.J.Appl.Phys.* **28**, L1265 (1989).
8. H. Kapitzka, R. Zentel, R.J. Twieg, C. Nguyen, S.U. Vallerien, F. Kremer, C.G. Willson, *Adv. Mater.* **2**, (1990) No. 11.
9. H. Poths, R. Zentel, S.U. Vallerien, F. Kremer, *Mol.Cryst.Liq.Cryst.* in press.
10. H. Kapitzka, R. Zentel, *Makromol.Chem.* in press.
11. H. Coles, R. Simon, H. Gleeson, G. Scherowski, A. Schliwa, and U. Müller, *Polymer Preprints, Japan (English Edition)*, Vol. 39, Nos. 1-4 (Supplement), p. S 5.
12. K. Skarp and G. Andersson, *Ferroelectrics Lett.* **6**, 67 (1986).
13. G. Andersson, I. Dahl, L. Komitov, M. Matuszczyk, S.T. Lagerwall, K. Skarp, B. Stebler, *Ferroelectrics* **114**, 137 (1991).

LINEAR ELECTROMECHANICAL EFFECT IN A POLYMERIC FERROELECTRIC LIQUID CRYSTAL

N. ÉBER, L. BATA

Central Research Institute for Physics, Hungarian Academy of
Sciences, H-1525 Budapest, P.O.Box 49

G. SCHEROWSKY, A. SCHLIWA

Institute für Organische Chemie, Technische Universität Berlin,
W-1000 Berlin 12, Germany

Abstract A linear electromechanical effect was detected in a ferroelectric side chain polymeric liquid crystal. Experimental data on temperature and frequency dependence are presented.

INTRODUCTION

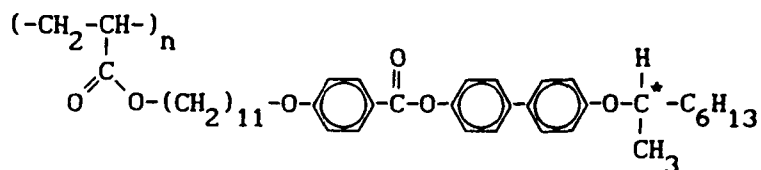
Ferroelectricity is one of the most remarkable features of the chiral smectic C^* (S_C^*) liquid crystals¹. Due to the presence of spontaneous polarization this phase exhibits a fast electrooptical switching² as well as a linear electromechanical effect³ which has been studied in detail for various monomeric liquid crystals.⁴⁻⁸

There exist polymeric liquid crystals which possess S_C^* phase, hence these polymers are ferroelectric too.⁹⁻¹² Two of us have synthesized even such polymers which exhibit fast electrooptical switching as well.¹³⁻¹⁵

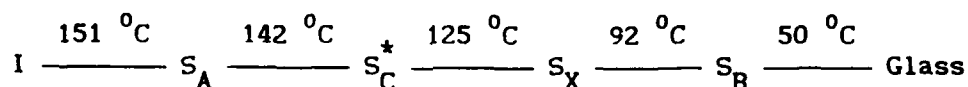
Recently a linear electromechanical effect, similar to that observed in low molar mass liquid crystals, has also been detected in polymeric S_C^* liquid crystals.^{16,17} In this paper we present some experimental data about this phenomenon.

SAMPLE AND EXPERIMENTAL SET-UP

Our measurements were carried out using a polyacrylate side chain polymer with a chemical formula^{13,14}



having $M_w=15000$ and its polydispersity characterised by $M_w/M_n=1.5$. Based on polarisation microscopy of $2 \mu\text{m}$ samples and DSC the phase sequence of this compound has been reported as:



In the S_C^* phase the sample exhibited fast ferroelectric switching, however, in the S_X phase only a switching of electroclinic type could be detected.¹⁴

In order to determine the electromechanical response of the polymer we used the experimental set-up shown in Figure 1, a similar one as for investigation of monomers.^{4,5,7} The polymeric liquid crystal was introduced in its isotropic phase in between two ITO coated glass plates separated by $15 \mu\text{m}$ thick teflon spacers. The lower glass plate was fixed to a thermostage while the upper one was connected to the membrane of a loudspeaker via a rigid metal rod, hence the upper glass could slide easily on the spacers. Parallelism of the cell was ensured by micropositioning supports. A piezoelectric accelerometer (Brüel&Kjær 4375) was attached to the connecting rod allowing detection of vibrations against the loudspeaker membrane, i.e. in a direction parallel to the glass plates. Using a charge amplifier we obtained an electric signal proportional to the acceleration (1000 mV/ms^{-2} at maximum sensitivity) which was analysed by a lock-in amplifier (Ithaco 3962). The AC voltage from the internal oscillator of the lock-in was applied to the electrodes via a high

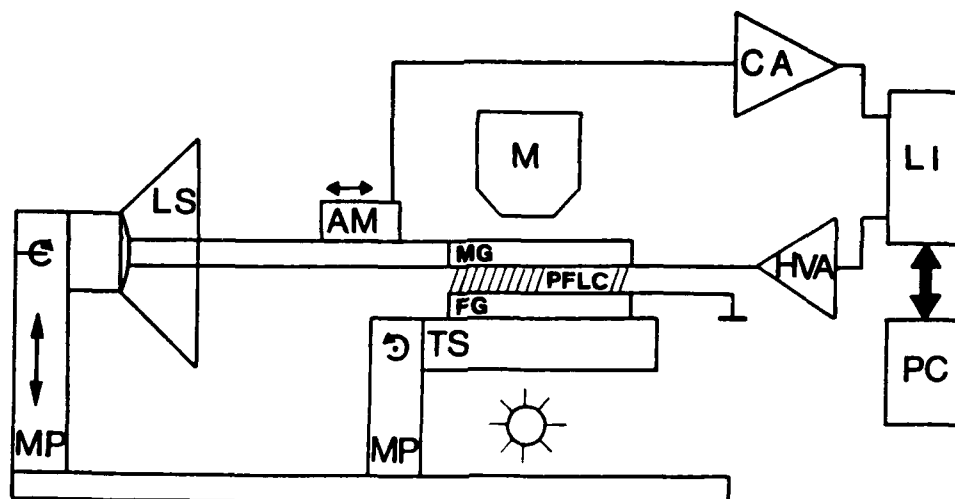


FIGURE 1 Experimental set-up for vibration measurements. MG: moving glass, FG: fixed glass, MP: micropositioning support, PFLC: polymeric ferroelectric liquid crystal, TS: thermostage, M: polarising microscope, LS: loudspeaker, AM: accelerometer, CA: charge amplifier, HVA: high voltage amplifier, LI: lock-in amplifier, PC: computer

voltage amplifier. During measurements the texture of the sample was observed by a polarizing microscope.

The glass plates were spincoated by polyimide but only one of them was rubbed, so in order to obtain a planar orientation the sample was sheared¹⁸ at the $I-S_A$ phase transition in an applied AC field.

Unfortunately our sample possessed a very broad $I-S_A-S_C^*$ phase transition, i.e. a coexistence of three phases was detected over a 10 °C temperature interval in the form of domains of different phases. Within a domain the transitions into the other smectic phases were sharp, however, in various domains they occurred at different temperatures within a range of 5-10 °C. This inhomogeneity of the cell remained even after repeated heating-cooling cycles. Due to this merging $I-S_A-S_C^*$ phase transitions the sample was only partially orientated with a lot of focal conics. We could not decide whether this feature was due to the larger sample thickness or to material degradation.

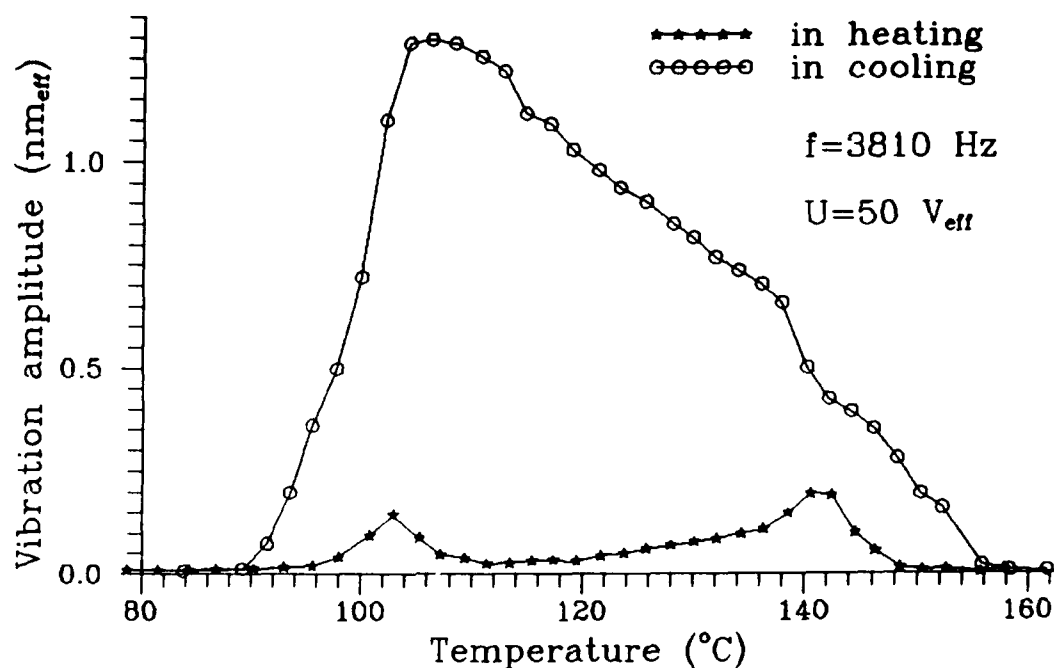


FIGURE 2 Temperature dependence of the vibration amplitude.

RESULTS AND DISCUSSION

When an AC voltage was applied onto the sample in the S_C^* phase, a mechanical vibration of the upper plate occurred just as in case of low molar mass S_C^* liquid crystals³. The direction of the displacement was parallel to the glass plates. In case of sine-wave excitation the waveform of the acceleration signal is typically a slightly distorted sine-wave of the same frequency, where the higher harmonic distortion is more pronounced at higher voltages and lower frequencies. This means that the linear electromechanical effect does exist in the investigated polymeric S_C^* liquid crystal. Since we were interested in this linear phenomenon we measured only the linear component of the acceleration by the lock-in amplifier.

In Figure 2 we present the temperature dependence of the vibration amplitude. Despite of the poor orientation, the vibration amplitudes are of similar order of magnitude as in S_C^* phase of low

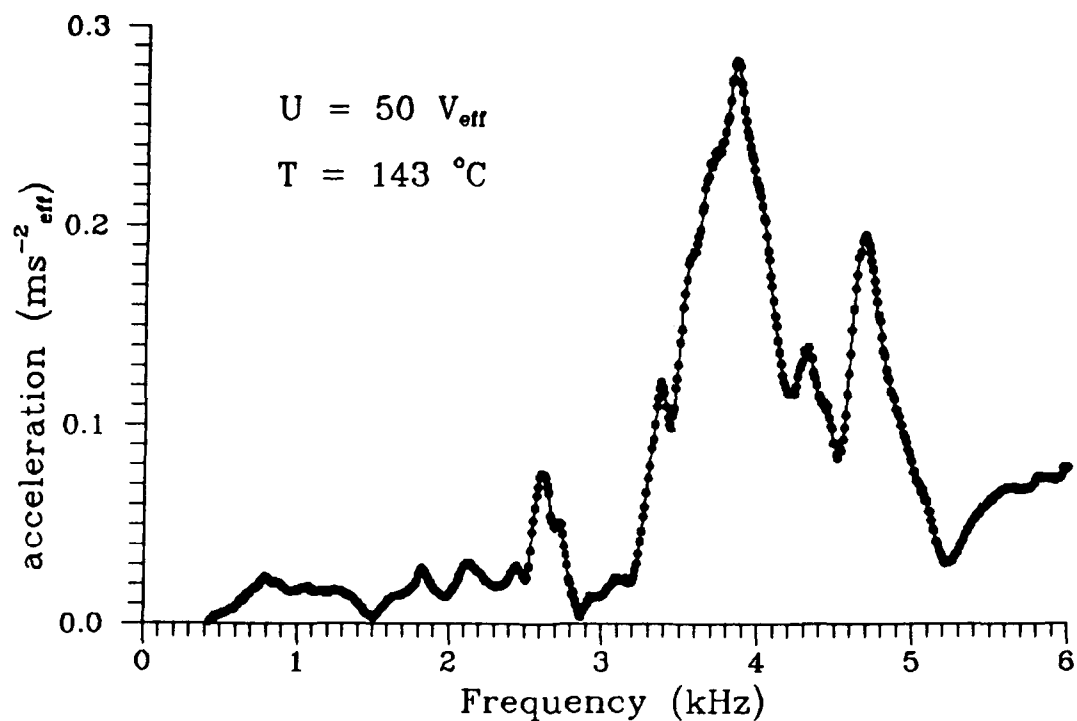


FIGURE 3 Frequency dependence of the acceleration in S_C^* phase.

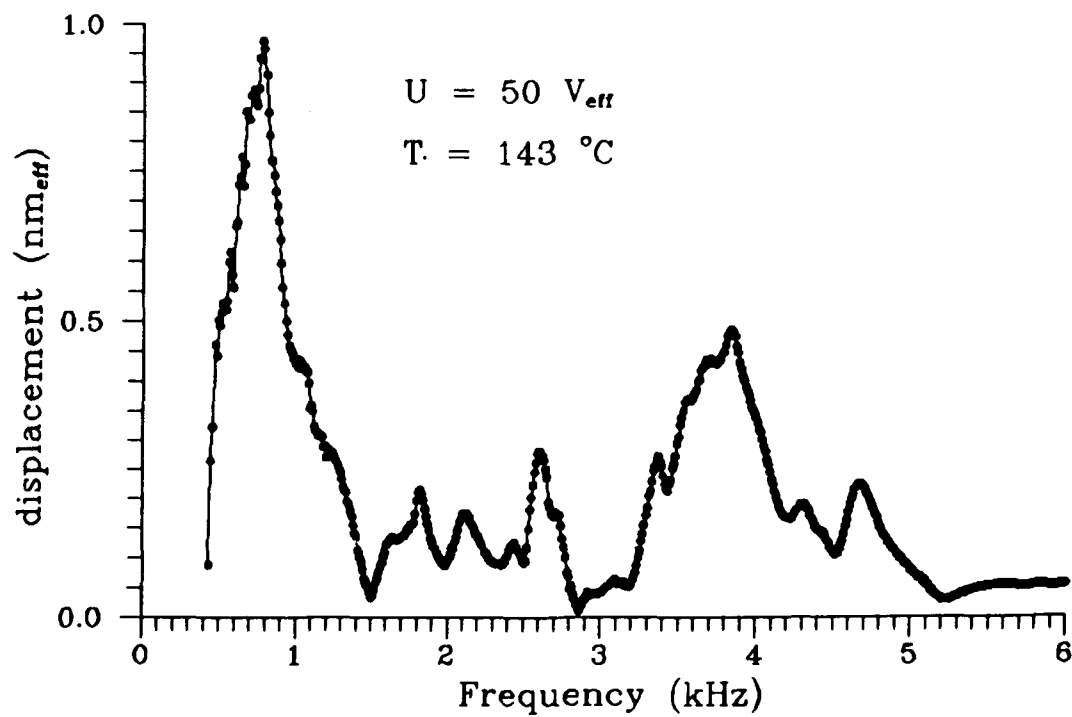


FIGURE 4 Frequency dependence of the displacement in S_C^* phase.

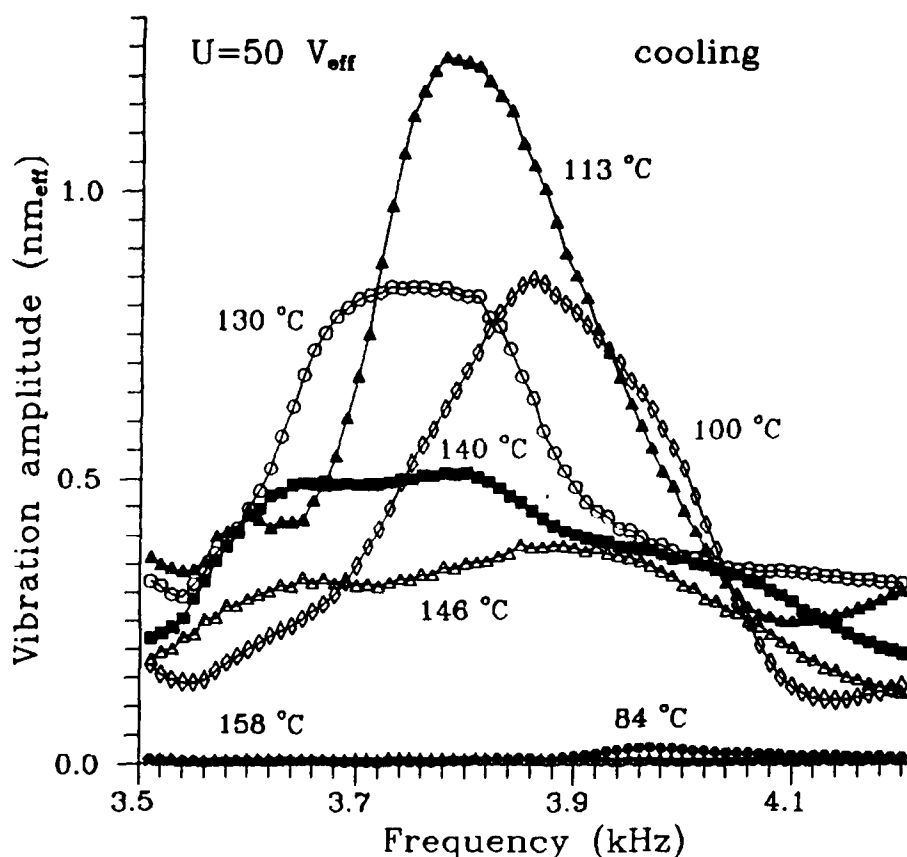


FIGURE 5 Frequency dependence of the vibration amplitudes at some temperatures during cooling.

molar mass compounds⁷ and are about three orders of magnitude larger than those reported recently for another ferroelectric polymer¹⁶. Figure 2 illustrates that this electromechanical effect is existing even in the lower temperature S_X phase of the same compound, moreover, it may be stronger in S_X than in S_C^* .

We have investigated the frequency dependence of the vibration amplitudes as well. It can be seen in Figure 3 that the acceleration versus frequency plot exhibits several maxima in the 0.5 - 6 kHz range, a behaviour similar to that of monomers⁷. The calculated displacement is plotted in Figure 4 illustrating that larger displacements are typically obtained from lower frequency vibrations.

In order to obtain information on the temperature dependence we

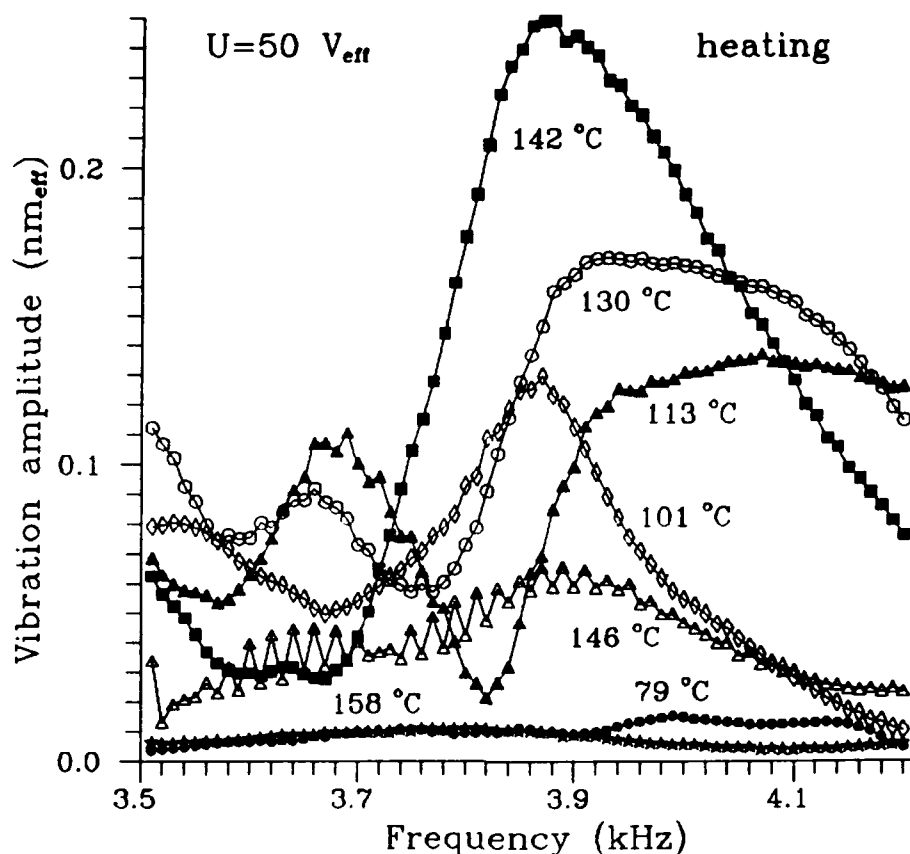


FIGURE 6 Frequency dependence of the vibration amplitudes at some temperatures during heating.

mapped the spectrum around the most pronounced resonance peak (3.81 kHz) at various temperatures by changing the frequency of excitation in 10 Hz increments while the amplitude of the applied voltage ($U=50 \text{ V}_{\text{rms}}$) was held constant. Some typical spectra are plotted in Figures 5 and 6 for cooling and heating the sample respectively.

The figures show that the behaviour of the sample is definitely different in heating or in cooling. This concerns the vibration amplitudes at a given frequency as well as the value of the resonance frequencies. The shift of the resonance frequency with temperature is more pronounced in the heating cycle which explains the appearance of the double peak in the temperature dependence of the vibration

amplitude in Figure 2.

The macroscopic properties of the polymeric liquid crystals should be influenced by the interaction of the long flexible main chains hindering molecular motions. This appears in higher viscosities as well as in difficulties of obtaining well aligned samples. However, S_C^* polymers possess the same symmetries as their low molar mass counterparts, i.e. the special properties related to the symmetries of the phase (e.g. ferroelectricity) should be similar. So we can expect that the main reason for the appearance of the linear electromechanical effect in ferroelectric polymers are the same as in ordinary S_C^* liquid crystals⁴.

The vibration amplitudes are very sensitive to texture changes. This may be responsible for the difference of behaviour between cooling and heating runs in Figures 2, 5 and 6. For example when the sample was cooled down from the isotropic phase it might have been more ordered (more planar) yielding larger vibration amplitudes than when it was heated up from the glassy or S_B phase.

For the existence of resonances we can list two reasons. First, any mass subjected to an elastic restoring force may show a resonance. In our set-up the elastic force acting on the upper glass plate is either due to the displacement of the loudspeaker membrane which behaves like a spring or it is the elastic surface force exerted by the liquid crystal due to deformation of smectic layers in the focal conics caused by the shear.

Secondly, as it has been shown recently,¹⁹ zig-zag defects of the chevron texture can cause resonances as well. Owing to these simultaneously acting mechanisms our cell is part of a mechanical system having several eigenfrequencies which may correspond to the complicated spectrum in Figure 3. Unfortunately our data are not enough to separate the various mechanisms.

This work was partially supported by the Hungarian National Research Fund (OTKA-1756).

REFERENCES

1. R.B. Meyer, L. Liebert, L. Strzelecki and P. Keller, J.Physique Lett., 36, 69 (1975)
2. N.A. Clark and S.T. Lagerwall, Appl.Phys.Lett., 36, 899 (1980)
3. A. Jákli, L. Bata, Á. Buka, N. Éber and I. Jánossy, J.Physique Lett., 46, L-759 (1985)
4. A. Jákli, L. Bata, Á. Buka and N. Éber, Ferroelectrics, 69, 153 (1986)
5. A. Jákli, N. Éber and L. Bata, Liquid Crystals, 5, 1121 (1989)
6. G. Pór and Á. Buka, J.Physique, 50, 783 (1989)
7. A. Jákli and L. Bata, Ferroelectrics, 103, 35 (1990)
8. A. Jákli and L. Bata, Liquid Crystals, 7, 105 (1990)
9. V.P. Shibaev, M.V. Kozlovsky, L.A. Beresnev, L.M. Blinov and N.A. Platé, Polym.Bull., 12, 299 (1984)
10. G. Decobert, J.C. Dubois, S. Esselin and C. Noel, Liquid Crystals, 1, 307 (1986)
11. R. Zentel, R. Reckert and B. Rack, Liquid Crystals, 2, 83 (1987)
12. G. Scherowsky, U. Müller, J. Springer, W. Trapp, A.M. Levelut and P. Davidson, Liquid Crystals, 5, 1297 (1989)
13. G. Scherowsky, A. Schliwa, J. Springer, K. Kühnpast and W. Trapp, Liquid Crystals, 5, 1281 (1989)
14. G. Scherowsky, A. Schliwa, E. Rhode, U. Müller and H.J. Coles, 8th Liq.Cryst.Conf.Soc.Countries, Krakow, Abstract H 17 (1989)
15. H.J. Coles, H.F. Gleeson, G. Scherowsky and A. Schliwa, Mol.Cryst. Liq.Cryst.Lett., 7, 117 (1990)
16. A. Jákli and A. Saupe, Liquid Crystals, 9, 519 (1991)
17. N. Éber, L. Bata, G. Scherowsky and A. Schliwa, Post deadline poster at 13th Int.Liq.Cryst.Conf., Vancouver, (1990)
18. A. Jákli, I. Jánossy, L. Bata and Á. Buka, Cryst.Res.Technol., 23, 949 (1988)
19. A. Jákli, L. Bata and N. Éber, Ferroelectrics, 113, 305 (1991)

A CHIRAL SIDE-CHAIN POLYMER WITH LAYERED STRUCTURE

LAJOS BATA, KATALIN FODOR-CSORBA, JÁNOS SZABON

Central Research Institute for Physics,
H-1525 Budapest, P.O.Box 49, Hungary

MIKHAIL V. KOZLOVSKY

Institute of Crystallography,
59. Leninskii pr., Moscow, 117333, USSR

SÁNDOR HOLLY

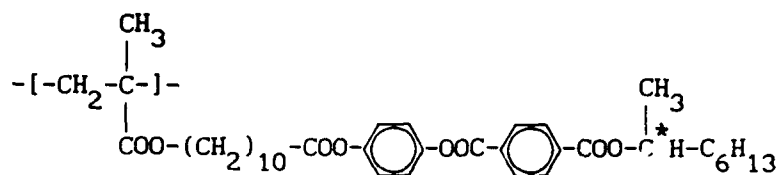
Central Research Institute for Chemistry,
H-1525 Budapest, P.O.Box 17, Hungary

Abstract A chiral side-chain polymer was synthesized and its chemical structure was proved by infrared spectroscopy. According to the X-ray diffraction studies the polymer exhibited smectic type ordering however it did not show any birefringence macroscopically.

INTRODUCTION

Comb-like polymers with chiral moieties in mesogenic side chains are widely studied recently, particularly since tilted smectic phases of such polymers have ferroelectric properties¹⁻⁶. Some dozens of polymers of that type have been synthesized, nevertheless careful studies of structure and physical properties have been carried out only for few of them.

To continue our study on comb-like polymethacrylates having chiral substituents in phenyl benzoate mesogenic side chains, we have synthesized a new polymer P8^{*}M with the following formula:



Chemical structure of the polymer P8^{*}M suggested possible existence of S_C^{*} phase and therefore presence of spontaneous polarization.

EXPERIMENTAL

The monomer 4-(11-methacryloyloxyundecanoyloxy)-phenyl-4'-(1-(S)-methylheptyloxycarbonyl)-benzoate (IV) has been synthesized using standard scheme² as shown in Fig. 1.

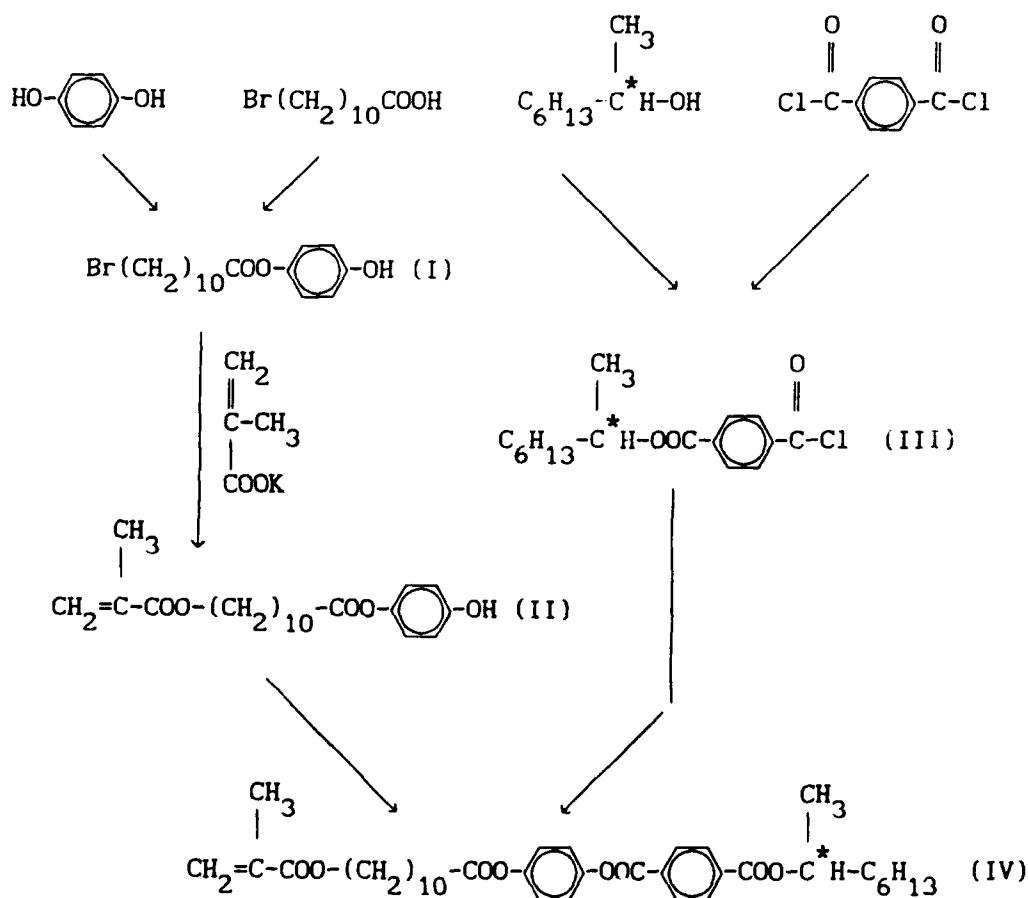


Figure 1. Scheme of synthesis of monomer (IV).

The purity of the intermediates and final product was checked by thin-layer chromatography using Kieselgel 60 F₂₅₄ (Merck) plates. The thin-layer plates were visualized by iodine vapour and later spraying with KMnO₄ solution (5% in water). The methacrylic group containing compounds appeared as green spots since the other easily oxydizable compounds gave white or yellow spots on a dark background.

The structure and physical properties of the compounds were characterized by the following methods:

Infrared spectra were taken with a Nicolet 170 SX FT-IR spectrometer in KBr pellets. The melting points were measured with a Boetius micro melting point equipment. DSC curves were taken with a Perkin Elmer DSC-2 equipment. X-ray curves were measured by diffractometer with a linear position sensitive detector using CuK_α radiation filtered by Ni film.

The 4-(11-bromoundecanoyl)-phenol (I) was obtained by semi-esterification of hydroquinone with 11-bromoundecanoic acid. Then bromine atom of I was replaced by methacryloyl group in reaction with potassium-methacrylate thus giving (II), as described earlier².

The 4-(11-methacryloyloxy)-undecanoyloxy-phenol (II) melted at 34°C. In its infrared spectrum the OH stretching vibration of the phenolic hydroxyl group was at 3340 cm⁻¹. The stretching vibrations of the methylene groups were at 2930 and 2850 cm⁻¹, the C=O vibrations of the phenolic ester group appeared at 1760 cm⁻¹, while the C=O vibration of the conjugated ester could be assigned at 1720 cm⁻¹. The C=C stretching vibration of the vinylidene group was at 1640 cm⁻¹, vibrations of the aromatic skeletal were at 1600 and 1510 cm⁻¹, the deformation vibrations of the para disubstituted benzene ring was observed at 820 cm⁻¹.

The 4-(1-(S)-methylheptyloxycarbonyl)-benzoyl chloride (III) was synthesized by semi-esterification of terephthaloyl dichloride with equimolar amount of S(-)-2-octanol in boiling benzene. After finishing the reaction the solvent was evaporated and the crude product distilled. Boiling point was 132°C at 0.026 kPa.

The 4-(11-methacryloyloxy-undecanoyloxy)-phenyl-4'-(1-(S)-methylheptyloxycarbonyl)-benzoate (IV) was synthesized by dropping the dry benzene solution of III (1 mole) into the well stirred mixture of II (1 mole) and triethylamine (1,2 mole) in dry benzene solution at room temperature. After two hours stirring the benzene was evaporated and the product separated by preparative column chromatography on Kieselgel 60 sorbent using ethyl acetate:benzene=1:14 mixture as eluant. The column chromatography was followed by thin-layer chromatography on Kieselgel 60 F₂₅₄ plates eluted with the same solvent mixture. The R_f value of the semicrystalline oil was 0.46.

Polymer P8^{*}M has been obtained by radical polymerization of the monomer (IV) in benzene solution using α,α' -azo-bis-isobutyro-nitril as initiator. Mean molar mass of the polymer appeared to be $m_w=99000$ with $m_w/m_n=2.7$ determined by gel permeation chromatography (GPC) using poly-(methyl-methacrylate) as standard.

The infrared spectrum of the P8^{*}M is shown in Fig.2. Stretching CH vibrations of the methylene groups appeared at 2920 and 2850 cm⁻¹. The stretching vibration of C=O in phenolic ester group was observed at 1760 cm⁻¹, while the C=O vibrations of the other esters could be assigned at 1730 and 1715 cm⁻¹. The vibrations of the aromatic skeletons can be characterized by the absorptions at 1495 cm⁻¹, and the CH deformation vibrations of the para disubstituted benzene rings were observed at 855 cm⁻¹.

Its optical rotation was $[\alpha]_D^{20}=-17.2^\circ$ (c=5, benzene).

RESULTS AND DISCUSSION

DSC curves of the polymer P8^{*}M (Fig.3) show one transition peak with pronounced supercooling ($T_m=64^\circ\text{C}$ in heating while $T_m=43^\circ\text{C}$ in cooling) having a transition heat of $\Delta H=15,5\pm 1$ J/g, and a glassing process at $T_g=30^\circ\text{C}$ (in the cooling cycle it seems to be covered by the transition peak).

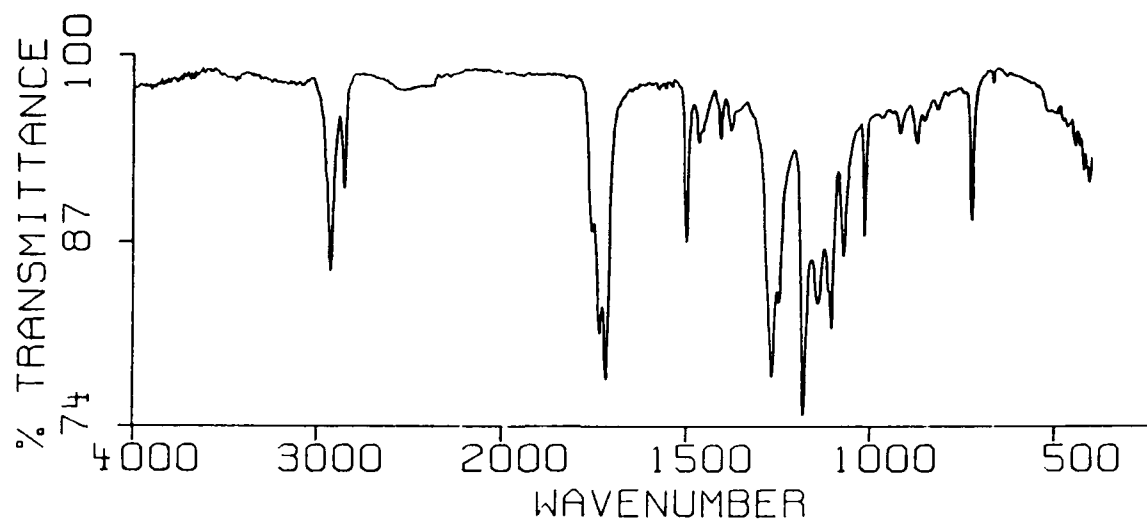


Figure 2. Infrared spectrum of the P8* M polymer

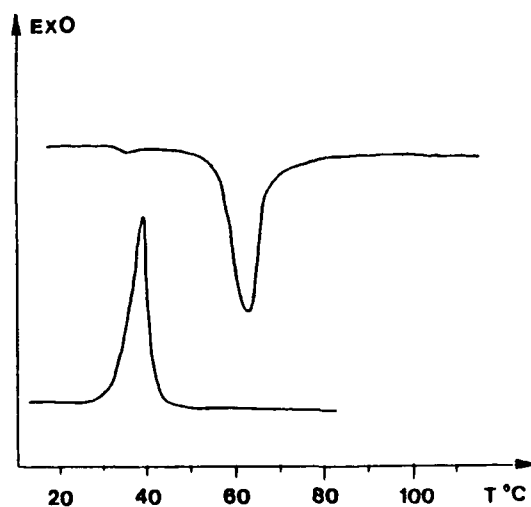


Figure 3. DSC curve of polymer P8* M

The surprising is the fact that polymer P8* M has no birefringence neither below nor above T_m value, so no phase transition can be observed by microscope. The polymer is completely transparent in bulk after precipitation and drying. Thin films of the polymer are transparent as well and do not show any birefringence, though polymer fibers can be observed in crossed polarizers as white

lines without any texture. (The latter is known for many polymers which are isotropic in bulk, e.g. polyethylene but orientation in this case is insufficient to be observable by X-ray diffraction).

Thus, layered structure of the polymer $P8^*M$ cannot be observed using visible light (with wavelength 300-700 nm), because of the short correlation length of the structure but it can be clearly observed by CuK_{α} X-rays with wavelength 0.15 nm. This is caused by the fact that the wavelength of the X-ray probe beam ($\lambda_{CuK_{\alpha}} = 0.15$ nm) is much shorter than the correlation length ($\xi_{\parallel} = 8.2$ nm) which is determined from the width of the basic X-ray peak.

The X-ray scattering pattern below T_m shows three orders of reflection (Fig. 4.), one at $2\theta = 1.4^{\circ}$ corresponding to a smectic type layered lattice with interlayer distance $d = 6.33$ nm: these three reflections disappear when the polymer is heated above T_m .

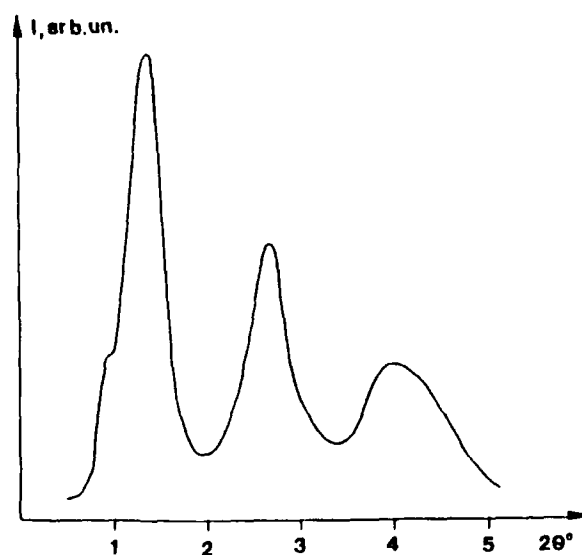


Figure 4. X-ray diffraction curve of $P8^*M$ at $20^{\circ}C$ with three orders of reflexion, $2\theta = 1.4^{\circ}$; 2.8° and 4.2°

To discuss the nature of low temperature phase of the polymer we should note first that interlayer distance is longer than the calculated length of mesogenic group (about 4.1 nm) but less than the doubled length. This suggests bilayer structure: either

S_A -like with mutual penetration of neighbouring layers i.e. $d=1.54 \times 4.1=6.3$ nm or S_C -like with tilt angle about 44° . The factor 1.54 is about the value what we used to get for such type bilayer structure. More precise determination of the structure would be possible only on the basis of X-ray diffraction on oriented sample, these experimental data attest the S_A like structure.

Furthermore it should be noted that the diffraction curve shows the presence of small part of other mesogenic groups package i.e. a shoulder at $2\theta=1^\circ$ on the first reflection peak in Fig.4 corresponds to a length of 8.5 nm at room temperature (marked \square in Fig.5) which coexists with S_A like structure.

One more consideration in favor of S_A -like structure of the polymer is the absence of pyroelectric effect near the transition temperature T_m .

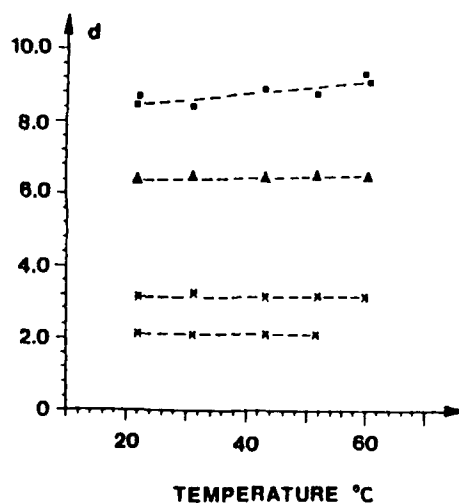


Figure 5. Layer spacings calculated from the X-ray diffraction peaks of P8^{*}M versus temperature.

- Δ corresponding to the smectic layer spacing ($d=6.33$)
- $*$ values calculated from the higher ordered reflections,
- \blacksquare corresponding to the shoulder peak at the first reflection

Practically, no clear temperature dependence could be observed either for positions of three orders of reflection (Fig.5) or for the value of correlation length $\xi_{||}$ calculated from the width of the basic X-ray peak (Fig.6). The only result of melting is in the decrease of the peak intensity until it completely vanishes (Fig.7).

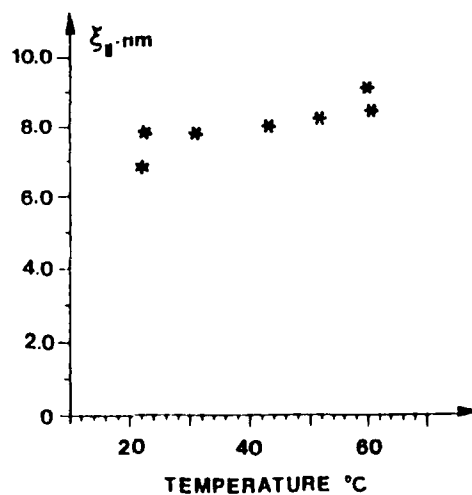


Fig.6. Correlation length $\xi_{||}$ calculated from the width of the basic X-ray peak versus temperature

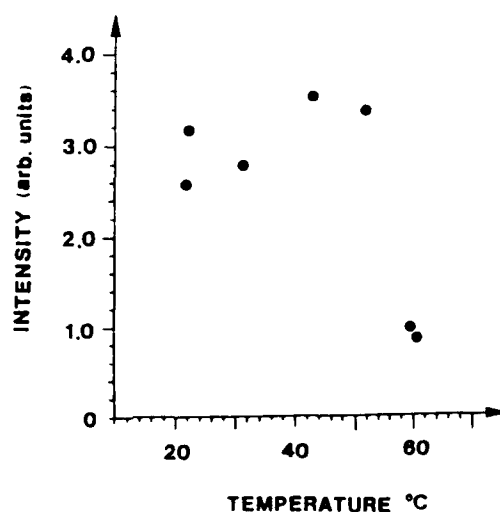


Figure 7. Relative intensity of the basic X-ray peak versus temperature

The whole picture of X-ray diffraction is not characteristic for true smectic phase, mainly due to extremely low values of the correlation length ($\xi_{\parallel} \sim 7-9$ nm, i.e. 1.5 "smectic" layers or two side chains). Diffraction curves of such type have been obtained for amorphous poly-(n-alkyl-methacrylates) with long enough aliphatic side chains⁷ and for nematic and cholesteric LC polymers⁸⁻¹⁰, but we have no evidence of orientational ordering in P8^{*}M below the phase transition point; on the contrary, the phase is macroscopically isotropic opposite to both cases mentioned above. From the other hand if we suggested it being "cibotactic isotropic phase", i.e. isotropic liquid with virtual areas of smectic order, it would be difficult to explain the rather high transition heat value.

CONCLUSION

The synthesized polymer P8^{*}M has chemical structure similar to ferroelectric polymers described earlier²; nevertheless it has no birefringence at all which could be attributed to an amorphous like polymer with some elements of smectic structure, probably of orthogonal bilayer one with superposition of mesogenic groups of neighbouring layers. More accurate and detailed investigations are necessary to determine the actual structure of the polymer below the phase transition point, e.g. X-ray diffraction patterns from a sample cooled slowly in strong magnetic field and study of IR dichroism in various sample geometry.

The polymer P8^{*}M itself has no ferroelectric properties but may be tested as component of composite ferroelectric materials or as the basis for copolymers with non-chiral S_C polymer matrix.

REFERENCES

1. V.P. Shibaev, M.V. Kozlovsky, L.A. Beresnev, L.M. Blinov, N.A. Plate, Polymer Bull., **12**, 299 (1984)
2. V.P. Shibaev, M.V. Kozlovsky, N.A. Plate, L.A. Beresnev, L.M. Blinov, Liquid Crystals, **8**, 545 (1990)
3. S. Esselin, C. Noel, G. Decobert, J.C. Dubois, Mol.Cryst.Liq. Cryst., **155**, 371 (1988)
4. P. Keller, Ferroelectrics, **85**, 425 (1988)
5. S. Uchida, K. Morita, K. Miyoshi, K. Hashimoto, K. Kawasaki, Mol.Cryst.Liq.Cryst., **155**, 93 (1988)
6. G. Scherowsky, A. Schliva, J. Springer, K. Kunpast, W. Trapp, Liquid Crystals, **5**, 1281 (1989)
7. Comb-shaped polymers and liquid crystals, ed. N.A. Plate and V.P. Shibaev, (Plenum Press, New York-London, 1987)
8. V.V. Tsukruk, V.V. Shilov, Structure of polymeric liquid crystals, (Naukova Dumka, Kiev 1990, 256. English version is to be published in 1991 by Springer Verlag, Germany.
9. P. Davidson, A.M. Levelut, M.F. Achard, F. Hardouin, Liquid Crystals, **4**, 561 (1989)
10. Ya.S. Freidzon, E.G. Tropsha, V.V. Tsukruk, V.V. Shilov, V.P. Shibaev, Yu.S. Lipatov, Vysokomol. Soed., **29**, 1371 (1987)

INDUCED SPONTANEOUS POLARIZATION IN A SIDE CHAIN POLYMER

GÜNTHER SCHEROWSKY, KIRSTEN GRÜNEBERG

Institut für Organische Chemie, Technische Universität
Berlin, Germany

KURT KÜHNPAST

Institut für Technische Chemie, Technische Universität
Berlin, Germany

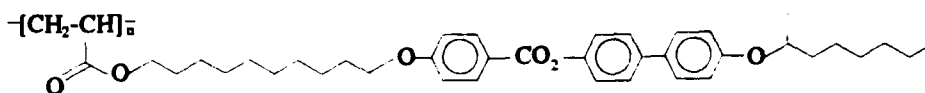
Abstract It is possible to induce a spontaneous polarization in a racemic side chain polyacrylate by doping with a low-molecular weight chiral compound. The spontaneous polarization was measured as a function of temperature and of concentration of the dopant.

INTRODUCTION

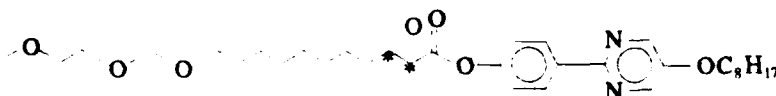
The phenomenon of induced spontaneous polarization in low-molecular weight S_C -liquid crystals is well known. Different concentration dependencies have been evaluated. As a rule the spontaneous polarization shows a nonlinear dependence on concentration of chiral dopant. In case of low concentrations a linear coherency was observed /1/.

Till now there exists only one example for the transformation of a S_C -phase in a polymer into a ferroelectric S_C^* - phase by adding a chiral mesogenic dopant /2/. This polymer was of the main chain type.

The aim of this work was to investigate the possibility of changing the S_C -phase of the racemic side chain polyacrylate A into a S_C^* -phase by doping with the low-molecular weight chiral compound B.



A



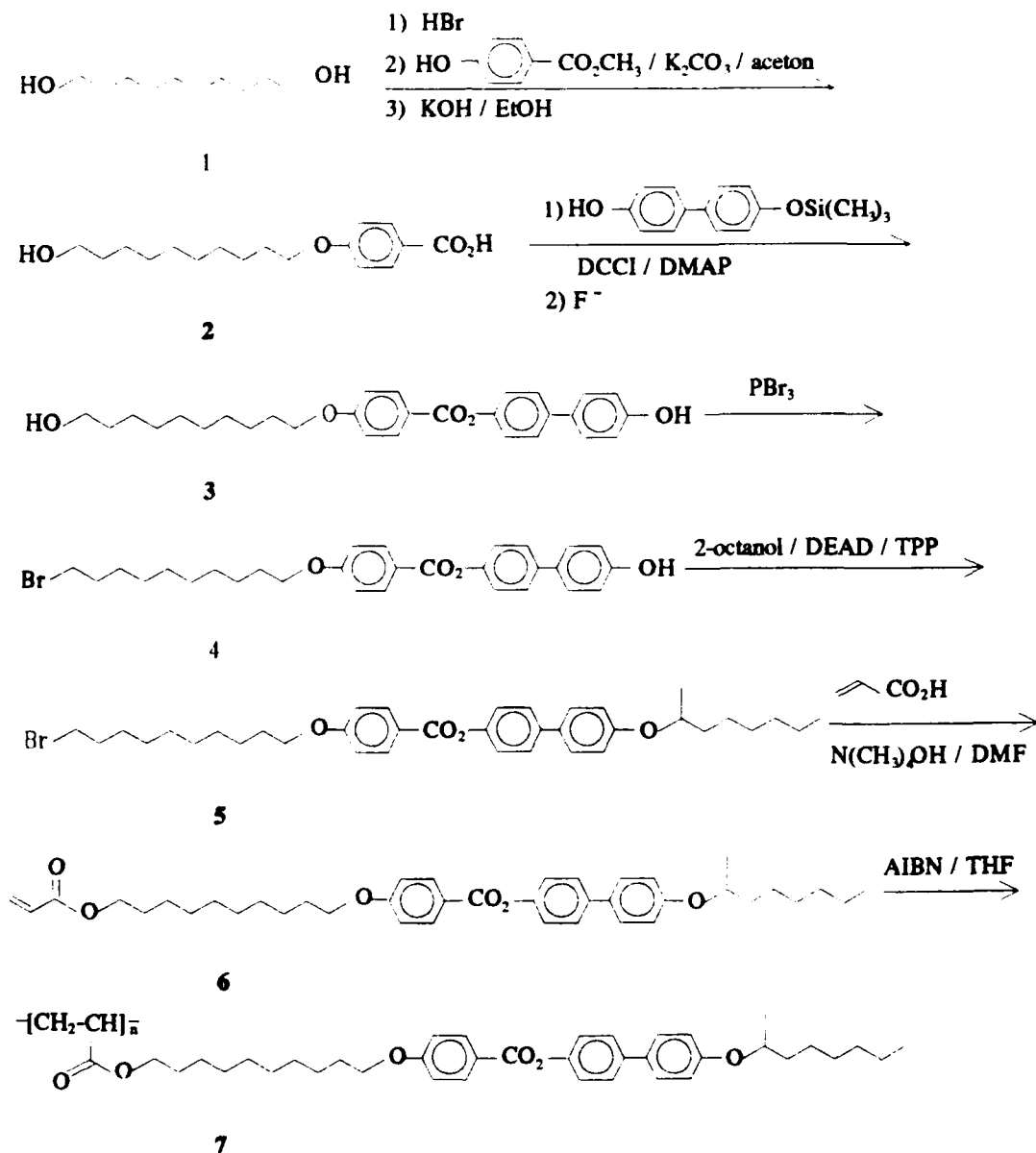
B

SYNTHESIS

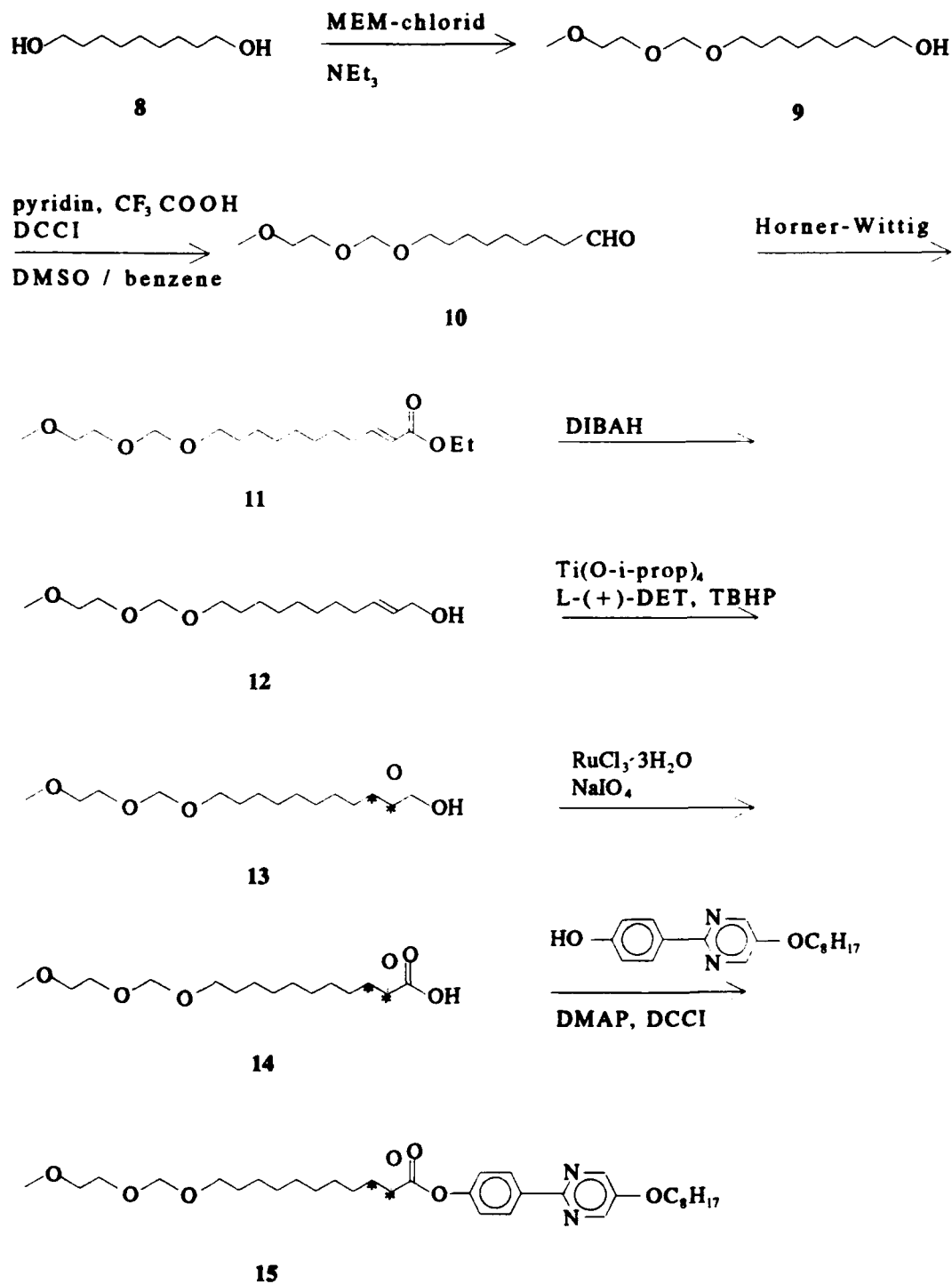
The nine step reaction sequence leading to the racemic side chain polyacrylate A is shown in scheme 1 /3/. 10-bromo-1-decanol, obtained by reaction of 1,10-decandiol 1 with HBr, was used to alkylate methyl-4-hydroxybenzoate to give methyl-4-(10-hydroxydecyloxy)-benzoate, which was saponified yielding 2. This product was combined with monosilylated 4,4'-dihydroxy-biphenyl to give after deprotection 3. Reacting 3 with phosphoroustribromide yielded 4. Etherification of 4 with 2-octanol using the Mitsunobu reaction [dimethyl azodicarboxylate (DEAD) plus triphenylphosphine (TPP)] /4/ yielded 5. Reaction with acrylic acid in presence of tetramethylammoniumhydroxide-hexahydrate gave the monomer 6. The polymerization in THF yielded the polymer 7 with a molecular weight of $M=12500$ g/mol ($M_w/M_n=1.43$).

Scheme 2 illustrates the reaction sequence for the chiral oxirane ester B used as dopant /5/. After one-sided protection of 1,9-nonandiol 8 as MEM-ether the second hydroxygroup was oxidized using dicyclohexylcarbodiimide (DCCI) and DMSO. The Horner-Wittig-reaction with ethyl-phosphonoacetate yielded 11, which was reduced to the allylic alcohol 12 using diisobutylaluminiumhydride (DIBAL).

The chiral oxirane 13 we obtained by asymmetric epoxidation of 12 via the Sharpless procedure /6/. The enantiomeric excess was determined by the Mosher method /7/ (ee>95). After oxidation of 13 with rutheniumtrichloride / sodiumperiodate to acid 14 the Steglich-reaction was used to esterificate with 2-(4-hydroxyphenyl)-5-octyloxy pyrimidine in presence of DCCI and dimethylaminopyridine (DMAP) to yield the mesogenic oxirane 15.



Scheme 1. Reaction pathway to the racemic polyacrylate



Scheme 2. Reaction pathway to the chiral dopant

INVESTIGATIONS

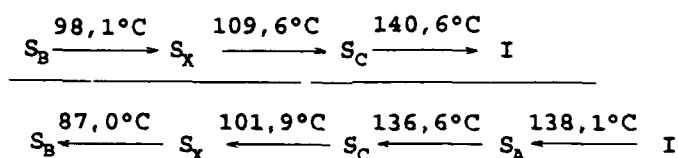
The phase behaviour was determined by polarizing microscopy, differential scanning calorimetry (DSC) and x-ray measurements.

The spontaneous polarization was measured by the triangular wave method using $4\mu\text{m}$ -cells coated with polyimide to give planar orientation.

The mixtures were prepared in the isotropic phase. The cells were filled using the temperature gradient method.

RESULTS AND DISCUSSION

We find four phase transitions for the polymer A.



The differential scanning calorimetry plots are shown in figure 1. The S_A -phase can only be observed on cooling. Due to x-ray

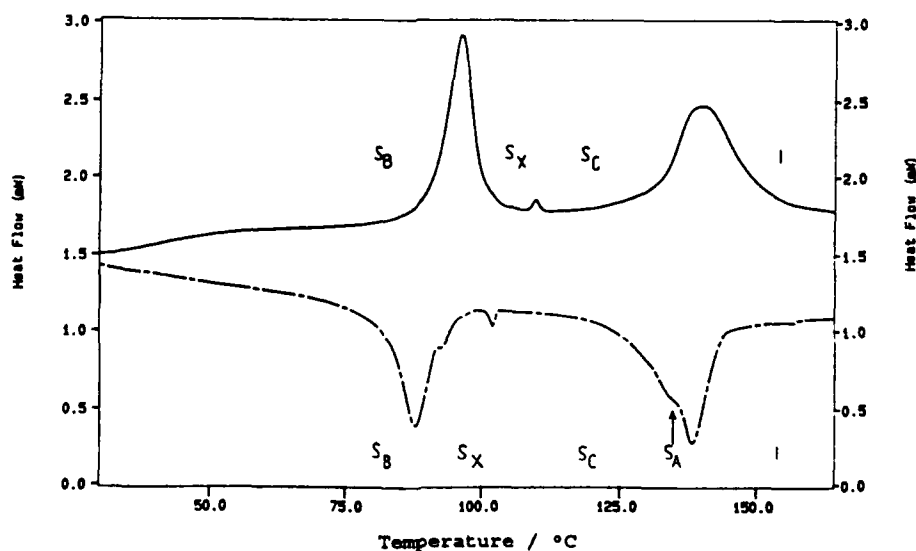


figure 1. Plots of the differential scanning calorimetry

investigations the S_x -phase probably is a S_C^* -phase as compared with detailed x-ray analyses of a homologue of polymer A /8/. In figure 2 the dependence of the transition temperatures of polymer A on concentration of the dopant is plotted.

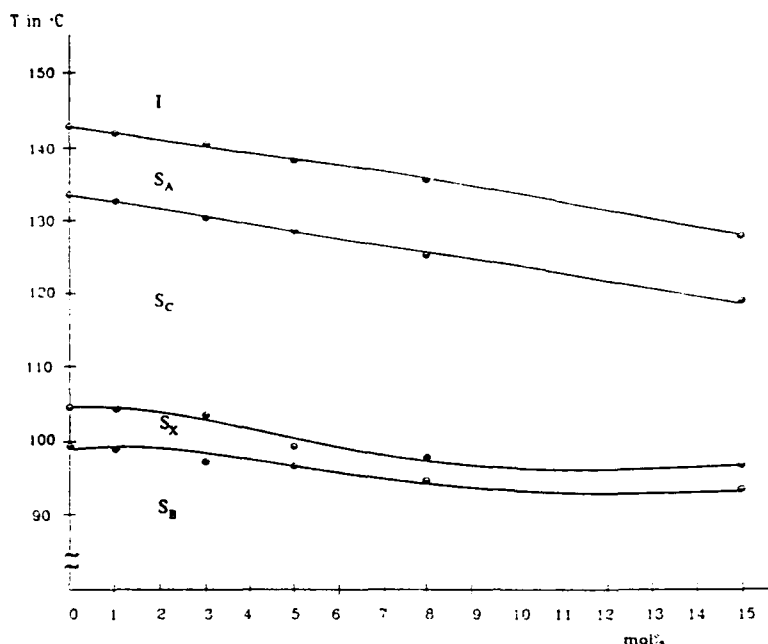


figure 2. Dependence of the transition temperature on the concentration of the dopant measured by cooling

Up to concentrations of 15 mol% dopant we observe no change in the phase sequence in the doped polymer. The transition temperatures decrease - as to be expected - with increasing concentration of the dopant.

The induced spontaneous polarization in these mixtures, displayed in figure 3 shows a maximum around 104°C. This maximum coincides with the transition of the proposed S_C^* -phase to S_C -phase observed in the DSC-curve. Coming down from the S_C -phase to a higher ordered phase one would expect an increase of the spontaneous polarization. A similar decrease in the spontaneous polarization has been observed by Ushida et al. /9/.

For the nonracemic polymer the highest value of $P_s = 42 \text{ nC/cm}^2$ has been measured /3/.

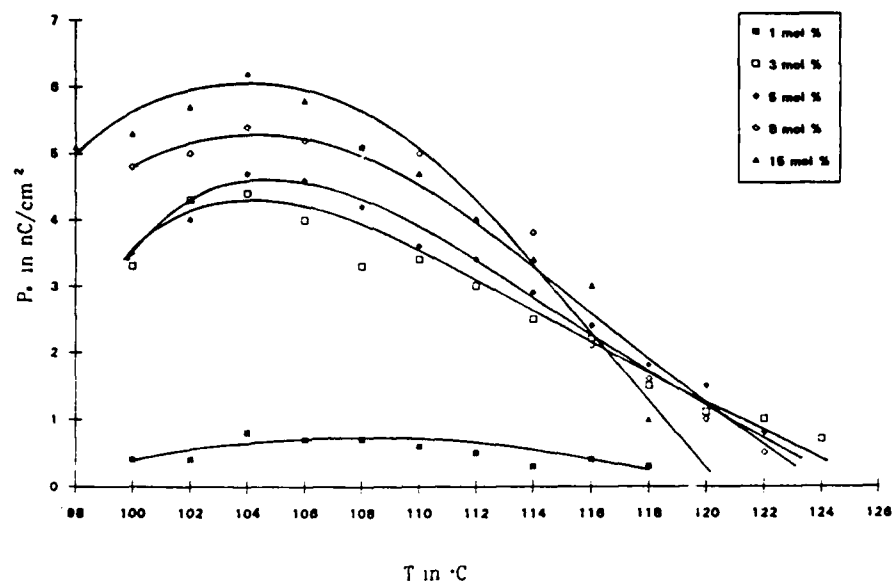


figure 3. Dependence of induced spontaneous polarization on temperature

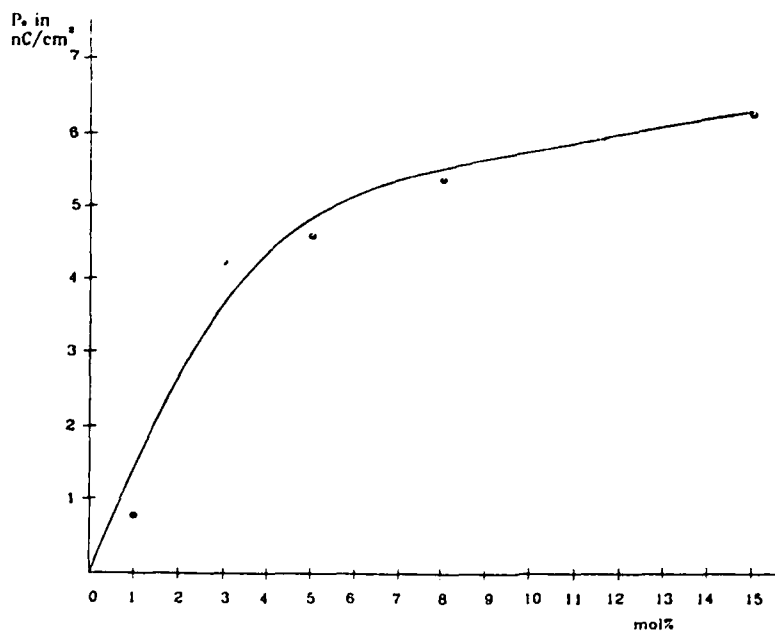


figure 4. Dependence of the maximum of spontaneous polarization on concentration of the dopant

In the doped racemic polymer we find a nonlinear increase of the maximum of P_{\parallel} with increasing dopant concentration (fig. 4).

ACKNOWLEDGEMENT

The support of this research by the Deutsche Forschungsgemeinschaft (Sonderforschungsbereich 335, Anisotrope Fluide) is gratefully acknowledged. The $4\mu\text{m}$ -cells were kindly supplied by Hoechst AG.

REFERENCES

- /1/ L.A.Beresnev; L.M.Blinov; M.A.Osipov; S.A.Pikin
Mol. Cryst. Liq. Cryst., 158A, (1988), 61-150
- /2/ C.Noel; F.Lampretze; C.Friedrich; B.Fayoll and L.Bosro
Polymer 25, 236 and 808, (1984)
- /3/ A.Schliwa; Dissertation; Technische Universität
Berlin, (1990), 32
see also
G.Scherowsky; A.Schliwa et al.
II. Int. FLC Conference Göteborg, (1989), O 24
- /4/ O.Mitsunobu, Synthesis, (1988), 1
- /5/ Details of the synthetic procedure will be published
elsewhere.
- /6/ Y.Gao; R.M.Hanson; J.M.Klunder; S.Y.Ko; H.Masamune;
K.B.Sharpless, J.Am.chem.Soc., 109, (1987), 5765
- /7/ J.A.Dale; D.L.Dull; H.S. Mosher; J.org.Chem., 34, 2543
- /8/ K.Kühnpast; J.Springer; G.Scherowsky; P.Davidson
to be published
- /9/ S.Ushida; T.Morita; K.Miyoshai; K.Hashimoto and
K.Kawasaki, Mol. Cryst. Liq. Cryst., 155, (1988),
93-102

SECTION G
CHIRAL SYSTEMS

ON THE APPEARANCE OF THE ANTIFERROELECTRIC PHASE

HIDEO TAKEZOE, ATSUO FUKUDA, ASAKO IKEDA, YOICHI
TAKANISHI, TSUYOSHI UMEMOTO, JUNJI WATANABE#,
HIROSHI IWANE@, MASAHIKO HARA* AND KEIZOU ITOH+

*Tokyo Institute of Technology, Department of Organic and
Polymeric Materials, #Department of Polymer Science,
O-okayama, Meguro-ku 152, Japan*

*@Mitsubishi Petrochemical Co. Ltd., Tsukuba Research
Center, 8-3-1, Chuo, Ami, Inashiki, Ibaraki 300-3, Japan*

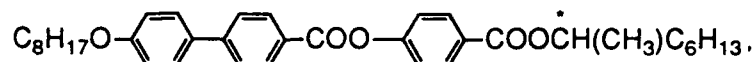
**Frontier Research Program, The Institute of Physical and
Chemical Research (RIKEN), Wako, Saitama 351-01, Japan*

*+Kashima Oil Co. Ltd., R & D Department, 4 Towada,
Kamisu-machi, Kashima-gun, Ibaraki 314-02, Japan*

Abstract As the origin of the appearance of the antiferroelectric phase, the importance of dimerization of molecules in adjacent layers is pointed out on the bases of some experimental results. In thermotropic main chain polymer liquid crystals, the appearance of the antiferroelectric molecular orientation shows the odd-even effect concerning the number of spacer methylene unit. The same kind of odd-even effect was observed in low molecular weight liquid crystals, when the number of carbon atom, n , in chiral end is changed; the antiferroelectric phase tends to appear when n is even. The phase diagram in enantiomeric mixtures of an antiferroelectric liquid crystal and the layer thicknesses in these mixtures also suggest the pairing of the molecules. The image of a scanning tunnelling microscope is also shown; the core parts of molecules align in a zigzag fashion.

INTRODUCTION

Since the antiferroelectric phase as the origin of the tristable switching¹ was discovered,² many attempts have been made to clarify the characteristics of the phase²⁻¹⁸ and to utilize as display devices.¹⁹⁻²² In addition, the other subphases have been extensively investigated.^{2-4,6,8-10,13-18} The molecular orientational structures of five phases, SmA-SmC_α*-SmC*-SmC_γ*-SmC_A*, in the first antiferroelectric liquid crystal, MHPOBC,



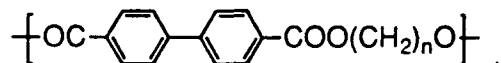
have been now clarified. The SmA and SmC* phases are well-known paraelectric and ferroelectric phases, respectively. The SmC_A* phase is the antiferroelectric phase, where molecules tilt to the opposite senses in adjacent layers so that no net spontaneous polarization exists and the optical extinction direction coincides with the layer normal.^{1-3,6,9,13} The SmC_γ* phase is a ferrielectric phase,^{6,9,13-15,18} where the unit cell (repeating unit) of the molecular orientation consists of three layers^{15,17,18} so that non-zero spontaneous polarization and average tilt angle exist.

Recently, Takanishi *et al.*²³ proposed that the SmC_α* phase exhibits the so-called Devil's staircase; the molecular orientational structure changes from the antiferroelectric to the ferroelectric through various ferrielectric structures with decreasing temperature within the SmC_α* phase. Therefore, we have the antiferroelectric molecular orientation in two phases, *i.e.* SmC_A* and SmC_α*, in other words, at least two different types of molecular interaction are necessary to be considered. As for the origin of the antiferroelectric structure in SmC_α*, the interaction between spontaneous polarizations in adjacent layers was pointed out to be responsible.²³ Actually, it is reasonable that the SmC_α* phase is observable only in substances with very high optical purity.^{4,16} On the other hand, the importance of dimerization of two like molecules, such as R and R or S and S, was proposed in

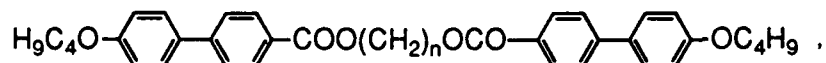
SmC_A^* .²³ In this paper, we will show some experimental results which suggest the dimerization.

THERMOTROPIC MAIN CHAIN LIQUID CRYSTALS OF POLYESTER

According to Watanabe and Hayashi,²⁴ thermotropic main chain liquid crystals of polyester,



show SmA and SmC_2 , when the number of methylene units is even and odd, respectively. The SmC_2 phase has the molecular orientational structure in which the successive mesogenic groups tilt to the opposite senses alternately. The molecular orientational structures of these phases were confirmed by X-ray diffraction.²⁴ It was confirmed that the dimers, $\text{BB}-n$



also have these phases according to n . The appearance of the two phases can be easily presupposed by assuming the trans-form of the spacer unit as shown in Figure 1, although the detailed discussion was made based on the calculation of the orientational

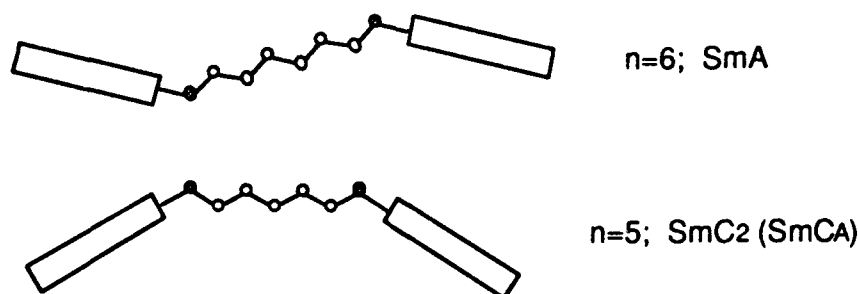
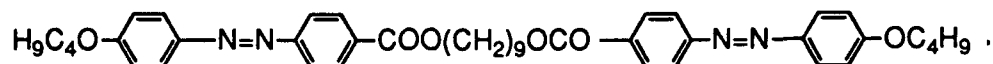


FIGURE 1 Molecular conformation by assuming the trans-form of the spacer unit in $\text{BB}-n$. Note that the appearance of SmA and SmC_2 (SmC_A) is easily understood.

probability as a function of connecting angle of two mesogenic cores.²⁵

The miscibility test was made between BAz-9,



and MHPOBC, and showed that SmC_2 is completely miscible with SmC_A^* , pointing out that both are the same phase. Thus, the importance of the number of carbon atoms in the spacer unit for the appearance of the zigzag structure is very suggestive.

ODD-EVEN EFFECT FOR THE APPEARANCE OF THE ANTIFERROELECTRIC PHASE

The same kind of odd-even effect was quite often observed in low molecular weight antiferroelectric liquid crystals. Figure 2 is a phase sequences of $m\text{BIMF}_n$ ($m=10$),

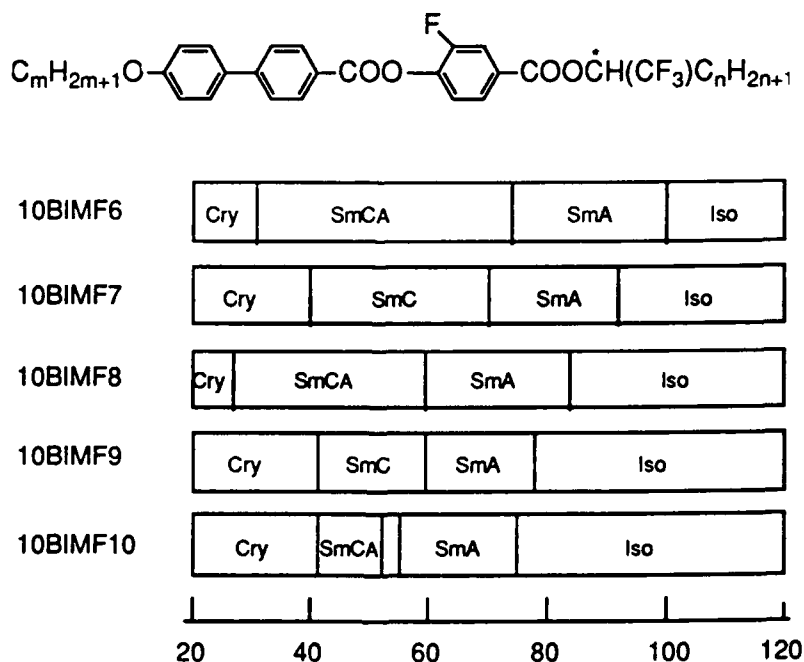


FIGURE 2 Phase sequences of 10BIMF_n ($n=6-10$) in the heating process.

in the heating process. The SmC_A^* phase appears only in the substances with even n . Otherwise, the normal SmC^* appears in the substances with odd n . It was also confirmed that the same phase sequences are obtained in the substances with $m=12$. This kind of odd-even effect for the appearance of the SmC_A^* phase is very interesting in the viewpoint of the similarity to the polymer liquid crystal mentioned above.

PHASE SEQUENCE AND LAYER THICKNESS IN ENANTIOMERIC MIXTURES

Another remarkable feature of the antiferroelectric liquid crystals is a phase diagram of enantiomeric mixtures.²⁶ In Figure 3 is displayed the phase diagram of the enantiomeric mixtures of TFMHPDOPB.^{26,27}

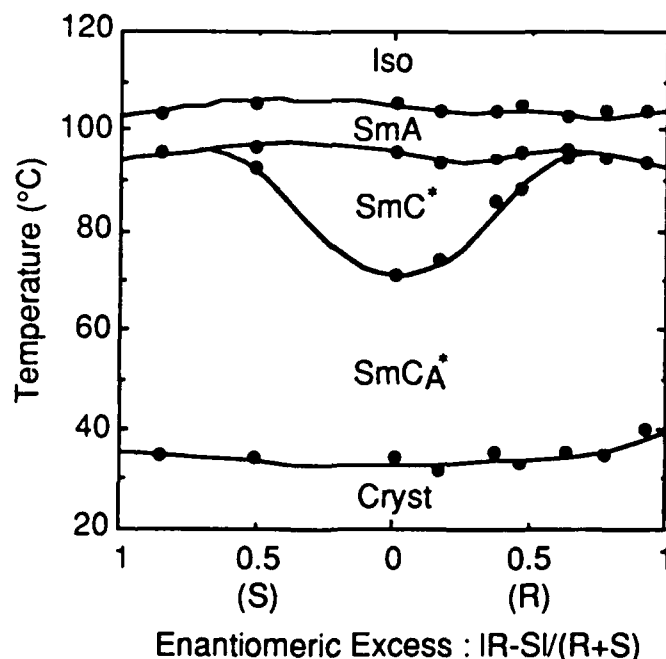
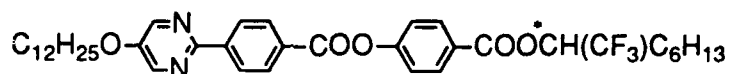
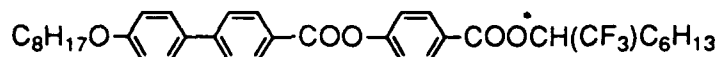


FIGURE 3 Phase diagram of the enantiomeric mixtures of TFMHPDOPB.

In the range of high enantiomeric excess, the direct transition from SmA to SmC_A* occurs, while SmC* is injected in the range of low enantiomeric excess; SmC* tends to be stabilized with decreasing optical purity. The similar phase diagram was also observed in TFMHPOBC,⁵



The expansion of the SmC* temperature range with decreasing optical purity was also observed in MHPOBC.^{4,16} Thus, the stabilization of SmC* with decreasing optical purity is quite common.

As pointed out above, molecules in the SmC_A* phase are supposed to form dimers in such a way that the dipole moments belonging to the adjacent layers make pair as shown in Figure 4. Here, each like molecule should form pairs to create bent-formed dimers, otherwise, each unlike molecule forms straight-formed

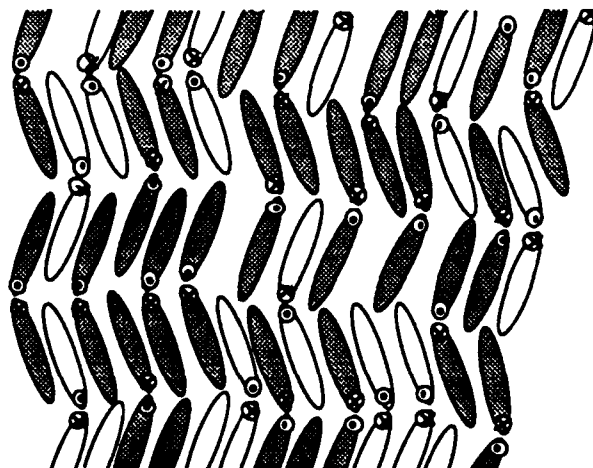


FIGURE 4 Proposed model orientational structure in SmC_A*, where R and S enantiomers are distinguished by open and shaded molecules. Note that pairing of the dipole moments belonging to the adjacent smectic layers and local spontaneous optical resolution.

dimers. This kind of phenomenon, *i.e.* molecules form supramolecules selectively, is often observed. By taking account of this situation, the phase diagram is quite understandable; in the range of high enantiomeric excess, molecules easily find their like molecules to form pairs, compared with the case in the range of low enantiomeric excess containing many unlike molecules. Thus, the SmC_A^* phase is more easily stabilized in compounds of higher optical purity. The observation was also made that there exists a wide coexisting temperature range of SmC^* and SmC_A^* in compounds of low optical purity.³ This fact is interpreted by taking account of the difference in the stabilization energies for the pair formation of like and unlike molecules.

This kind of pair formation may give the explanation for the optical purity dependence of the smectic layer thickness as shown in Figure 5. The temperature dependences of the layer thickness

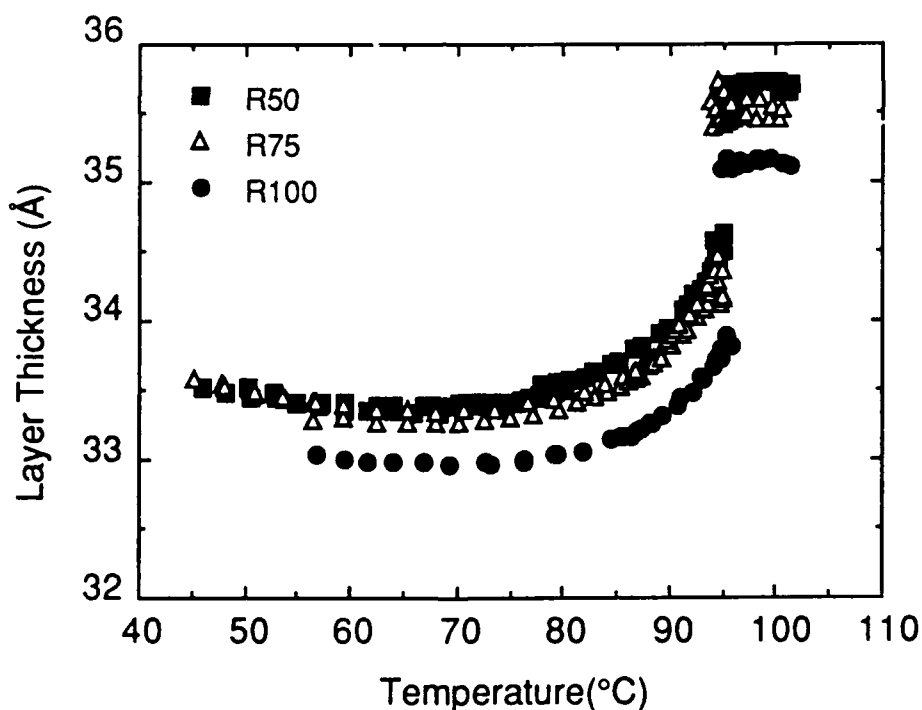


FIGURE 5 Temperature dependence of the layer thickness in enantiomeric mixtures of TFMHPDOPB.

in three enantiomeric mixtures show similar first-order phase transition behaviors as a whole, but exhibit distinct difference in their absolute values. The layer thickness dependence on the optical purity even in SmA can be speculated as follows; the molecules may tend to make pairs even in SmA depending on the temperature range of SmC* between SmA and SmC_A*. We are in the process of confirming this using many kinds of substances.

SCANNING TUNNELING MICROSCOPE IMAGES

Clear scanning tunnelling microscope (STM) images were obtained in several materials. One of them exhibits a novel quadruple zigzag structure on a molybdenum disulphide (MoS₂) substrate. The material used was MOBIPC,

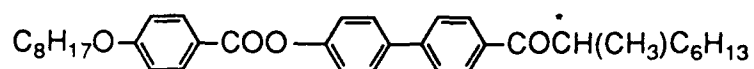
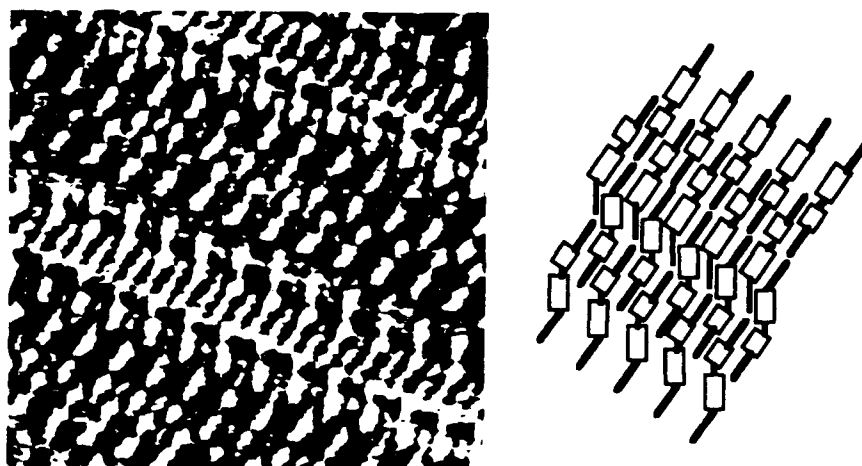


Figure 6 shows an STM image taken in air at room temperature using NanoScope II (Digital Instruments). Individually distinguishable molecules and regular alignment can



See Color Plate IX.

FIGURE 6 STM image of MOBIPC on MoS₂.

be clearly observed. According to the packing of phenyl and biphenyl groups distinguishable on each molecule, it is obvious that the direction of the molecular cores is tilted alternately, although the repeating unit consists of four molecular layers, *i.e.* a quadruple structure, instead of two. Thus, the pairing of molecules is strongly suggested by the interfacial structure. The details of the STM work will be reported elsewhere.

CONCLUSION

Some experiments were reported to show the importance of the pairing of like molecules (R & R or S & S) in the SmC_A^* phase. Direct structural information using such as X-ray diffraction and direct evidence of the pairing using microscopic techniques such as NMR and IR spectroscopies are needed.

REFERENCES

1. A. D. L. Chandani, T. Hagiwara, Y. Suzuki, Y. Ouchi, H. Takezoe and A. Fukuda, Jpn. J. Appl. Phys., **27**, L729 (1988).
2. A. D. L. Chandani, E. Gorecka, Y. Ouchi, H. Takezoe and A. Fukuda, Jpn. J. Appl. Phys., **28**, L1265 (1989).
3. A. D. L. Chandani, Y. Ouchi, H. Takezoe, A. Fukuda, K. Terashima, K. Furukawa and A. Kishi, Jpn. J. Appl. Phys., **28**, L1261 (1989).
4. M. Fukui, H. Orihara, Y. Yamada, N. Yamamoto and Y. Ishibashi, Jpn. J. Appl. Phys., **28**, L849 (1989).
5. Y. Yamada, K. Mori, N. Yamamoto, H. Hayashi, K. Nakamura, M. Yamawaki, H. Orihara and Y. Ishibashi, Jpn. J. Appl. Phys., **28**, L1606 (1989).
6. K. Hiraoka, A. Taguchi, Y. Ouchi, H. Takezoe and A. Fukuda, Jpn. J. Appl. Phys., **29**, L103 (1990).
7. M. Johno, Y. Ouchi, H. Takezoe, A. Fukuda, K. Terashima and K. Furukawa, Jpn. J. Appl. Phys., **29**, L111 (1990).
8. H. Orihara and Y. Ishibashi, Jpn. J. Appl. Phys., **29**, L115 (1990).
9. E. Gorecka, A. D. L. Chandani, Y. Ouchi, H. Takezoe and A. Fukuda, Jpn. J. Appl. Phys., **29**, 131 (1990).
10. M. Fukui, H. Orihara, A. Suzuki, Y. Ishibashi, Y. Yamada,

- N. Yamamoto, K. Mori, K. Nakamura, Y. Suzuki, and I. Kawamura, Jpn. J. Appl. Phys., **29**, L329 (1990).
11. H. Orihara, T. Fujikawa, Y. Ishibashi, Y. Yamada, N. Yamamoto, K. Mori, K. Nakamura, Y. Suzuki, T. Hagiwara and I. Kawamura, Jpn. J. Appl. Phys., **29**, L333 (1990).
12. A. Suzuki, H. Orihara, Y. Ishibashi, Y. Yamada, N. Yamamoto, K. Mori, K. Nakamura, Y. Suzuki, T. Hagiwara, I. Kawamura and M. Fukui, Jpn. J. Appl. Phys., **29**, L336 (1990).
13. J. Lee, A. D. L. Chandani, K. Itoh, Y. Ouchi, H. Takezoe and A. Fukuda, Jpn. J. Appl. Phys., **29**, 1122 (1990).
14. K. Hiraoka, A. D. L. Chandani, E. Gorecka, Y. Ouchi, H. Takezoe and A. Fukuda, Jpn. J. Appl. Phys., **29**, L1473 (1990).
15. J. Lee, Y. Ouchi, H. Takezoe, A. Fukuda and J. Watanabe, J. Phys.: Condens. Matter, **2**, SA271 (1990).
16. H. Takezoe, J. Lee, A. D. L. Chandani, E. Gorecka, Y. Ouchi, A. Fukuda, K. Terashima and K. Furukawa, Ferroelectrics, **114**, 187 (1991).
17. J. Li, H. Takezoe and A. Fukuda, Jpn. J. Appl. Phys., **30**, 532 (1991).
18. H. Takezoe, J. Lee, Y. Ouchi and A. Fukuda, Mol. Cryst. Liq. Cryst., in press.
19. M. Yamawaki, Y. Yamada, N. Yamamoto, K. Mori, H. Hayashi, Y. Suzuki, Y. S. Negi, T. Hagiwara, I. Kawamura, H. Orihara and Y. Ishibashi, Japan Display '89, 26 (1989).
20. M. Johno, K. Itoh, J. Lee, Y. Ouchi, H. Takezoe, A. Fukuda and T. Kitazume, Jpn. J. Appl. Phys., **29**, L107 (1990).
21. M. Johno, A. D. L. Chandani, J. Lee, Y. Ouchi, H. Takezoe, A. Fukuda, K. Itoh and T. Kitazume, Proc. of SID, **31/2**, 129 (1990).
22. K. Itoh, M. Johno, Y. Takanishi, Y. Ouchi, H. Takezoe and A. Fukuda, Jpn. J. Appl. Phys., **30**, 735 (1991).
23. Y. Takanishi, K. Hiraoka, V. K. Agrawal, H. Takezoe, A. Fukuda and M. Matsushita, Jpn. J. Appl. Phys., submitted.
24. J. Watanabe and M. Hayashi, Macromolecules, **22**, 4083 (1989).
25. A. Abe, Macromolecules, **17**, 2280 (1984).
26. A. Ikeda, Y. Takanishi, H. Takezoe, A. Fukuda, S. Inui, S. Kawano, M. Saito and H. Iwane, Jpn. J. Appl. Phys., **30**, L1032 (1991).
27. S. Inui, S. Kawano, M. Saito, H. Iwane, Y. Takanishi, K. Hiraoka, Y. Ouchi, H. Takezoe and A. Fukuda, Jpn. J. Appl. Phys., **29**, L987 (1990).

PHASE TRANSITIONS AND SWITCHING PROPERTIES IN ANTIFERROELECTRIC LIQUID CRYSTALS

HIROSHI ORIHARA AND YOSHIHIRO ISHIBASHI
*Synthetic Crystal Research Laboratory, School of Engineering,
Nagoya University, Nagoya 464-01, Japan*

Abstract The advantages of antiferroelectric liquid crystals(AFLCs) in application are clearly shown by comparing the hysteresis loops of AFLC and FLC(ferroelectric liquid crystal) derived theoretically. The competition between the antiferroelectric and ferroelectric interactions is observed by means of dielectric measurements. The origin of the antiferroelectricity is briefly discussed.

INTRODUCTION

From the viewpoint of application to display devices, the bistability is one of the most important properties, since two different states should coexist over a certain range of applied voltage for multiplex driving. In ordinary surface stabilized ferroelectric liquid crystal(SSFLC) cells, however, it has been pointed out that the bistability is difficult to obtain, contrary to previous expectations. On the other hand, antiferroelectric liquid crystals(AFLCs)¹ have a bistability as is clearly shown in an optical response. In fact, prototype AFLC display of 6 inches in diagonal was fabricated last year by Yamada et al.²

In this paper, first we point out that FLC should have no bistability without surface anchoring, while in AFLC bulk itself should have bistability, by showing hysteresis loops of FLC and AFLC derived theoretically. Then, dielectric measurements are presented to clarify the fundamental aspect of phase transitions in AFLC. Finally, we briefly discuss the origin of antiferroelectricity, i. e., the interaction between molecules stabilizing the antiferroelectric state.

HYSTERESIS LOOP

First, we derive the hysteresis loop of FLC, ignoring the helical structure for simplicity. Let us introduce a vector ξ_f defined as

$$\begin{aligned}\xi_f &= (\xi_{fx}, \xi_{fy}) \\ &= (-n_y n_z, n_x n_z),\end{aligned}\tag{1}$$

where $\mathbf{n}=(n_x, n_y, n_z)$ is the director. The macroscopic polarization \mathbf{P}_f is given as

$$\mathbf{P}_f = -\lambda_f \chi_f \boldsymbol{\xi}_f + \chi_f \mathbf{E}, \quad (2)$$

where λ_f and χ_f are constants needed in a phenomenological theory³ and \mathbf{E} is the applied field. The free energy density may be generally expressed as

$$f = h(\xi_f) - c \boldsymbol{\xi}_f \cdot \mathbf{E}, \quad (3)$$

where ξ_f is the norm of $\boldsymbol{\xi}_f$ and $c = -\lambda_f \chi_f$. The equilibrium condition and the stability condition lead to

$$\boldsymbol{\xi}_f / \xi_f = c / h'(\xi_f) \cdot \mathbf{E}, \quad (4)$$

$$h''(\xi_f) > 0, \quad (5. a)$$

$$c \boldsymbol{\xi}_f \cdot \mathbf{E} > 0. \quad (5. b)$$

Equation (4) implies that $\boldsymbol{\xi}_f$ should be parallel or antiparallel to \mathbf{E} . The direction of $\boldsymbol{\xi}_f$ relative to \mathbf{E} is determined by eq. (5.b), which is a remarkable aspect in a two-component system. Hereafter, we assume that c is positive for convenience. Then, such a state that $\boldsymbol{\xi}_f$ is antiparallel to \mathbf{E} (\mathbf{P} is also antiparallel to \mathbf{E}) is always unstable. In a uniaxial ferroelectric crystal, on the contrary, this state can be metastable, since eq. (5.b) should not be imposed on a one-component system. These results mean that under a reversed field the polarization can rotate in FLC, but can not do in the uniaxial ferroelectric crystal because of the constraint. We show a typical hysteresis loop of ξ_f - \mathbf{E} in Fig. 1(a), where ξ_f includes the sign. The stable states (bold lines) cease on ξ_f -axis, and so there exists no bistable region. In the uniaxial ferroelectric crystal, on the

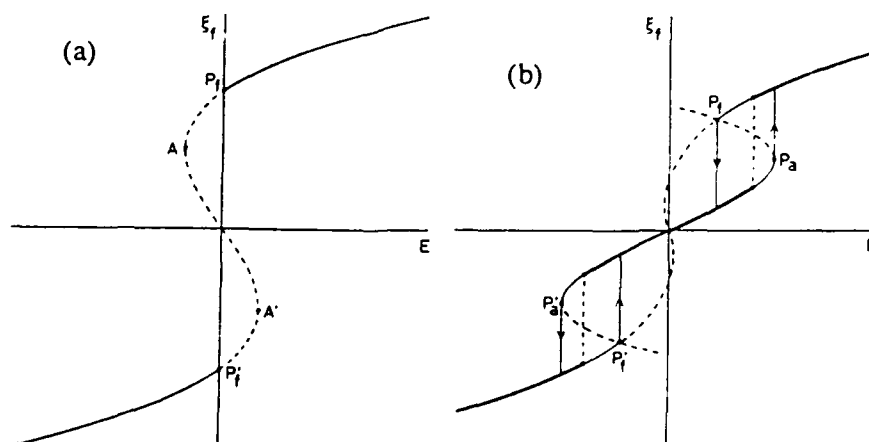


Fig. 1. Hysteresis loops of FLC (a) and AFLC (b).

other hand, metastable states appear in the regions of P_f-A and P'_f-A' , resulting in the bistability between A and A' .

Next, we show a typical double hysteresis loop of AFLC in Fig. 1(b), which has been phenomenologically obtained by the present authors.³ Metastable states (thin lines) are clearly seen, and therefore the bistability between $P_f(P'_f)$ and $P_a(P'_a)$ is obtainable. Thus, the bistability in AFLC is ascribable to the metastable states typical of the first order phase transition.

At the end of this section, we present the experimental results which demonstrate the bistability of AFLC. The sample used in the present experiment is a mixture of several AFLCs.² Well-aligned cell with a thickness of $2.0 \mu\text{m}$ was prepared by rubbing after coating indium-tin oxide (ITO) glass plate with polyimide. The optical hysteresis in transmission under a triangular voltage is shown in Fig. 2. The ferroelectric state (bright) and the antiferroelectric state (dark) can exist in the same voltage range. Figure 3 demonstrates the bistability under pulse trains. The first 4 pulses are for selecting one of two states and the selected state is maintained by the following pulse trains.

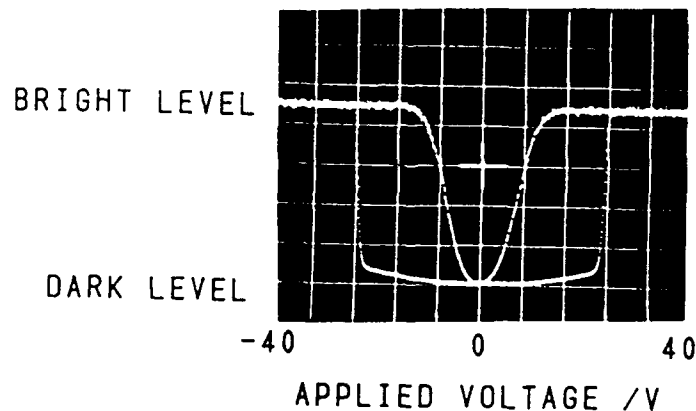


Fig. 2. Optical hysteresis in transmission as a function of applied voltage.

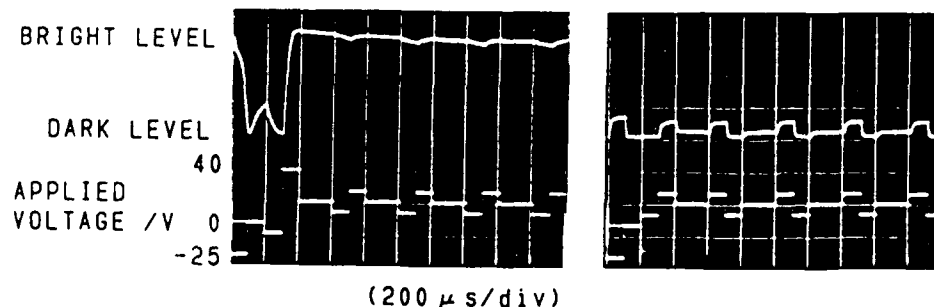


Fig. 3. The ferroelectric and antiferroelectric states are maintained in the left and right figures, respectively.

PHASE TRANSITIONS

In this section, the results of dielectric measurements in TFMHPOBC are presented in order to show the general properties of phase transitions in AFLC. TFMHPOBC changes its phase sequence due to the optical purity, i.e., SmA-SmC_A* (antiferroelectric phase) in pure sample and SmA-SmC*-SmC_A* in a mixture of R- and S-enantiomers.^{4,5} Therefore, TFMHPOBC is a suitable material for investigation of the competition between the ferroelectric and antiferroelectric interactions.

We prepared 2- μ m-thick homogeneous cells aligned by rubbing after coating the plates with a polyimide film. The area of the electrode was 2.25 mm². Dielectric measurements were performed with an impedance analyzer(HP4194A).

In Figs. 4(a) and (b), we show the temperature dependence of the dielectric constant at several frequencies for the pure(R:S=10:0) sample and for the mixture(R:S=8:2) sample, respectively. In the pure sample, the dielectric constant increases as the transition temperature is approached in SmA, while it drops in SmC_A*. In the mixture, on the other hand, the SmC* phase appears between SmA and SmC_A*, and the dielectric constant keeps large values due to the Goldstone mode in SmC*.

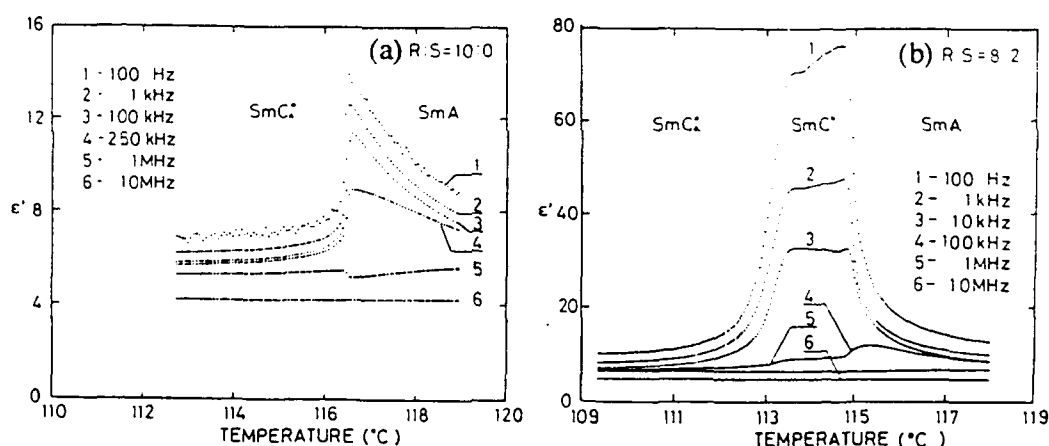


Fig. 4. Temperature dependences of the dielectric constant in the pure sample (a) and in the mixture sample (b).

The relaxation frequency obtained by the dielectric measurements are shown in Fig. 5. In SmA the relaxation frequency decreases as the transition point is approached both for the pure and mixture samples. Here, we would like to emphasize that two types of soft modes should be considered, i. e., a ferroelectric soft mode and an antiferroelectric soft mode, which induce the SmC* phase and the SmC_A* phase, respectively. These two modes are illustrated in Fig. 6. It is the antiferroelectric mode that should condense in the pure sample. In addition, the ferroelectric mode observable by the dielectric measurements is found to tend to be soft as well, as is seen in Fig. 6(a). This fact

suggests that the ferroelectric and antiferroelectric modes should tend to be soft simultaneously and the competition between them should take place.

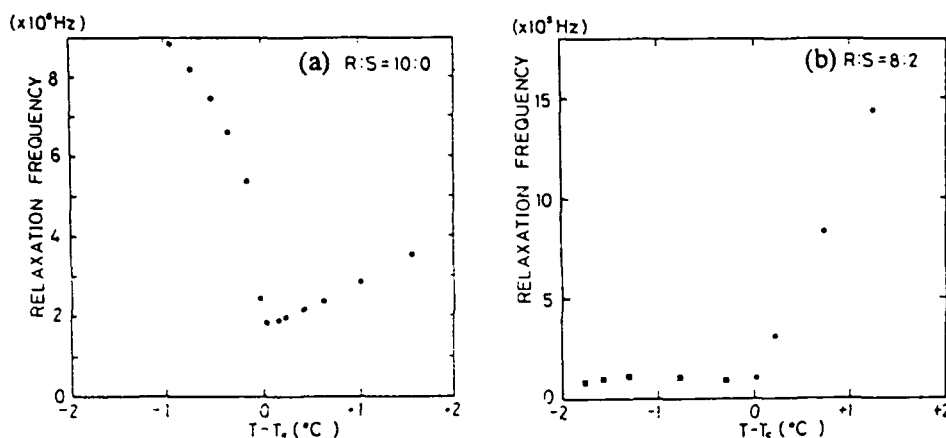


Fig. 5. Temperature dependences of the relaxation frequency in the pure sample (a) and in the mixture sample (b).

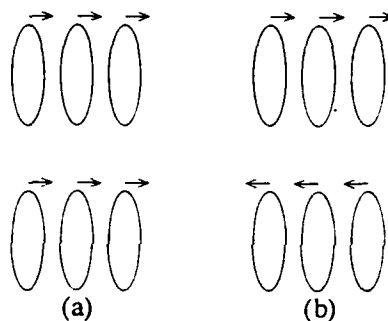


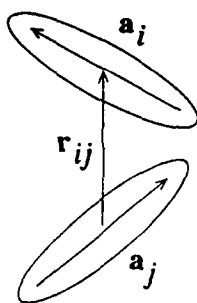
Fig. 6. Ferroelectric soft mode (a) and antiferroelectric soft mode (b).

ORIGIN OF ANTIFERROELECTRICITY

Finally, we point out that the dispersion interaction may play a role as an origin of antiferroelectricity. Maier and Saupe calculated the dispersion energy between two anisotropic molecules i and j taking into account the dipole-dipole interaction.⁶ In their calculation, however, they averaged the energy over the direction of the vector r_{ij} between the molecules i and j (see Fig. 7). This averaging is valid in nematic liquid crystals, but not in smectic liquid crystals. The dispersion energy without averaging is easily obtained as

$$V_{ij} = -1/(8r_{ij}^6) \cdot [2\alpha_i(\alpha_1 + 2\alpha_t) + 3\Delta\alpha\alpha_t\{(a_i \cdot r_{ij})^2 + (a_j \cdot r_{ij})^2\} + \Delta\alpha^2\{a_i \cdot a_j - 3(a_i \cdot r_{ij})(a_j \cdot r_{ij})\}^2], \quad (6)$$

where a_i and a_j are, respectively, unit vectors along the molecules i and j , and α_1 and

Fig. 7. Configuration of two molecules i and j .

α_t are the susceptibilities along and perpendicular to the molecule, respectively, and $\Delta\alpha = \alpha_l - \alpha_t$ and I the ionization energy of the molecule. When r_{ij} is along z -axis, eq. (6) is rewritten as

$$V_{ij} = -I/(8r_{ij}^6) \cdot [2\alpha_t(\alpha_l + 2\alpha_t) + 6\Delta\alpha\alpha_t + 3\Delta\alpha\alpha_t(b_i^2 + b_j^2) + \Delta\alpha^2\{-4a_{iz}a_{jz}b_i \cdot b_j + 4a_{iz}^2a_{jz}^2 + (b_i \cdot b_j)^2\}], \quad (7)$$

where we have defined two projected vectors as $b_i = (a_{ix}, a_{iy})$ and $b_j = (a_{jx}, a_{jy})$. The term with $b_i \cdot b_j$ in eq. (6) prefers the antiferroelectric state to the ferroelectric one. Therefore, the dipole-dipole dispersion interaction may be one of the most important interactions inducing the antiferroelectric phase.

ACKNOWLEDGMENTS

We would like to thank Professor H. Kimura of Nagoya University for his valuable discussion of the interaction energy. This work was partly supported by TEPCO Research Foundation.

REFERENCES

1. A. D. L. Chandani, E. Gorecka, Y. Ouchi, H. Takezoe and A. Fukuda, Jpn. J. Appl. Phys., **28**, L1256(1989).
2. Y. Yamada, N. Yamamoto, K. Mori, K. Nakamura, T. Hagiwara, Y. Suzuki, I. Kawamura, H. Orihara and Y. Ishibashi, Jpn. J. Appl. Phys., **29**, 1757(1990).
3. H. Orihara and Y. Ishibashi, Jpn. J. Appl. Phys., **29**, L115(1990).
4. Y. Yamada, K. Mori, N. Yamamoto, H. Hayashi, K. Nakamura, M. Yamawaki, H. Orihara and Y. Ishibashi, Jpn. J. Appl. Phys., **28**, L1606(1989).
5. H. Orihara, T. Fujikawa, Y. Ishibashi, Y. Yamada, N. Yamamoto, K. Mori, K. Nakamura, Y. Suzuki, T. Hagiwara and I. Kawamura, Jpn. J. Appl. Phys., **29**, L333(1990).
6. W. Maier and A. Saupe, Z. Naturforsch., **13a**, 564(1958).

POLYMER-DISPERSED CHOLESTERIC LIQUID CRYSTALS
- CHALLENGE FOR RESEARCH AND APPLICATION

HEINZ-S. KITZEROW^{*)} and PETER P. CROOKER^{*)}

^{*)}Iwan-N.-Stranski-Institut, Technische Universität Berlin
Straße des 17. Juni 135, 1000 Berlin 12

^{*)}Department of Physics and Astronomy, University of Hawaii
2505 Correa Road, Honolulu, HI 96822, USA

ABSTRACT. - Polymer dispersed cholesteric liquid crystals are a new class of systems which might be suitable for application in colored electrooptic displays. For materials with negative dielectric anisotropy and with sufficiently short pitch it is possible to induce a texture showing bright selective reflection by application of ac electric fields. We give a summary of the basic experimental results on these new systems.

I. INTRODUCTION

Polymer dispersed nematic liquid crystals (PDLC) have been intensively studied during the last few years^{1,2}. Due to the possibility of electric field controlled light scattering³, these systems are used for application in large area flexible displays. Usually, such devices contain microdroplets of nematic liquid crystals with positive dielectric anisotropy. The samples appear opaque in the

Invited Lecture at the 3rd International Conference on Ferroelectric Liquid Crystals, Boulder (CO), 1991
(Session on Chiral Systems)

absence of electric fields when the droplets are randomly oriented and become transparent under the influence of an electric field due to uniform director alignment, provided that the ordinary refractive index of the liquid crystal is properly matched with the refractive index of the polymer. In contrast to conventional liquid crystal displays, no polarizers are used for this application.

Crooker and Yang⁴ have proposed the use of polymer-dispersed cholesteric liquid crystals (PDCLC) for display applications. In contrast to nematic PDLC displays, the PDCLC device is colored and works in reflection (fig. 1, 2). In the absence of electric fields, the randomly oriented cholesteric droplets exhibit a director configuration characterized by double twist (section V), and the sample appears colorless. If sufficiently high ac voltages are applied, a uniformly oriented uniaxial cholesteric structure can be induced. If the cholesteric pitch p of the liquid crystal

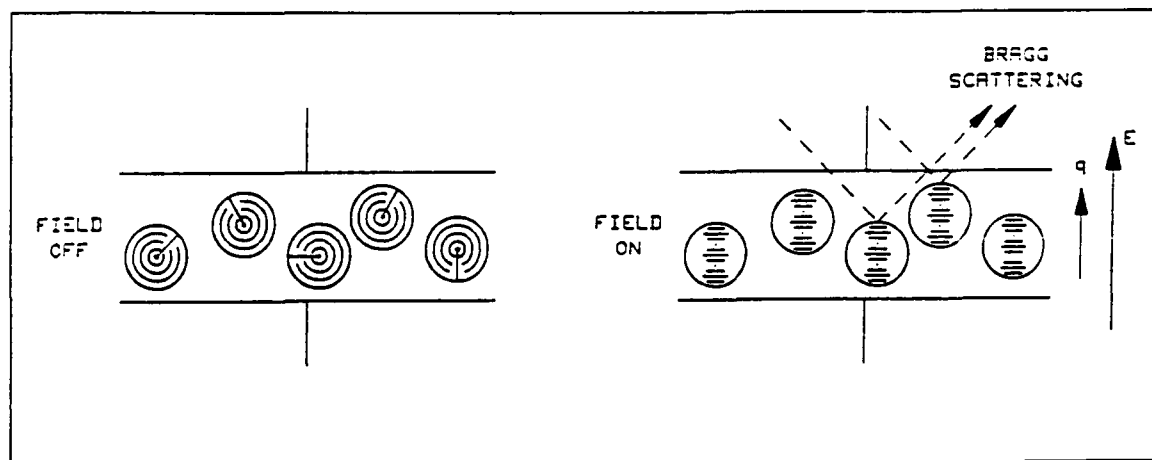


FIGURE 1. - Schematic representation of a PDCLC display. (a) Field off state: Cholesteric droplets dispersed in a polymer matrix exhibit a randomly oriented double twist director configuration. The sample appears transparent or slightly diffuse scattering. (b) For materials with negative dielectric anisotropy, electric fields induce a uniformly oriented uniaxial helix structure. The sample shows selective reflection of circularly polarized light due to Bragg scattering.

is of the same order of magnitude as the wavelength of visible light, the cholesteric drops oriented by the field show selective reflection of circularly polarized light⁵ at the Bragg wavelength

$$\lambda_0 = n p, \quad (1)$$

where n is a mean refractive index. As indicated by this relation, the color of the display depends on the cholesteric pitch, while the intensity is controlled by the field strength. In sections III and V of this article we describe the static and dynamic behaviour of this electrooptical effect.

Fundamental information on the director field in cholesteric droplets can be obtained by microscopic observation of the textures obtained for systems with large cholesteric pitch ($p \approx$ several μm)⁶⁻¹³. Such systems have been considered as a model system to study the mechanism of the influence of electric fields on chiral droplets^{14,15}. Some results of such observations are presented in section IV.

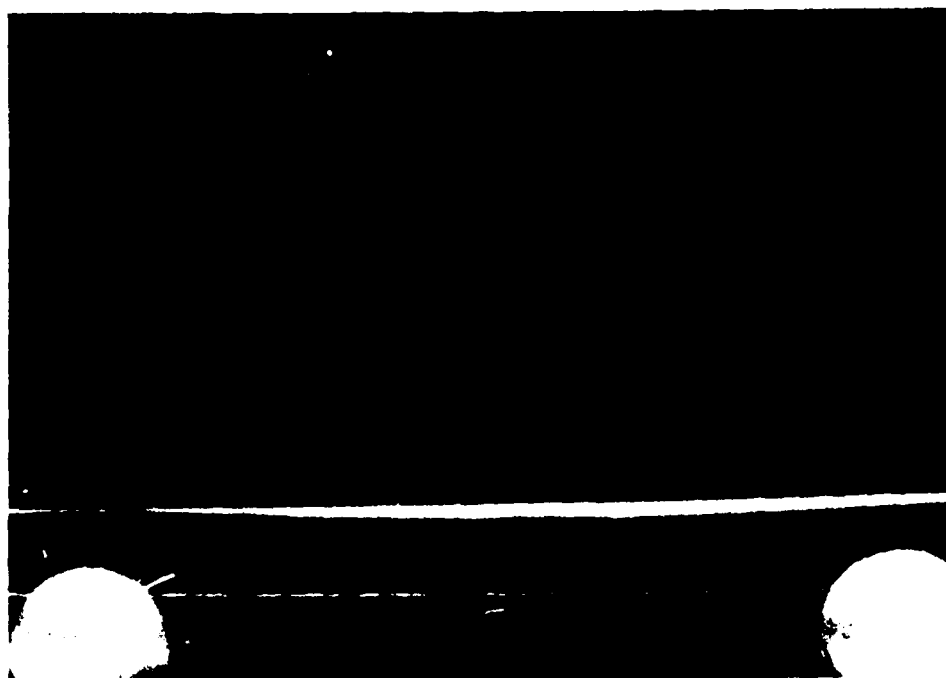
II. SAMPLE PREPARATION

For polymer-dispersed cholesteric systems so far investigated in electric fields, monomer mixtures consisting of a nematic component with negative dielectric anisotropy (e. g. ZLI 2806, E. Merck, Germany) and a non-polar chiral dopant (e. g. CE2, British Drug House, England) have been used. The matrix consisted in most cases of a thermoplastic material, such as Poly(methyl methacrylate) or Poly(vinyl butyral).

The pitch and thus the field-induced color of the display can be controlled by the fraction of chiral dopant in the monomer mixture (fig. 2). As for many induced cholesteric mixtures, this relation can be approximately described¹⁶ by

POLYMER-DISPERSED CHOLESTERIC LIQUID CRYSTALS

(a)



(b)

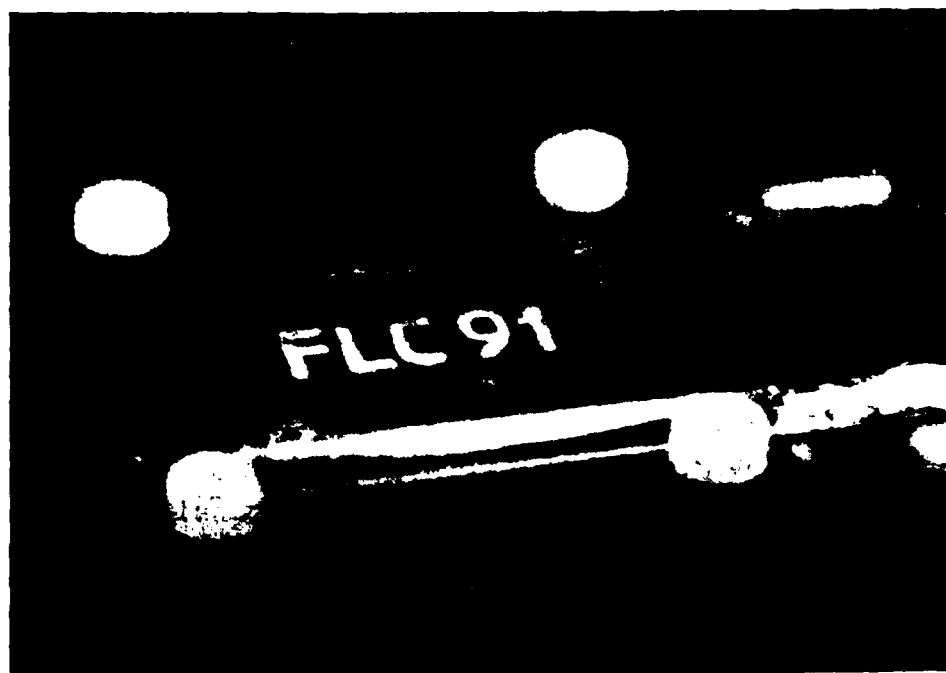


FIGURE 2. - Two PDCLC samples exhibiting different chirality:
(a) 18% chiral CE2, 32% nem. ZLI 2806, 50% Poly(vinylbutyral),
(b) 15% chiral CE2, 34% nem. ZLI 2806, 51% Poly(vinylbutyral).
The colored inscription corresponds to the shape of the electrode areas ($E_{rms} = 50 \text{ V} / 11 \mu\text{m}$ with $f = 1 \text{ kHz}$).
See Color Plate X.

$$p * x_{\text{chiral}} = \text{constant}, \quad (2)$$

where x_{chiral} is the mole fraction of the chiral compound in the monomer component. Slight deviations occur, possibly due to uncompleted phase separation between the liquid crystal mixture and the polymer.

FIGURE 2 (see color plate at the end of this issue).

- Two PDCLC samples exhibiting different chirality:
(a) 18% chiral CE2, 32% nem. ZLI 2806, 50% Poly(vinylbutyral),
(b) 15% chiral CE2, 34% nem. ZLI 2806, 51% Poly(vinylbutyral).
The colored inscription corresponds to the shape of the electrode areas ($E_{\text{rms}} = 50 \text{ V} / 11 \mu\text{m}$ with $f = 1 \text{ kHz}$).

In order to produce monodisperse samples, the cholesteric droplets are formed - due to thermally induced phase separation^{17,18} - by controlled cooling of a homogeneous mixture containing the liquid crystalline monomer and the non-mesogenic polymer. An organic solvent (chloroform) which is allowed to evaporate at high temperatures prior to the phase separation is useful to mix these components homogeneously. The droplet size is governed by the cooling rate (fig. 3).

Alternatively to thermoplastic materials, Crooker and Yang⁴ have used an epoxy matrix in order to obtain room temperature PDCLC samples. The respective preparation is well known from the first nematic PDLC samples described by Doane et al.³: The liquid crystal is mixed with a polymerizable monomer and the droplets are formed due to polymerization induced phase separation^{3,19-23}.

We point out that other methods known to prepare nematic PDLC displays are potentially capable of producing polymer-dispersed cholesteric droplets: Vaz et al.²⁴ have demonstrated that UV-curable polymers can be used to obtain PDLC samples by polymerization-indu-

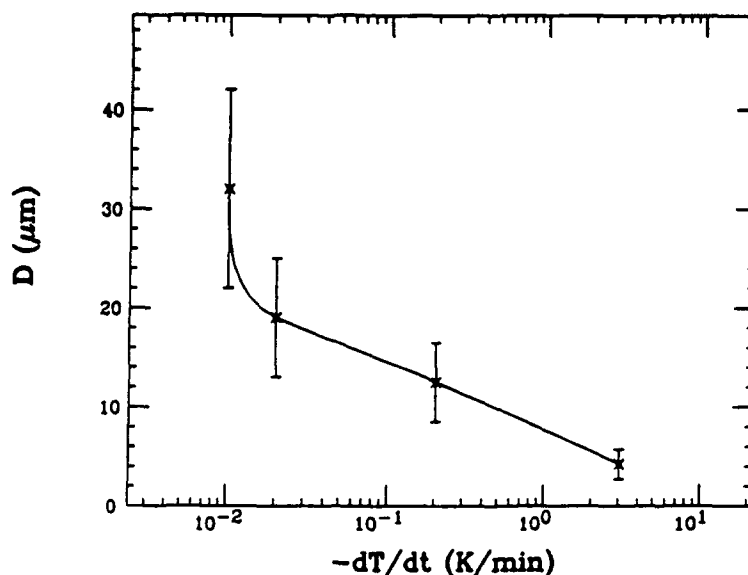


FIGURE 3. - Dependence of the drop diameter on the cooling rate for a sample prepared by temperature induced phase separation [22% CE2, 28% ZLI 2806 and 50% Poly(vinyl butyral)].

ced phase separation^{24,25}. Using solvent-induced phase separation^{1,17}, the liquid crystal and the polymer can be dissolved and the droplet formation can happen during the evaporation of the organic solvent. Besides phase separation in monomer/polymer mixtures, also the encapsulation of liquid crystal droplets in aqueous solutions of poly(vinyl- alcohol)^{26,27} or gelatin²⁸ are known. A detailed review of preparation methods has recently been given by Doane².

III. OPTICAL PROPERTIES

For PDCLC samples with suitable pitch (equation 1), application of a sufficiently high ac voltage causes an increase of the reflectivity at the Bragg wavelength as shown in figure 4. The electro-optic characteristics shows a distinct threshold field strength E_0 . A typical value of this threshold is $E_0 \approx 25 \text{ V} / 10 \mu\text{m}$ for droplets exhibiting a diameter of 6 - 8 μm . The value of E_0 decreases with increasing droplet size. Due to the small slope of the

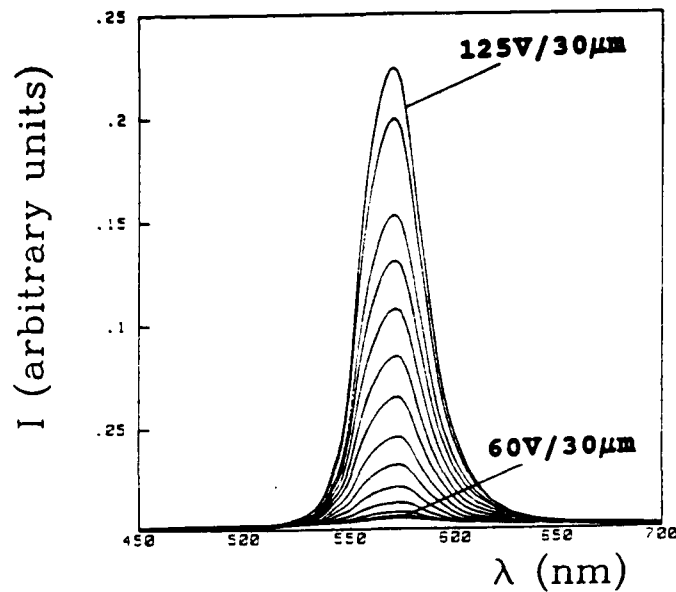


FIGURE 4. - Reflectivity spectra of a PDCLC sample for different field strengths (increment $5 V_{rms} / 30 \mu m$).

reflectivity-voltage characteristics [$\gamma \equiv (V_{50} - V_{10}) / V_{10} \approx 0.3 - 0.4$], PDCLC samples are suitable for controlling the reflected intensity by the applied field strength.

The halfwidth (full width at half-maximum) of the Bragg peaks is typically about 30 nm - 40 nm for droplets with diameters of 10 μm - 15 μm . The reflected light is circularly polarized, exhibiting the same handedness as the helical structure of the cholesteric phase^{4,5}. If the samples are illuminated with unpolarized light, the circularly polarized part of light with opposite handedness is transmitted at the Bragg wavelength.

According to Bragg's law, the wavelength λ of selective reflection depends on the angle θ between the direction of observation and the surface normal:

$$\lambda(\theta) = \lambda_0 \cos \theta' = \lambda_0 \sqrt{1 - \sin^2 \theta / n^2}. \quad (3)$$

(The angle θ' is related to θ by Snell's law.) This strong angular

dependence may be a disadvantage for some possible applications but it can also be used to control the color by tilting the sample with respect to the direction of light incidence (especially in a transmissive display).

Corresponding to the narrow spectral halfwidth of the reflection peaks, the chromaticity coordinates [characterizing the color impression of a standard colorimetric observer according to the recommendations of the International Commission on Illumination (CIE 1931)²⁹] are very close to the chromaticity coordinates of monochromatic light³⁰. As a consequence, a large part of the chromaticity diagram is accessible by additive color mixing of light reflected from three samples with different chirality (fig. 5).

With respect to both brightness and chromaticity coordinates of the light reflected by PDCLC samples, large droplets are favorable since the intensity scattered from cholesteric domains increase with increasing diameter D of these domains ($I \propto D^4$) and the spectral halfwidth decreases with increasing diameter ($\Delta\lambda \propto 1/D$).

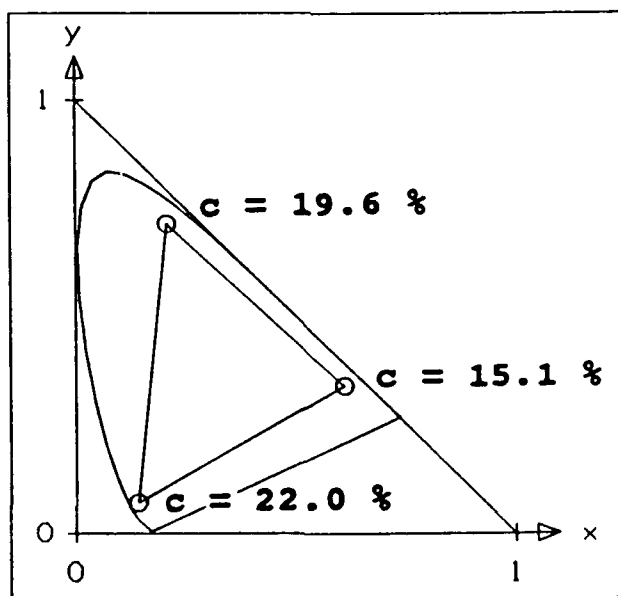


FIGURE 5. - Chromaticity coordinates for samples with different chirality [composition: $c\%$ CE2, $(50-c)\%$ ZLI 2806, 50% Poly(vinyl butyral)].

IV. DIRECTOR CONFIGURATION WITHIN THE DROPS

Microscopic investigations on cholesteric droplets with large cholesteric pitch have proved to be a tool to obtain information on the director configuration. If the pitch of a dispersed cholesteric liquid crystal is of the order of several μm , characteristic fingerprint textures can be observed in the microscope between crossed polarizers⁶. The distance of these fingerprint lines corresponds to one half of the pitch. Characteristic patterns of these fingerprint lines indicate the director configuration in the droplets.

Respective observations have been reported since the early history of thermotropic liquid crystals. Lehmann⁶ and Friedel⁷ investigated liquid crystal droplets on free surfaces and in an isotropic environment close to the clearing temperature. Later, cholesteric droplets were intensively studied in lyotropic systems such as polypeptide solutions in organic solvents⁸⁻¹⁰, and in aqueous solutions¹¹ of DNA or of polysaccharides. Dispersions of thermotropic liquid crystals in solvents like glycerol¹² or toluene¹¹, or in polyurethane elastomers¹³ were prepared. Investigations on the influence of magnetic fields on cholesteric drops in both thermotropic¹² and lyotropic systems¹⁰ revealed the deformation of the fingerprint texture leading to an oval shape for weak fields, and the occurrence of a uniform appearing texture in the drop center above a threshold field strength.

Yang and Crooker¹⁴ have studied the behaviour of cholesteric droplets in electric fields microscopically, using the same components as in the colored PDCLC display, but lower concentrations of the chiral compound. Their observations indicate that the director configuration in the field off state is described by a model proposed by Frank and Pryce^{7,8} (fig. 6) which is characterized by planar alignment of the director at the drop surface and a radial disclination line of strength $s = +2$. Application of an electric

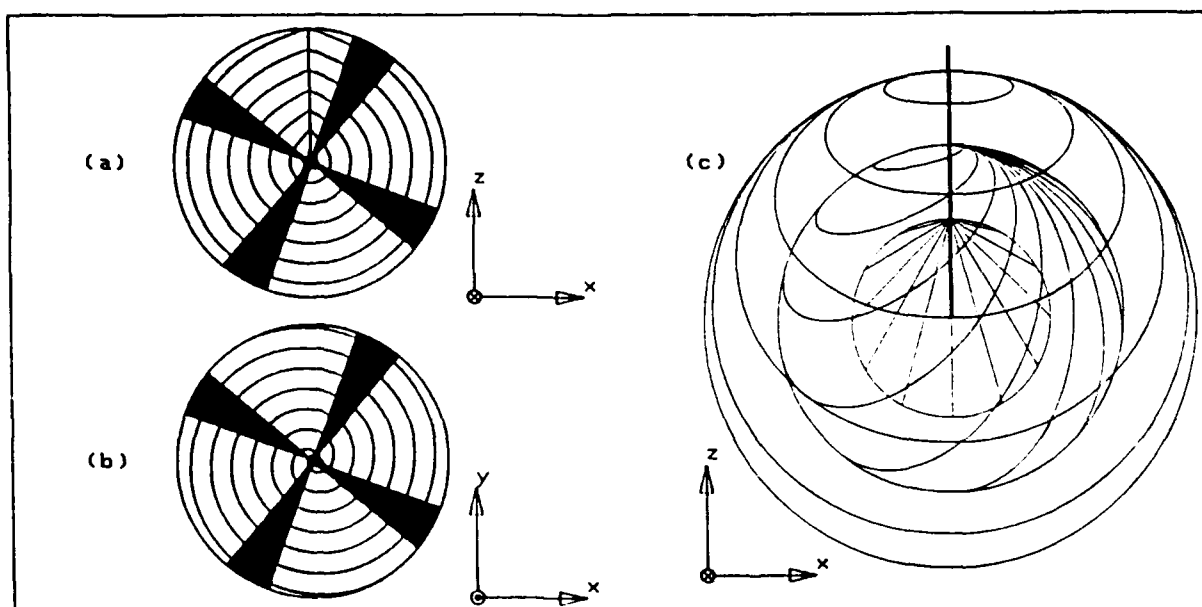


FIGURE 6. - (a,b) Fingerprint patterns of cholesteric droplets with large pitch for two different orientations, as observed in a polarizing microscope in transmission. (c) Visualization of the Frank-Pryce model for cholesteric droplets with planar anchoring: The lines along the spherical surfaces represent the director orientation. The straight vertical line corresponds to a radial disclination line of strength $s = 2$.

field above a threshold value E_0 results in the occurrence of a uniformly oriented region in the center of the drop. The diameter d of this central region is a monotonically increasing function of the field strength which, for a single droplet, can be approximately described¹⁵ by the function $d(E) = D [1 - \exp\{(E-E_0)/E'\}]$. We have found¹⁵ that the threshold value E_0 and the parameter E' decrease with increasing drop diameter D . Changes of the diameter d are associated with rotation of the radial disclination line.

V. DYNAMIC BEHAVIOUR

Microscopic observations on the dynamic behaviour of large pitch droplets if a step voltage is applied to the sample show that the reorientation starts in the drop center. The diameter of the reoriented region increases continuously, if the voltage is

switched on. However, the relaxation when the voltage is switched off was found to exhibit a more complicate three step mechanism¹⁵.

In order to investigate the dynamic behaviour of colored PDCLC displays, the reflected intensity I at the Bragg wavelength was monitored while the ac voltage was switched on/off. Minimum switching times down to a few tenth of a second were found⁴. More detailed studies¹⁵ show that the function $I(t)$ for the switching on process fits a sum of two exponentials

$$I(t) = I_0 + \Delta I (x \exp[-t/\tau_{1,on}] + (1-x) \exp[-t/\tau_{2,on}]). \quad (4)$$

The time constants $\tau_{1,on}$ and $\tau_{2,on}$ were found to decrease with increasing voltage and with increasing temperature T

$$\ln \tau_{i,on} \propto -E_{rms}/T. \quad (5)$$

As a consequence, the values of $\tau_{1,on}$ and $\tau_{2,on}$ vary from a few tenths

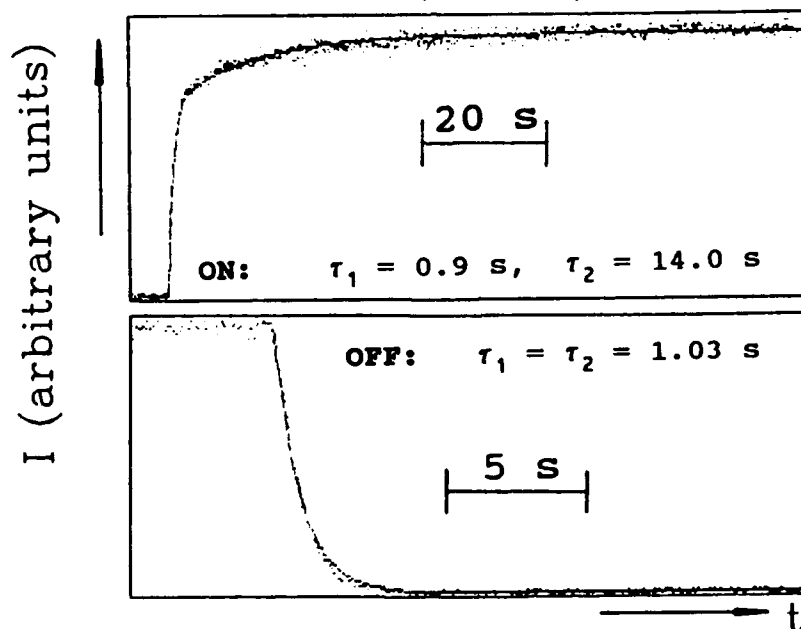


FIGURE 7. - Time dependence of the reflectivity at the Bragg wavelength when an ac voltage ($E_{rms} = 150 \text{ V} / 31.2 \mu\text{m}$) is switched (a) on or (b) off. (90°C , same composition as indicated in figure 3). The time constants τ_1 and τ_2 correspond to a least square fit to equation (4).

of a second to about one minute and from a few seconds to several minutes, respectively. The time constants measured for constant voltage and at constant temperature increase with increasing droplet size¹⁵.

Dynamic investigations for the switching off process indicate that two different relaxation mechanisms can occur, depending on the applied field strength. For low voltages, $I(t)$ fits to a sum of two exponentials with similar time constants as for the case of switching on. However, for high voltage, $I(t)$ exhibits a shape similar to a Gaussian and the relaxation becomes extremely slow. Microscopic investigations show that the latter behaviour occurs if the entire drop has been reoriented by the field. The textures of the droplets occurring during the relaxation are entirely different from those occurring during the switching on process.

Due to the texture change occurring in PDCLC samples, their dynamic behaviour is quite different from the dynamics of nematic PDLC samples. Compared to the values for PDCLC, much smaller time constants (≈ 1 ms) were found for the director reorientation in nematic PDLC displays³. However, besides the fast response (0.1 ms - 1 ms)³¹ related to the pure director reorientation, a much slower process (10 ms - 1 s), related to changes in the surface layer, was observed in elliptically shaped nematic PDLC droplets³¹. In both PDCLC and nematic PDLC displays, small droplet sizes were found to favor fast switching. The drop size in the latter samples is usually smaller ($d \approx 0.4 \mu\text{m}$)³ than the size of the drops in the investigated PDCLC displays (with d ranging from a few μm to $\approx 50 \mu\text{m}$). It is interesting to note that the switching times for nematic PDLC depend not only on the size but also to considerable extent on the shape of the drops³¹.

VI. SUMMARY

PDCLC displays have some very promising properties for applications, namely the possibility of producing flexible polymer sheets and the field-induced occurrence of a bright color which - in contrast to many conventional LCD's - can be observed without polarizers. Due to the small spectral halfwidth of the reflected light the chromaticity coordinates are suitable to access a large area of the chromaticity diagram by additive or subtractive color mixing. Concerning display applications, it should be noted that the aims of fast switching times and bright color are in contradiction, since small time constants require small droplets. Typically, nematic PDLC samples utilize droplet sizes of a few hundred nm³. (For NMR studies, droplets with diameters even less than 20 nm have been produced.³²) However, for PDCLC displays, the droplet size should be sufficiently large compared to the cholesteric pitch ($p \approx 300 \text{ nm} - 500 \text{ nm}$) in order to obtain selective reflection.

We have reviewed the first experimental results on polymer dispersed cholesteric droplets which give some characteristic values for the electrooptical properties and their qualitative dependence on temperature and droplet size. However, systematic variations of the material parameters, such as elastic coefficients or the magnitude of the dielectric anisotropy are still to be performed. Moreover, theoretical considerations are lacking in order to understand the rather complicated dynamics of the relaxation.

REFERENCES

1. J. W. Doane, A. Golemme, J. L. West, J. B. Whitehead and B.-G. Wu: Mol. Cryst. Liq. Cryst., **165**, 511-532 (1988)
2. J. W. Doane in: Liquid Crystals - Applications and Uses, Vol. 1, pp. 361-395, edited by B. Bahadur, World Sci. Pub., Singapore (1990)
3. J. W. Doane, N. A. Vaz, B.-G. Wu and S. Zumer: Appl. Phys. Lett., **48**, 269-271 (1986)

4. P. P. Crooker and D. K. Yang:
Appl. Phys. Lett., **57**, 2529-31 (1990)
5. H. L. de Vries: Acta Crystallog. **4**, 219-229 (1951)
6. O. Lehmann: Flüssige Kristalle und die Theorien des Lebens,
Verlag Johann Ambrosius Barth, Leipzig (1908)
7. G. Friedel:
Annales de Physique, Série 9, Tome **18**, 273-474 (1922)
8. C. Robinson, J. C. Ward and R. B. Beevers:
Disc. Faraday Soc., **25**, 29-42 (1958)
9. C. Robinson: Molecular Crystals **1**, 467-494 (1966)
10. D. L. Patel and D. B. DuPré:
J. Polymer Sci., **18**, 1599-1607 (1980)
11. Y. Bouligand and F. Livolant:
J. Phys. France, **45**, 1899-1923 (1984)
12. S. Candau, P. Le Roy and F. Debeauvais:
Mol. Cryst. Liq. Cryst., **23**, 283-297 (1973)
13. J. R. Quigley and W. J. Benton:
Mol Cryst. Liq. Cryst., **42**, 43-51 (1977)
14. D. K. Yang and P. P. Crooker:
Liquid Crystals, **9**, 245-51 (1990)
15. H.-S. Kitzerow, J. Rand and P. P. Crooker: Results presented
at the European Conference on Liquid Crystals, Courmayeur /
Italy (1991)
16. P. G. de Gennes: The Physics of Liquid Crystals,
Clarendon Press, London (1974)
17. J. L. West: Mol. Cryst. Liq. Cryst., **157**, 427-41 (1988)
18. B.-G. Wu, J. H. Erdmann and J. W. Doane:
Liquid Crystals, **5**, 1453-1465 (1989)
19. N. A. Vaz, G. W. Smith and G. P. Montgomery:
Mol. Cryst. Liq. Cryst., **146**, 17-34 (1987)
20. N. A. Vaz and G. P. Montgomery:
J. Appl. Phys., **62**, 3161-3172 (1987)
21. B.-G. Wu, J. L. West and J. W. Doane:
J. Appl. Phys., **62**, 3925-3931 (1987)
22. G. W. Smith and N. A. Vaz: Liquid Crystals, **5**, 543-571 (1988)
23. G. Chidichimo, G. Arabia and A. Golemme:
Liquid Crystals, **5**, 1443-1452 (1989)
24. N. A. Vaz, G. W. Smith and G. P. Montgomery:
Mol. Cryst. Liq. Cryst., **146**, 1-15 (1987)
25. J. D. Margerum, A. M. Lackner, E. Ramos, K.-C. Lim and W. H.
Smith: Liquid Crystals, **5**, 1477-1487 (1989)
26. J. L. Ferguson: SID Digest of Technical Papers, **16**, 68 (1985)
27. P. S. Drzaic: J. Appl. Phys., **60**, 2142-2148 (1986)
28. A. Seeboth and H. Hermel:
Thin Solid Films, **173**, L119-L121 (1989)
29. Commission Internationale de l'Éclairage (CIE):
Publication No. **15**, E-1.3.1. (1971)
30. H.-S. Kitzerow and P. P. Crooker: to be published.
31. P. S. Drzaic: Liquid Crystals, **3**, 1543-1559 (1988)
32. A. Golemme, S. Zumer, D. W. Allender and J. W. Doane:
Phys. Rev. Lett., **61**, 2937-2940 (1988)

FERROELECTRIC LIQUID CRYSTALS AS FLOW-FIELD SENSORS IN BOUNDARY LAYER INVESTIGATION

D. S. PARMAR*

NASA Langley Research Center, Hampton, Va. 23665

Abstract Utilization of Ferroelectric Liquid Crystals in a simple new configuration, one rigid surface and the other exposed directly to the flow field, for non-intrusive global as well as local 2D surface stress field determination is reported. Shear flow-field induced optical switching on the boundary layer has been used both in the transmission as well as in the reflection mode operation of the sensor. Characteristics of domain formation in an A - C* and a N* - C* material and the optical response of domains to an applied shear stress in the plane of the C* layers are described. Optical polarization microscopy has been used to measure the transmitted and the reflected light intensities as function of flow parameters. Using micro wind tunnel in conjunction with polarizing microscopy, change in director orientation as a function of the shear stress field has been determined. Director dynamics has been discussed from free energy considerations in the present context.

INTRODUCTION

Optical visualization of the air or gas flow-field and the quantitative measurement of the boundary layer shear stress field are important for a variety of applications. For example in fluid mechanics, it is important to know the flow patterns and from them to determine the conditions for the transition from laminar to the turbulent flow. A complete understanding of the boundary layer phenomena is also important in aerodynamics for the development of high efficiency aircraft. In all such situations, knowledge of

* Supported under master agreement with the Old Dominion University Research Foundation, Task # NAS1-18584-111

the instantaneous conditions and mechanisms responsible for the boundary layer transition is essential. This can be accomplished by constantly viewing the boundary layer in the vicinity of the transition from laminar to the turbulent flow through the entire transition process. Liquid crystals because of their optical anisotropic properties are considered as good candidates for optical visualization of flow patterns. There have been a number of experimental efforts to use cholesteric and chiral nematic liquid crystals^{1,2} by utilizing the phenomenon of selective reflection in the shear sensitive and the temperature sensitive modes. Although it has been possible to calibrate the shear sensitivity of the cholesteric liquid crystals³, their response to an applied shear stress (like for any mechanical, electrical or magnetic) field is relatively slow (1 - 100 ms). Hence rapid changes in the flow-field taking place at the time scales on the order of micro- and even submicroseconds can not be recorded. This limits the utility of these systems in the transition region.

In a simple flow experiment, Pieranski et al.⁴ obtained helix unwinding effects in a ferroelectric liquid crystal (FLC) sandwiched between two plates by shearing the FLC layers perpendicular to the helix axis. These effects were similar to the one obtained by applying an electric field in the plane of the smectic layers. In a thin ($\sim 1 \mu\text{m}$) sample of FLC, the bounding surface interactions suppress the helix. This led to the discovery of Surface Stabilized FLC (SSFLC) by Clark and Lagerwall⁵ in 1980. Sandwiched between two transparent conducting electrodes and crossed polarizers, the SSFLC exhibited submicrosecond bistable optical switching⁶. In a recent experiment, domain switching in FLC was utilized as a boundary layer sensor⁷ in a new configuration, a rigid surface and the other exposed directly to the gas flow. In the present paper utilization of this new configuration for non-intrusive global as well as local 2D surface stress field determination is reported.

EXPERIMENTAL

The liquid crystal thin film is prepared on a glass substrate by filling the material in between two buffed nylon coated glass plates separated by $\sim 1.7 \mu\text{m}$ polyballs. The liquid crystal is heated to the isotropic liquid (I) phase and the cell is filled by capillarity. The sample is cooled down slowly to the chiral smectic C (C^*) phase through the smectic A (A) or the nematic (N^*) phase depending on whether the material demonstrates the A - C^* or the N^* - C^* transition. Not far below the transition from the higher temperature phase, a chevron layer texture⁸ is seen in the C^* phase. The top glass plate is sheared gently parallel to the bottom one in the direction of the chevron until it is completely out of the configuration. This provides a FLC thin film ($\sim 1.7 \mu\text{m}$) on a rigid (bottom) glass substrate and free top surface. The sample is examined with the help of an experimental arrangement of Ref. 7 for the reflection and the transmission mode polarizing microscopy under shear stress from a gas flow on the exposed surface.

RESULTS

Experimental results on two FLC mixtures, namely the ZLI-3654 from E. Merck and the CS2004 from Chisso Corporation with the following transition sequence are reported here:

ZLI-3654 I 86 N^* 76 A 62 C^* < -30 X
 CS2004 I 71 N^* 62 C^* -9 X

where X is the crystalline phase. In these experiments, the two mixtures have been found to give different Schilieren textures depending on whether the higher temperature phase to C^* is the A or the N^* phase.

A - C* Transition

In this case the typical Schlieren texture, as seen in the microscope under the crossed polarizers in the transmission mode, consists essentially of two domains separated by a domain wall. The two domains and the domain wall in absence of the gas flow are shown in Fig. 1(a). On the impingement of gas flow in the direction of the arrow, the domain on the left hand side becomes brighter whereas the one on the right hand side becomes darker as shown in Fig. 1(b) for a gas flow differential pressure $\sigma = 3.3$ Torr. Further increase in the rate of gas flow increases the contrast between the bright and the dark states as shown in Fig. 1(c) for $\sigma = 8.8$ Torr. For the brighter domain, the change $\Delta I = (I_S - I_0)/I_0$, where I_S and I_0 are respectively the light intensities in



Fig. 1 Schlieren texture of the A - C* sample viewed in transmission under crossed polarizers. σ in Torr (a) 0, (b) 3.3, and (c) 8.8.

presence and absence of gas flow, in the transmitted light intensity as a function of differential pressure σ is shown in Fig. 2. In the range of σ (0 - 15 Torr) used in the present experiment, the variation is linear. Saturation effects in ΔI start appearing at higher values of σ .

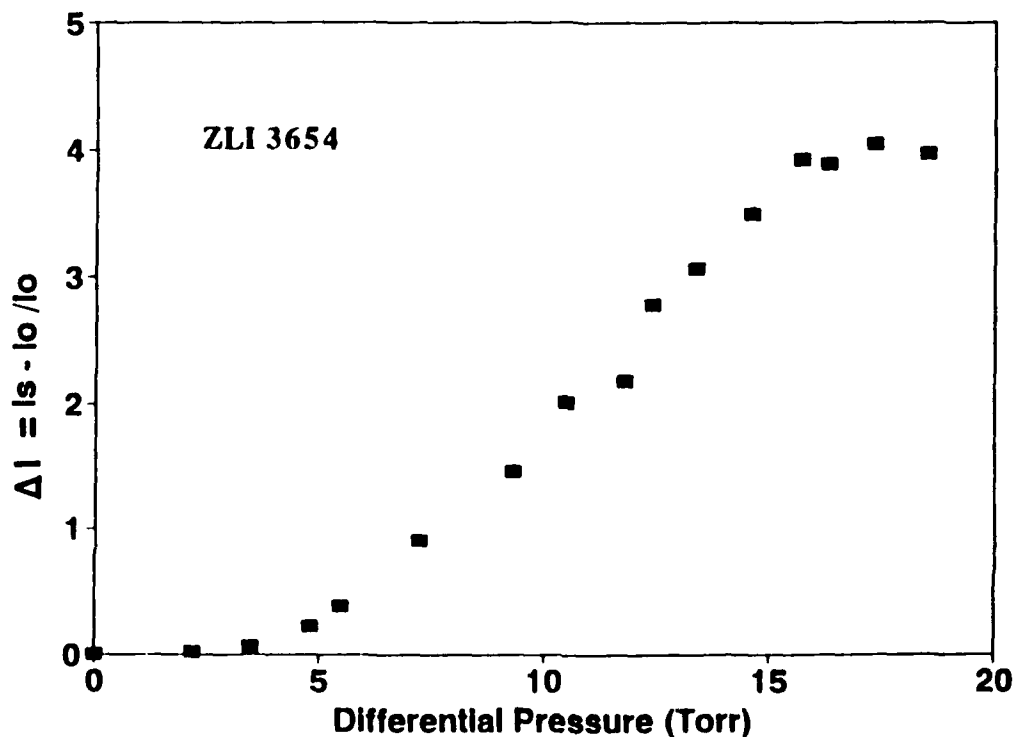


Fig. 2 Variation of ΔI with σ for ZLI-3654.

Domain Walls

The domain walls appear as closed loops with varying shapes and sizes but with definite wall structure. A typical wall structure, shown in Fig. 3(a), is a natural boundary between the domains of two degenerate orientations. The mechanism representing formation of the wall corresponding respectively to the director n tilt angle θ and $-\theta$ in the homeotropic orientation of the smectic layers is shown in Fig. 4(a). The two orientations are constrained by the surface interactions at the substrate surface and the

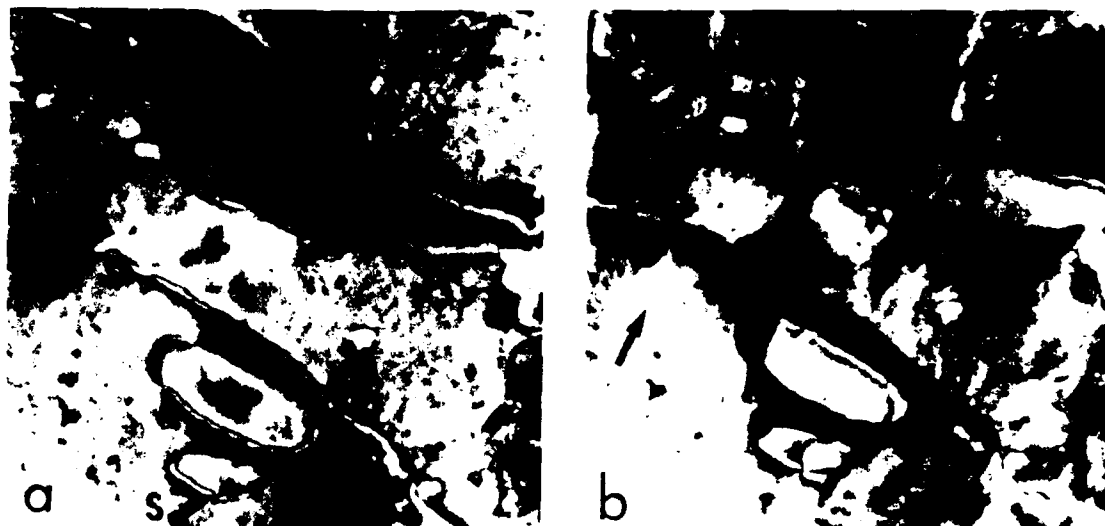


Fig. 3: A typical domain wall structure of an $A - c^*$ material. (a) $\sigma = 0$, (b) $\sigma = 2.6$ Torr.

forces of surface tension on the upper free surface. The director \mathbf{c} in Fig. 4(a) is the projection of \mathbf{n} on the smectic layer parallel to the substrate in the x - y plane. The two positions of \mathbf{c} , namely \mathbf{c} and \mathbf{c}' , correspond respectively to the two different positions of \mathbf{n} on the cone of revolution (Fig. 4b). Topographical defect structures, such as point singularity S_+ , are induced in the domain wall as a natural consequence of the change in the \mathbf{c} orientation across it as shown in the Schilieren texture photograph of Fig. 3(a) and its geometrical representation in Fig. 4(a). S_- point singularity, will also be induced as a result of the similar director distribution across the wall.

The polarizer P_1 and the analyzer P_2 are aligned along the y - and the x - axes respectively and extinction is achieved in absence of the gas flow. Shear stress σ due to gas impingement along y - axis forces \mathbf{c} in state 1 (Fig. 4b) to reorient towards the polarizer P_1 increasing extinction. The directors \mathbf{c} in state 2, on the other hand, tend to reorient away from the analyzer P_2 thus increasing transmission in these areas. The domains formed by \mathbf{c} at 1 on one side of the domain wall become darker and those

formed by c at 2 on the other side of the domain wall become brighter. This situation is demonstrated unambiguously in the photograph of Fig. 3(b) obtained for gas impingement of $\sigma = 2.6$ Torr in the direction of the arrow. The rotation and sharpness of the brushes of the 8 defect under shear stress (Fig. 3b) in comparison to that in Fig. 3(a) for zero shear is striking. This further demonstrates that the observed effects are a result of the director rotation under the influence of σ .

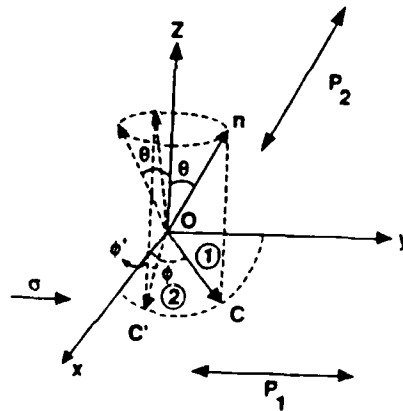
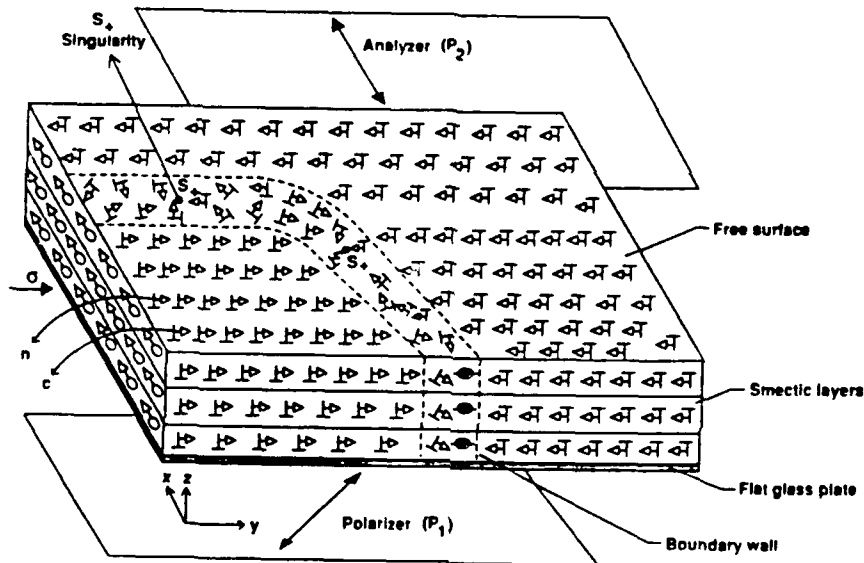


Fig. 4 (a) Director orientation on a glass substrate and the free upper surface.
(b) Coordinate system representing the c distribution.

A Domain wall with two S type point singularities is shown in Fig. 5(a) for $\sigma = 0$ and in Fig. 5(b) for $\sigma = 2.1$ Torr. It is interesting to note that on the impingement of gas flow in the direction of the arrow, black and bright areas grow on the opposite sides of the defect and also when the defect is traversed along the wall (Fig. 5b). The fact that the domain wall actually separates the domains of two

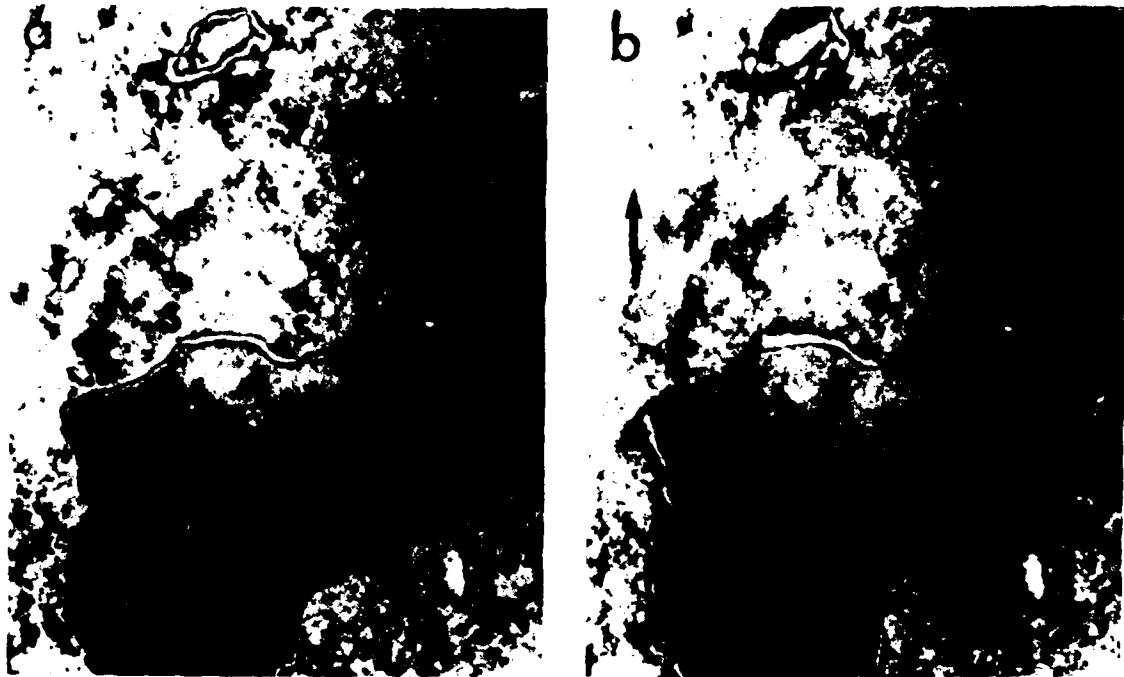


Fig. 5 (a) A domain wall with two S defects. (b) Areas of black and bright orientations grow on the opposite sides of the defect both along and across the wall.

unidirectional director orientations is further demonstrated in the photographs of Fig. 6(a,b) where the domain wall appears in the form of a zig-zag defect. The domain wall, like in Figs. 3 and 5 also, is a double line boundary, a bright border confined by black boundaries on each side, for $\sigma = 0$ as shown in Fig. 6(a). Gas flow impingement of $\sigma = 1.9$ Torr in the direction of the arrow in Fig. 6(b) switches the

domains on the two sides of the zig-zag respectively to black and bright. This clearly demonstrates that not only the two opposite sides of the zig-zag wall form domains of

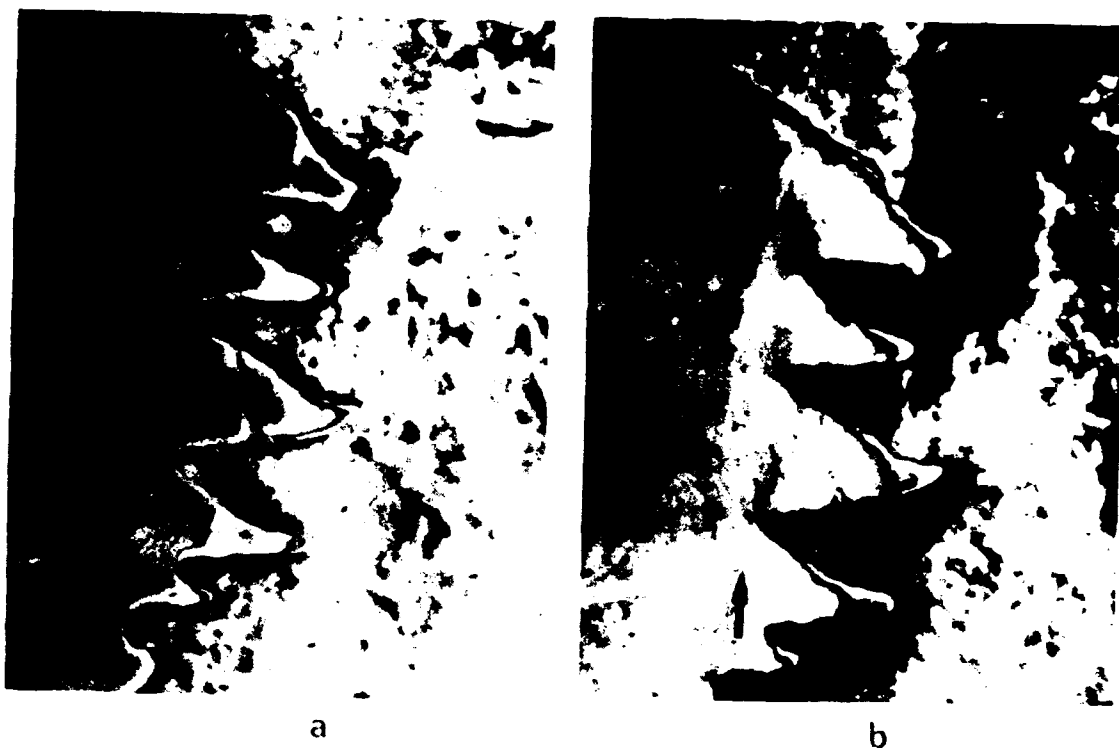


Fig. 6 (a) A zig-zag shaped domain wall, $\sigma = 0$.
(b) The opposite sides of the zig-zag switch to black and bright states, $\sigma = 1.9$ Torr.

different director orientation but also that the observed shear - optic effects are due entirely to the molecular reorientation in the stress field and not due to any hydrodynamic flow of the liquid crystal.

N* - C* Transition

Monodomain liquid crystal samples were obtained for CS2004 which demonstrates a N* - C* transition with a wide C* range (-9 - 62°C) and a large but constant θ ($\sim 44^\circ$). Schlieren texture for C* monodomains as seen in transmission is shown in Fig. 7(a,b,c,d) for $\sigma = 0, 8.5, 13.8$ and 16.0 Torr respectively. σ is arranged along the direction of buffing of the glass plates. It may be noted that all the landmarks in the texture formed by the polystyrene balls ($1.7 \mu\text{m}$) mixed with the liquid crystal during the sample preparation remain undisturbed by the gas flow. This ensures that the change ΔI in the transmitted light intensity is a result

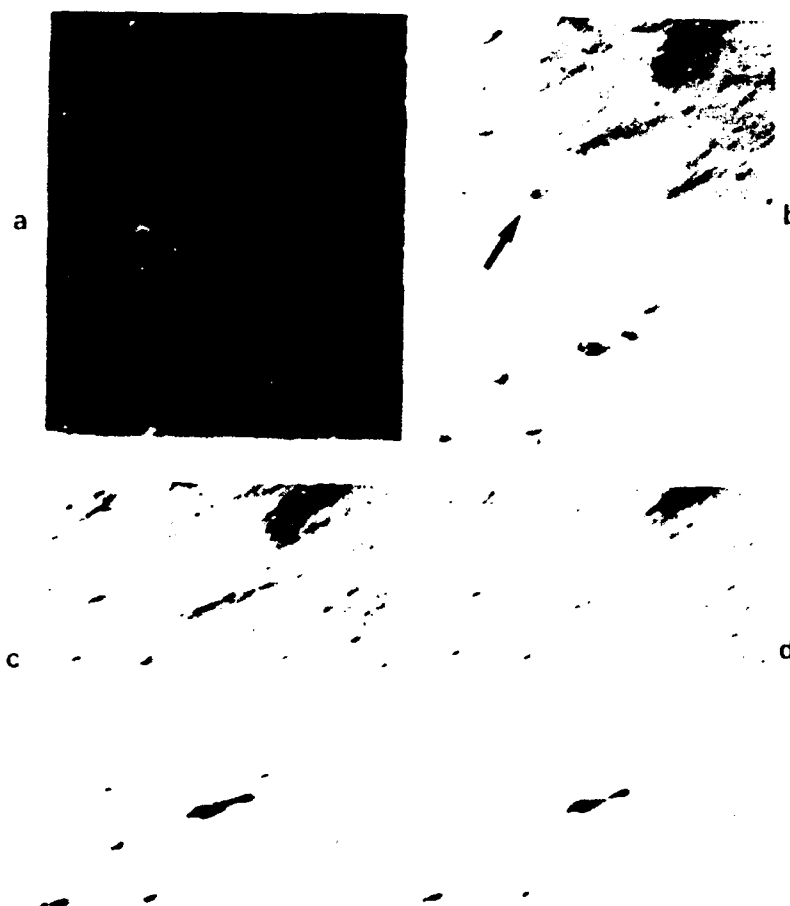


Fig. 7 Schlieren texture for the monodomain sample of CS2004 for σ (Torr): (a) 0, (b) 8.5, (c) 13.8 and (d) 16.0

of the molecular reorientations. Further, ΔI increases with σ as shown in Fig. 8. Similar ΔI behavior, shown in Fig. 9, is observed when the sample is viewed in normal reflection after adequate adjustment of the polarizers for maximum extinction in absence of shear stress.

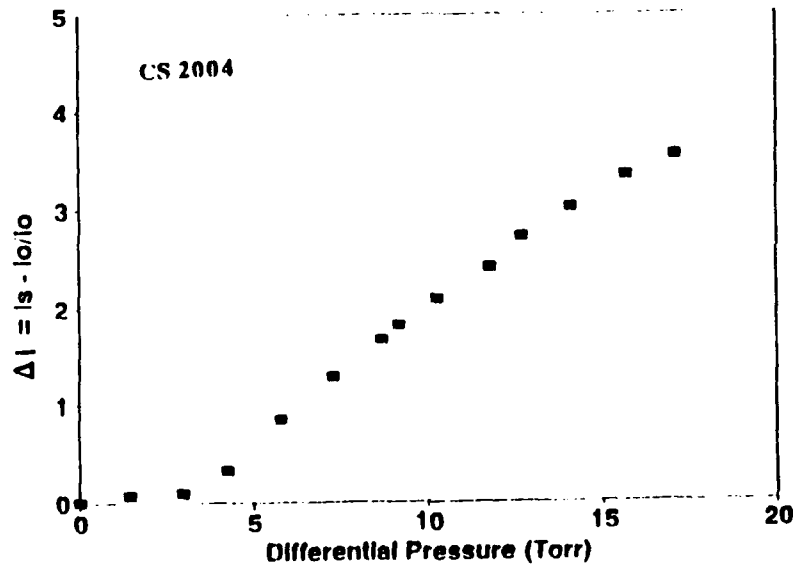


Fig. 8 Variation of ΔI with σ in the transmission mode for CS2004.

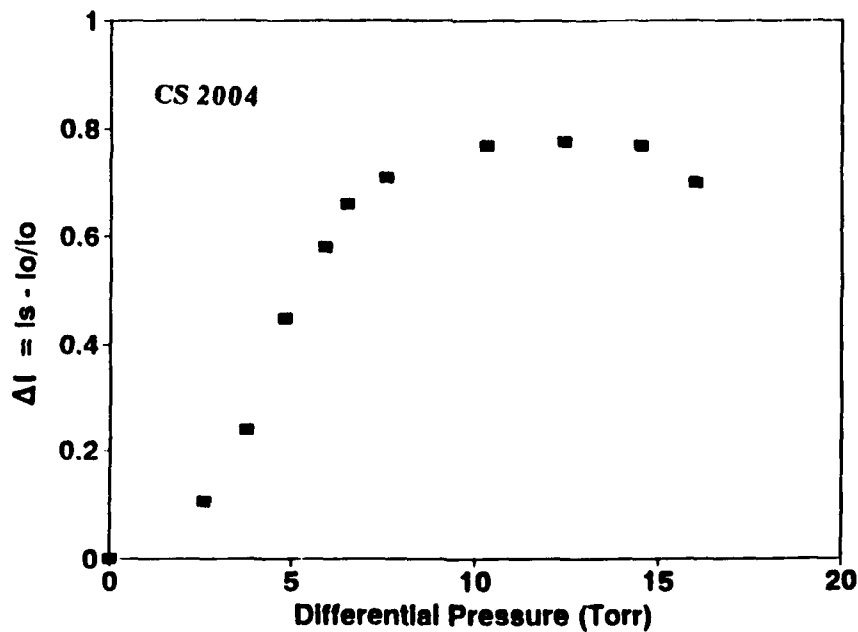


Fig. 9 Variation of ΔI with σ in the reflection mode of CS2004.

Shear stress induced director rotations, $\Delta\phi$ were measured by rotating the microscope stage until extinction is achieved. This realigns σ in the $\sigma = 0$ position with respect to P_1 . The micro wind tunnel used for gas flow impingement being attached to the stage, relative orientation of σ and σ is always maintained. For transmission mode, $\Delta\phi$ is a linear function of σ as shown in Fig. 10(a). Variation of $\Delta\phi$ for the reflection mode is similar as shown in Fig. 10(b).

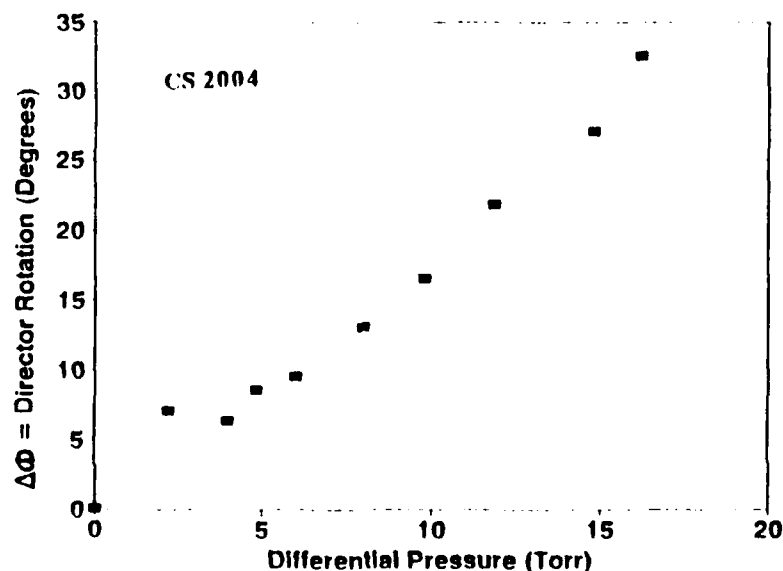


Fig. 10 (a) Variation of $\Delta\phi$ with σ in the transmission mode for CS2004.

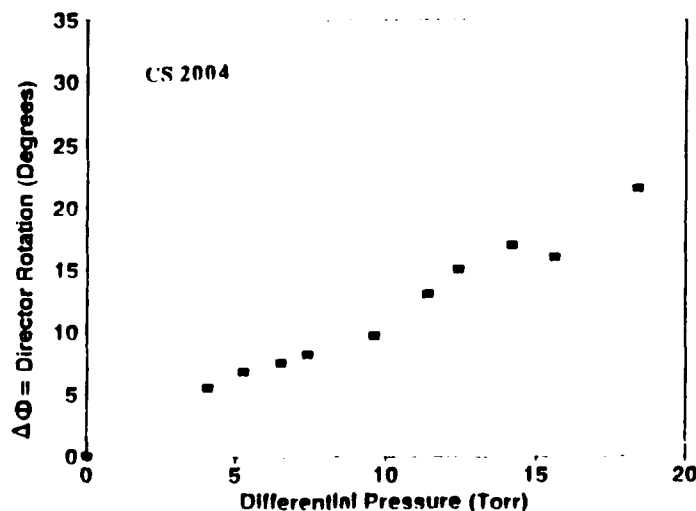


Fig. 10 (b) Variation of $\Delta\phi$ with σ in the reflection mode for CS2004

FREE ENERGY OF THE SYSTEM

The system free energy f in presence of σ is the sum of contributions from the elastic deformations, f_{elast} , the shear stress, f_{shear} , and the free surface energy f_{surf} , i.e.

$$f = f_{\text{elast}} + f_{\text{shear}} + f_{\text{surf}} \quad (1)$$

The elastic free energy consists of the conventional splay, twist, and the bend deformation terms and is written as⁹:

$$f_{\text{elast}} = \frac{1}{2} K_1 (\nabla \cdot \mathbf{n})^2 + \frac{1}{2} K_2 (\mathbf{n} \cdot \nabla \times \mathbf{n})^2 + \frac{1}{2} K_3 (\mathbf{n} \times \nabla \times \mathbf{n})^2 \quad (2)$$

where K_i are the corresponding elastic constants. From Fig. 4(b), $f_{\text{shear}} = \sigma \sin \theta \cos \phi = \sigma \cos \phi$. If Ω° is the energy due to surface tension on the free surface and θ' is the apparent tilt angle, f_{surf} is given by:

$$f_{\text{surf}} = \Omega^\circ \sin^2 (\theta - \theta') \quad (3)$$

In the frame of reference of Fig. 4(b), the director equation of motion can be obtained by solving eq. (1). The Euler - Langrange equation in the most commonly used one elastic constant approximation can be solved to result⁷:

$$\eta \partial \phi / \partial t = \sigma \times c = \sigma' \sin \phi \quad (4)$$

where $\sigma' = \sigma \sin \theta = \sigma c$ and the elastic term has been neglected because of its smallness. Integrating eq. (4):

$$\log \{ \tan(\phi/2) / \tan(\phi_0/2) \} = (\sigma' / \eta) t \quad (5)$$

where ϕ , for an applied step input σ , increases from $\phi = \phi_0$ at $t = 0$ to saturate after a characteristic time t . In the present experimental situation where σ was arranged orthogonal to c in the x - y plane, eq. (4) may be solved to

give:

$$\Delta\phi = \phi - \phi_0 = \alpha\sigma t \quad (6)$$

where α ($= n\sin\theta/\eta$) is a constant. For a given σ , $\Delta\phi$ is a linear function of t and the saturated value of $\Delta\phi$ is a linear function of σ . This explains the linearity in the σ vs. $\Delta\phi$ curve of Fig. 10. Measurements of $\Delta\phi$ in different parts of the sample give $\partial\Delta\phi/\partial\sigma \sim 2.0 \pm 0.2$ °/Torr.

In the present situation, ΔI for an applied input σ can be expressed by the relation

$$I = I_0 \sin^2(\Gamma/2) \quad (7)$$

where $\Gamma = (\Delta n + \delta\Delta n)k_0d$ is the amplitude of the phase retardation for an incident light of wavevector k_0 propagating in a medium of birefringence Δn . The shear stress induced change in birefringence is $\delta\Delta n$. For a monodomain sample of the director configuration of Fig. 11, $I_0 = I_p \sin^2(\Psi - \beta)$, where I_p is the transmitted light intensity for the parallel polarizers and β the angle by which the frame of reference would have to be rotated with respect to the polarizer for maximum extinction for a given σ . From Fig. 11, $\tan\Psi = \tan\theta\cos\phi_0$ and thus $\sin\beta = \sin\theta\cos\phi$. With these substitutions in eq. (7) under the assumption that $\delta\Delta n$ is negligibly small for the range of σ in the present experiment, ΔI is obtained as a \sin^2 function of $\Delta\phi$. This explains the $\Delta I - \sigma$ behavior in Figs. 8 and 9. In case $\delta\Delta n$ is appreciable, ΔI would further be a \sin^2 function of σ and a linear function of $\Delta\phi$ because of its linearity with σ from eq. 6 as in Fig. 10.

The calculations presented in this paper are for the smectic layer orientation parallel to the substrate surface according to the geometries of Figs. 4(b) and 11. The homeotropic alignment of the sample has been concluded from the texture determination. However, further studies are necessary to ascertain the layer alignment and structure in

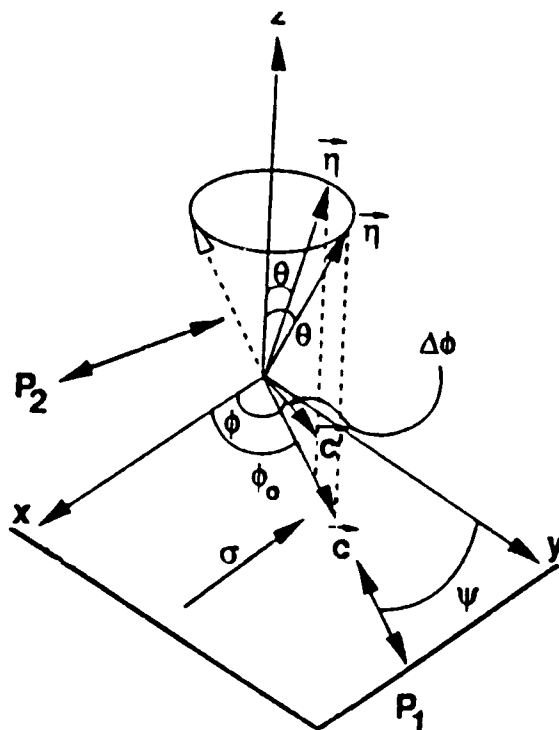


Fig. 11 Orientation of σ relative to c used in the calculations of $\Delta\phi$.

the sample geometry of the present experiments.

The author expresses his sincere thanks to Jag J. Singh, Harlan K. Holmes and Bruce A. Conway for many helpful discussions and their continued encouragement for this work.

REFERENCES

1. B.J. Holmes, C.G. Groom, P.D. Gall, G.S. Manuel and D.L. Carraway, AIAA-86-Q786(1986).
2. L. Gaudet and T.G. Gell, Int. Conf. on Instrumentation in Aerospace Facility, Göttingen, W. Germany, 1989, p. 66.
3. D.S. Parmar, Rev. Sci. Instrum., **62**, 1596(1991).
4. P. Pieranski, E. Guyon, P. Keller and L. Liebert, Mol. Cryst. Liq. Cryst., **38**, 275(1977).
5. N.A. Clark and S.T. Lagerwall, Appl. Phys. Lett., **36**, 899(1980).
6. N.A. Clark and S.T. Lagerwall, Ferroelectrics, **59**, 25(1984).
7. D.S. Parmar, Rev. Sci. Instrum., **62**, 474(1991).
8. T.P. Rieker, N.A. Clark, G.S. Smith, D.S. Parmar, E.B. Sirota and C.R. Safinya, Phys. Rev. Lett., **59**, 2658(1987).
9. P.G. deGennes, The Physics of Liquid Crystals (Clarendon, Oxford, 1974).

DIRECTOR STRUCTURES OF A CHIRAL SMECTIC I LIQUID CRYSTAL IN THE SURFACE STABILIZED GEOMETRY

Renfan Shao, Zhiming Zhuang and Noel A. Clark
Department of Physics
Condensed Matter Laboratory
Optoelectronic Computing Systems Center
University of Colorado
Boulder, CO 80309-0390, U.S.A.

Abstract The director structures of the Smectic I* (SmI^*) liquid crystal 8SI, confined in the surface stabilized ferroelectric liquid crystal cell geometry, were studied using the polarized light microscope. Upon cooling from smectic C* (SmC^*) to SmI^* phase, the zigzag defects of the C^* phase were unchanged indicating that the chevron layer structure remains in the SmI^* phase. This phase transition is first order with SmI^* domains growing from the SmC^* background. Eight stable states were observed in the SmI^* phase. These states were divided into two groups of four, separated by the chevron interface transition, revealed by its characteristic boat shaped switching domains. Additionally there were three surface transitions at each bounding glass plate with stripe shaped domains. The polarization P-director n configurations for all eight states are presented.

INTRODUCTION

Since the discovery of Surface Stabilized Ferroelectric Liquid Crystal (SSFLC) geometry in SmC^* phase¹, there have been several studies of SSFLC switching phenomena in higher ordered phases like smectic I* and smectic J (SmJ) phases^{2,3}. The influences of the inplane hexagonal bond orientational order and translational order and their orientation relative to the surface boundary are the major focus of the interest. Previously Ouchi *et al.*³ proposed a four state multistable switching scheme based on the simple bookshelf geometry¹. They observed two type switching domains in their SmI^* sample: one is of stripe shape and the other looked like the $\pm 2\pi$ disclination loops (speedy boats) commonly seen in the SSFLC cells in SmC^* phase. In the light of the chevron layer structure revealed by high resolution X-ray experiment^{4,5}, it is generally recognized now that those $\pm 2\pi$ disclination loop are

caused by molecular reorientation at the chevron interface⁶⁻⁸. Also stripe shaped switching domains has been observed in SmC^* SSFLC cells when the molecules reorient at the surface (FLC-glass plate interface)⁷⁻⁹. Comparing these new research results of SSFLC cells with what Ouchi *et al.* observed in their experiments indicates that what may actually happened in their sample was a surface director reorientation and a chevron interface director reorientation. However our recent investigation shows that the reorientation process in SmI^* is more complicated and both the inplane hexagonal order and the chevron layer structure have to be considered to get a complete picture. In this paper we will present our experimental observations on the $SmC^* - SmI^*$ phase transition and switching processes in SmI^* phase, and our model of director-polarization configurations for the multi-stable states of SmI^* phase in SSFLC geometry. This model differs significantly from those proposed previously^{2,3}.

EXPERIMENTAL OBSERVATIONS

The liquid crystal we used is the 8SI from BDH, with the nominal phase sequence $Iso \xrightarrow{140^\circ} N^* \xrightarrow{134^\circ} SmA \xrightarrow{82.5^\circ} SmC^* \xrightarrow{67.9^\circ} SmI^* \xrightarrow{62.0^\circ} SmJ \xrightarrow{56.6^\circ} SmG \xrightarrow{50.5^\circ} Cryst$. The sample was made using the SSFLC geometry with the liquid crystal (LC) being sandwiched between two clean ITO coated glass plates separated by $1.7\mu m$ spacerballs. The LC material was filled in by capillary in the isotropic phase and the alignment in the smectic phases was achieved by shearing method when the sample was cooled from nematic phase to SmA phase. The observed SmC^* to SmI^* transition temperature is $69.0^\circ C$.

Fig. 1 (a) shows the photomicrographs of the 8SI sample cooling through SmC^* to SmI^* transition (from (i) to (vi)), taken with a Zeiss polarized light microscope with crossed the polarizer and analyzer. The polarizer and analyzer directions are indicated in the photographs and the projection of smectic layer normal onto the glass plates can be determined using the zigzag defects line clearly seen in the figure⁵. Fig. 1 (i) shows the sample in SmC^* phase. In the photographed area we can see two zigzag wall lines across the picture separating areas with different chevron direction, and some speedy boat shaped polarization reorientation domain walls, trapped at the chevron interface, separating average polarization UP state (the dark grey region) and average polarization DOWN state (the brown region). Both of these states are twist states which is typical in SmC^* SSFLC cells⁶. As

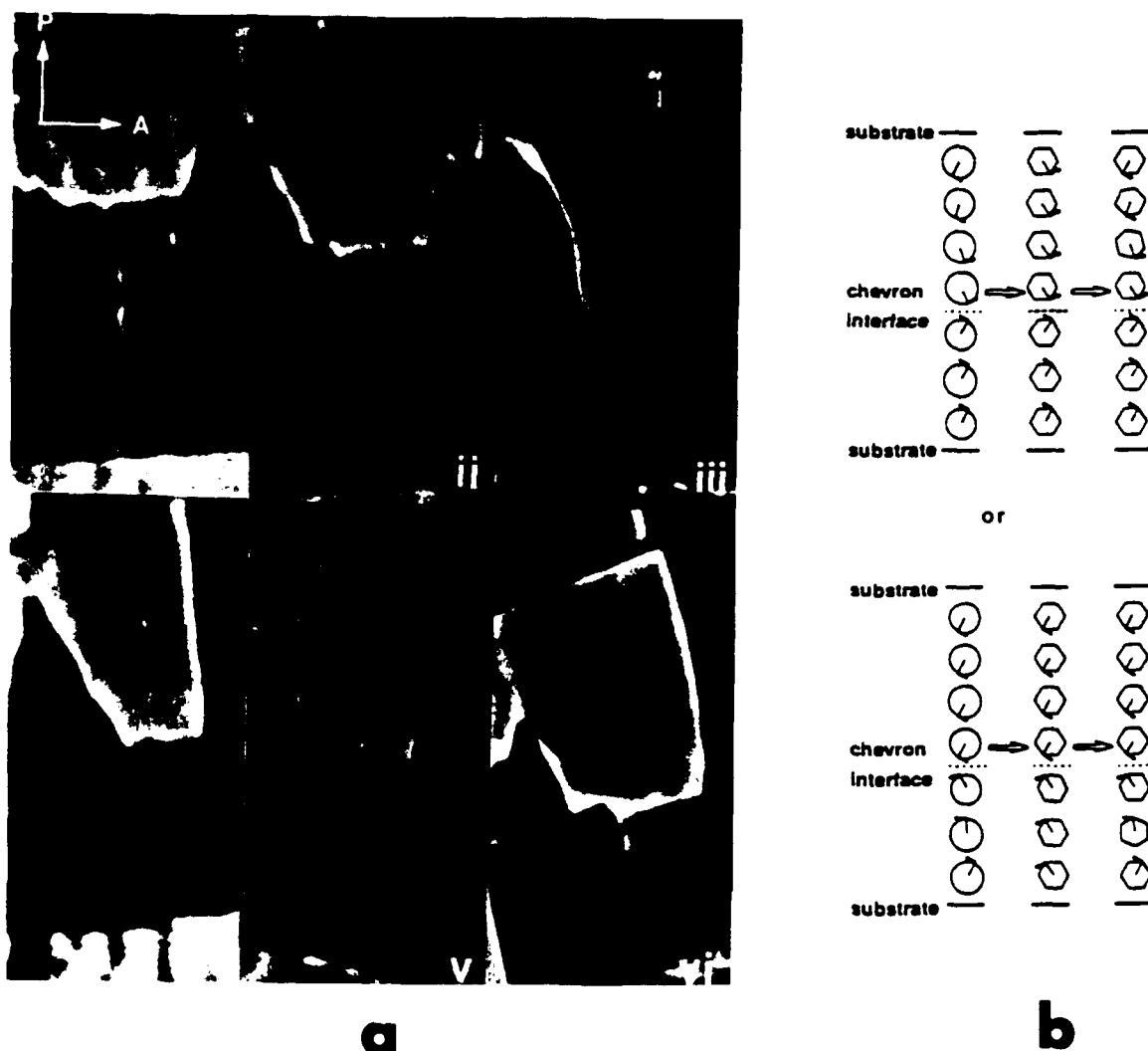


Figure 1: (a) Photomicrographs of SmC^* to SmI^* phase transition.

- (i) $T = 75^\circ C$ (SmC^*), $\alpha = +7.4^\circ$;
- (ii) $T = 68.9^\circ C$ ($SmC^* \rightarrow SmI^*$), $\alpha = +7.4^\circ$;
- (iii) $T = 68.7^\circ C$ (SmI^*), $\alpha = +7.4^\circ$;
- (iv) $T = 65^\circ C$ (SmI^*), $\alpha = +7.4^\circ$;
- (v) $T = 65^\circ C$ (SmI^*), $\alpha = -16.4^\circ$;
- (vi) $T = 65^\circ C$ (SmI^*), $\alpha = +16.4^\circ$.

α is the angle between the analyzer direction and the projection of layer normal on the glass plate. (b) Proposed P-n configurations changes at phase transition.

See Color Plate XI.

we decrease the temperature two SmI^* states (the green and dark green region) started to nucleate and expand from the SmC^* texture, as shown in Fig. 1 (ii) and (iii). Both of this two SmI^* states were found to be uniform states because they could give very good extinction between crossed polarizer and analyzer, as can be seen in Fig. 1 (v) and (vi). The difference between their extinction angle is found to be $\sim 28.8^\circ$. When we kept cooling the sample in SmI^* phase after the two uniform states covered the whole cell (see Fig. 1 (c)) two new SmI^* states appeared in the sample, shown as the yellow and grey region in Fig. 1 (iv). These two new states are twist states since we could not find a extinction position for them. The appearance of these four states are very similar to those observed by Ouchi *et al*³. It is noticeable that the domain boundaries separating the two twist SmI^* states are leftovers of the domain boundaries separating the two twist states in SmC^* phase. This fact leads us to suspect that these domain boundaries, described by Ouchi *et al* in their paper as 2π disclination loops, are actually same the switching domains commonly seen in SmC^* chevron SSFLC cells. *An important feature to be noticed in Fig. 1 (a) is that the zigzag defects were unchanged through the $SmC^* - SmI^*$ phase transition, indicating that the chevron layer structure remains in the SmI^* phase and there was no significant change in the layer tilt angle.*

When we applied external voltage V_a across the cell, as depicted in Fig. 2, an eight state multistable switching process was formed. We will denote these eight states with number 1 to 8. In Fig. 2 from (i) to (iv) the sample was switched successively from the first state to the fourth state through three director reorientations with stripe shaped switching domains, similar to those observed in SmC^* cells when director reorients at surfaces (FLC-glass plate interfaces). Symmetrically from Fig. 2 (x) to (vii) the sample was switched from the eighth state to the fifth state. Meanwhile the switching between the fourth and the fifth states, as shown in Fig. 2 (v) and (vi), showed some unique features different from all other transitions observed. It generates boat shaped reorientation domain walls, which are similar to those commonly seen in the chevron interface switching in SmC^* SSFLC cells. All these observations indicate that for the seven director orientation transitions observed, six of them occurred at surfaces and only one ($4 \leftrightarrow 5$) occurred at chevron interface. Among all eight states, states 1, 2 and 3 are uniform DOWN states and states 6, 7 and 8 are uniform UP states judging by their extinction color and the direction of applied fields, while states 4 and 5 are twist states because they do not extinguish between crossed polarizer and analyzer. The applied voltage mismatch

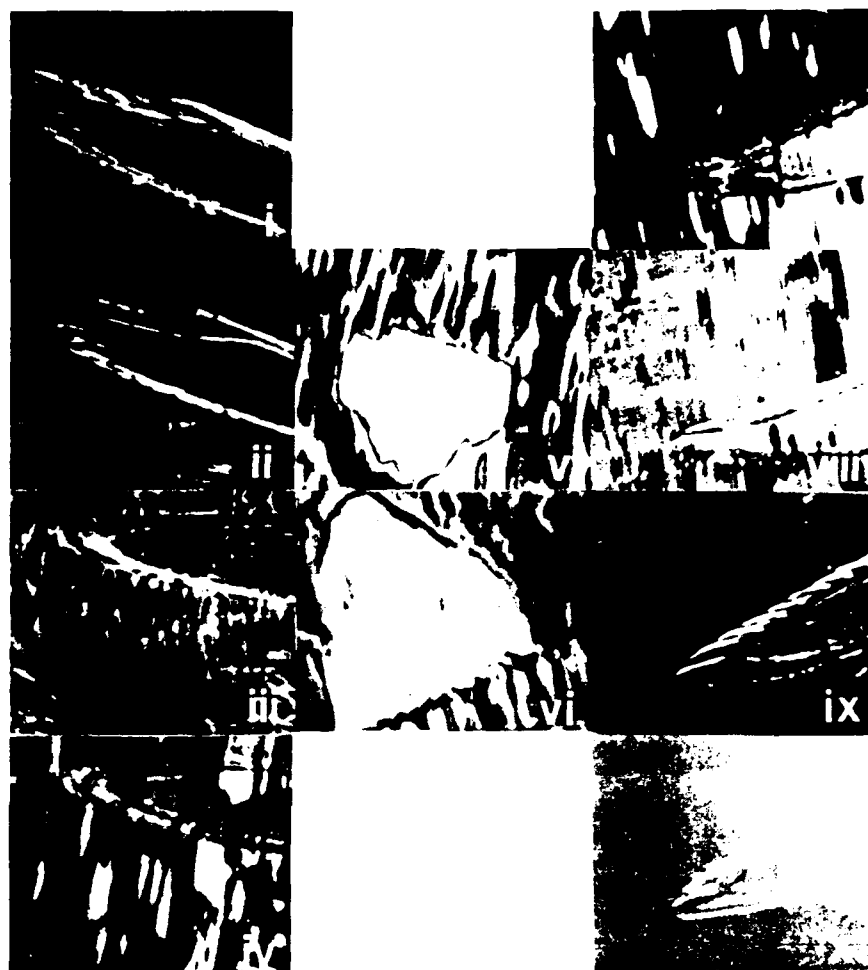


Figure 2: Multistable switching process in SmI^* phase.

- (i) $V_a = -25V, \alpha = -22.5^\circ$. The state 1 in extinction.
- (ii) $V_a = -11.1V, \alpha = -18.5^\circ$. $1 \rightarrow 2$ transition. State 2 is the dark state.
- (iii) $V_a = -0.7V, \alpha = -11.5^\circ$. $2 \rightarrow 3$ transition. State 3 is the dark state.
- (iv) $V_a = +0.27V, \alpha = -11.5^\circ$. $3 \rightarrow 4$ transition. State 3 is the dark state.
- (v) $V_a = +0.5V, \alpha = -11.5^\circ$. $4 \rightarrow 5$ transition. State 5 is the yellow state.
- (vi) $V_a = -0.2V, \alpha = +11.5^\circ$. $5 \rightarrow 4$ transition. State 4 is the yellow state.
- (vii) $V_a = -0.1V, \alpha = +11.5^\circ$. $6 \rightarrow 5$ transition. State 6 is the dark state.
- (viii) $V_a = +0.8V, \alpha = +11.5^\circ$. $7 \rightarrow 6$ transition. State 6 is the dark state.
- (ix) $V_a = +10.6V, \alpha = +21^\circ$. $8 \rightarrow 7$ transition. State 7 is the dark state.
- (x) $V_a = +20.9V, \alpha = 25^\circ$. State 8 in extinction.

The colors in (i) and (x) are due to the deliberate overexposure so the sample texture can be seen. See Color Plate XII.

between Fig. 2 (iv,v) and (vi,vii) shows the hysteresis of the switching process.

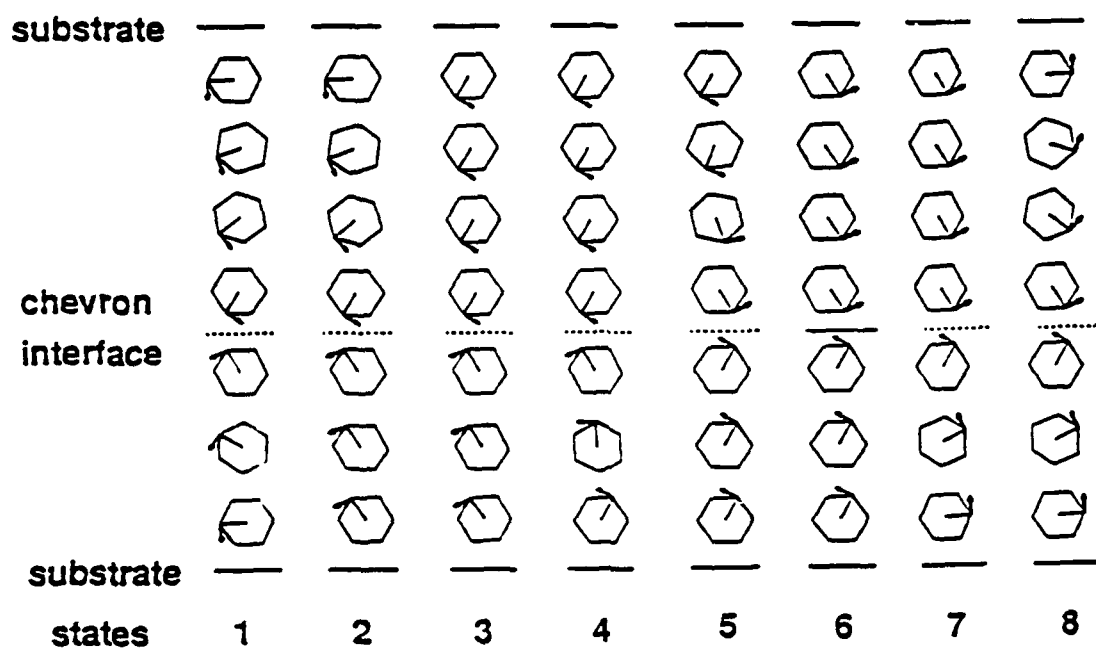
DISCUSSIONS

Based on above experimental observations we propose the following polarization **P**-director **n** configurations for the *SmI** states in SSFLC geometry, as depicted in Fig. 3 (a). The eight observed states are divide into two group of four, (1, 2, 3, 4) and (5, 6, 7, 8), separated by the chevron interface transition. Additionally those states within one group are separated by three similar surface transitions. Since the spontaneous polarization of 8SI is positive we presume here the polar surface interaction prefers the polarization **P** to point into the liquid crystal⁹. According to this configuration model states 1, 2, 3 (or 8, 7, 6) are uniform or relatively uniform DOWN (or UP) states which is consistent with the observed extinction for these states, while states 4 and 5 should be twist states which is why they never extinguish. The measured extinction angle difference between the two uniform states, state 3 and state 6, is $2\gamma = 23^\circ$, where γ is the apparent tilt angle for state 3 (or 6). Using the simple geometry shown in Fig. 3 (b), which assumes the layer tilt makes the director cone intersect the surface plane exactly at *SmI* hexagonal positions, we can get following relations between the half tilt cone angle θ , layer tilt angle δ , and γ :

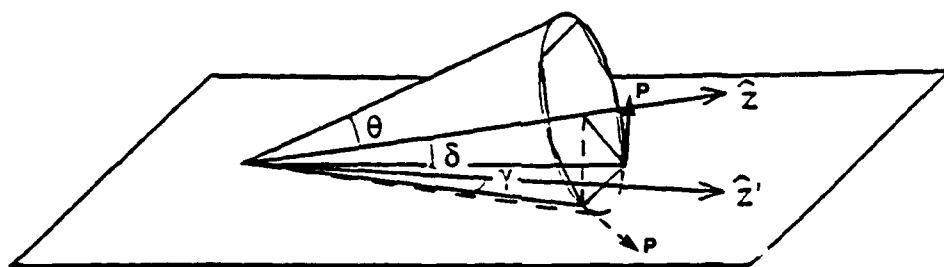
$$\sin\theta = 2\sin\gamma \quad (1)$$

$$\cos\delta = \frac{\cos\theta}{\cos\gamma} \quad (2)$$

With the observed value of γ , it is easy to find $\theta = 23^\circ$, and $\delta = 20^\circ$ using above relations. These θ and δ values are similar to those observed in other commonly used *SmA* \rightarrow *SmC** FLC materials. We can also approximately predict the extinction angle $2\gamma'$ difference between states 1 and 2. Simple calculation will give $2\gamma' = 2\tan^{-1}(\tan\theta\cos\delta) = 44^\circ$, which compares reasonably to the observed value of 47.5° . The fact that even at the highest field observed there is no evidence for any discontinuous (domain mediated) director orientation transition of the $2 \leftrightarrow 3$ or $6 \leftrightarrow 7$ type at the chevron interface indicates a strong director coupling at the chevron interface. Only the configurations giving the same **n** orientation on the opposite sides of and immediate adjacent to the chevron interface are energetically achievable. All these facts support our **P**-**n** configuration model and the proposed relation between the *SmI* hexagonal bond orientation and the surface boundary in



a



b

Figure 3: (a) Polarization *P*-director *n* configurations in *SmI** SSFLC cell. The hexagons in the figure denote the in-layer hexagonal order of the *SmI** phase. The arrows indicate the polarization field and the line segments inside the hexagons represent the projections of the director onto the layer plane. (b) Schematic view of the *SmI** tilt cone intersection with bounding plates

the SSFLC geometry which has the nearest neighbor molecular row (the (1,0) row) parallel to the glass substrates.

Finally we want to point out the phase transition phenomena observed in Fig. 1 (a) can be understood using the proposed **P-n** configurations. The two uniform states first appearing in SmI^* phase were states 3 and 6, judging by the difference between their extinction angle. Then part of these area relaxed to states 4 and 5, the two twist states respectively (see Fig. 1 (b)). The reason for this sequence is unknown. It could be related to the relative strength of the director elasticity and the polar surface interaction through the $SmC^* - SmI^*$ phase transition.

ACKNOWLEDGEMENTS

This work was supported by NSF Grant DMR 8901657, ARO contract DAAL03 - 86 - K - 0053 and NSF Engineering Research Center for Optoelectronic Computing Systems Grant CDR 8622236.

REFERENCES

1. N. A. Clark and S. T. Lagerwall, Appl. Phys. Lett. **36**, 899(1980).
2. J. W. Goodby, J. S. Patel, and T. M. Leslie, Ferroelectrics **59**, 121(1984).
3. Y. Ouchi, T. Uemura, H. Takezoe, and A. Fukuda, Jpn. J. Appl. Phys. **24**, 893(1985).
4. T. P. Rieker, N. A. Clark, G. S. Smith, D. S. Parmar, E. B. Sirota, and C. R. Safinya, Phys. Rev. Lett. **59**, 2658(1987).
5. N. A. Clark and T. P. Rieker, Phys. Rev. A **37**, 1053(1988).
6. J. E. MacLennan, N. A. Clark, M. A. Handschy, and M. R. Meadows, Liq. Cryst. **7**, 753(1990).
7. T. P. Rieker, N. A. Clark, G. S. Smith, and C. R. Safinya, Liq. Cryst. **6**, 565(1989).
8. Z. Zhuang, N. A. Clark, and J. E. MacLennan, Liq. Cryst. **10**, 409(1991).
9. J.-Z. Xue, N. A. Clark, and M. R. Meadows, Appl. Phys. Lett. **53**, 2397 (1988).

SECTION H

ANTIFERROELECTRICS

LANDAU-KHALATNIKOV DYNAMICS OF HELICOIDAL ANTIFERROELECTRIC LIQUID CRYSTALS

BOŠTJAN ŽEKŠ,^{a,b} ROBERT BLINC,^b and MOJCA ČEPIČ^b

^aInstitute of Biophysics, Medical Faculty, Lipičeva 2, 61105
Ljubljana, Yugoslavia

^bJ. Stefan Institute, Jamova 39, 61111 Ljubljana, Yugoslavia

Abstract A phenomenological model of helicoidal antiferroelectric liquid crystals is analysed and the relaxational eigenfrequencies of ferroelectric and antiferroelectric modes are evaluated in the smectic A phase, in the ferroelectric smectic C* phase and in the antiferroelectric phase. In the intermediate ferrielectric phase the eigenmodes are mixtures of ferroelectric and antiferroelectric fluctuations.

INTRODUCTION

In last few years a series of antiferroelectric liquid crystals has been discovered¹⁻⁷. This new antiferroelectric phase of chiral smectic C liquid crystals, usually denoted as SmC_A^* , has a structure, where the molecules in the neighbouring layers are tilted from the normal to smectic layers in almost opposite directions. Two types of phase sequences including the antiferroelectric phase have been reported so far. One is smectic A (SmA) - ferroelectric chiral smectic C* (SmC^*) - SmC_A^* , observed in MHPOBC¹, and the other is SmA - SmC_A^* (observed in pure TFMHPOBC⁵). For a mixture of R- and S-enantiomers of TFMHPOBC the phase sequence changes into the former type. For an optically pure MHPOBC⁴, there exist two additional intermediate phases between SmA and SmC^* and between SmC^* and SmC_A^* , respectively. The last one seems to be a ferrielectric phase.

Recently, a phenomenological theory of the antiferroelectric phase transition has been introduced⁸. The model, which implicitly assumes the existence of long range forces between smectic layers, consists of a Landau expansion in ferroelectric and antiferroelectric order parameters. The first one represents a homogeneous tilt of molecules from the normal to smectic layers and the second one corresponds to the Brillouin zone-boundary tilt mode. Because of the chirality of the system, the expansion includes the Lifshitz invariants with respect to the antiferroelectric as well as ferroelectric order

parameters and also bilinear couplings between the two tilt order parameters and the ferroelectric and antiferroelectric polarizations.

In the equilibrium analysis of the model⁸ the terms related to the modulations of the two order parameters were neglected for simplicity, because the pitch of the helical structures is much larger than the layer spacing and the helicity of the system can be expected to be not important for the antiferroelectric phase transition.

In this contribution, we shall take into account also the effects of the chirality and analyse the dynamic properties of the Orihara - Ishibashi model⁸ in the Landau - Khalatnikov approximation.

THE MODEL AND THE ORDER PARAMETER FLUCTUATIONS IN THE SMECTIC PHASE

The tilt of molecules in the i -th smectic layer can be described by a two-component tilt vector

$$\vec{\xi}_i = (n_{ix} \ n_{iz}, n_{iy} \ n_{iz}) , \quad (1)$$

where $\vec{n}_i = (n_{ix}, n_{iy}, n_{iz})$ is the director of the i -th layer and the z -axis is normal to the layers. The ferroelectric tilt order parameter $\vec{\xi}_f$ can be defined as the Brillouin zone-center component of $\vec{\xi}_i$ and corresponds to a homogeneous tilt of molecules, while the antiferroelectric order parameters $\vec{\xi}_a$, which is equal to the Brillouin zone-boundary component of $\vec{\xi}_i$, corresponds to the antiferroelectric order. The Landau free energy density expansion in $\vec{\xi}_f$ and $\vec{\xi}_a$ can be expressed as

$$\begin{aligned} g(z) = & \frac{1}{2} \alpha_f |\vec{\xi}_f|^2 + \frac{1}{4} \beta_f |\vec{\xi}_f|^4 + \delta_f \left(\xi_{fx} \frac{\partial \xi_{fy}}{\partial z} - \xi_{fy} \frac{\partial \xi_{fx}}{\partial z} \right) + \frac{1}{2} \kappa_f \left[\left(\frac{\partial \xi_{fx}}{\partial z} \right)^2 + \left(\frac{\partial \xi_{fy}}{\partial z} \right)^2 \right] + \\ & + \frac{1}{2} \alpha_a |\vec{\xi}_a|^2 + \frac{1}{4} \beta_a |\vec{\xi}_a|^4 + \delta_a \left(\xi_{ax} \frac{\partial \xi_{ay}}{\partial z} - \xi_{ay} \frac{\partial \xi_{ax}}{\partial z} \right) + \frac{1}{2} \kappa_a \left[\left(\frac{\partial \xi_{ax}}{\partial z} \right)^2 + \left(\frac{\partial \xi_{ay}}{\partial z} \right)^2 \right] + \\ & + \frac{1}{2} \gamma_1 |\vec{\xi}_a|^2 |\vec{\xi}_f|^2 + \frac{1}{2} \gamma_2 (\vec{\xi}_a \cdot \vec{\xi}_f)^2 . \end{aligned} \quad (2)$$

Here the α and β terms represent the expansion up to the fourth order in the magnitude of the $\vec{\xi}_f$ and $\vec{\xi}_a$, respectively. The δ terms are Lifshitz terms, which appear in the expansion because of the chirality of the molecules, and the κ terms represent the elastic energy. The γ terms describe the coupling between

the two order parameters. The above free energy can be obtained from the one introduced by Orihara and Ishibashi⁸ after the elimination of the ferroelectric and antiferroelectric polarization. We should also point out that the vector $\vec{\xi}$ (Eq.1) is defined in a standard way⁹ and is perpendicular to the one in Ref.(8).

In the above free energy only the coefficients α_f and α_a are assumed to be temperature dependent

$$\alpha_f = a(T - T_{f,o}) , \quad (3a)$$

$$\alpha_a = a(T - T_{a,o}) . \quad (3b)$$

Here it is assumed that the entropy contribution to α , i.e. the part proportional to T , is the same for ferroelectric and for antiferroelectric ordering, while the energies of the two states are different giving rise to different transition temperatures $T_{f,o} \neq T_{a,o}$ to homogeneously ordered ferroelectric and antiferroelectric states, respectively.

In the SmA phase the tilt is equal to zero, i.e. $\vec{\xi}_f = \vec{\xi}_a = 0$. We are interested only in small deviations from the equilibrium state and we therefore consider only quadratic terms in $\vec{\xi}_f$ and $\vec{\xi}_a$ in the free energy density (Eq.2). The fluctuations can be expressed as a linear combination of helicoidal fluctuations with wave-vectors q

$$\xi_{f,x} = \sum_q (a_{f,q} \cos qz - b_{f,q} \sin qz) , \quad (4a)$$

$$\xi_{f,y} = \sum_q (a_{f,q} \sin qz + b_{f,q} \cos qz) , \quad (4b)$$

$$\xi_{a,x} = \sum_q (a_{a,q} \cos qz - b_{a,q} \sin qz) , \quad (4c)$$

$$\xi_{a,y} = \sum_q (a_{a,q} \sin qz + b_{a,q} \cos qz) , \quad (4d)$$

and the harmonic part of the free energy density (g_2) can be expressed as

$$g_2 = \sum_q \frac{1}{2} (\alpha_f + 2\delta_f q + \kappa_f q^2) (a_{f,q}^2 + b_{f,q}^2) + \sum_q \frac{1}{2} (\alpha_a + 2\delta_a q + \kappa_a q^2) (a_{a,q}^2 + b_{a,q}^2). \quad (5)$$

One can see from this expression that the helicoidal ferroelectric and antiferroelectric fluctuations are not coupled in the SmA phase and that both types of fluctuations are doubly degenerate. The equations of motion for the tilt can be expressed as

$$\begin{aligned} \dot{a}_{f,q} &= -\Gamma \frac{\partial g_2}{\partial a_{f,q}}, & \dot{b}_{f,q} &= -\Gamma \frac{\partial g_2}{\partial b_{f,q}}, \\ \dot{a}_{a,q} &= -\Gamma \frac{\partial g_2}{\partial a_{a,q}}, & \dot{b}_{a,q} &= -\Gamma \frac{\partial g_2}{\partial b_{a,q}}. \end{aligned} \quad (6)$$

Here the kinetic coefficients Γ for ferroelectric and antiferroelectric fluctuations are assumed to be equal, representing the inverse viscosity for the molecular tilt motion.

From Eqs.(5) and (6) one can easily obtain two double degenerate wave vector dependent relaxation frequencies, i.e. inverse relaxation times, for ferroelectric and for antiferroelectric fluctuations

$$\frac{1}{\tau_{f,q}} = \Gamma (\alpha_f + 2\delta_f q + \kappa_f q^2), \quad (7a)$$

$$\frac{1}{\tau_{a,q}} = \Gamma (\alpha_a + 2\delta_a q + \kappa_a q^2). \quad (7b)$$

Both dispersion relations are quadratic in q and have minimal values for the relaxation frequencies at $q = q_f = -\delta_f/\kappa_f$ for the ferroelectric case and at $q = q_a = -\delta_a/\kappa_a$ for the antiferroelectric case. The temperature dependence of the minimal value of the relaxation frequencies can be expressed as

$$\frac{1}{\tau_f} = \frac{1}{\tau_{f,q=q_f}} = \Gamma a (T - T_f), \quad (8a)$$

$$\frac{1}{\tau_a} = \frac{1}{\tau_{a,q=q_a}} = \Gamma a (T - T_a), \quad (8b)$$

where $T_f = T_{f,o} + \delta_f/a\kappa_f^2$ and $T_a = T_{a,o} + \delta_a/a\kappa_a^2$. In the SmA phase all eigenfrequencies are positive. The SmA phase becomes unstable at a temperature

where the first eigen-frequency becomes equal to zero. Here we shall treat explicitly only the case $T_a > T_f$, where the relaxation frequency of antiferroelectric fluctuations (Eq.8b) goes to zero at T_a while the ferroelectric relaxation frequency remains positive. The SmA phase becomes unstable with respect to antiferroelectric fluctuations and the system transforms via a second order phase transition into the helicoidal antiferroelectric phase with the wave-vector q_a (Figs. 1 and 2).

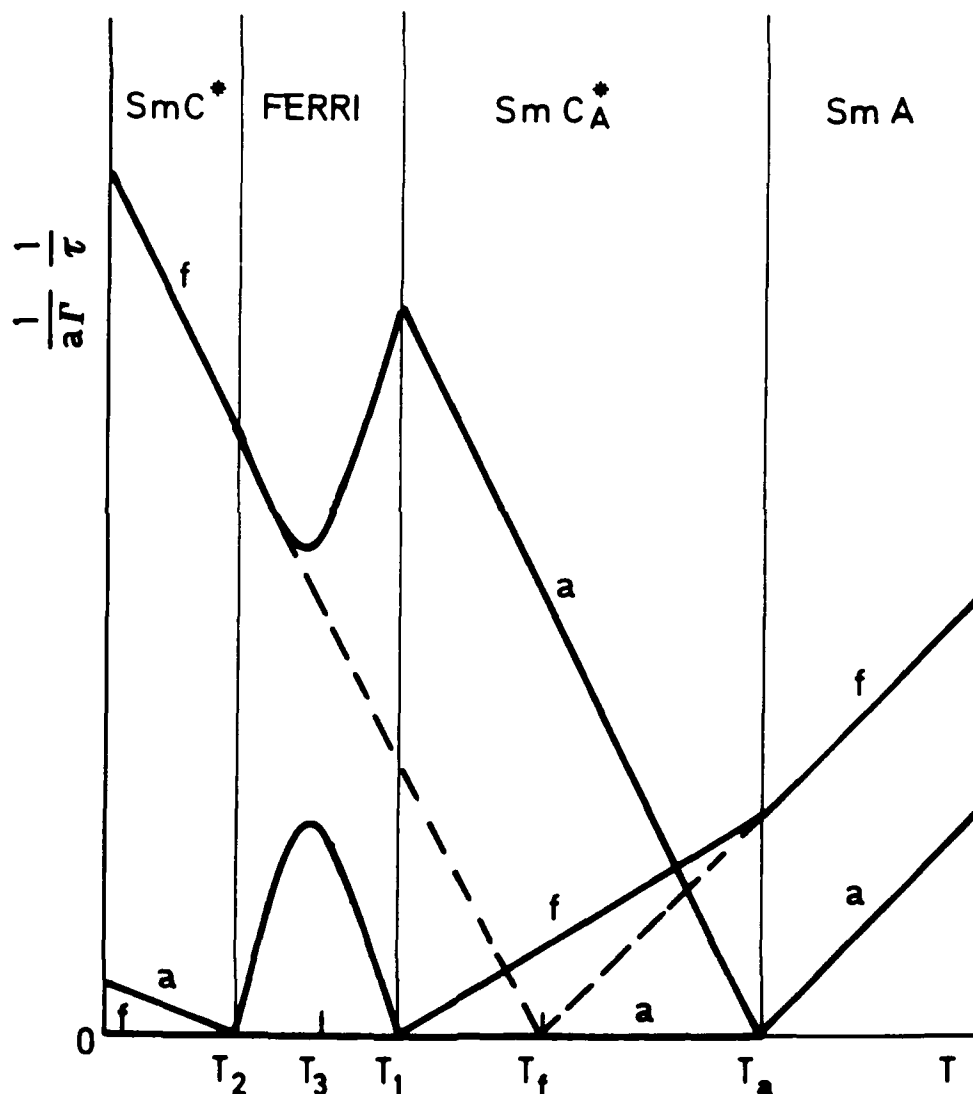


FIGURE 1 Relaxational frequencies of antiferroelectric and ferroelectric modes for $q = q_a$ and $q = q_f$, respectively, as functions of temperature for $\beta_a/\beta_f = 4$, $\sqrt{\beta_a\beta_f}/\gamma_1 = 1.2$ and $\gamma_2 = 0$.

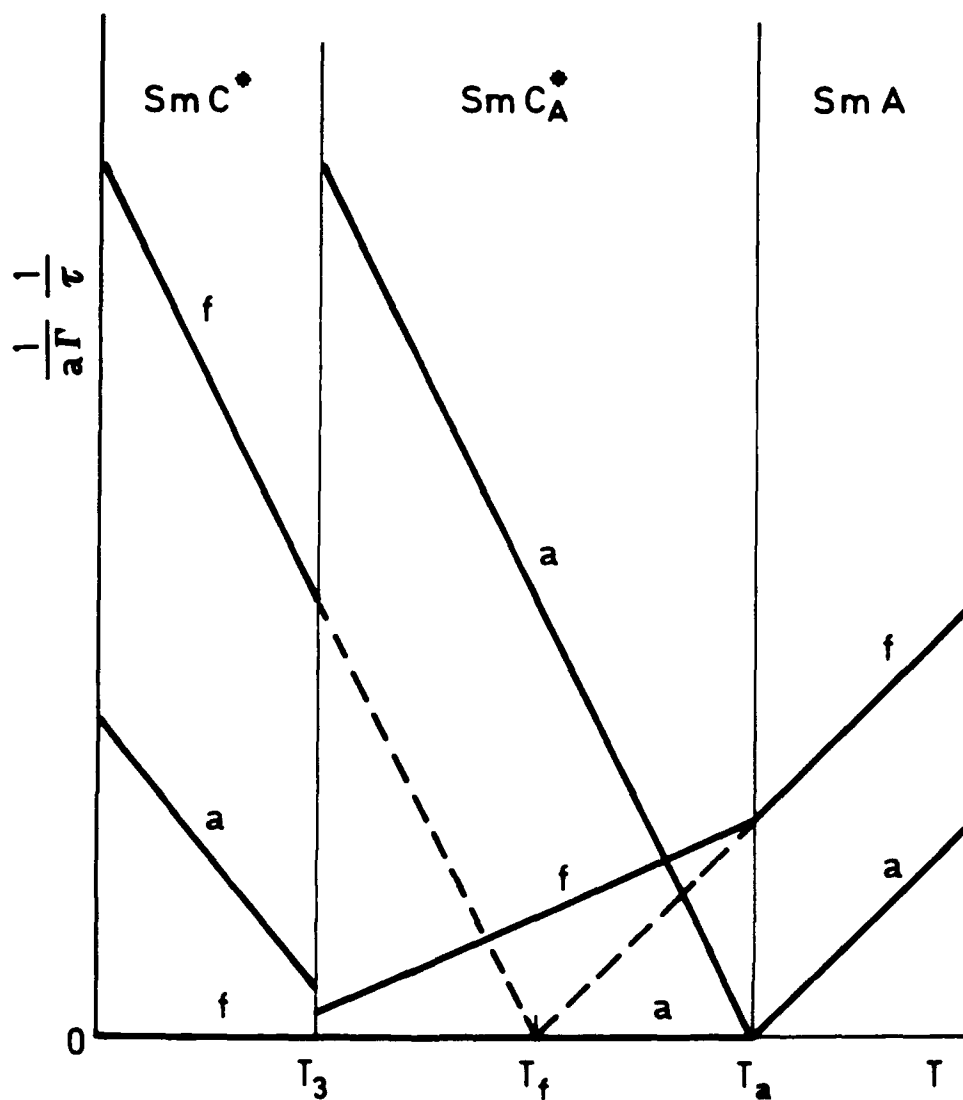


FIGURE 2 Relaxational frequencies of antiferroelectric and ferroelectric modes for $q = q_a$ and $q = q_f$, respectively, as functions of temperature for $\beta_a/\beta_f = 4$, $\sqrt{\beta_a\beta_f}/\gamma_1 = 0.9$ and $\gamma_2 = 0$.

ANTIFERROELECTRIC SmC_A^* PHASE

In the antiferroelectric phase $\tilde{\xi}_f = 0$ and

$$\xi_{ax} = \vartheta_a \cos q_a z, \quad (9a)$$

$$\xi_{ay} = \vartheta_a \sin q_a z, \quad (9b)$$

with

$$\vartheta_a^2 = \frac{a}{\beta_a} (T_a - T). \quad (10)$$

The ferroelectric and the antiferroelectric fluctuations remain decoupled. The critical, antiferroelectric fluctuations, which were degenerate above T_a , split into an amplitude part (soft mode) with the increasing relaxational frequency with decreasing temperature, and a phason part (Goldstone mode) with the relaxational frequency which is for $q = q_a$ identically equal to zero (Figs.1 and 2). The noncritical ferroelectric mode also splits into the amplitude and the phase part, but remains for $\gamma_2 = 0$ degenerate (Figs.1 and 2).

FERRIELECTRIC PHASE

When the ferroelectric relaxation frequency becomes zero in the antiferroelectric phase at $T = T_1$ (Fig.1), the SmC_A^* phase becomes unstable with respect to ferroelectric fluctuations and there is a transition to a phase where both order parameters are different from zero. This phase is composed, at least close to T_1 , of two helices: the antiferroelectric one with the wave-vector q_a and the ferroelectric one with the wave-vector q_f . In general this two wave-vectors are not commensurate and the two helices can freely slide one with respect to the other. Therefore, two Goldstone modes are expected in this phase. For $\gamma_2 \neq 0$, at lower temperatures the sinusoidal behaviour changes into soliton-like lattice and finally transforms into a commensurate phase, where $\bar{\xi}_f$ and $\bar{\xi}_a$ get a constant phase difference and form a periodic structure. In this phase only one Goldstone mode exists. If the lock-in term in the free energy (γ_2) is strong enough, the antiferroelectric phase can transform into the commensurate ferrielectric phase directly by a first order transition above T_1 .

In Fig.1 the case for $\gamma_2 = 0$ is shown. The ferrielectric phase is incommensurate and two Goldstone modes exists. The two amplitude modes have mixed ferroelectric and antiferroelectric character and only one of them is critical.

FERROELECTRIC PHASE

In general, a ferroelectric phase can exist at low temperatures with $\bar{\xi}_a = 0$ and

$$\xi_{fx} = \vartheta_f \cos q_f z, \quad (11a)$$

$$\xi_{fy} = \vartheta_f \sin q_f z, \quad (11b)$$

with

$$\vartheta_f^2 = \frac{a}{\beta_f} (T_f - T). \quad (12)$$

In this phase in analogy to the antiferroelectric phase the ferroelectric fluctuations are split into a phason part (Goldstone mode) and an amplitude part, while the antiferroelectric mode remains degenerate for $\gamma_2 = 0$ (Figs.1 and 2). This low temperature ferroelectric phase becomes unstable with respect to antiferroelectric fluctuations at $T = T_2$, where the antiferroelectric relaxation frequency goes to zero, and transforms above T_2 into a sinusoidally modulated ferroelectric phase.

If $T_2 > T_1$ (Fig.2) a stable ferroelectric phase does not exist and there is a first order transition between SmC^* and SmC_A^* phases at $T = T_3$, where the free energy of the two phases are equal.

In Figs. 1 and 2 the relaxation frequencies are shown for the two scenarios. The other two possibilities can be obtained by exchanging a and f , SmC_A^* and SmC^* , and T_1 and T_2 .

REFERENCES

1. A. D. L. Chandani, T. Hagiwara, Y. Suzuki, Y. Ouchi, H. Takezoe, and A. Fukuda, Jpn. J. Appl. Phys., **27**, L729 (1988).
2. A. D. L. Chandani, Y. Ouchi, H. Takezoe, A. Fukuda, K. Terashima, K. Fukuwara, and A. Kishi, Jpn. J. Appl. Phys., **28**, L1261 (1989).
3. A. D. L. Chandani, E. Gorecka, Y. Ouchi, H. Takezoe, and A. Fukuda, Jpn. J. Appl. Phys., **28**, L1265 (1989).
4. M. Fukui, H. Orihara, Y. Yamada, N. Yamamoto, and Y. Ishibashi, Jpn. J. Appl. Phys., **28**, L849 (1989).
5. Y. Suzuki, T. Hagiwara, I. Kawamura, N. Okamura, T. Kitazume, M. Kakimoto, Y. Imai, Y. Ouchi, H. Takezoe, and A. Fukuda, Liq. Cryst., **5**, 167 (1989).
6. Y. Yamada, K. Mori, N. Yamamoto, H. Hayashi, K. Nakamura, M. Yamawaki, H. Orihara, and Y. Ishibashi, Jpn. J. Appl. Phys., **28**, L1606 (1989).
7. H. Orihara, T. Fujikawa, Y. Ishibashi, Y. Yamada, N. Yamamoto, K. Mori, K. Nakamura, Y. Suzuki, T. Hagiwara, and I. Kawamura, Jpn. J. Appl. Phys., **29**, L333 (1990).
8. H. Orihara and Y. Ishibashi, Jpn. J. Appl. Phys., **29**, L115 (1990).
9. S. A. Pikin and V. L. Indenbom, Sov. Phys. Usp., **21**, 487 (1987).

SECTION I

OPTICS

NONLINEAR OPTIC PROPERTIES OF HETEROCYCLIC COMPOUNDS HYPERPOLARIZABILITY-STRUCTURE CORRELATION

GIRIJA SUBRAMANIAM*, SUSAN POLASHENSKI, KARI KENNEDY
Department of Chemistry, Penn State University,
Hazleton, Pennsylvania 18201-1291

Abstract In an attempt towards understanding the relation between molecular structure-nonlinear optic activity (NLO) among heterocycles, with special reference to the identity, number and position of the heteroatom, semiempirical calculations were carried out on a number of nitrogen heterocycles and their thia and carbon analogs using MNDO, AM1 and PM3 approaches. The results indicate that given the same number and type of atoms and double bonds in a molecule, linear conjugation excels over cyclic or crossed conjugation in enhancing hyperpolarizabilities and it seems to be far more critical than a chiral center. The data also show that adjacent nitrogens tend to lower second and third order polarizabilities considerably. All the three methods predicted the same correct trends.

INTRODUCTION

There is a great demand for high bandwidth optical switching and processing devices as well as materials capable of processing information and storing data.¹⁻⁴ Nonlinear optic (NLO) materials have these desired properties.

Qualitatively, nonlinear optics deals with that behavior of electromagnetic field in which the properties (e.g. phase change, frequency change, amplitude change) of the incident and the output beam cannot be related by simple proportionality. Quantitatively, NLO is mainly concerned with the response of a dielectric material to a strong electronic field. This response arises due to the polarization(P) of the molecule in an intense electric field(E) and can be expressed as a power series term (Equations. 1 and 2).⁵

$$P = \alpha E + \beta E^2 + \gamma E^3 + \dots \quad (\text{Eq. 1})$$

or macroscopically,

$$P = \chi^1 E + \chi^2 E + \chi^3 E + \dots \quad (\text{Eq. 2})$$

where

α, χ^1 = First order/linear polarizability

β, χ^2 = Second order/nonlinear polarizability

γ, χ^3 = Third order/nonlinear polarizability

The tensorial character of χ^2 makes it vanish automatically ($\chi^2 = 0$) in a centrosymmetric medium. This imposes restriction that the design of NLO material should be such that it allows the molecule to reside in a non-centrosymmetric environment.

It would be helpful to aim at potential target molecules, if one has an idea of their hyperpolarizability. This is where computational calculations come in handy, at least, to predict the trends in a chosen set of target molecules. This paper describes semiempirical calculations of hyperpolarizability using MOPAC-5 package. Most of the compounds studied were heterocycles or carbocycles with heteroatom side chains. A total of 20 (1-20) compounds were chosen for calculation to study the influence of structural variation on hyperpolarizabilities. Growing interest in exploiting the spontaneous polarization of ferroelectric liquid crystal to enhance nonlinear polarizabilities prompted us to study specifically the effect of chiral center on these chosen sets. Calculations were done using the three widely used semiempirical methods, MNDO, AM1 and PM3 to see their relative merits in predicting polarizabilities.

Effect of Linear vs Cyclic ConjugationResults

The two sets of molecules used in this study were pyrazole analogs 1-8 (Figure 1) and pyrrole analogs 9-16 (Figure 2). The influence of linear vs cyclic conjugation is clearly brought out from the study of compounds 1-4 and 9-12. The calculated β values are shown in Table I and Table II and the γ values in Table III and Table IV respectively.

Discussion

Careful study of the calculated β and γ values of both the series shows that the more linear the conjugation in a molecule is the larger is its nonlinear polarizability. For the same number of double bonds, atoms and for the same functional groups, a five fold increase is evident in compounds 4 and 12 relative to 1 and 9. Comparison between the two series comprising 1-4 and 9-12 reveals the deleterious effect of the second nitrogen on these values. Clearly, 9-12 are far better NLO materials than compounds 1-4, having adjacent nitrogen functions.

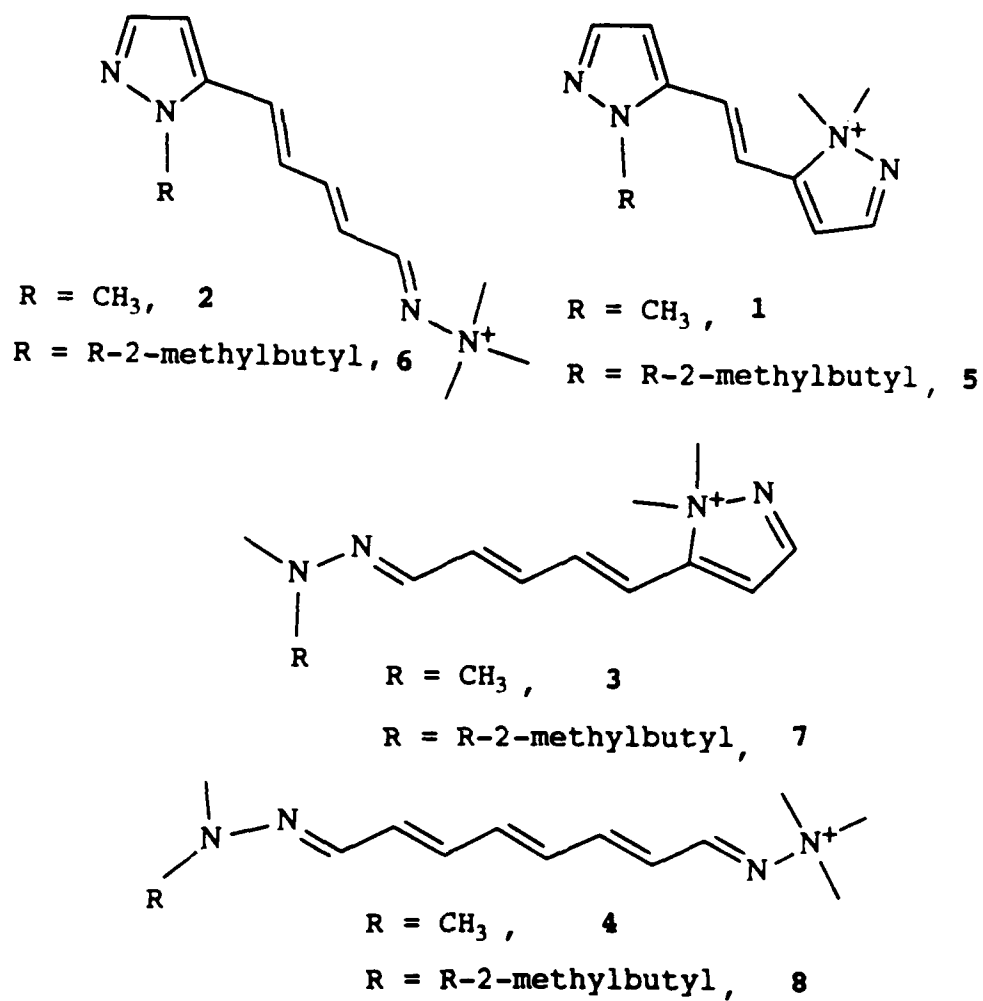
TABLE I Beta ($\times 10^{-30}$ esu)

Compound	MNDO	AM1	PM3
1	-34.02	-38.32	-55.10
2	-89.31	-89.31	-103.2
3	-163.8	-200.5	-216.1
4	-189.2	-235.2	-235.1

TABLE II Gamma ($\times 10^{-34}$ esu)

Compound	MNDO	AM1	PM3
1	1.212	0.940	1.146
2	2.802	2.585	2.602
3	6.431	6.190	7.330
4	8.418	10.23	9.891

FIGURE 1 Pyrazole analogs

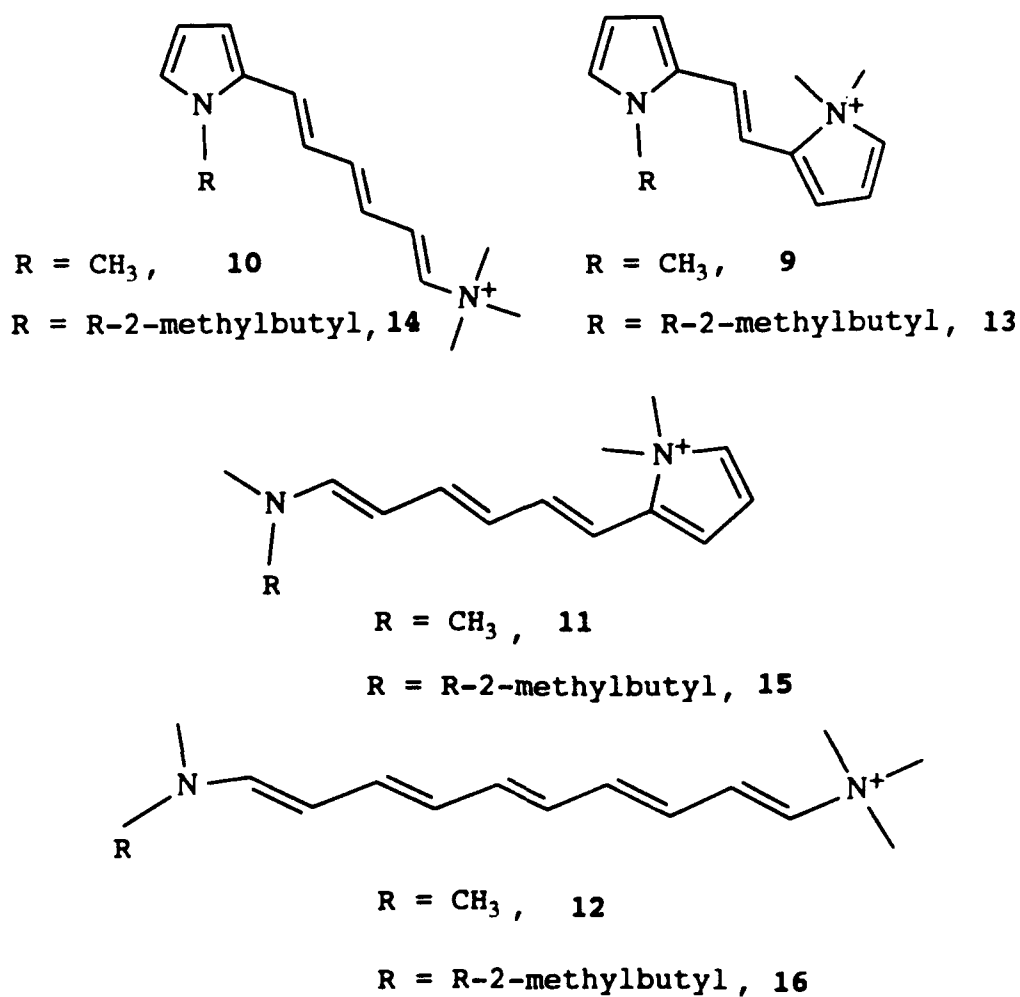
TABLE III Beta ($\times 10^{-30}$ esu)

Compound	MNDO	AM1	PM3
9	-48.68	-61.60	-59.41
10	-132.8	-126.9	-119.5
11	-221.1	-229.2	-242.7
12	-203.4	-331.8	-294.2

TABLE IV Gamma (X 10⁻³⁴ esu)

Compound	MNDO	AM1	PM3
9	1.672	1.500	1.392
10	4.514	3.652	3.043
11	7.881	5.400	7.439
12	9.909	13.66	12.81

FIGURE 2 Pyrrole analogs



Another interesting observation from this study is the importance of availability of electron density on the donor atom. As the lone pair of nitrogen locked in cyclic delocalization (in 2 and 10) is released and is fully available on the donor nitrogen as in 3 and 11, a doubling of β and γ values are noticeable.

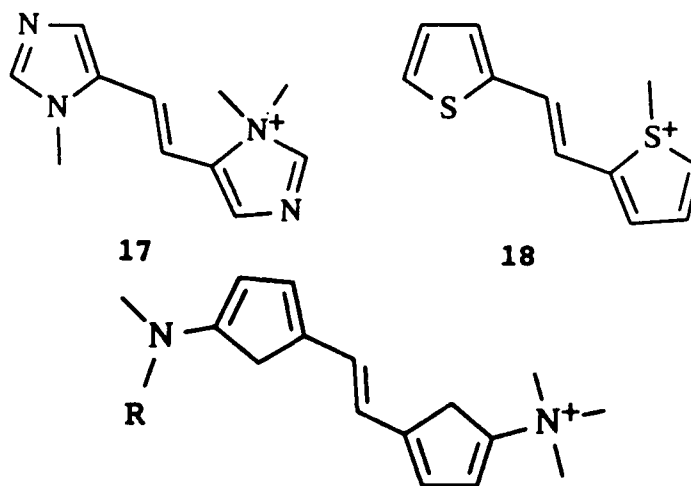
Effect of Position, Number and Nature of Hetero Atoms

Results

Since adjacent nitrogens seem to be undesirable for enhanced hyperpolarizabilities, calculations were done by changing the positions to 1,3 as in 17, the imidazole analog of 1. Calculations were also done on 18 and 19, the thia and carbon analog of 9 to study the influence of the presence of other atoms in the ring. Table V lists the calculated values of β and Table VI those of γ for 17-19.

Structures of these analogs were shown in Figure 3.

FIGURE 3 Imidazole, thia, carbon analogs



$R = \text{CH}_3$, 19

$R = \text{R-2-methylbutyl}$, 20

Discussion

Position of nitrogens within the ring matter little as far as both second and third order values are concerned. Comparison of 9 and 18 shows that changing -N to -S did not affect these values, a great deal. However, making these nitrogens as side chains as in 19 dramatically boost up both β and γ values, once again emphasizing the importance of complete availability of lone pair on the donor atom. These data point out at least one rule for the design of an efficient NLO material: The donor atom should not be involved in cyclic delocalization, if it is a part of the ring.

TABLE V Beta ($\times 10^{-30}$ esu)

Compound	MNDO	AM1	PM3
17	-17.01	-30.13	-33.29
18	-35.72	-55.32	-
19	-96.98	-209.2	-180.4

TABLE VI Gamma ($\times 10^{-34}$ esu)

Compound	MNDO	AM1	PM3
17	0.355	0.780	0.908
18	1.046	1.690	-
19	2.126	6.653	6.783

Effect of Chiral CenterResults

A very high β value does not assure always a large bulk second order polarizability (χ^2). Presence of a chiral center in a molecule assures a noncentrosymmetric alignment macroscopically and generally expected to lead to a large χ^2 . To investigate whether the chiral center enhances β on

the chiral center enhances β on the molecular level, calculations were done on compounds 5-8, 13-16, and 20 (Figures 1, 2 and 3). All these molecules have the chiral (R)-2-methylbutyl chain on the donor nitrogens. Results from these calculations are shown in Table VII and Table VIII.

Discussion

Both β and γ values are notably increased only in compounds with complete linear conjugation. The values are unaffected practically for compounds with cyclic delocalization e.g. 1 vs 5 and 9 vs 13. When one compares the series 1-4 with 5-8 and 9-12 with 13-16, one sees that the effect of chiral center is not remarkable in enhancing nonlinear polarizabilities.

TABLE VII Beta ($\times 10^{-30}$ esu)

Compound	MNDO	AM1	PM3
5	-39.41	-45.58	-54.66
6	-90.28	-92.75	-106.8
7	-194.0	-229.7	-255.2
8	-225.5	-327.6	-312.8
13	-70.62	-70.17	-66.12
14	-133.6	-125.3	-120.5
15	-243.5	-251.8	-269.8
16	-322.3	-393.1	-341.6
20	-218.3	-231.2	-202.3

These data suggest that at the molecular level linear conjugation plays a far more important role than chiral center even though latter is a definite boon at the macroscopic level.

TABLE VIII Gamma ($\times 10^{-34}$ esu)

Compound	MNDO	AM1	PM3
5	1.255	1.172	1.451
6	2.271	1.774	1.698
7	8.449	5.844	6.556
8	2.846	2.662	2.667
13	7.885	7.342	7.802
14	10.51	14.46	13.34
15	4.652	3.772	3.042
16	8.944	5.747	6.593
20	15.85	15.83	14.71

Conclusions

To test the reliability of these semiempirical methods, calculations were carried out for compounds with experimentally determined β values. All the three methods underestimated the second order polarizabilities; but predicted the correct trends. Choice of the semiempirical methods depends on the type of system to be investigated. Our earlier calculations⁷ showed that for 1,2-diaza compounds MNDO and PM3 are far superior than AM1. Having chosen the right method, one can use these calculations to predict the trends in a given set of molecules to facilitate better design of a superior NLO material. The number of compounds used in this study may not be very significant statistically; nevertheless it did reveal the following interesting clues to the design of future NLO materials:

Linear delocalization is anytime better than a closed one.

Locking the electrons of donor group in cyclic delocalization is deleterious to nonlinear

polarizabilities.

Addition of chiral centers is not a great advantage at the molecular level, even though they are a must to assure non-centrosymmetric environment to lead to large χ .

REFERENCES

1. D. R. Ulrich, Mol. Cryst. Liq. Cryst., 160, 1 (1988).
2. R. Burzynski, B. P. Singh, P. N. Prasad, R. Zanoni and G. I. Stegeman, Appl. Phys. Lett., 53, 2011 (1988).
3. K. b. Rochford, R. Zanoni, Q. Gong and G. I. Stegeman, Appl. Phys. Lett., 55, 1161 (1990).
4. P. D. Townsend, G. L. Baker, N. E. Scholetter, C. F. Klausner and S. Etemad, Appl. Phys. Lett., 53, 1782 (1988).
5. D. J. Williams, Angew. Chem. Int. Ed. Engl. 23, 690 (1984).
6. A. Ulman, J. Phys. Chem., 92, 2385 (1988).
7. Submitted to J. Computational Chem.

SECTION J

INTERFACES

FERROELECTRIC LIQUID CRYSTAL ALIGNMENT BY OBLIQUE EVAPORATION OF SiO₂

DAVID ARMITAGE

Research and Development Division, Lockheed Missiles & Space Company Inc.
3251, Hanover St., Palo Alto, CA94304, USA.

Abstract A study of the alignment of a ferroelectric liquid crystal (FLC) on various obliquely deposited silicon oxide substrates is presented. The FLC is further aligned by an electric field $>10 \text{ V}/\mu\text{m}$ at 10 Hz. Improved bistability and full cone-angle switching are achieved for 10 nm small angle depositions set at a glancing angle of 5° to the substrate. Thicker depositions $\geq 30 \text{ nm}$ inhibit full cone-angle switching. Flow effects consistent with piezoelectric flow are observed at high electric fields and kHz frequencies.

INTRODUCTION

Obliquely deposited silicon dioxide, known as the Janning method, has been used for many years to provide liquid-crystal alignment. The alignment mechanism can be explained in terms of the surface topology of the obliquely deposited film.¹ If sufficient material is deposited the surface structure is clearly visible in the SEM.²⁻⁴ Small angle deposition (SAD), at a glancing angle $<10^\circ$ to the substrate surface, gives columnar growth tilted in the direction of the source. Medium angle evaporation (MAD), where the deposition angle is increased to approximately 30° , gives a non-columnar structure which appears to be corrugated orthogonal to the source direction, similar to wind or water waves on sand. The surface structure is determined by nucleation, growth, and self shadowing effects.

Nematic liquid crystal (NLC) alignment on SAD follows the column direction when tangential boundary conditions apply, since the intercolumn elastic energy is minimized. Nematic tilt angles in the range 0° - 45° can be achieved according to the material and deposition conditions. Surfactant treatment of SAD to give perpendicular boundary conditions will generally result in the complimentary nematic tilt angle alignment. The surfactant behavior suggests an effective average surface tilt. NLC alignment with tangential boundary conditions on MAD is along the corrugation direction, which minimizes the elastic energy. Nematic MAD alignment is non-tilted and orthogonal to the SAD nematic alignment, for a common source direction. Reliable low-tilt alignment is achieved by sequential SAD/MAD, with 90° substrate rotation between depositions.

Uniform nematic alignment is generally achieved by MAD of approximately 10-nm thickness. The nematic tilt angle is sensitive to SAD thickness and saturates at <10-nm thickness.⁵ Controlled tilt directions close to 90° can be achieved by omni-azimuthal oblique evaporation of SiO, which is achieved by SAD on a rotating substrate.⁴

Oblique angle deposition is also an alignment method for ferroelectric liquid crystals (FLC).⁶⁻¹⁵ However, no detailed study of the influence of deposition conditions and materials has been reported. Rubbed polymeric alignment methods are expected to dominate large volume production, because of lower manufacturing cost as shown by the NLC display industry. For small production demonstration devices, or high quality optical processing devices, the higher cost of oblique evaporation alignment is acceptable. Moreover, rubbing techniques are difficult to apply in integrated silicon applications.¹⁶ Therefore, it is of more than academic interest to establish the alignment behavior of FLC on evaporated surfaces.

The alignment of FLC is generally achieved by SAD of silicon oxide in the range 30-200 nm, where the thickness is monitored at perpendicular incidence and not corrected for obliqueness.⁸⁻¹¹ Uniform alignment of NLC can be achieved by SAD of thickness <10 nm, although thicker layers are generally employed in production. The NLC precursor phase is essential in SAD alignment of FLC because the smectic phase does not directly align at an isotropic-smectic transition. The SAD controls the NLC alignment, which in turn determines the FLC alignment. However, details of the smectic structure are directly influenced by the alignment film.

The application of a high electric field to convert a FLC chevron structure to a pseudo-bookshelf arrangement has been demonstrated for various polymer alignments. Similar experiments on SAD alignments should prove interesting.¹⁴ We are particularly interested in finding a high quality alignment method which provides bistable full cone-angle director switching for *planar optic* devices.¹⁷ Planar optic devices operate under off-axis optical conditions and are therefore more demanding in director switching angle.

We present some preliminary results on oblique evaporated film alignment and electric field effects on FLC device structures.

FILM STRUCTURE AND ALIGNMENT

Oblique evaporated film structures are readily established by SEM observation for thicknesses >100 nm.²⁻⁴ The structure of thinner films is inferred from thick film observations. Silicon oxide can be thermally evaporated from SiO source or e-beam evaporated from SiO₂ source. The resultant deposition is silicon rich and is generally described as SiO_x. The structure is influenced by deposition rates and starting material.

E-beam deposition has the advantage of precise control of deposition rate, and our experiments use this method.

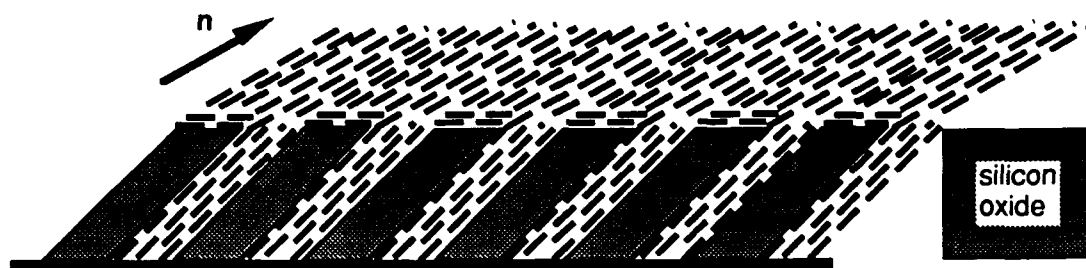


FIGURE 1. Structure of small angle deposited silicon oxide and nematic alignment.

The columnar structure produced by SAD is sketched in Figure 1., together with the nematic alignment and director n . The initial slope of the columns $\sim 30^\circ$, and increases to $\sim 50^\circ$ for e-beam SiO_2 .² The nematic alignment approximates the column direction where the details are determined by nematic-substrate interactions and elastic constants.

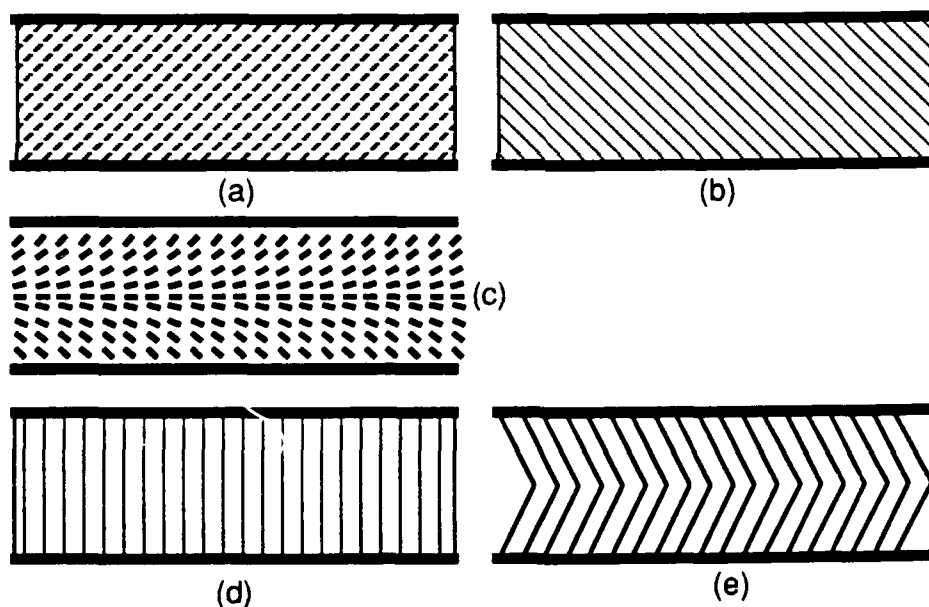


FIGURE 2. (a) Antiparallel SAD substrates and resultant nematic alignment. (b) Antiparallel SAD substrates and smectic layer alignment. (c) Parallel SAD substrates and nematic alignment. (d) Parallel SAD substrates and smectic-A layer alignment. (e) Parallel SAD substrates and FLC chevron layers.

A liquid crystal cell can be assembled from SAD substrates in parallel or antiparallel arrangements as shown in Figure 2., together with the liquid-crystal alignments.⁹⁻¹¹ The antiparallel cell is the standard NLC configuration, and the smectic layer format is

consistent with the NLC alignment with little or no discontinuity at the N-S_A transition.² The parallel cell gives a nematic distribution with bend and splay distortion. Close to the N-S_A phase transition the bend/splay elastic ratio increases and the splayed nematic state will be favored. The transition to an S_A bookshelf arrangement is plausible, but tilted or curved layers are also reported, as determined by surface interaction details and sample history.⁹⁻¹¹ Chevron structures essentially identical to polymeric planar alignment are reported for the S_C* phase aligned on SAD silicon oxide.¹⁰⁻¹²

The SAD surface is rough on a scale important to liquid crystal behavior, in comparison with a smooth glass or indium tin oxide surfaces. The smooth surface promotes the formation of a smectic phase, whereas the rough surface is expected to inhibit the smectic formation. The SAD surface may depress the N-S transition temperature significantly in the surface regions; therefore a slowly cooled sample could begin the phase transformation in the bulk material rather than the surface region.

CELL PREPARATION

The substrates are 25 mm square, cut from indium tin oxide (ITO) coated glass of thickness 3 mm (Donnelly), and cleaned in chromic acid. The evaporation conditions are: cryopumped e-beam evaporator (Temescal); starting material SiO₂ chips; deposition rate 0.3 nm/sec; source to substrate distance 70 cm; SAD angle 5°; MAD angle 30°. The cells are assembled with UV curing cement (Norland 61), filled with FLC at 120° C in a vacuum oven, and slow cooled by switching off the oven at atmospheric pressure.

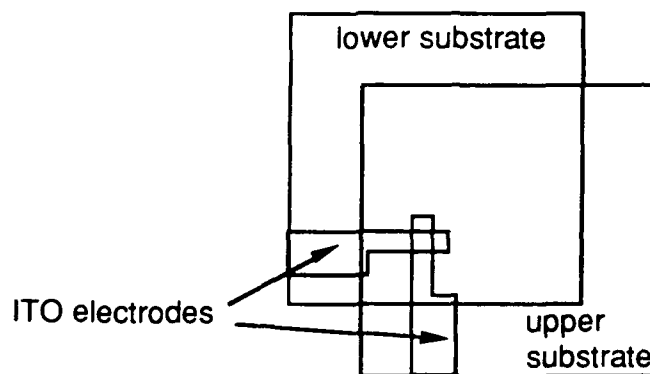


FIGURE 3. Electrode pattern of cell.

Some substrates have a simple crossed electrode pattern as shown in Figure 3. This facilitates a comparison between passive and electrically driven regions, and allows the cell thickness to be determined by capacitance measurements. The small active 1 mm² area of the crossed electrode cells favors high breakdown voltage. The thickness

distribution of non-patterned cells is inferred from white light interference colors in comparison with capacitance calibrated cells. The cell thicknesses are generally in the range 1-3 μm .

A well known FLC (Merck ZLI3654) with high polarity ($P_s=30 \text{ nC/cm}^2$) is employed in most of the experiments to provide direct comparison with published work. High P_s is important in electric field realignment experiments. Abrupt changes in the surface alignment conditions on a given substrate can be achieved by partial surface masking during the deposition.

SMALL ANGLE DEPOSITION

Cells prepared from SAD of SiO_2 in the range 1-100 nm (measured at perpendicular incidence by quartz crystal monitor), are examined for uniformity by polarizing microscopy. For parallel SAD alignment the zigzag defects are fewer for increasing deposition thickness, and the detailed texture changes in a characteristic way. The appearance in the vicinity of the electrode region is shown in Figure 4., where the cell is rotated between crossed polarizers to show the texture both on and off the electrode. The electrodes were driven by $\pm 40 \text{ V}$ at 10 hz to improve the alignment over the square overlap region, and then shorted. The electric field induced alignment has a characteristic striped texture. The original texture is preserved outside the electrode overlap region.

The 10 nm SAD provides uniform alignment as seen outside the electrode region in Figure 4a, where stripes are absent. Typically some regions of the sample are striped, and some regions clear. Increasing the SAD thickness to 30 nm provides alignment with stripes similar to the electroded region as shown in Figure 4b, and a submillimeter random domain pattern. Further increase of SAD to 100 nm gives a smaller domain structure as shown in Figure 4c, and the stripes are less obvious. In all cases, with cell rotation a given domain cannot be made extinct and appears grey-blue. Poor extinction indicates the lack of a unique optic axis, and is generally identified as a twisted state.

The ITO electrodes are fabricated by lithography under clean-room conditions. However, there are variations from sample to sample which may be due to surface contamination, and Figure 4 represents typical results. Examination of virgin cells shows no systematic variation in alignment on the ITO surface in comparison with the glass surface, or SiO_2 overcoated ITO.

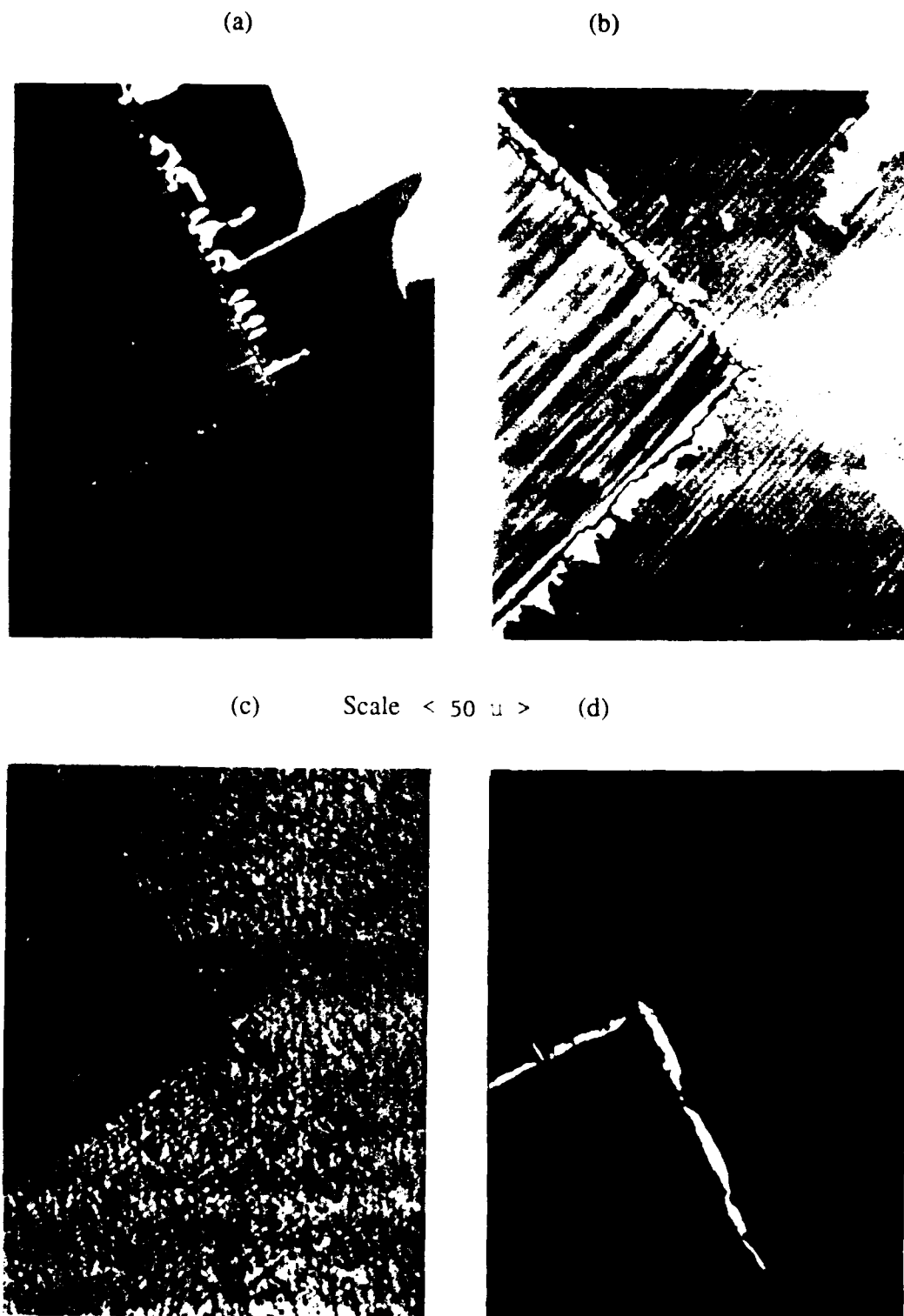


FIGURE 4. FLC texture within and around the electrode structure after electric field alignment. (a) SAD 10 nm (b) SAD 30 nm (c) SAD 100 nm (d) MAD/SAD 10/5 nm.

MIXED DEPOSITION

The thickness of SAD required to control liquid-crystal alignment uniformity results in high surface tilt conditions. The high tilt can be avoided without compromising alignment uniformity by mixed deposition, where a sequential SAD/MAD or vice versa is employed. The effectiveness of thermally evaporated silicon monoxide MAD/SAD in FLC alignment was recently reported, but details of the deposition conditions and thicknesses were omitted.¹³ We are guided by the early work on nematic alignment, where the surface tilt alignment is readily measured at room temperature. A MAD thickness of 10 nm is generally sufficient to provide uniform alignment. The tilt produced by the SAD is strongly dependent on the sequence MAD/SAD or SAD/MAD. In the former case the tilt angle increases rapidly and saturates at an SAD thickness of 3 nm, while in the latter case a slower rise with an SAD saturation of about 7 nm is found.⁵ For low-tilt nematic alignment the SAD/MAD sequence is employed because the lower sensitivity provides better control and uniformity.

We experimented with the SAD/MAD sequence at SAD thicknesses of 1, 2, 3, 4, and 10 nm and constant MAD thickness of 10 nm. The alignment is poor at SAD of 1-2 nm, giving a focal-conic fan texture with majority alignment in the SAD direction. An SAD of 3 nm gives the SSFLC appearance with many zigzag defects. Increasing the SAD thickness decreases the defect density.

The alternative sequence MAD/SAD was also studied with a constant MAD thickness of 10 nm, and SAD thicknesses of 2.5, 5, and 10 nm. The alignment is substantially improved relative to the SAD/MAD sequence. Figure 4d illustrates the alignment for a MAD/SAD sequence of 10-nm/5-nm. Striped-texture regions appear in all the samples and are more probable with thicker SAD.

In all the samples (except the focal-conic fan textures) the virgin state is a twisted state as described for the pure SAD alignment.

ELECTRIC FIELD ALIGNMENT

The applied electric field interacts with the large $P_s = 30 \text{ nC/cm}^2$ and the negative dielectric anisotropy ($\Delta\epsilon$) of the FLC. The relative $\Delta\epsilon \sim -2$ at frequencies above 1 kHz, but changes rapidly to values < -10 at lower frequency of order 100 Hz.¹⁸ The electrical response of the sample is sensitive to frequency, and we chose an initial test frequency of 10 Hz, in accordance with previous experiments on electric field treatment of polymer aligned FLC.¹⁹ The voltage is applied through a decoupling capacitor to eliminate any dc component, and the cell is terminated by a resistor when the voltage is switched off.

The applied voltage is gradually increased while changes in the texture are observed. The texture changes such as *roofed-shaped* and *striped-pattern* reported for polymer aligned samples are observed here at similar electric fields beyond $10\text{V}/\mu\text{m}$. A typical *roof-texture* is shown in the overlapping electrode region of Figure 5., and the final *striped-texture* appears in electrically active regions of Figure 4. In the striped-texture the cell can be rotated to give good extinction, apart from the stripe defects. The roof-texture is less pronounced in cells with thick SAD alignments $\geq 30\text{ nm}$.



FIGURE 5. FLC *roof-texture* for MAD/SAD 10/2.5 nm cell with 1x1-mm electrode addressed area.

The cell bistability and switching angle are sensitive to the SAD thickness. Reliable bistability and full cone-angle switching are generally achieved with SAD of 10 nm or less, including the MAD/SAD combinations. The thicker SAD alignment sometimes favors one of the bistable states, and the switching angle $\sim 40^\circ$ is significantly less than the 50° full cone-angle. Increasing the electric field treatment to $30\text{ V}/\mu\text{m}$ causes a deterioration in switching angle. The bistability is assessed by randomly switching off the ac drive voltage, while observing the cell in the polarizing microscope. The bistable optic axis directions are measured on a rotating microscope stage to a precision $\pm 1^\circ$. The driven switching angle is assessed by the same microscope methods, at low drive frequencies of order 1 hz, where close to the full cone-angle switching is observed for all samples.

Minor defects in the alignment of the thin oxide SAD or SAD/MAD cells are removed by the electric field alignment, but the thick oxide SAD cells preserve such defects. Moreover, in the thick oxide cells the defects and bistable switching angle cannot be improved by electric fields as high as $100 \text{ V}/\mu\text{m}$.

ELECTRIC FIELD EFFECTS

A variety of interesting patterns and textures can be seen in the SSFLC cell when subjected to high-voltages in the audio-frequency range. This electrohydrodynamic behavior is difficult to interpret, but has been discussed in terms of electric field alignment technique.²⁰ At frequencies of order 6 kHz the electric field effects extend well beyond the electrode boundary in a direction parallel to the smectic planes. A defect structure is created beyond the electrode, which remains in the field-off state as shown in Figure 6. The extent of the electric response is far beyond the direct influence of fringe fields.

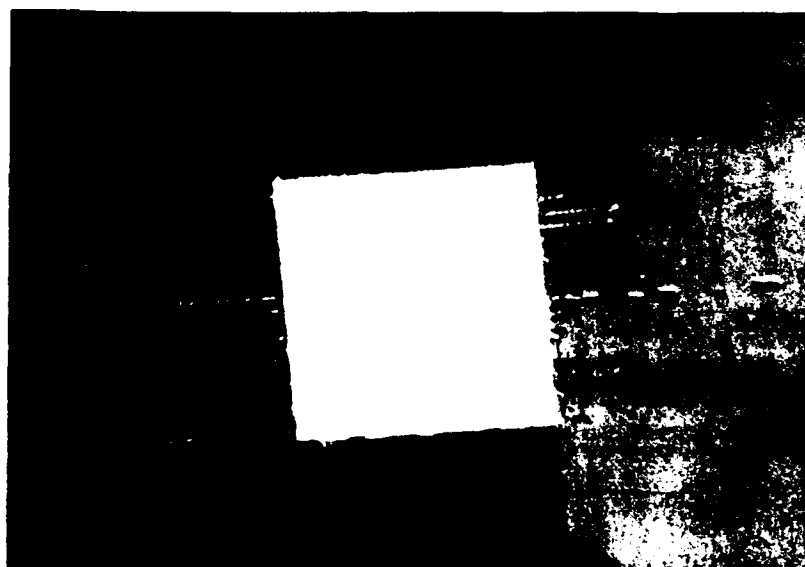


FIGURE 6. Electric field induced defects beyond 1x1-mm addressed region.

Thermal expansion in response to local heating might explain the behavior, where layer incompressibility would direct flow parallel to the smectic layers. However, the estimated temperature rise is low at $\sim 0.1^\circ \text{C}$. The heating is calculated from V^2/R , where the low-voltage measured resistance $R \sim 3 \text{ M}\Omega$ at 10 kHz, plus $4VP_s f$, with $P_s = 0.3 \text{ nC}/\text{mm}^2$, and $V = 30 \text{ volts}$. The temperature rise is estimated by approximating the electrically active region with a continuous heat source of 0.5-mm gaussian radius in an infinite

medium.²¹ The electrical response appears in a few seconds, so the cell boundaries can be ignored.

The behavior is probably due to piezoelectric effects, and a connection can be made to electromechanical experiments.^{22,23} The layer flow directions are consistent with the piezoelectric effect. In the electromechanical experiments a resonant frequency is observed ~ 2 kHz, while we observe a resonance at 6 kHz for a different FLC material.

Increasing the applied voltage to 50 V/ μ m at the resonant frequency, or higher, produces an alignment distortion as shown in Figure 7. The cell cannot be restored by the original 10 Hz electric field treatment.



FIGURE 7. Electric field induced alignment distortion.

ABRUPT CHANGES IN ALIGNMENT

An abrupt change in surface alignment conditions can be achieved by masking part of the substrate during the evaporation process. The substrates are held by 1-mm thick clamps, which mask part of the surface during the film deposition. However, oblique evaporation magnifies the mask thickness shadow, creating a poorly defined region at the edge of the mask. The behavior of a masking line parallel to the SAD direction is illustrated in Figure 8., for an SAD thickness of 50 nm. There is a transition region of approximately 0.5 mm before a severely striated texture is established, associated with one alignment coating and

a clean planar aligning surface. In the transition region the striations are rotated by approximately 45° and have the form of elongated focal-conics. The transition region is probably associated with the ill-defined region of the masking, which may be coated indirectly by scattered material, altering the local alignment direction. The transition region is absent for SAD thickness ≤ 10 nm, but reappears for MAD/SAD combinations.



FIGURE 8. Texture at termination of 50-nm SAD alignment film. Scale $<200\ \mu\text{m}>$

DISCUSSION

Dielectric alignment layers isolating the FLC from the conducting electrodes have a deleterious effect on the cell bistability due to ionic charging by the FLC depolarization field.²⁴ Although evaporated silicon oxide is a poor insulator, there is an incentive to reduce the film thickness as a precaution against ionic charging effects. Moreover, aside from ionic effects, we find much better cell performance with thinner alignment layers.

The thicker SAD alignments are associated with smaller effective switching cone-angles and poorer bistability, which is identified with a chevron rather than a psuedo-bookshelf structure. On cooling into the S_A -phase a bookshelf or near bookshelf alignment is formed, followed by a typical chevron structure on further cooling through the FLC phase.¹⁰⁻¹² It is surprising that the FLC cannot be voltage driven into the bookshelf FLC arrangement, when the S_A favors the bookshelf arrangement. Therefore the thick SAD ≥ 30 nm prevents the establishment of the bookshelf structure in the FLC phase. Higher voltage treatment at 10 hz reduces the switching angle, suggesting the more ordered structure is dominated by surface effects. The thin SAD alignments allow an electric field induced psuedo-bookshelf arrangement to be established in the FLC phase, as judged by the apparant cone-angle. This desirable behavior must be determined

by a weaker surface alignment or lower effective surface tilt. The columnar film structure resulting from SAD will have more FLC-surface interaction with increasing deposition, simply because of increasing contact area. The tilt angle is also known to increase with increasing SAD thickness. Therefore it is plausible that bookshelf structure is achieved for sufficiently thin alignment films.

More work is required to explore the SAD range 10-30 nm, where the texture changes and electric field alignment fails. The MAD range above 10-nm should be explored to establish the thickness required for uniform parallel alignment, which should result in an FLC structure dominated by zigzag defects. It would be interesting to determine if thick MAD layers, followed by thin SAD layers, inhibit the switching angle and bistability.

Oblique evaporation structures are determined by nucleation and growth mechanisms, and may be sensitive to substrate surface conditions. Spurious surface influences can be eliminated by an initial evaporation of silicon oxide at perpendicular incidence. We observe no significant variation in comparing ITO and glass regions of a surface, or SiO₂ coated surfaces. Nevertheless, a perpendicular deposited oxide film followed by SAD should be compared with the SAD and MAD/SAD results. Contaminated regions of the substrate are not corrected by a thin SAD coating and generate defects. Therefore it would be an advantage to establish an optimum evaporated alignment method including surface defects and FLC ionic issues.

We have concentrated on a particular well known FLC, but considerable variation in the alignment of different FLC materials can be expected. It would be of interest to study the tilt alignment of the high temperature precursor N* phase in relation to the FLC alignment.

The striped texture always emerges with electric field alignment, and has been analysed in terms of an undulation of the smectic layer structure.²⁵ We observe a similar low contrast striped texture in most samples before the electric field is applied, and while the twisted domain structure is present. The continuity of the striped texture can be seen in Figure 4. One might speculate that a buckling of the S_A layer structure to accommodate the S_C* could give rise to transverse buckling or undulation of the layers under these alignment conditions. Some similarity with the field induced roof texture is seen in the virgin texture of Figure 4C.

The FLC response outside the electrode region, which we identify with piezoelectric behavior, is of academic interest. The voltage level required for the effect is generally higher than practical device voltage levels. Progress is being made in electromechanical studies related to FLC piezoelectricity, but difficulties remain.²⁶ It would be interesting to provide auxiliary electrodes to sample the voltage associated with the piezoelectric flow induced by the active electrodes. Voltage measurement would allow a quantitative study

of the effect.

The striped texture created by the 10-hz electric field treatment can sometimes be returned to the virgin texture by raising the frequency to ~6 khz; thus demonstrating that the surface conditions are unchanged. At high-voltage levels of 40V/ μm , at the 6-khz resonant frequency or higher, the alignment is severely distorted and cannot be restored by electrical treatment. This implies that the piezoelectric flow process disturbs the surface alignment. Rubbed nylon aligned cells are not disturbed by a similar electric field treatment, where piezoelectric flow processes are observed. The stability of the nylon cells in this respect is probably related to their ability to directly align the smectic phase.

The masking effects on the alignment film are difficult to interpret because the deposition geometry we used does not abruptly terminate the film. However, it is interesting to observe the alignment behavior on a surface region screened from the direct source deposition path, but subject to surface migration and scattered deposition. With a small change in the substrate holder position we should achieve a controllable abrupt change in the alignment film. Precise control of masking is achieved by lithography, but disturbance of the deposited film may result from the photoresist removal process.³

ACKNOWLEDGEMENT

The electrode lithography was performed by Angie Ortega. The ZLI3654 sample was provided by EM Chemicals. The work is supported by a Lockheed Research & Development Division Program.

REFERENCES

1. J. Cognard, Mol. Cryst. Liq. Cryst., Supplement 1, (1982)
2. D. Armitage, J. Appl. Phys., **51**, 2552 (1980)
3. J. Cheng, G. D. Boyd, and F. G. Storz, Appl. Phys. Lett., **37**, 716 (1980).
4. K. Hiroshima, S. Kondo, and M. Kyoshima, Proc. 6th Int. Disp. Res. Conf., **3**, 5 (1986).
5. F. J. Kahn, Mol. Cryst. Liq. Cryst., **38**, 109 (1977).
6. T. Uemura, N. Ohba, N. Wakita, H. Ohnishi, and I. Ota, Proc. 6th Int. Display Res. Conf., 464 (1986)
7. C. Bowry, M. G. Clark, A. Mosley, and B. M. Nicholas, EuroDisplay Proc., **33** (1987)
8. P. J. Bos, K. R. Koehler/Beran, Ferroelectrics, **85**, 15 (1988).
9. M. Kuwahara, Y. Kawata, H. Onnagawa, and K. Miyashita, J. J. Appl. Phys., **27**, 1365 (1988).
10. Y. Ouchi, J. Lee, H. Takezoe, A. Fukuda, K. Kondo, T. Kitamura, and A. Mukoh, J. J. Appl. Phys., **27**, L1993 (1988).
11. Yamada, N. Yamamoto, T. Inoue, H. Orihara, and Y. Ishibashi, J. J. Appl. Phys., **28**, 50 (1989)
12. T. P. Rieker, N. A. Clark, G. S. Smith, C. R. Safinya, Liq. Cryst., **6**, 565 (1989)

13. Y. S. S. Bawa, A. M. Biradar, K. Saxena, S. Chandra, Appl. Phys. Lett., **57**, 1398 (1990)
14. R. C. Chittick, W. A Crossland, and J. R. Brocklehurst, SLM & Applications, OSA Tech. Digest 14, 136 (1990)
15. N. Wakita, Y. Iwai, T. Uemura, S. Fujiwara, Y. Gohara, I. Ota, Y. Masumoto, Y. Miyatake, T. Tsuda, Y. Horio, Ferroelectrics, **114**, 27 (1991)
16. D. Armitage and D. K. Kinell, SPIE, **1296**, 158 (1990).
17. D. Armitage and A. J. Ticknor, SPIE, **1455**, in press (1991).
18. EM Chemicals data sheet.
19. W. J. A. M. Hartmann and A. M. M. Luyckx-Smolters, J. App. Phys., **67**, 1153 (1990).
20. J. S. Patel, Sin-Doo Lee, and J. W. Goodby, Phys. Rev. A., **40**, 2854 (1989).
21. D. Armitage, J. App. Phys., **52**, 1294 (1981)
22. A. Jakli, L. Bata, A. Buka, and N. Eber, Ferroelectrics, **69**, 153 (1986)
23. A. Jakli, N. Eber, and L. Bata, Ferroelectrics, **113**, 305 (1991)
24. T. C. Chieu and K. H. Yang, App. Phys. Lett., **56**, 1326 (1990)
25. L. Lejcek and Pirkel, Liq. Cryst., **8**, 871 (1990).
26. A. Jakli and A. Saupe, Liq. Cryst., **9**, 519 (1991)

ELECTRIC FIELD INDUCED MACROSCOPIC FLOW IN FREE-STANDING FERROELECTRIC FILMS

GERD HAUCK and HANS DIETER KOSWIG
Zentralinstitut für Elektronenphysik, Hausvogteiplatz 5/7,
D-1086 Berlin, FRG

Abstract Free-standing ferroelectric films were investigated in a rotating electric field. Depending on the applied voltage and the period of the field rotation a domain switching or a macroscopic rotation of the film could be observed. At special conditions the rotating film shows spontaneously the formation of a bubble domain structure. A model for the interpretation is proposed.

INTRODUCTION

Free-standing ferroelectric smectic liquid crystal films offer the possibility to study dynamical properties without the influence of stabilizing orientational layers at the substrates of a sample. The normal picture of the free-standing film accepts arrangements of smectic layers parallel to the free surface. Recently¹, we presented at the first time the determination of the rotational viscosity of a free-standing FLC-film in comparison to the value in a surface stabilized cell. The use of the four-electrode equipment (described by Kremer et al.¹ for a normal cell construction) at the free-standing film opens the facility to study the change in the orientation by a rotating electric field.

EXPERIMENTAL

We investigated a free-standing film stretched on a hole of about 1 mm diameter at a film thickness between 500 - 800 nm. On the sample four electrodes are arranged perpendicular to each other (Figure 1). The rotating electric field results from rectangular voltage impulses: two opposite electrodes are at plus/minus U and the two perpendicular to the first electrodes at the same time at zero voltage (Figure 2). The amplitude U of the impulses can be varied between 0 and 50 V and the impulse length between 2.5 s and 0.1 ms. The period of the rotation of

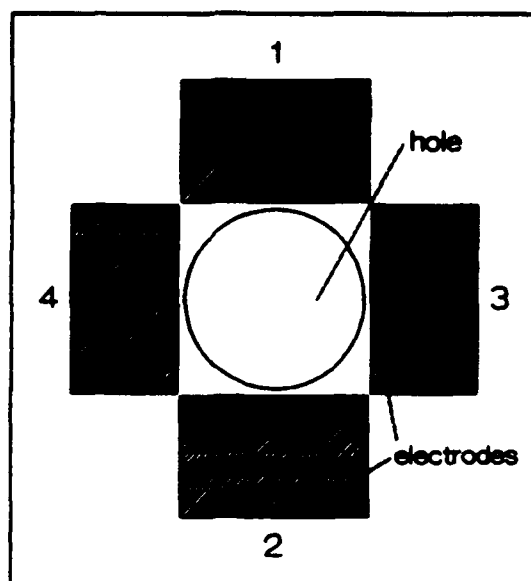


FIGURE 1 Experimental setup.

the field T is, therefore, between 10 s and 0.4 ms (frequency $f = 1/T$ between 0.1 Hz and 2.5 kHz).

The experiments were carried out on a hot stage in a polarizing microscope with crossed polarizers. The optical response has been controlled by a CCD-camera with video recording, and the optical transmission by a photomultiplier connected with an oscilloscope.

The ferroelectric smectic liquid crystals used in the experiments are

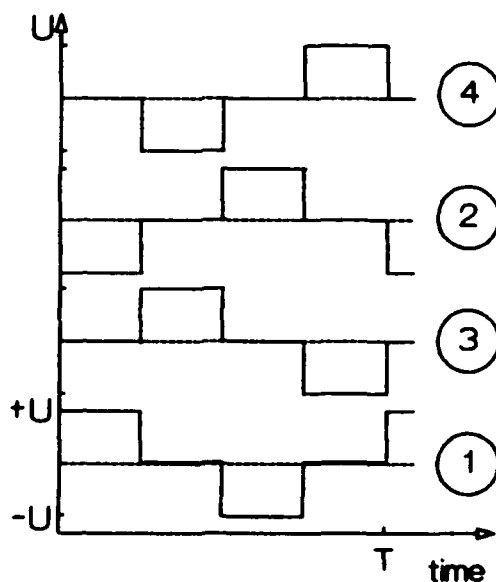


FIGURE 2 Impulse diagram for electrodes 1-4.

the mixtures:

- 15/2 (MLU Halle) with a spontaneous polarization of 60 nC/cm^2 ,
 $C - < 15^\circ\text{C} - \text{SmC}' - 31^\circ\text{C} - \text{SmA} - 61^\circ\text{C} - \text{N}' - 69^\circ\text{C} - \text{I}$,
- SCE 12 (BDH) with 16 nC/cm^2 ,

$\text{SmI} - < -20^\circ\text{C} - \text{SmC}' - 66^\circ\text{C} - \text{SmA} - 81^\circ\text{C} - \text{N}' - 119^\circ\text{C} - \text{I}$.

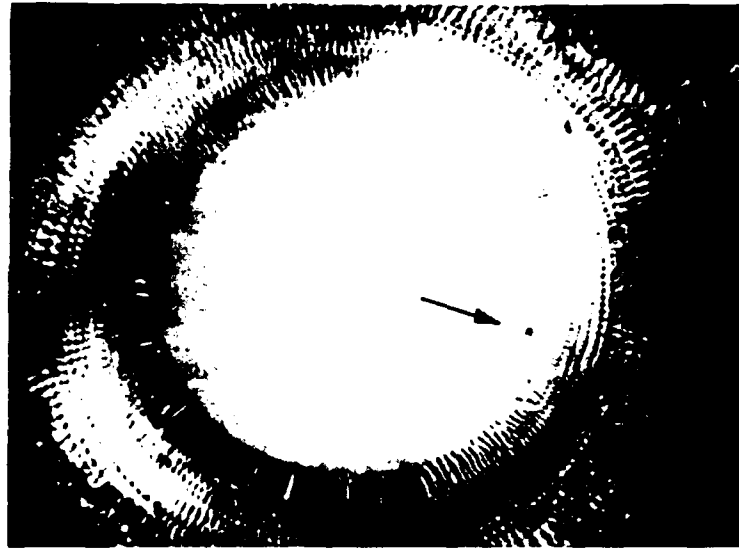
Both FLC-mixtures exhibit the SmC' -phase at room temperature.

RESULTS

In the SmC' -phase measured at 24°C the electric field induces the well known rotational motion of the director on the smectic cone with the axis perpendicular to the layer and the free surfaces of the film. This is evident from the motion of the optical axis in the conoscopical picture. At low voltages a domain switching could be observed in the film which is visible by the different brightness of the domains. Simultaneously, an inhomogeneous field distribution can be noticed. This results from the non-unified orientation of the molecules in the film.

In the mixture 15/2 a macroscopic rotational flow has been observed at voltages above 30 V and not too small periods T : the individual rotation of the directors on the cone induces a collective rotational movement in the film. The angular velocity depends on U and T . In the transition region to the solid substrate the thickness of the film increases and a striped pattern is formed^{1,4}. In this region the angular velocity decreases because of hindering forces from the substrate. The stripes are moving slower in the thicker part. If there are dust particles on the film, the motion is visible also in the inner part of the film because the particles take part in the macroscopic rotation (Figure 3). From the uniform brightness of the film (with possible deviations near the dust particles) we must conclude that the electric field induces a homogeneous orientation of the dipole moments of the individual molecules in the film. This homogeneous orientation rotates with the period of the field.

At special values of U and T (between the conditions of the domain switching and the homogeneously oriented film) one can observe that the rotating film shows spontaneously the formation of a bubble domain structure (Figure 4), known from magnetic materials¹: a central or spiral system of rotating lines which are dividing dark and bright



(a)



(b)

FIGURE 3 A dust particle in the rotating free-standing film ($U = 50$ V, $T = 30$ ms) is shifted from the right side (a) to the left one (b). Near the particle the homogeneous orientation is disturbed. See Color Plate XIII.

ring-shaped regions is formed. It is possible to choose such a combination of voltage and period that a quasi-stationary regime of the rotating bubble domain is realized ($U = 12$ V and $T = 40$ ms in Figure 4). In this case the system is formed immediately after the switching-on of the field in the whole film (region C in Figure 5). In the non-

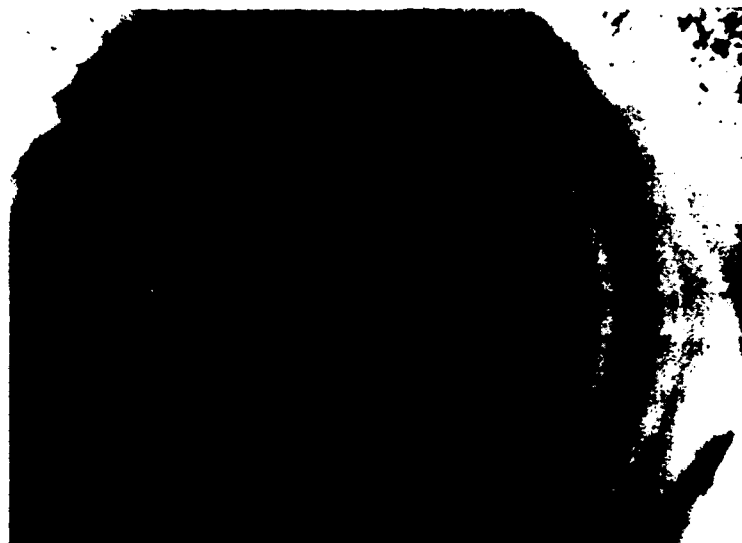


FIGURE 4 Bubble domain structure with dark and bright rings. See Color Plate XIV.

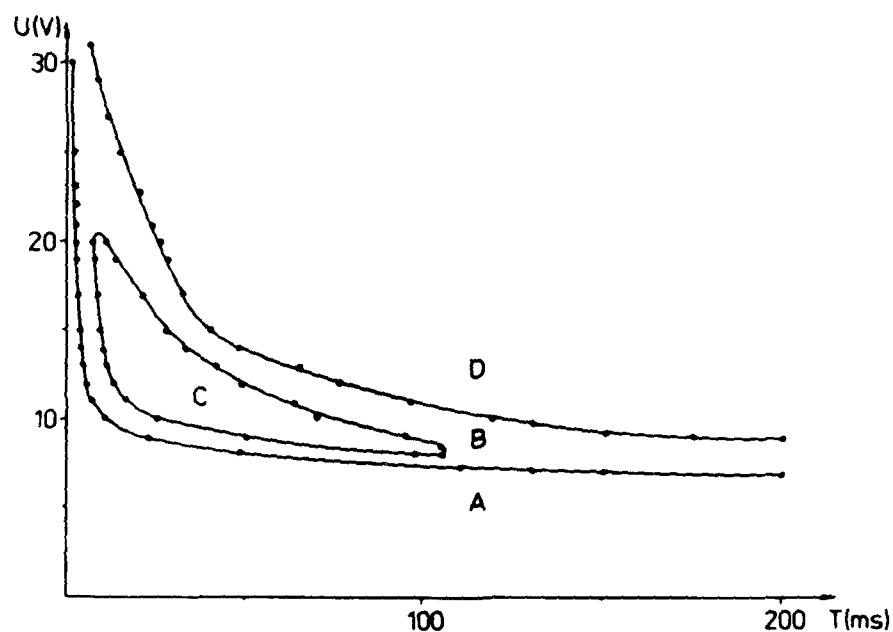


FIGURE 5 Dependence of switching behaviour on the voltage between a pair of electrodes U and the period of the field T ; A: domain switching; B: non-stationary mode; C: quasi-stationary mode; D: homogeneously rotating film.

stationary mode (region B in Figure 5) a symmetrical bubble domain is created only in the middle of the film or as a ring system in the outside part. It can growth to fill out the whole film or may be destroyed at the border of the hole. In the FLC-mixture SCE 12 the stability region is shifted to higher values of U and T in comparison to Figure 5.

The formation of the rotating line system must not be central symmetrical. It is possible that the spontaneous formation of the bubbles takes place at different parts of the film as a consequence of an inhomogeneous orientation of the molecules throughout the film (e.g. near dust particles). The development of these different bubbles depends also on the electric field conditions and will be described otherwise⁶.

In the SMA-phase the formation of similar structures could not been observed because of the uniform orientation of the molecules perpendicular to the layers. It may be possible that at the electroclinic effect the spontaneous formation of structures can be observed. But, the electric fields which we used are too small to induce an observable electroclinic effect.

DISCUSSION

Our interpretation of the experimental results accepts the usual picture of the field induced reorientation of the molecules in the chiral smectic-C phase. As a consequence of the parallel arrangement of the smectic layers to the surfaces of the free-standing film the axis of the cone will be perpendicular to the electric field. The tilted director with the dipole moment perpendicular to the molecule axis rotates at the cone determined by the tilt angle. A switching of the electric field from the electrode pair 1-2 to 3-4 induces a 90° -rotation of the dipole. Under special conditions a synchronous run of the reorientation of the individual molecules is possible, resulting in the visible macroscopic flow (resonance state). This macroscopic rotational flow is connected with a rotation of the field-induced unified dipole orientation, or, in other words, a mono-domain rotation results.

The homogeneously oriented, rotating mono-domain becomes unstable at special parameters of the electric field, and a bubble domain is

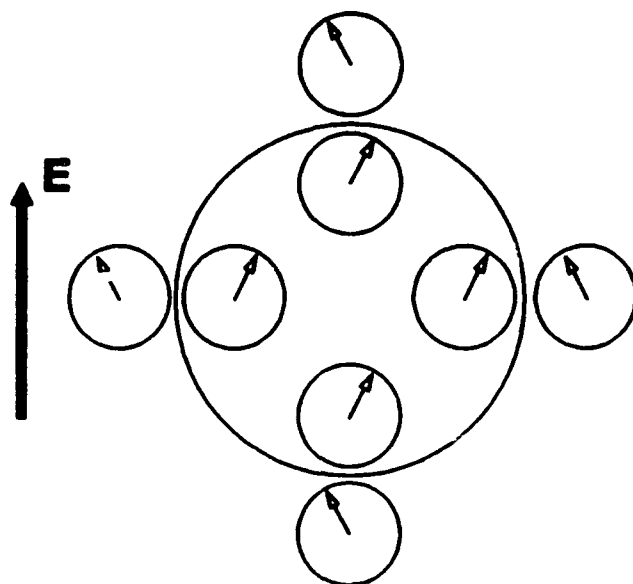


FIGURE 6 Supposed arrangement of orientational directions in the ring system.

spontaneously formed. The bubble system with dark and bright ring systems requires different orientation of the molecules in the dark and bright parts, but with a constant and field-determined angle between them. The central or spiral rings act as lines dividing regions with different orientation like an antiferroelectric system. The main orientation of the different parts in the ring system is determined at every time by the electric field direction.

Figure 6 shows this concept. Dark and bright parts of the ring are separated by the circle. The possible molecular reorientation at the cone inside and outside the circle in the direction of the four electrodes is indicated by the arrows. From this view it is evident, that it is possible to realize an arrangement which represents a homogeneous quasi-antiferroelectric orientation through the film following the rotating electric field. Slow-motion reproduction of the video recording shows, that the brightness of the dark and bright parts in the ring system is changed periodically with the field. This transmission distribution can also be changed by a rotation of the crossed polarizers, indicating again the variation of the orientational directions.

The financial support of the Deutsche Forschungsgemeinschaft is acknowledged.

REFERENCES

1. G. Hauck, H. D. Koswig, and Ch.Selbmann, 20. Freiburger Arbeitstagung Flüssigkristalle (Freiburg, 1991), P10.
2. F. Kremer, S. V. Vallerian, and L. R. Zente, Phys. Lett. A **146**, 237 (1990).
3. G. Hauck and H. D. Koswig, Mol. Cryst. Liq. Cryst. **199**, 159 (1991).
4. J. MacLennan, Europhys. Lett. **13**, 435 (1990).
5. A. H. Bobeck and E. Della Torre: Magnetic Bubbles (North-Holland Publishing Company, Amsterdam, 1975).
6. G. Hauck and H. D. Koswig, in preparation.

RELATIONS BETWEEN SURFACE PROFILE AND FREE SURFACE ENERGY OF SMECTIC C LIQUID CRYSTALS

PETER SCHILLER

Martin-Luther-Universität

Institut für Physikalische Chemie

Mühlpforte 1, O-4020 Halle, Germany

Abstract Using symmetry arguments, order parameter expansions for the free surface energy of chiral and nonchiral smectic C liquid crystals anchored at a solid plate are derived. Surface forces are sensitive to surface profiles obtained by rubbing the plate. The free surface energy can be combined with a Landau expansion for the free energy of the bulk phase. In an equilibrium configuration the sum of the surface and the bulk free energy is a minimum. The theoretical approach is useful to predict stable configurations of the smectic layer planes and the director with respect to boundaries.

INTRODUCTION

As well known, the Landau theory is a useful method to understand various physical properties of the chiral smectic C phase. If the Landau expansion includes a sufficient number of terms, a fairly good description is obtained as long as the order parameters remain small close to the smectic A-smectic C phase transition temperature. In accordance with Indenbom, Pikin and Loginov /1/ a two component order parameter Ψ can be introduced, the components of which are approximately

$$\Psi_1 = \theta \cos \phi \quad \text{and} \quad \Psi_2 = \theta \sin \phi, \quad (1)$$

where θ is the tilt angle (polar angle) enclosed by the long molecules and the smectic layer normal, and ϕ is their azimuthal angle. The chiral smectic C phase possesses a spontaneous polarization, which is directed perpendicular to the plane spanned by the tilted molecules and the normal of smectic layers. Besides the primary order parameters ξ_1 and ξ_2 both components of this in-plane polarization \mathbf{P} can be taken into account as secondary order parameters /2/. There are some hints, however, from dielectric spectroscopy /3/ that rotations of the macroscopic polarization are already described by the azimuthal angle ϕ , which defines the position of the long molecular axes on a cone with aperture 2θ . In this case only the components of \mathbf{P} and the absolute value of the polarization $|\mathbf{P}|$ are sufficient to define uniquely the state avoiding redundant variables.

At a substrate the free surface energy should also depend on θ and ϕ , and an order parameter expansion similar to the procedure used in the bulk phase may be reasonable.

First let us consider a smooth surface (Figure 1). A reference configuration is the smectic A^* phase, which has a planar molecular alignment. In this configuration the normal \mathbf{N}_0 of the smectic layers is parallel to the surface. If the A^* phase is cooled below the phase transition temperature, θ becomes nonzero and the layer normal can be tilted with respect to the boundary. Consequently, besides ξ_1 and ξ_2 the components of $\delta\mathbf{N} = \mathbf{N} - \mathbf{N}_0$ are additionally introduced as surface order parameters to describe a small rotation of the layer normal from its initial position. This behaviour is expected, if the surface is smooth.

Of practical interest are also other surface geometries. For instance, the substrate can be rubbed in such a manner, that a twofold rotation axis is generated. If the plate is only rubbed in one direction the twofold rotation axis of the surface profile disappears. For rubbed plates we define the reference configuration of the smectic A phase in a similar way as for a smooth plate: The smectic layer normal in the reference state

is parallel to the rubbing direction. However, this reference state is not necessarily a stable configuration characterized by a minimum of the free energy. The stability of a surface configuration can be checked by analysing the surface energy expansion. Excluding the case of a strong anchoring of molecules at the surface, we restrict the expansion to terms which are linear or quadratic in the order parameter components.

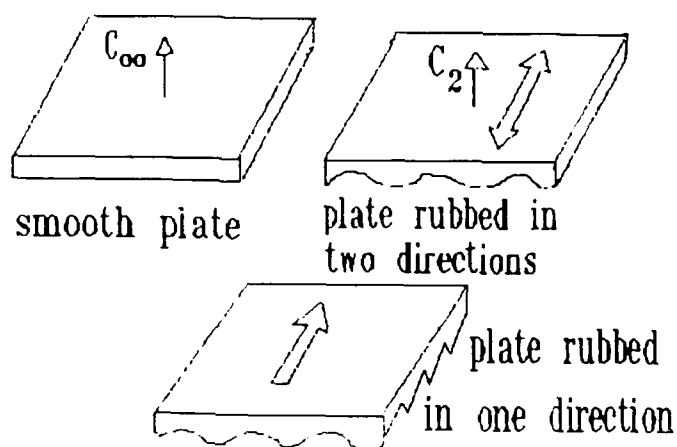


FIGURE 1 Surface profiles of a bounding plate.

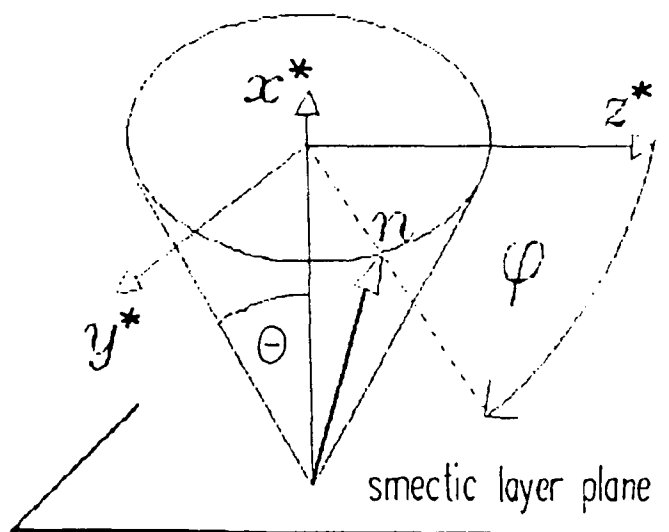


Figure 2 Cartesian coordinate system fixed at the smectic layer plane (y^* - z^* -plane). θ is the angle between the director n and the normal N of the smectic layer plane; ϕ is the azimuthal rotation angle.

FREE ENERGY EXPANSIONFree energy of the bulk phase

Using the coordinate system fixed at the smectic layer planes (Figure 2) and definitions (1) the free energy F_b for the bulk phase of a chiral smectic phase is /4/

$$\begin{aligned}
 F_b = & \frac{1}{2}a \theta^2 + \frac{1}{4}b \theta^4 + \frac{1}{2} G' \theta_{\mathbf{x}}^2 + \frac{1}{2} G (\theta_{\mathbf{y}}^2 + \theta_{\mathbf{z}}^2) \\
 & + \frac{1}{2} K' \theta^2 \phi_{\mathbf{x}}^2 + K \theta^2 \phi_{\mathbf{x}} + C (\varphi_{2,z} - \varphi_{1,y}) \\
 & + \frac{1}{2} B_1 (\varphi_{1,z} + \varphi_{2,y})^2 + \frac{1}{2} B_2 (\varphi_{2,z} - \varphi_{1,y})^2 \\
 & + D \theta^2 \phi_{\mathbf{x}} (\varphi_{2,z} - \varphi_{1,y}) \quad (2)
 \end{aligned}$$

where the bold typed subscripts \mathbf{x}, \mathbf{y} and \mathbf{z} define the partiell derivatives

$$\theta_{\mathbf{x}} = \partial \theta / \partial x^*, \quad \theta_{\mathbf{y}} = \partial \theta / \partial y^*, \quad \varphi_{1,y} = \partial \varphi_1 / \partial y^* \quad \text{etc..}$$

In the cases of a nonchiral smectic C phase the coefficients K and C are zero.

For combinig the bulk free energy with the free surface energy a different coordinate system fixed at a bounding plate (x - y - z -system in Fig.3) must be introduced. As seen in Figure 3 the x - y - z -system is obtained when the x^* - y^* - z^* -system is rotated by the angles μ and σ . Then the free energy (2) is transformed by replacing the spatial derivatives in the following way:

$$\begin{bmatrix} \partial / \partial x^* \\ \partial / \partial y^* \\ \partial / \partial z^* \end{bmatrix} = \begin{bmatrix} 1 - \frac{1}{2}(\mu^2 + \sigma^2) & \sigma & \mu \\ -\sigma & 1 - \frac{1}{2}\sigma^2 & 0 \\ -\mu & -\mu\sigma & 1 - \frac{1}{2}\mu^2 \end{bmatrix} \begin{bmatrix} \partial / \partial x \\ \partial / \partial y \\ \partial / \partial z \end{bmatrix}$$

where terms of third and higher order like μ^3 , $\mu^2 \sigma$ etc. are neglected in the transformation matrix. In the case of a thin cell with a chevron defect structure /5/ the transformation should be done separately for the regions below and above the chevron kink.

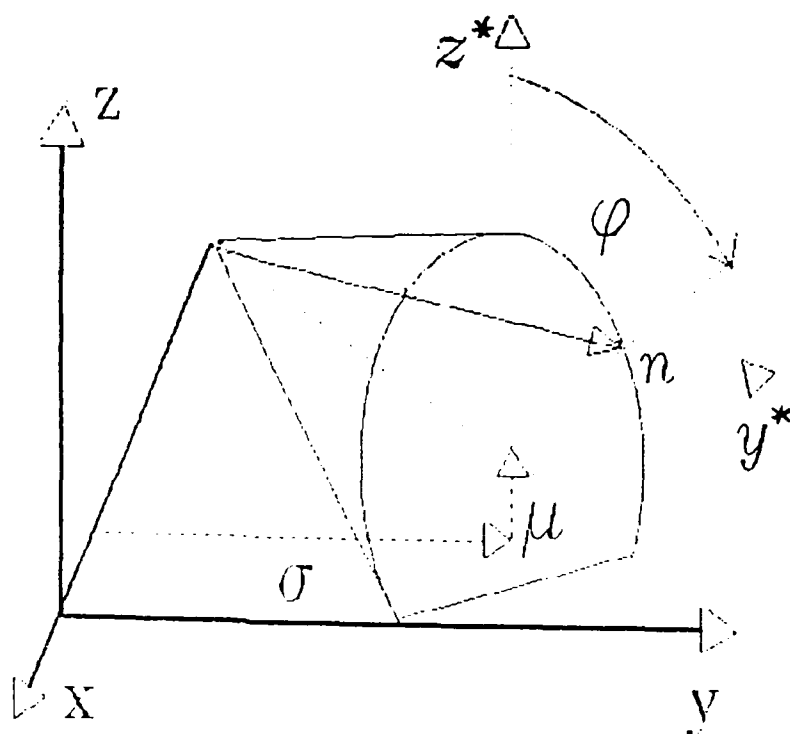


FIGURE 3. Coordinate system fixes at the lower bounding plate (x-y-plane). μ , angle between the plate and the smectic layer normal; σ , lateral deviation of the layer normal from the rubbing direction.

Free energy of the surface

Figure 3 demonstrates how the layer normal and the preferred direction of long molecular axes are arranged with respect to the surface of a lower bounding plate, which coincides with the x-y-plane of a cartesian coordinate system. Using the notation

$$\mathbf{N} = (N_x, N_y, N_z)$$

for the normal of smectic layers and

$$\mathbf{n} = (n_x, n_y, n_z)$$

for the director, the components of these vectors in the

reference state (smectic A phase) are

$$N_x = 1, N_y = N_z = 0 \text{ and } n_x = 1, n_y = n_z = 0. \quad (3)$$

If the plate is rubbed, the x-axis coincides with the rubbing direction. A surface configuration, which deviates from the reference state, is characterized by a rotation of \mathbf{n} and \mathbf{N} . The components

$$\begin{aligned} N_z &= \mu \quad (\text{layer tilt angle}) \\ N_y &= \sigma \quad (\text{lateral deviation of the layer} \\ &\quad \text{normal from the rubbing direction}) \\ n_z &= \theta \cos \phi + O(3) \quad \text{and} \quad n_y = \theta \sin \phi + O(3) \end{aligned} \quad (4)$$

($O(3)$ symbolizes that third order surface terms are neglected.)

are small close to the smectic A-smectic C phase transition point. We regard these as first order terms. Consequently, products like $n_y n_z$, $n_y N_z$, $N_y N_y$ and so on are second order terms.

Now we can expand the free surface energy of a chiral smectic C phase up to terms of second order. Since the chiral smectic C phase possesses a twofold rotation axis as symmetry element /5/, \mathbf{N}, \mathbf{n} and $-\mathbf{N}, -\mathbf{n}$ correspond to the same configuration of the smectic layers and the long molecular axes. Vector components in the expansion should therefore occur in pairs. Some terms in this expansion can be cancelled because the relations

$$N_x^2 = 1 - (N_y^2 + N_z^2), \quad n_x^2 = 1 - (n_y^2 + n_z^2)$$

$$N_x N_y = n_x N_y + O(3), \quad N_x N_z = n_x N_z + O(3)$$

$$N_x n_y = n_x n_y + O(3), \quad N_x n_z = n_x n_z + O(3) \quad \text{and}$$

$$N_x n_x = 1 - 1/2 (n_y^2 + n_z^2 + N_y^2 + N_z^2) + O(4)$$

are satisfied. The free surface energy is composed of the remaining terms:

$$\begin{aligned}
 2F_S = & \alpha_2 N_Y^2 + \alpha_3 N_Z^2 + 2\alpha_{12} N_X N_Y + 2\alpha_{23} N_Y N_Z \\
 & + 2\alpha_{13} N_X N_Z + \beta_2 n_Y^2 + \beta_3 n_Z^2 + 2\beta_{23} n_Y n_Z \\
 & + 2\Gamma_2 N_Y n_Y + 2\Gamma_3 N_Z n_Z + 2\Gamma_{23} N_Y n_Z + 2\Gamma_{32} N_Z n_Y \\
 & + 2\Gamma_{12} N_X n_Y + 2\Gamma_{13} N_X n_Z
 \end{aligned} \tag{5}$$

It should be noted, that (5) is valid for a nonchiral and a chiral smectic C phase, when the profile of the bounding plate excludes both a rotation axis and a mirror plane in the reference state (3). Let us consider some surface profiles shown in Figure 1.

Plate rubbed in only one direction

In Figure 1 the surface profile is shown for a plate which is rubbed only in one direction so that the directions parallel and antiparallel to the x-axis are distinguishable. For such a surface a twofold rotation axis does not exist and the complete expression (5) should be used to describe the surface anchoring energy:

$$\begin{aligned}
 2F_S = & \alpha_2 \sigma^2 + \alpha_3 \mu^2 + 2\alpha_{12} \sigma + 2\alpha_{23} \sigma \mu + 2\alpha_{13} \mu \\
 & + \beta_2 \theta^2 + (\beta_3 - \beta_2) \theta^2 \cos^2 \phi + 2\beta_{23} \theta^2 \sin \phi \cos \phi \\
 & + 2\Gamma_2 \sigma \theta \sin \phi + 2\Gamma_3 \mu \theta \cos \phi + 2\Gamma_{23} \sigma \theta \cos \phi \\
 & + 2\Gamma_{12} \theta \sin \phi + 2\Gamma_{13} \theta \cos \phi
 \end{aligned} \tag{6}$$

This expression is considerably simplified if a nonchiral smectic phase is regarded because the reference configuration has a mirror plane, which is parallel to the x-z-plane of the cartesian coordinate system. As the mirror plane is accompanied with the symmetry operation $y \rightarrow -y$, terms linearly proportional to n_Y and N_Y are forbidden. Writing down the remaining

terms of (6) we have

$$2F_S = \alpha_2 \sigma^2 + \alpha_3 \mu^2 + 2\alpha_{13} \mu + \beta_2 \theta^2 + (\beta_3 - \beta_2) \theta^2 \cos^2 \phi \\ + 2\Gamma_2 \sigma \theta \sin \phi + 2\Gamma_3 \mu \theta \cos \phi + 2\Gamma_{13} \theta \cos \phi. \quad (7)$$

The influence of chirality on the surface anchoring energy can be studied by comparing (6) and (7).

Plate with twofold rotation axis

Figure 1 demonstrates a plate equally rubbed parallel and antiparallel to the x-axis. In this case a twofold rotation axis exists in the reference state. The rotation by an angle π is accompanied with the operation

$$N_X, n_X \rightarrow -N_X, -n_X, N_Y, n_Y \rightarrow -N_Y, -n_Y \text{ and } N_Z, n_Z \rightarrow N_Z, n_Z. \quad (8)$$

Taking into account (8), the expansion (7) is simplified to

$$2F_S = \alpha_2 \sigma^2 + \alpha_3 \mu^2 + 2\alpha_{12} \sigma + \beta_2 \theta^2 + (\beta_3 - \beta_2) \theta^2 \cos^2 \phi \\ + 2\Gamma_2 \sigma \theta \sin \phi + 2\Gamma_3 \mu \theta \cos \phi + 2\Gamma_{12} \theta \sin \phi. \quad (9)$$

The free surface energy for a nonchiral smectic phase is obtained by cancelling some terms in (9):

$$2F_S = \alpha_2 \sigma^2 + \alpha_3 \mu^2 + \beta_2 \theta^2 + (\beta_3 - \beta_2) \theta^2 \cos^2 \phi \\ + 2\Gamma_2 \sigma \theta \sin \phi + 2\Gamma_3 \mu \theta \cos \phi \quad (10)$$

Smooth plate

Since there is not a preferred direction parallel to the plate, the surface energy cannot depend on N_Y . Cancelling all terms in (9) and (10) which are proportional to N_Y or N_Y^2 , we obtain

$$2F_S = \alpha_3 \mu^2 + \beta_2 \theta^2 + (\beta_3 - \beta_2) \theta^2 \cos^2 \phi \\ + 2\Gamma_3 \mu \theta \cos \phi + 2\Gamma_{12} \theta \sin \phi \quad (11)$$

for the chiral smectic C phase and

$$2F_S' = \alpha_3 \mu^2 + \beta_2 \theta^2 + (\beta_3 - \beta_2) \theta^2 \cos^2 \phi + 2\Gamma_3 \mu \theta \cos \phi \quad (12)$$

for the nonchiral phase. In practical cases the liquid crystal is confined between two parallel plates. All previously obtained expansions for the free energy refer to a cartesian coordinate system fixed at a lower plate. Using this coordinate system the free surface energy for the upper plate is usually different since there the plate normal is inversely oriented. Furthermore, the rubbing direction of the plates can be either parallel or antiparallel.

For predicting the correct free surface energy of the upper plate another representation of the free surface energy which avoids the introduction of a special coordinate system can be helpful. Using the unit vectors

\mathbf{K} , plate normal pointing into the liquid crystal phase

\mathbf{N} , normal of the smectic layers

\mathbf{n} , the director

\mathbf{R} , unit vector parallel to the rubbing direction, and

$\mathbf{K} \times \mathbf{R}$, unit vector parallel to the plates and perpendicular to the rubbing direction

the vector components in expansion (5) are replaced by the skalar products

$$\begin{aligned} N_x &\rightarrow (\mathbf{R}, \mathbf{N}), \quad N_y \rightarrow (\mathbf{K} \times \mathbf{R}, \mathbf{N}), \quad N_z \rightarrow (\mathbf{K}, \mathbf{N}) \\ n_y &\rightarrow (\mathbf{K} \times \mathbf{R}, \mathbf{n}), \quad n_z \rightarrow (\mathbf{K}, \mathbf{n}). \end{aligned} \quad (13)$$

However, a preferred direction defined by a vector \mathbf{R} does not exist for a smooth plate. In this case we obtain a correct expression for the free surface energy when \mathbf{R} is formally replaced by \mathbf{N} in the scalar products (13), so that

$$\begin{aligned}
 N_x &\rightarrow 1, \quad N_y \rightarrow 0, \quad N_z \rightarrow (K, N) \\
 n_y &\rightarrow (K \times N, n), \quad n_z \rightarrow (K, n)
 \end{aligned}
 \tag{14}$$

As an example we consider expansion (11) which represents the surface anchoring energy for a lower smooth plate. Applying the transformations (14) it is checked easily that the surface energy for the upper smooth plate differs from formula (11), as the coefficient Γ_{12} is replaced by $-\Gamma_{12}$.

EQUILIBRIUM CONDITION

The free energy of the smectic C phase consists of a bulk term and two surface terms

$$F = \int_V F_b \, dV + \int_S F_s \, dS + \int_{S'} F_{s'} \, dS' \tag{15}$$

where V denotes the volume, S is the surface of the lower plate and S' the surface of the upper plate. In an equilibrium state F is a minimum.

In most cases the tilt angle θ is not constant, but it is a function of the distance to the surface. Even in the smectic A phase θ can be nonzero near the boundary.

The equilibrium configuration of a smectic A or smectic C phase confined between two parallel bounding plates is obtained by minimizing functional (15) with respect to μ , σ , θ and ϕ . In this case the variational procedure leads to the equations

$$\frac{\partial F_b}{\partial \theta} - \frac{d}{dx} \frac{\partial F_b}{\partial \theta_x} - \frac{d}{dy} \frac{\partial F_b}{\partial \theta_y} - \frac{d}{dz} \frac{\partial F_b}{\partial \theta_z} = 0 \tag{16}$$

$$\frac{\partial F_b}{\partial \phi} - \frac{d}{dx} \frac{\partial F_b}{\partial \phi_x} - \frac{d}{dy} \frac{\partial F_b}{\partial \phi_y} - \frac{d}{dz} \frac{\partial F_b}{\partial \phi_z} = 0 \tag{17}$$

with the boundary conditions

$$\left. \frac{\partial F_b}{\partial \theta_z} \right|_S = \frac{\partial F_s}{\partial \theta}, \quad \left. \frac{\partial F_b}{\partial \phi_z} \right|_S = \frac{\partial F_s}{\partial \phi}, \quad \frac{\partial F_s}{\partial \mu} = 0$$

$$\frac{\partial F_s}{\partial \sigma} = 0 \quad (18)$$

for the lower plate, and

$$\left. \frac{\partial F_b}{\partial \theta_z} \right|_{S'} = - \frac{\partial F_{s'}}{\partial \theta}, \quad \left. \frac{\partial F_b}{\partial \phi_z} \right|_{S'} = - \frac{\partial F_{s'}}{\partial \phi}, \quad \frac{\partial F_{s'}}{\partial \mu} = 0$$

$$\frac{\partial F_{s'}}{\partial \sigma} = 0 \quad (19)$$

for the upper plate. It should be noted that the dynamics of a liquid crystal cell is described in the usual manner /5/ by adding friction terms $\Gamma_A \theta_\tau$ and $\Gamma_B \theta^2 \phi_\tau$ (Γ_A, Γ_B viscosity coefficients, τ time) to the equations (16) and (17), respectively. Furthermore, an external electrical field can be taken into account by generalizing the expression for F_b /5/. Unfortunately, it is already a rather tedious task to solve the static nonlinear equations (16) and (17) with nonlinear boundary conditions.

Assuming that θ is constant the mathematical problem is considerably simplified. This assumption is justified a little beyond the smectic A - smectic C phase transition temperature and if the surface anchoring of the director at the plate is not too strong.

If also free elastic energy contributions associated with spatial derivatives of ϕ are neglected in the overall free energy (15), then stability of a surface configuration at the lower plate requires

$$\partial F_s / \partial \phi = 0, \quad \partial F_s / \partial \mu = 0 \quad \text{and} \quad \partial F_s / \partial \sigma = 0. \quad (20)$$

EXAMPLES

For a first analysis we only consider the simplified conditions (20) to predict stable surface configu-

rations. Three different surface profiles are taken into account which are shown in Figure 1.

Reference state

Let us check whether the reference state $\mu = 0$ and $\sigma = 0$ of the smectic A phase anchored at a substratum can be stable or not:

As $\theta = 0$ is assumed to be valid also in the vicinity of the surface, F_p does not depend on ϕ and the first stability condition (20) is satisfied for all surface profiles.

In the case of a smooth plate the remaining conditions (20) are satisfied for the nonchiral and the chiral smectic A phase. This is proven easily by inserting (11) and (12) in (20).

For a rubbed plate with twofold rotation axis the stability conditions (20) are satisfied, when the smectic A phase is nonchiral. Inspection of (9) reveals, that stability of the chiral smectic A phase requires

$$\mu = 0 \quad \text{and} \quad \sigma = -\alpha_{12}/\alpha_2 . \quad (21)$$

According to (21) surface forces associated with the chirality of molecules generally cause a small lateral deviation of the smectic layer normal from the rubbing direction.

Finally, for a plate rubbed in only one direction both σ and the layer tilt angle μ are nonzero when the smectic A phase is chiral. For a nonchiral smectic A phase σ is zero, but μ is nonzero.

Bookshelf geometry

The bookshelf geometry characterized by a perpendicular orientation of the smectic layer planes with respect to the bounding plates is often presumed in the interpretation of experiments with chiral smectic C liquid crystals /6/. Of some practical interest is the surface alignment defined by

$$\mu = 0 \quad \text{and} \quad \phi = +\pi/2 \quad \text{or} \quad \phi = -\pi/2 , \quad (22)$$

that means that both the normal of smectic layer planes and long molecular axes are parallel to the plates. Using the free surface energies (6), (9) and (11) and the conditions (20), we decide for a chiral smectic C phase whether such a configuration can be stable.

It is easily shown, that (22) is a solution of (20) in the case of a smooth plate. For a plate with twofold rotation axis (22) is also a possible solution of equations (20). However, in this case the angle σ , which defines the lateral deviation of the layer normal from the rubbing direction is nonzero.

In the third case, if the profile of the plate excludes a twofold rotation axis, the bookshelf geometry (22) is not an equilibrium configuration because both μ and σ are generally nonzero.

It should be noted, that in some circumstances several different surface states can be stable simultaneously. To estimate the stability of a surface configuration obtained by conditions (20), data about the magnitude and the sign of the coefficients in surface energy expansions are needed. A variety of possible surface configurations which depend on the preparation of the bounding plate are discussed in /7/.

Influence of elastic forces on the bookshelf configuration in a thin layer

Since the ground-state of a chiral smectic C phase is nonuniform, elastic forces influence the surface alignment. Let us regard a thin layer of a chiral smectic C material confined between two smooth plates. The distance between the bounding plates should be small enough to unwind the helix alignment of the long molecular axis, which is stable in a thick sample. In a very thin slab the boundary conditions can stabilize a bookshelf configuration with parallel orientation of director and smectic layer normal to the plates. Handschy et al. /8/ have shown that in somewhat thicker slabs this homogeneous state is replaced by a nonuniform stable director structure called the splayed state. In this case the angle ϕ at the lower plate is different

from that one at the upper plate. Finally, if the plate distance is increased further, then the helix ordering of the director appears.

Let us discuss the stability of the bookshelf configuration for a thin slab by using the present theoretical approach.

As previously we assume that θ is constant in space for temperatures a little beyond the smectic A-smectic C phase transition point, and μ is zero for smooth plates. The splayed state, in which ϕ depends on z , is influenced by elastic forces in chiral materials, as a The liquid crystal layer is confined between the plates at $z = 0$ and $z = d$ of the cartesian coordinate system. Inserting (2) and (7) in (15) and disregarding terms which do not depend on $\phi(z)$, the free energy per unit area

$$\begin{aligned}
 F = & \frac{1}{2} \int_0^d dz \{ B \theta^2 \phi_z^2 + C \theta (\sin \phi)_z \} \\
 & + \frac{1}{2} \beta \theta^2 (\cos^2 \phi_2 + \cos^2 \phi_1) \\
 & - \Gamma_{12} \theta (\sin \phi_2 - \sin \phi_1)
 \end{aligned} \tag{23}$$

is derived, where $B_1 = B_2 = B$ is assumed and the notation

$$\phi_1 = \phi(0), \quad \phi_2 = \phi(d) \quad \text{and} \quad \beta = \beta_3 - \beta_2$$

is introduced. Stability of a planar director alignment requires that $\beta > 0$. The Eulerian equation $\phi_{zz} = 0$ related to the functional (23) has the solution

$$\phi(z) = \phi_1 + z (\phi_2 - \phi_1)/d \tag{24}$$

Now we check whether the homogeneous director configuration in the sample $\phi = \pi/2$ (or $\phi = -\pi/2$) is stable with respect to small perturbations. For this

purpose we define the angles

$$\Omega_1 = \phi_1 - \pi/2 \quad \text{and} \quad \Omega_2 = \phi_2 - \pi/2 \quad (25)$$

which correspond to small deviation from the initial alignment at the boundaries. Combining (23), (24) and (25) yields

$$\begin{aligned} f = & \frac{1}{2} \theta^2 (\Omega_2 - \Omega_1)^2 + \frac{1}{2} w \theta^2 (\Omega_2^2 + \Omega_1^2) \\ & - \frac{1}{2} p \theta (\Omega_2^2 - \Omega_1^2) + O(4) \end{aligned} \quad (26)$$

where

$$f = Fd/B, \quad w = \beta d/B, \quad p = (C - \Gamma_{12})d/B$$

and $O(4)$ symbolizes that terms proportional to Ω_1^4 and Ω_2^4 are neglected. The coefficients p and w characterize the effectiveness of polar and nonpolar surface forces of a slab with thickness d , respectively.

Stability of the homogeneous state $\Omega_1 = \Omega_2 = 0$ implies that f is positive definite ($f \geq 0$). This condition is satisfied, when

$$(w^2 + 2w) \theta^2 \geq p^2. \quad (27)$$

Obviously, if θ is decreased below a critical value the homogeneous director alignment becomes unstable. Thus the splayed state is always expected to occur in the vicinity of the smectic C-smectic A phase transition temperature of a chiral material, since there the angle θ tends to zero.

It should be possible to compensate partially the polar boundary interaction by using plates consisting of a chiral material which has the correct type of handedness. (Chiral compounds occur in two complementary structures, a right-handed and a left-handed variety.) It is highly probable that the handedness of both the chiral plate material and the chiral smectic C compound are decisive when the coefficient p for the polar

boundary interaction is decreased. There are many possibilities to observe effects caused by the presence of a solid surface.

Symmetry arguments suggest that a polar boundary interaction can be induced at the surface of a nonchiral smectic C phase when the bounding plate consists of a chiral compound. In this case also an electric polarisation of the surface is possible. Similarly, a tilt angle and an electric polarization is induced in the surface region of a chiral smectic A phase anchored at a smooth solid plate.

CONCLUDING REMARKS

The expansions of the free surface energy are useful to predict stable configurations of the smectic layers and the director of the smectic C phase with respect to the boundaries. The stable state is influenced by the surface profile of the bounding plates.

Frequently the smectic C sample is not in an equilibrium state defined by a minimum of the free energy, because the relaxation of the sample is hindered. Especially, the angles μ and σ , which define the configuration of the smectic layer planes, can be fixed by several defects. For instance, the chevron defect in the mid-plane of a thin slab is accompanied with a layer tilt angle $/5/$. In these cases formulas (6), (9) and (11) are suitable to predict how the surface energy for a chiral smectic C phase depends on the azimuthal angle ϕ . The correct choice of the free surface energy is important to describe the static configurations and the dynamics of electric field induced transitions with surface switching $/6/, /8/, /9/$.

A more complete description of a sandwich cell is possible by applying equations (16) and (17) with boundary conditions (18) and (19). But there remains a problem concerning the chevron kink of the smectic layers, which usually appears in thin cells. It is not clarified yet how the director position is influenced by

this defect.

ACKNOWLEDGMENT

The author wishes to thank Prof. P. Barber (Longwood College, Farmville, Virginia) for useful discussions.

REFERENCES

- /1/V.L. Indenbom, S.A. Pikin and E.B. Loginov, Kristallografiya, **21**, 1093 (1976)
- /2/R. Blinc and B. Zeks, Phys. Rev. A, **18**, 740 (1978)
- /3/F. Kremer, S.U. Vallerien, A. Hoffmann, N. Schwenk and E.. Fischer, The Molecular Origin of Ferroelectricity in FLC: A Challenge for Dielectric Spektroskopy at Microwave Frequencies, Proceedings of "Freiburger Arbeitstagung Flüssigkristalle", Freiburg 1991
- /4/S. A. Pikin, Strukturniye Prevrasceniya v zidkikh kristallach, Nauka, Moscow 1981
- /5/K. Skarp and M.A. Handschy, Mol. Cryst. Liq. Cryst., **165**, 439, (1988)
- /6/N.A. Clark and S.T. Lagerwall, Appl. Phys. Lett., **36**, 899 (1980)
- /7/N.A. Clark and S.T. Lagerwall, Ferroelectrics, **59**, 25 (1984)
- /8/M.A. Handschy, N.A. Clark and S.T. Lagerwall, Phys. Rev. Lett., **51**, 471 (1983)
- /9/P. Schiller, Cryst. Res. Technol., **21**, 176 (1986) and **21**, 301 (1986)

SECTION K

THEORY

ON THE ELASTIC FREE ENERGY OF SmC^* AND SmCa^* PHASES

MASAHIRO NAKAGAWA

Department of Electrical Engineering, Faculty of Engineering, Nagaoka University of Technology, Kamitomioka 1603-1, Nagaoka, Niigata 940-21, Japan

Abstract Complete elastic free energy expressions for ferroelectric SmC^* and antiferroelectric SmCa^* phases are derived within a quadratic expansion in terms of the spatial derivatives of the biaxial tensor order parameter Q_{ij} as well as an orthogonal triad. It is found that there exist 25 non-chiral terms, 5 of which are found to be eventually reduced as certain surface contributions, and 5 chiral terms in bulk elastic energy. As a few simple applications of the present free energy, the SmCa^* - SmC^* phase transition is discussed and the helical pitch in SmCa^* and SmC^* phases is explicitly derived in terms of the molecular tilt angle and the microscopic order parameters.

INTRODUCTION

The elastic free energy expressions of SmC and SmC^* liquid crystals have been extensively studied up to date¹⁻⁸. Recently the present author generalised the free energy so as to be concerned with the layer compression and the C-director distortion⁸. Utilising such an extended elastic free energy for compressible smectics, the chevron layer structure observed in homogeneously aligned SmC^* samples⁹⁻¹² has been analysed and found to be described as a soliton-like solution¹³⁻¹⁵ in qualitatively consistence with the experimentally observed temperature dependence of the chevron layer profile showing the layer inclination angle and the sharpness of the chevrons⁹⁻¹².

Antiferroelectric smectic phase SmCa^* was recently found by Chandani et al.^{16,17} Recently the phenomenological free energy of SmC^* derived by Pikin and Indenbom⁴ was extended by Orihara and Ishibashi in

order to account for the possible phase transitions¹⁷. As far as we are aware, there has not been reported a general expression for SmCa^* elastic free energy concerned with the layer distortion as well as the molecular alignment.

In the present paper, a complete expression of the elastic free energy of SmC^* which includes SmCa^* will be derived in similar way to the previously studied biaxial cholesterics¹⁶. As a few simple applications, we shall focus our interest on the $\text{SmCa}^*-\text{SmC}^*$ phase transition as well as the above-mentioned temperature dependence of the helical pitch near the critical points^{21-27, 29}.

ELASTIC FREE ENERGY

First of all let us mention the biaxial tensor order parameter which characterize the microscopic molecular alignments. Choosing an orthogonal triad a - b - c as principal axes in the local frame, the elastic free energy may be expanded in terms of spatial gradients of the biaxial traceless tensor order parameters, Q_{ij} as follows

$$\begin{aligned} Q_{ij} &= (2S/3)a_i a_j + (-S/3+B)b_i b_j + (-S/3-B)c_i c_j \\ &= S(a_i a_j - \delta_{ij}/3) + B(b_i b_j - c_i c_j), \end{aligned} \quad (1)$$

where S and B represent the uniaxial and the biaxial orderings about a , respectively. These microscopic order parameters, S and B may depend on the temperature and also on the molecular tilt angle θ_m and are assumed to be constant throughout an isothermal sample under consideration. a is assumed to be the average molecular orientation which is coincident with the layer normal unit vector k in SmCa^* phase^{16, 17}. On the other hand, the principal axis a just corresponds to the n -director in the SmC^* phase.⁸ Thus, in the present model, a is chosen as a principal axis in the local D_2 symmetry. Noting that $Q_{ij,k} p_j = 0$ ($p_i = a_i, b_i, c_i$), the basic scalar quantities constructed by $Q_{ij,k}$ and $P_i = P b_i$ as well as a - b - c triad are defined as follows,

$$\left. \begin{array}{lll} (a \cdot \nabla Q : bc)^* & (a \cdot \nabla Q : ca) & (a \cdot \nabla Q : ab)^* \\ (b \cdot \nabla Q : bc) & (b \cdot \nabla Q : ca)^* & (b \cdot \nabla Q : ab) \\ (c \cdot \nabla Q : bc)^* & (c \cdot \nabla Q : ca) & (c \cdot \nabla Q : ab)^* \\ & (b \cdot P)^* & \end{array} \right\} \quad (2)$$

where $(x \cdot \nabla Q : yz) = x_k Q_{ij,k} y_j z_k$, $(x \cdot P) = x_i P_i$ ($P_i = p_i, p_i$), *

stands for the chiral quantities or the pseudo-scalars which change their signs under improper transformations. Since we choose a-b-c triad as axes of the local D_2 symmetry, the above scalars are sufficient to derive the elastic free energy concerned with Q_{ijk} and P_i . Then \mathbf{p} and \mathbf{p} are the spontaneous polarization vectors in the odd-numbered layers and in the even-numbered ones, respectively^{16,17}. If we consider only a unit layer, the dipole alignment is ferroelectric even in the SmC_A^* phase.^{16,17} In similar to the Pikin and Indenbom's phenomenological theory of SmC^* phase,⁴ the polarization vectors, \mathbf{p} and \mathbf{p} , in each layer must be determined by minimizing the local electrostatic energy concerned with them. Since we assume that \mathbf{a} and \mathbf{c} are genuine vectors, $\mathbf{b} = \mathbf{c} \times \mathbf{a}$ is defined as an axial vector, or a pseudo-vector. Making an isotropic scalar as the free energy within possible combinations between the above scalars in (2) up to 2nd order in Q_{ijk} and p_i and p_i , and ignoring some surface contributions, one may derive the following elastic free energy in C_2 symmetry of SmC^* phase as

$$F = F_{non} + F^* + F_p, \quad (3)$$

where F_{non} is a non-chiral part, F^* a chiral part, and F_p a ferroelectric part, divided into F_p^0 and F_p^1 , as follows

$$\begin{aligned} F_{non} = & \frac{L_1}{2} (\mathbf{a} \cdot \nabla \mathbf{Q} : \mathbf{bc})^2 + \frac{L_2}{2} (\mathbf{a} \cdot \nabla \mathbf{Q} : \mathbf{ca})^2 + \frac{L_3}{2} (\mathbf{a} \cdot \nabla \mathbf{Q} : \mathbf{ab})^2 \\ & + \frac{L_4}{2} (\mathbf{b} \cdot \nabla \mathbf{Q} : \mathbf{bc})^2 + \frac{L_5}{2} (\mathbf{b} \cdot \nabla \mathbf{Q} : \mathbf{ca})^2 + \frac{L_6}{2} (\mathbf{b} \cdot \nabla \mathbf{Q} : \mathbf{ab})^2 \\ & + \frac{L_7}{2} (\mathbf{c} \cdot \nabla \mathbf{Q} : \mathbf{bc})^2 + \frac{L_8}{2} (\mathbf{c} \cdot \nabla \mathbf{Q} : \mathbf{ca})^2 + \frac{L_9}{2} (\mathbf{c} \cdot \nabla \mathbf{Q} : \mathbf{ab})^2 \\ & + L_{10} (\mathbf{a} \cdot \nabla \mathbf{Q} : \mathbf{bc}) (\mathbf{a} \cdot \nabla \mathbf{Q} : \mathbf{ab}) + L_{11} (\mathbf{a} \cdot \nabla \mathbf{Q} : \mathbf{bc}) (\mathbf{b} \cdot \nabla \mathbf{Q} : \mathbf{ca}) \\ & + L_{12} (\mathbf{a} \cdot \nabla \mathbf{Q} : \mathbf{bc}) (\mathbf{c} \cdot \nabla \mathbf{Q} : \mathbf{bc}) + L_{13} (\mathbf{a} \cdot \nabla \mathbf{Q} : \mathbf{bc}) (\mathbf{c} \cdot \nabla \mathbf{Q} : \mathbf{ab}) \\ & + L_{14} (\mathbf{a} \cdot \nabla \mathbf{Q} : \mathbf{ab}) (\mathbf{b} \cdot \nabla \mathbf{Q} : \mathbf{ca}) + L_{15} (\mathbf{a} \cdot \nabla \mathbf{Q} : \mathbf{ab}) (\mathbf{c} \cdot \nabla \mathbf{Q} : \mathbf{ab}) \\ & + L_{16} (\mathbf{b} \cdot \nabla \mathbf{Q} : \mathbf{ca}) (\mathbf{c} \cdot \nabla \mathbf{Q} : \mathbf{bc}) + L_{17} (\mathbf{b} \cdot \nabla \mathbf{Q} : \mathbf{ca}) (\mathbf{c} \cdot \nabla \mathbf{Q} : \mathbf{ab}) \\ & + L_{18} (\mathbf{c} \cdot \nabla \mathbf{Q} : \mathbf{bc}) (\mathbf{c} \cdot \nabla \mathbf{Q} : \mathbf{ab}) + L_{19} (\mathbf{a} \cdot \nabla \mathbf{Q} : \mathbf{ca}) (\mathbf{c} \cdot \nabla \mathbf{Q} : \mathbf{ca}) \\ & + L_{20} (\mathbf{b} \cdot \nabla \mathbf{Q} : \mathbf{bc}) (\mathbf{b} \cdot \nabla \mathbf{Q} : \mathbf{ab}), \end{aligned} \quad (4)$$

$$\begin{aligned} F^* = & D_1 (\mathbf{a} \cdot \nabla \mathbf{Q} : \mathbf{bc}) + D_2 (\mathbf{a} \cdot \nabla \mathbf{Q} : \mathbf{ab}) + D_3 (\mathbf{b} \cdot \nabla \mathbf{Q} : \mathbf{ca}) \\ & + D_4 (\mathbf{c} \cdot \nabla \mathbf{Q} : \mathbf{bc}) + D_5 (\mathbf{c} \cdot \nabla \mathbf{Q} : \mathbf{ab}), \end{aligned} \quad (5)$$

$$\begin{aligned} F_p^0 = & 1/(2\chi) (\mathbf{p}^2 + \mathbf{p}^2) + d_0 \{ (\mathbf{b} \cdot \mathbf{p}) + (\mathbf{b} \cdot \mathbf{p}) \} \\ & + d_c (\mathbf{b} \cdot \mathbf{b}) + d_a (\mathbf{b} \cdot \mathbf{b})^2, \end{aligned} \quad (6)$$

$$\begin{aligned} F_p^1 = & d_1 (\mathbf{a} \cdot \nabla \mathbf{Q} : \mathbf{bc}) (\mathbf{b} \cdot \mathbf{p}) + d_2 (\mathbf{a} \cdot \nabla \mathbf{Q} : \mathbf{ab}) (\mathbf{b} \cdot \mathbf{p}) \\ & + d_3 (\mathbf{b} \cdot \nabla \mathbf{Q} : \mathbf{ca}) (\mathbf{b} \cdot \mathbf{p}) + d_4 (\mathbf{c} \cdot \nabla \mathbf{Q} : \mathbf{bc}) (\mathbf{b} \cdot \mathbf{p}) \\ & + d_5 (\mathbf{c} \cdot \nabla \mathbf{Q} : \mathbf{ab}) (\mathbf{b} \cdot \mathbf{p}) \end{aligned}$$

$$\begin{aligned}
& + d_1(a \cdot \nabla Q:bc)(\underline{b} \cdot \underline{p}) + d_2(a \cdot \nabla Q:ab)(\underline{b} \cdot \underline{p}) \\
& + d_3(b \cdot \nabla Q:ca)(\underline{b} \cdot \underline{p}) + d_4(c \cdot \nabla Q:bc)(\underline{b} \cdot \underline{p}) \\
& + d_5(c \cdot \nabla Q:ab)(\underline{b} \cdot \underline{p}) ,
\end{aligned} \tag{7}$$

respectively, where while L_1-L_{20} are the non-chiral elastic constants, D_1-D_5 are chiral ones, χ is the dielectric susceptibility related to the local dipole-dipole interaction, d_0 is the piezo-electric constant, d_1-d_5 are the flexo-electric coefficients related to the director distortion, b and \underline{b} are a couple of unit vectors defined by $(c \times a)$ in the odd-numbered layers and the even-numbered ones, respectively, d_0 is a polar coupling constant between b (or p) and \underline{b} (or \underline{p}) and considered to be positive to prefer $b \cdot \underline{b} = -1$ in SmC_A^* phase and negative to prefer $b \cdot \underline{b} = 1$ in SmC^* one , respectively, and d_4 is a quadrupole coupling between molecules in the adjacent layers. Here F_p^0 is introduced phenomenologically in analogous to the Landau approach for SmC^* phase by Pikin and Indenbom.⁴ For SmC_A^* phase with the local D_2 symmetry, $L_{10} = L_{12} = L_{14} = L_{15} = L_{16} = L_{18} = L_{19} = L_{20} = L_{23} = L_{24} = 0$, $D_2 = D_4 = 0$, and $d_2 = d_4 = 0$ because the elastic free energy in SmC_A^* phase must be invariant under such independent operation as $a \rightarrow \pm a$, $b \rightarrow \pm b$ and $c \rightarrow \pm c$ with $b = -\underline{b}$.

Then minimizing $F_p = F_p^0 + F_p^1$ with respect to p and \underline{p} , one readily finds

$$\begin{aligned}
p &= -\chi \{ d_0 + d_1(a \cdot \nabla Q:bc) + d_2(a \cdot \nabla Q:ab) \\
&+ d_3(b \cdot \nabla Q:ca) + d_4(c \cdot \nabla Q:bc) + d_5(c \cdot \nabla Q:ab) \} b \\
&= P b ,
\end{aligned} \tag{8}$$

$$\begin{aligned}
\underline{p} &= -\chi \{ d_0 + d_1(a \cdot \nabla Q:bc) + d_2(a \cdot \nabla Q:ab) \\
&+ d_3(b \cdot \nabla Q:ca) + d_4(c \cdot \nabla Q:bc) + d_5(c \cdot \nabla Q:ab) \} \underline{b} \\
&= P \underline{b} .
\end{aligned} \tag{9}$$

While $b = \underline{b}$, or $p = \underline{p}$ in SmC^* phase , $b = -\underline{b}$ or $p = -\underline{p}$ in SmC_A^* phase. Substituting (8) and (9) into (6), one has

$$\begin{aligned}
F &= \frac{L_1}{2} (a \cdot \nabla Q:bc)^2 + \frac{L_2}{2} (a \cdot \nabla Q:ca)^2 + \frac{L_3}{2} (a \cdot \nabla Q:ab)^2 \\
&+ \frac{L_4}{2} (b \cdot \nabla Q:bc)^2 + \frac{L_5}{2} (b \cdot \nabla Q:ca)^2 + \frac{L_6}{2} (b \cdot \nabla Q:ab)^2 \\
&+ \frac{L_7}{2} (c \cdot \nabla Q:bc)^2 + \frac{L_8}{2} (c \cdot \nabla Q:ca)^2 + \frac{L_9}{2} (c \cdot \nabla Q:ab)^2 \\
&+ \underline{L}_{10} (a \cdot \nabla Q:bc)(a \cdot \nabla Q:ab) + \underline{L}_{11} (a \cdot \nabla Q:bc)(b \cdot \nabla Q:ca) \\
&+ \underline{L}_{12} (a \cdot \nabla Q:bc)(c \cdot \nabla Q:bc) + \underline{L}_{13} (a \cdot \nabla Q:bc)(c \cdot \nabla Q:ab) \\
&+ \underline{L}_{14} (a \cdot \nabla Q:ab)(b \cdot \nabla Q:ca) + \underline{L}_{15} (a \cdot \nabla Q:ab)(c \cdot \nabla Q:ab)
\end{aligned}$$

$$\begin{aligned}
& + \underline{L}_{16}(\mathbf{b} \cdot \nabla \mathbf{Q} : \mathbf{ca})(\mathbf{c} \cdot \nabla \mathbf{Q} : \mathbf{bc}) + \underline{L}_{17}(\mathbf{b} \cdot \nabla \mathbf{Q} : \mathbf{ca})(\mathbf{c} \cdot \nabla \mathbf{Q} : \mathbf{ab}) \\
& + \underline{L}_{18}(\mathbf{c} \cdot \nabla \mathbf{Q} : \mathbf{bc})(\mathbf{c} \cdot \nabla \mathbf{Q} : \mathbf{ab}) + \underline{L}_{19}(\mathbf{a} \cdot \nabla \mathbf{Q} : \mathbf{ca})(\mathbf{c} \cdot \nabla \mathbf{Q} : \mathbf{ca}) \\
& + \underline{L}_{20}(\mathbf{b} \cdot \nabla \mathbf{Q} : \mathbf{bc})(\mathbf{b} \cdot \nabla \mathbf{Q} : \mathbf{ab}) \\
& + \underline{D}_1(\mathbf{a} \cdot \nabla \mathbf{Q} : \mathbf{bc}) + \underline{D}_2(\mathbf{a} \cdot \nabla \mathbf{Q} : \mathbf{ab}) + \underline{D}_3(\mathbf{b} \cdot \nabla \mathbf{Q} : \mathbf{ca}) \\
& + \underline{D}_4(\mathbf{c} \cdot \nabla \mathbf{Q} : \mathbf{bc}) + \underline{D}_5(\mathbf{c} \cdot \nabla \mathbf{Q} : \mathbf{ab}) \\
& + d_c(\mathbf{b} \cdot \underline{\mathbf{b}}) + d_a(\mathbf{b} \cdot \underline{\mathbf{b}})^2, \tag{10}
\end{aligned}$$

where we omitted a surface contribution as well as a trivial constant $-(\chi/2)d_0^2$, and the underlined, i.e. renormalized, the elastic coefficients are defined by

$$\begin{aligned}
\underline{L}_1 &= L_1 - 2\chi d_1^2, \quad \underline{L}_3 = L_3 - 2\chi d_2^2, \quad \underline{L}_5 = L_5 - 2\chi d_3^2, \\
\underline{L}_7 &= L_7 - 2\chi d_4^2, \quad \underline{L}_9 = L_9 - 2\chi d_5^2, \quad \underline{L}_{10} = L_{10} - 2\chi d_1 d_2, \\
\underline{L}_{11} &= L_{11} - 2\chi d_1 d_3, \quad \underline{L}_{12} = L_{12} - 2\chi d_1 d_4, \\
\underline{L}_{13} &= L_{13} - 2\chi d_1 d_5 - 2\chi d_2 d_4, \quad \underline{L}_{14} = L_{14} - 2\chi d_2 d_3, \\
\underline{L}_{15} &= L_{15} - 2\chi d_2 d_5, \quad \underline{L}_{16} = L_{16} - 2\chi d_3 d_4, \\
\underline{L}_{17} &= L_{17} - 2\chi d_3 d_5, \quad \underline{L}_{18} = L_{18} - 2\chi d_4 d_5, \\
\underline{D}_1 &= D_1 - 2\chi d_0 d_1, \quad \underline{D}_2 = D_2 - 2\chi d_0 d_2, \quad \underline{D}_3 = D_3 - 2\chi d_0 d_3, \\
\underline{D}_4 &= D_4 - 2\chi d_0 d_4, \quad \underline{D}_5 = D_5 - 2\chi d_0 d_5. \tag{11}
\end{aligned}$$

On the other hand, in the SmC_A^* phase with D_2 symmetry, we have

$$\begin{aligned}
F &= \frac{\underline{L}_1}{2}(\mathbf{a} \cdot \nabla \mathbf{Q} : \mathbf{bc})^2 + \frac{\underline{L}_2}{2}(\mathbf{a} \cdot \nabla \mathbf{Q} : \mathbf{ca})^2 + \frac{\underline{L}_3}{2}(\mathbf{a} \cdot \nabla \mathbf{Q} : \mathbf{ab})^2 \\
&+ \frac{\underline{L}_4}{2}(\mathbf{b} \cdot \nabla \mathbf{Q} : \mathbf{bc})^2 + \frac{\underline{L}_5}{2}(\mathbf{b} \cdot \nabla \mathbf{Q} : \mathbf{ca})^2 + \frac{\underline{L}_6}{2}(\mathbf{b} \cdot \nabla \mathbf{Q} : \mathbf{ab})^2 \\
&+ \frac{\underline{L}_7}{2}(\mathbf{c} \cdot \nabla \mathbf{Q} : \mathbf{bc})^2 + \frac{\underline{L}_8}{2}(\mathbf{c} \cdot \nabla \mathbf{Q} : \mathbf{ca})^2 + \frac{\underline{L}_9}{2}(\mathbf{c} \cdot \nabla \mathbf{Q} : \mathbf{ab})^2 \\
&+ \underline{L}_{11}(\mathbf{a} \cdot \nabla \mathbf{Q} : \mathbf{bc})(\mathbf{b} \cdot \nabla \mathbf{Q} : \mathbf{ca}) + \underline{L}_{13}(\mathbf{a} \cdot \nabla \mathbf{Q} : \mathbf{bc})(\mathbf{c} \cdot \nabla \mathbf{Q} : \mathbf{ab}) \\
&+ \underline{L}_{17}(\mathbf{b} \cdot \nabla \mathbf{Q} : \mathbf{ca})(\mathbf{c} \cdot \nabla \mathbf{Q} : \mathbf{ab}) \\
&+ \underline{D}_1(\mathbf{a} \cdot \nabla \mathbf{Q} : \mathbf{bc}) + \underline{D}_3(\mathbf{b} \cdot \nabla \mathbf{Q} : \mathbf{ca}) + \underline{D}_5(\mathbf{c} \cdot \nabla \mathbf{Q} : \mathbf{ab}) \\
&+ d_c(\mathbf{b} \cdot \underline{\mathbf{b}}) + d_a(\mathbf{b} \cdot \underline{\mathbf{b}})^2. \tag{12}
\end{aligned}$$

APPLICATION

In this section, let us present a few applications of the presently derived free energy.

1. SMC_A^* - SMC^* TRANSITION

First of all, let us discuss below the phase transition between SmC^* and SmC_A^* , assuming that the system is in a homogeneous helicoidal state, with a long helical pitch P_0 , along z axis. Since we can neglect the

spatial change of Q_{ij} compared with the non-elastic contribution F_p^0 for a relatively long helical pitch such that $P_0 \gg$ (layer distance \sim molecular length). In practice one can realize such a homogeneous state in the surface-stabilized thin film sample between two bounding plates.^{16, 17} In such a situation, we find that $p = -\chi d_0 b$, and $\underline{p} = -\chi d_0 \underline{b}$ as seen in the surface-stabilized sample between two bounding plates.^{16, 17}

$$F = d_0(b \cdot b) + d_1(b \cdot \underline{b})^2 \quad (13)$$

Here d_0 represents the polar interaction and is regarded as a function of temperature such that $d_0 > 0$ in SmC_A^* phase (lower temperature region) and $d_0 < 0$ in SmC^* phase (upper temperature region) as will be mentioned in the next section. It should be borne in mind that such a polar interaction results from the dipole-dipole interaction between the pairing molecules in the adjacent layers^{3, 2} and also from the excluded volume effect of the banana-like molecules.^{3, 3} Denoting $2\pi/P_0$ as q and assuming that the layer normal unit vector \mathbf{k} is coincident with z axis, \mathbf{b} and $\underline{\mathbf{b}}$ may be put into

$$\mathbf{b} = (\cos(\phi + qz), \sin(\phi + qz), 0) \quad (14a)$$

and

$$\underline{\mathbf{b}} = (\cos(\phi + qz), \sin(\phi + qz), 0) \quad (14b)$$

respectively, where ϕ and ϕ are the angles between \mathbf{b} and X axis, which rotates with the twist angle qz , and $\underline{\mathbf{b}}$ and X axis, respectively. Substituting these expressions into (13), we have

$$F = d_0 \cos \Phi + d_1 \cos^2 \Phi \quad (15)$$

where Φ is the phase difference between \mathbf{b} and $\underline{\mathbf{b}}$ and defined by $\phi - \phi$. Then we have the following derivatives to determine the $SmC_A^* - SmC^*$ transition point.

$$\frac{\partial F}{\partial \Phi} = -d_0 \sin \Phi - 2d_1 \sin \Phi \cos \Phi = 0 \quad (16a)$$

$$\frac{\partial^2 F}{\partial \Phi^2} = -d_0 \cos \Phi - 2d_1 \cos 2\Phi = 0 \quad (16b)$$

or

$$\sin 2\Phi = \kappa \sin \Phi \quad (17)$$

$$\cos 2\Phi = \frac{\kappa}{2} \cos \Phi \quad (18)$$

where κ is defined by $\kappa = -d_0/d_1$. From these, one readily has

$$\sin\Phi = \{(4-\kappa^2)/(3\kappa^2)\}^{1/2}, \cos\Phi = 2\{(\kappa^2-1)/(3\kappa^2)\}^{1/2}. \quad (19)$$

Therefore, to assure the existence of Φ at the transition point, κ^2 has to be restricted between 1 and 4. Then substituting (19) into (17), one readily finds

$$\kappa^2 = 4, 4/3. \quad (20)$$

Hence, corresponding to $\kappa^2=4$ and $\kappa^2=4/3$, we have

$$\sin\Phi = 0, \cos\Phi = 1 \quad (\kappa^2=4), \quad (21a)$$

and

$$\begin{aligned} \sin\Phi &= \{(8/3)/4\}^{1/2} = (2/3)^{1/2} \\ \cos\Phi &= 2\{(1/3)/4\}^{1/2} = (1/3)^{1/2} \end{aligned} \quad \left. \vphantom{\begin{aligned} \sin\Phi \\ \cos\Phi \end{aligned}} \right\} (\kappa^2=4/3). \quad (21b)$$

Here only the former case with $|\kappa|=2$ is non-trivial because $\Phi=0$ (Ferro) and $\Phi=\pi$ (AntiFerro) must be stable solutions which satisfy $\partial^2 F/\partial\Phi^2 > 0$ and $\partial F/\partial\Phi = 0$, simultaneously. From (17) to satisfy $\partial F/\partial\Phi = 0$, one has

$$\sin\Phi = 0, \quad (22a)$$

or

$$\cos\Phi = \kappa/2. \quad (22b)$$

Then the corresponding values of $\partial^2 F/\partial\Phi^2$ are given by

$$\frac{\partial^2 F}{\partial\Phi^2} = -d_a(2-\kappa) \quad (\Phi=0), \quad (23a)$$

$$\frac{\partial^2 F}{\partial\Phi^2} = -d_a(2+\kappa) \quad (\Phi=\pi), \quad (23b)$$

$$\frac{\partial^2 F}{\partial\Phi^2} = -2^{-1}d_a(\kappa^2-4) \quad (\Phi=\cos^{-1}(\kappa/2)). \quad (23c)$$

Therefore one has the following three possible states depending on $\Phi = 0, \pi$ and $\cos^{-1}(\kappa/2)$.

$$F = d_c + d_a = d_a(1-\kappa), \quad (\Phi=0) \quad (24a)$$

$$F = -d_c + d_a = d_a(1+\kappa), \quad (\Phi=\pi) \quad (24b)$$

$$F = d_c\kappa/2 + d_a\{2(\kappa/2)^2 - 1\} = -d_a, \quad (\Phi=\cos^{-1}(\kappa/2)) \quad (24c)$$

From these energies together with (23a)-(23c), one finds the following two possible phase sequences corresponding to the sign of d_a .

(Case I : $d_a < 0$)

$$\Phi = 0 \quad (\kappa < 0) \quad \text{SmC}^* \text{ state} \quad (25a)$$

$$\Phi = \pi \quad (\kappa > 0) \quad \text{SmC}_A^* \text{ state} \quad (25b)$$

(Case II : $d_q > 0$)

$$\Phi = 0 \quad (\kappa > 2) \quad \text{SmC}^* \text{ state} \quad (26a)$$

$$\Phi = \cos^{-1}(\kappa/2) \quad (-2 < \kappa < 2) \quad \text{Ferrielectric State} \quad (26b)$$

$$\Phi = \pi \quad (\kappa < -2) \quad \text{SmC}_A^* \text{ state} \quad (26c)$$

Therefore it is concluded that while the $\text{SmC}_A^* - \text{SmC}^*$ transition is of the first-order for the Case I with $d_q < 0$, it is of the second-order one via a ferrielectric phase state for the Case II with $d_q > 0$. In practice since the molecules prefer the parallel alignment, d_q is expected to be negative in general. Hence the polarization vectors in the adjacent layers in the SmC_A^* phase are anti-parallel each other in consistence with the experimental finding.^{16, 17} Now assuming that d_c is a linear function of the temperature T defined by $d_c^\theta(1-T/T_{cA})$ ($d_c^\theta > 0$, T_{cA} : $\text{SmC}_A^* - \text{SmC}^*$ transition temperature) and d_q is a negative constant, the entropy Σ and the internal energy U can be readily derived as,

$$\Sigma = - \frac{\partial F}{\partial T} = + \frac{d_c^\theta}{T_{cA}} \cos \Phi, \quad (27a)$$

$$\begin{aligned} U &= F + \Sigma T \\ &= d_c^\theta \cos \Phi + d_q \cos^2 \Phi \end{aligned} \quad (27b)$$

Therefore, for the Case I showing a first-order $\text{SmC}_A^* - \text{SmC}^*$ transition, the transition entropy $\Delta\Sigma$ and the latent heat ΔU are given by

$$\begin{aligned} \Delta\Sigma &= \Sigma(\Phi=0) - \Sigma(\Phi=\pi) \\ &= 2d_c^\theta/T_{cA} \end{aligned}, \quad (28a)$$

and

$$\begin{aligned} \Delta U &= U(\Phi=0) - U(\Phi=\pi) \\ &= 2d_c^\theta \end{aligned}, \quad (28b)$$

respectively. Finally a normalized total polarization p_r may be defined by

$$\begin{aligned} p_r &= \cos(\phi + qz - \phi_n) + \cos(\phi + qz - \phi_n) \\ &= 2\cos(\Phi/2) \end{aligned}, \quad (29)$$

where $\phi_n = (\phi + \phi)/2 + qz$. In conclusion, for the above-mentioned two cases, one finds the following phase sequences.

(Case I : $d_q < 0$)

$$\left. \begin{array}{lll} p_r = 0 & (\kappa > 0) & (\text{SmC}_A^*) \\ p_r = 2 & (\kappa < 0) & (\text{SmC}^*) \end{array} \right\} \quad (30a)$$

(Case II : $d_q > 0$)

$$\left. \begin{array}{lll} p_r = 0 & (\kappa < -2) & (\text{SmC}_A^*) \\ p_r = 2^{1/2}(1+\kappa/2)^{1/2} & (-2 < \kappa < 2) & (\text{Ferri}) \\ p_r = 2 & (\kappa > 2) & (\text{SmC}^*) \end{array} \right\} \quad (30b)$$

Although we neglected here the spatial change of Q_{ij} for simplicity similar to the previous work by Orihara and Ishibashi,¹⁷ the present result remains to be qualitatively correct even in the helicoidal structure as far as such a structural change is in the macroscopic range such that $P_0 \gg$ molecular length.

2. HELICAL PITCHES IN SMC^* AND SMC_A^* PHASES

In this subsection let us derive to the temperature dependent helical pitch in SmC^* and SmC_A^* phases^{21-27,29}. For simplicity let us assume that S and B are constant throughout the sample in an isothermal state.

First of all let us take the z axis along the layer normal direction, k . Supposing a homogeneous helicoidal structure along z axis, one may put a - b - c as follows

$$a = (\eta \cos qz, \eta \sin qz, \xi) \quad , \quad (31a)$$

$$b = (\sin qz, -\cos qz, 0) \quad , \quad (31b)$$

$$c = (\xi \cos qz, \xi \sin qz, -\eta) \quad , \quad (31c)$$

where q is the wave number of the homogeneous helix, $\eta = \sin \theta$ and $\xi = \cos \theta$; here θ is the angle between a and k , which is equal to θ_m in SmC^* phase and to 0 in SmC_A^* phase as was previously noted. Substituting (31a)-(31c) into (11) and ignoring such a constant as $d_c(b \cdot b) + d_a(b \cdot b)^2 = d_a \pm d_c$ ($d_a < 0$), one finds

$$F = \frac{1}{2} L(S, B, \theta) q^2 + D(S, B, \theta) q \quad , \quad (33)$$

where $L(S, B, \theta)$ and $D(S, B, \theta)$ are defined by

$$\begin{aligned} L(S, B, \theta) = & \underline{L}_1 \{2B\}^2 \xi^4 + \underline{L}_3 (S-B)^2 \eta^2 \xi^2 + \underline{L}_7 \{2B\}^2 \eta^2 \xi^2 \\ & + \underline{L}_9 (S-B)^2 \eta^4 - \underline{L}_{10} \{2B\} (S-B) \eta \xi^3 - \underline{L}_{12} \{2B\}^2 \eta \xi^3 \\ & + \underline{L}_{13} \{2B\} (S-B) \eta^2 \xi^2 - \underline{L}_{15} (S-B)^2 \eta^3 \xi - \underline{L}_{18} \{2B\} (S-B) \eta^3 \xi \quad , \end{aligned} \quad (34a)$$

and

$$D(S, B, \theta) = \underline{D}_1 \{2B\} \xi^2 - \underline{D}_2 (S-B) \eta \xi - \underline{D}_4 \{2B\} \eta \xi + \underline{D}_5 (S-B) \eta^2 \quad , \quad (34b)$$

respectively. From this one derives the equilibrium value of q as

$$q = - \frac{D(S, B, \theta)}{L(S, B, \theta)} = - \frac{2\pi}{P_\theta} \quad , \quad (35)$$

where P_θ is the natural pitch. The molecular tilt angle θ_m may be determined by minimizing the following free energy, F_{LD} , which includes the free energy related to the molecular tilt^{4, 24, 30}

$$F_{LD} = \frac{\alpha^\theta (T - T_c)}{2} \theta_m^2 + \frac{\beta}{4} \theta_m^4 + F \quad , \quad (36a)$$

where α^θ and β are assumed to be positive constants, and T_c denotes the Curie temperature. Furthermore, making use of (36a), we have

$$F_{LD} = \frac{\alpha^\theta (T - T_c)}{2} \theta_m^2 + \frac{\beta}{4} \theta_m^4 - \frac{\{D(S, B, \theta)\}^2}{2 L(S, B, \theta)} \quad . \quad (36b)$$

Minimizing F_{LD} with respect to θ_m at a given temperature, one can determine the temperature dependent tilt angle $\theta_m(T)$ and also the helical pitch $P_\theta(T)$ from (35). As a first approximation one may approximate θ_m as $\theta_m \approx \{(\alpha^\theta/\beta)(T_c - T)\}^{1/2}$.

To the end of this section, let us present the temperature dependence of the wave number q for SmC^* phase given by (35), i.e.

$$q_c = - \frac{\tau_1 \xi^2 + \tau_2 \eta^2 - \tau_1^* \eta \xi}{\lambda_1 \xi^4 + \lambda_2 \eta^2 \xi^2 + \lambda_3 \eta^4 - \lambda_1^* \eta \xi^3 - \lambda_2^* \eta^3 \xi} \quad , \quad (37a)$$

where we defined as

$$\lambda_1 = \underline{L}_1 \{2B\}^2 \quad , \quad : \xi^4 \quad (38a)$$

$$\lambda_2 = \underline{L}_3 (S-B)^2 + \underline{L}_7 \{2B\}^2 + \underline{L}_{13} \{2B\} (S-B) \quad , \quad : \eta^2 \xi^2 \quad (38b)$$

$$\lambda_3 = \underline{L}_9 (S-B)^2 \quad , \quad : \eta^4 \quad (38c)$$

$$\lambda_1^* = \underline{L}_{10} \{2B\} (S-B) + \underline{L}_{12} \{2B\}^2 \quad , \quad : \eta \xi^3 \quad (38d)$$

$$\lambda_2^* = \underline{L}_{15} (S-B)^2 + \underline{L}_{18} \{2B\} (S-B) \quad , \quad : \eta^3 \xi \quad (38e)$$

$$\tau_1 = \underline{D}_1 \{2B\} \quad , \quad : \xi^2 \quad (38f)$$

$$\tau_2 = \underline{D}_5 (S-B) \quad , \quad : \eta^2 \quad (38g)$$

$$\tau_1^* = \underline{D}_2 (S-B) + \underline{D}_4 \{2B\} \quad . \quad : \eta \xi \quad (38h)$$

Here $\eta = \sin \theta_m$, $\xi = \cos \theta_m$ because of $\theta = \theta_m$ in SmC^* phase. On the other hand, for SmC_A^* phase with D_2 symmetry^{16, 17} with $\theta = 0$ and $\theta_m \neq 0$, or $b + \underline{b} = 0$. Then the corresponding wave number q_{cA} is reduced to

$$q_{cA} = - \frac{\tau_1}{\lambda_1} = - \frac{\underline{D}_1}{\underline{L}_1 (2B)} \quad (37b)$$

Since $B=B(\theta_*)$ can be put as $B=B_0\cos^2\theta_*+B_1\sin^2\theta_*$ in SmC_A^* phase, where B_0 and B_1 are constants, q_{cA} may also show a temperature dependence through the temperature dependence of θ_* . From (37a) and (37b) one may infer that the helical pitch shows a jump at the first-order SmC_A^* - SmC^* transition point as was observed in experiments²⁹.

DISCUSSIONS AND CONCLUSIONS

In this work, we have obtained a complete expression of the elastic free energy in SmC^* and SmC_A^* on the basis of an tensor order parameter expansion approach¹⁸. For SmC^* phase, one finds 20 non-chiral and 5 chiral terms in addition to 5 surface terms, two of which are significantly dependent on each other. On the other hand, for SmC_A^* phase, it is found that there exist 12 non-chiral and 3 chiral terms in similar to the biaxial cholesterics¹⁸⁻²⁰. We have also investigated the phase transition between SmC_A^* and SmC^* phases and also derived the helical pitches in SmC^* and SmC_A^* phases in terms of the possible elastic constants as well as the microscopic order parameters³¹.

Now let us here discuss the presently derived SmC_A^* - SmC^* phase transition. In the experiments, SmC_A^* - SmC^* transition has been observed as the first-order one²⁹. From the present results, in fact, one may see that the transition between SmC_A^* and SmC^* is always first-order if $d_q < 0$. In practice one may expect $d_q < 0$ in general since the molecules prefer the parallel alignment such that $\mathbf{b} \cdot \mathbf{b} = \pm 1$. Finally let us mention the origin of the temperature dependence of d_c . In the lower temperature region with $T < T_{cA}$, the electrostatic dipole-dipole interaction has to be dominant to assure $\mathbf{b} \cdot \mathbf{b} < 0$, or $d_c > 0$. In an actual system, such an electrostatic interaction must be localized because of the pairing of permanent dipoles in the adjacent layers as was noted by Takanishi et al³². On the other hand, as the temperature increases or $T > T_{cA}$, the packing entropy due to the steric hindrance between the rod-like molecules will overcome the above dipole-dipole interaction to assure $\mathbf{b} \cdot \mathbf{b} > 0$, or $d_c < 0$. This is considered as the reason why SmC_A^* phase always appears in the lower temperature range, whereas SmC^* does in the upper one.

As a future problem, it seems to be worthwhile to compare quantitatively the presently derived helical pitch with the experimental ones²⁹ and also to extend the present free energy for the ferrielectric

phase^{16,17,29}.

REFERENCES

1. A. Saupe: Mol. Cryst. & Liq. Cryst., **7**, 59 (1969).
2. Orsay Group: Solid State Commun., **9**, 653 (1971).
3. A. Rapini: J. Phys. (Paris), **33**, 237 (1972).
4. S. A. Pikin and V. L. Indenbom: Sov. Phys. Usp., **21**, 487 (1978).
5. I. Dahl and S. T. Lagerwall: Ferroelectrics, **58**, 215 (1984).
6. L. A. Beresnev, L. M. Blinov, M. A. Osipov and S. A. Pikin: Mol. Cryst. & Liq. Cryst., **158A**, 3 (1988).
7. M. Nakagawa: J. Phys. Soc. Jpn., **58**, 2346 (1989).
8. M. Nakagawa: Liq. Cryst., **8**, 651 (1990).
9. N. A. Clark and S. T. Lagerwall: Proc. 6th International Display Research Conf. Tokyo, Japan, 456 (1986).
10. T. R. Rieker, N. A. Clark, G. S. Smith, D. S. Parmer, E. B. Sirota and C. R. Safinya: Phys. Rev. Lett., **59**, 2658 (1987).
11. Y. Ouchi, Ji Lee, H. Takezoe, A. Fukuda, K. Kondo, T. Kitamura and A. Mukoh: Jpn. J. Appl. Phys., **27**, L725 (1988).
12. N. A. Clark and T. P. Rieker: Phys. Rev. A (Rapid Commun.), **37**, 1053 (1988).
13. M. Nakagawa: Mol. Cryst. & Liq. Cryst., **174**, 65 (1989).
14. M. Nakagawa: Displays, **April**, 67 (1990).
15. M. Nakagawa: J. Phys. Soc. Jpn., **59**, 1995 (1990).
16. A. D. L. Chandani, Y. Ouchi, H. Takezoe, A. Fukuda, K. Terashima, K. Furukawa and A. Kishi: Jpn. J. Appl. Phys., **28**, L1261 (1989).
17. H. Orihara and Y. Ishibashi: Jpn. J. Appl. Phys., **29**, L115 (1990).
18. M. Nakagawa: J. Phys. Soc. Jpn., **59**, 4313 (1990).
19. H. R. Brand and H. Pleiner: Phys. Rev., **A26**, 1783 (1982).
20. E. Govers and G. Vertogen: Phys. Rev., **A30**, 1998 (1984).
21. R. Blinc and B. Zeks: Phys. Rev., **A18**, 740 (1987).
22. K. Kondo, H. Takezoe, A. Fukuda and E. Kuze: Jpn. J. Appl. Phys., **21**, 224 (1982).
23. R. Blinc, B. Zeks, I. Musevic and A. Levstik: Mol. Cryst. & Liq. Cryst., **114**, 189 (1984).
24. M. Nakagawa: Liq. Cryst., **3**, 573 (1988).
25. M. Yamashita and H. Kimura: J. Phys. Soc. Jpn., **51**, 2419 (1982).
26. C. C. Huang and S. Dumrongrattana: Phys. Rev., **A34**, 5020 (1987).
27. B. Zeks: Mol. Cryst. & Liq. Cryst., **114**, 259 (1984).
28. P. G. de Gennes: Mol. Cryst. & Liq. Cryst., **12**, 193 (1971).
29. Ji Li, H. Takezoe and A. Fukuda: Jpn. J. Appl. Phys., **30**, 532 (1991).

30. M. Nakagawa: Liq. Cryst., **3**, 63 (1988).
31. N. Kirov, I. Dozov, M. Petrov, M. P. Fontana and M. Rosi: Mol. Cryst. & Liq. Cryst., **103**, 71 (1984).
32. Y. Takanishi, K. Hiraoka, V. K. Agrawal, H. Takezoe, A. Fukuda and M. Mastushita: Jpn. J. Appl. Phys. (to be appeared).
33. M. Nakagawa: J. Phys. Soc. Jpn. (to be submitted).

OPTICAL STUDIES OF SMECTIC C* DISPLAYS

J.M. Otón, J.M.S. Pena, A. Serrano and F. Olarte

Dpt. Tecnología Fotónica - ETSI Telecomunicación

Ciudad Universitaria, 28040 Madrid Spain

ABSTRACT An accurate description of spectral and angular optical transmission is needed to characterize and optimize a liquid crystal display. Actual FLC display prototypes have been modelled from their director profiles. When broad spectrum backlights, color filters, and real polarizers are used, and several hundreds of oblique incidences are calculated, the running time may reach unpractical limits. A complete calculation process with reasonable running time is described. The results are compared to experimental measurements.

INTRODUCTION

The use of ferroelectric liquid crystals (FLC) for manufacturing high quality displays has drawn considerable attention since surface stabilized (SSFLC) bistable structures of these materials were reported by Clark and Lagerwall¹. A simple bookshelf geometry with uniform layers perpendicular to the glass plates was proposed, and a fast electrooptical switching was demonstrated. Further work by them and other researchers²⁻⁴, however, showed that the usual configurations found in real structures are far more complex: tilted bookshelf, chevrons, splayed chevrons, etc. Moreover³, the presence of either configuration depends on bulk properties of FLC materials as well as anchoring treatment of glass plates. The picture is further complicated by the usual presence of several kinds of defects. This behavior has somewhat delayed the manufacturing of FLC based commercial displays. Nevertheless, much effort has been done in the last few years^{5,6} to produce high performance display prototypes. In fact, FLC displays (FLCD) are the only current alternative to active matrix LC displays in the high end applications market, i.e. video rate, color, large area displays.

Several analyses of FLC optical transmission have been already presented⁷⁻⁹. In most cases, only normal incidence and/or monochromatic light input is considered. These approaches, though valuable, are not suitable to study the behavior of a real display in working conditions, where parameters such as viewing angle, angular contrast and color response are most important¹⁰. In any case, the optical transmission of the system can be calculated from the director profile. Much work has been done to derive the director orientation from molecular and energy-related parameters of the material¹¹⁻¹⁵, and boundary conditions^{14,16} but, unfortunately, the problem has not been completely solved yet. A semiempirical approach has been employed in this work, using experimental data when available, and completing the input parameters with assumptions based on physical grounds.

PROBLEM FORMULATION

As mentioned above, data from real optical elements must be used. The wavelength region from 380 nm to 770 nm in 10 nm steps is chosen, for most data from literature (C.I.E., for example) are expressed in this way. The following wavelength-dependent tables are needed to describe a FLC:

Backlight. Normalized emission spectrum. If RGB color filters are used, the normalized transmission of the combined backlight/filter system is employed.

Polarizers. Real and imaginary refractive indices of major and minor transmission axes.

FLC material. Ordinary and extraordinary refractive indices. No absorption is considered in the wavelength range.

In addition, data for tilt angles (i.e. smectic C cone angles) at different temperatures are needed to study transmission variations in the working range of temperatures. This range is usually well below the SmC \leftrightarrow SmA transition; therefore no "near transition" phenomena have been taken into account. In the examples given below, the following elements are used:

Backlight: C.I.E. D65¹⁷

Color filters: EMI RGB/standard fluorescent lamp¹⁸

Polarizers: G1220¹⁹

Material: ZLI 3654 (Merck)²⁰

Running times refer to a 25 MHz AT-386 microcomputer with 80387 mathematical coprocessor. The software packages are written in FORTRAN. A Microsoft 5.0 optimizing compiler has been used.

Normal and oblique incidence FLCD transmissions have been measured on a optical bench using a 5 mW unpolarized He-Ne laser and a large area (1 cm²) Hamamatsu photodiode connected to a Tektronix 100 MHz digital oscilloscope. Color coordinates experiments have been obtained from an EG&G optical multichannel analyzer (OMA) with a 5 ns-gated, 1024 photodiode/intensifier array. This setup allows the recording of time-resolved spectra at different times after switching.

MATHEMATICAL TREATMENT

The calculation is based on a 4×4 matrix formulation for anisotropic, stratified media, first applied to liquid crystals by Berreman^{21,22}. This provides a general method not limited to the case of normal incidence or special profiles, as it happens in Jones matrix formalism²³, Poincaré sphere methods²⁴ or geometrical optics²⁵. The truncated series expansion of Berreman's method is avoided using explicit expressions for 4×4 propagation matrices of homogeneous uniaxial slices of the material, as proposed by Wöhler *et al.*²⁶.

A single propagation matrix is computed for every wavelength and angle of incidence. This matrix is calculated as:

$$\mathcal{M}_T = \mathcal{M}_{P_2} \mathcal{M}_G \left(\prod_{i=1}^n \mathcal{M}_{LCi} \right) \mathcal{M}_G \mathcal{M}_{P_1} \quad (1)$$

where P, G, and LC stand for polarizer, glass, and liquid crystal. \mathcal{M}_P may be computed in a standard 4×4 matrix formulation, providing complex refractive indices are used. \mathcal{M}_G is computed as a single slice of isotropic material. Some adjustments needed to fit this procedure in the original Berreman's formulation are shown below.

To speed up the calculation, LC strata are computed propagating the beam in the opposite direction (i.e. from the exit side to the incidence side). This strategy avoids a matrix inversion at every wavelength and viewing angle; besides, these matrices –when polarizers are included– are quite ill-conditioned. When working with these matrices, the index of the product for \mathcal{M}_{LC} runs from 1 to n (i.e. from the incidence side to the exit side as opposed to the usual backwards calculation), as stated in Eq. (1).

A Fabry-Perot correction is applied to the results. As pointed out by Yang²⁷, this correction is needed to avoid unrealistic transmission oscillations produced by the use of several monochromatic wavelengths in the simulation of broad spectra. In practice, the only relevant Fabry-Perot interference affecting the calculations comes from the outermost air-glass interfaces. This is corrected in our model assuming two semi-infinite volumes of index-matching material at both sides of the cell (i.e. the interfaces are eliminated). Refraction of oblique incidences and Fresnel losses are taken into account in separate calculations.

A complete case for optical display characterization consists of the computation of clear and dark-state transmissions at 40 wavelengths (380-770 nm) for about 250 oblique incidences (viewing angle circles from normal to grazing incidence, 10° steps). Depending on the director profile, the FLC sample is split into 1-100 strata. Thus the worst case may lead to the calculation of roughly 2×10^6 transmission matrices for the liquid crystal and several thousand complex matrices for the polarizers. Our present running time for such a case is about 90 minutes for each state. No further big savings are expected unless parallel processing is used. For every angle and wavelength, two whole structures per second are computed. In any case, fairly good estimations of display transmission may be obtained in much less time, reducing the number of computed wavelengths or viewing angles. For example, a sketch of a display rotating in the computer screen, while varying its brightness and contrast, may be achieved almost in real time, for only a viewing angle need to be computed for every frame.

Besides this main module, several related packages have been derived, their running times being below 60 seconds in most cases: single wavelength transmission, spectral transmission for a given angle, color coordinates, and optimization of polarizer orientations.

In the following paragraphs, a geometrical study of the director orientation across the sample is performed. The main goal of this study is to narrow down the number of possible profiles for a given set of experimental conditions. Several configurations yield more than one (mathematical) solution for the director profile. In these cases, experimental data or energy considerations must be applied to decide the actual profile.

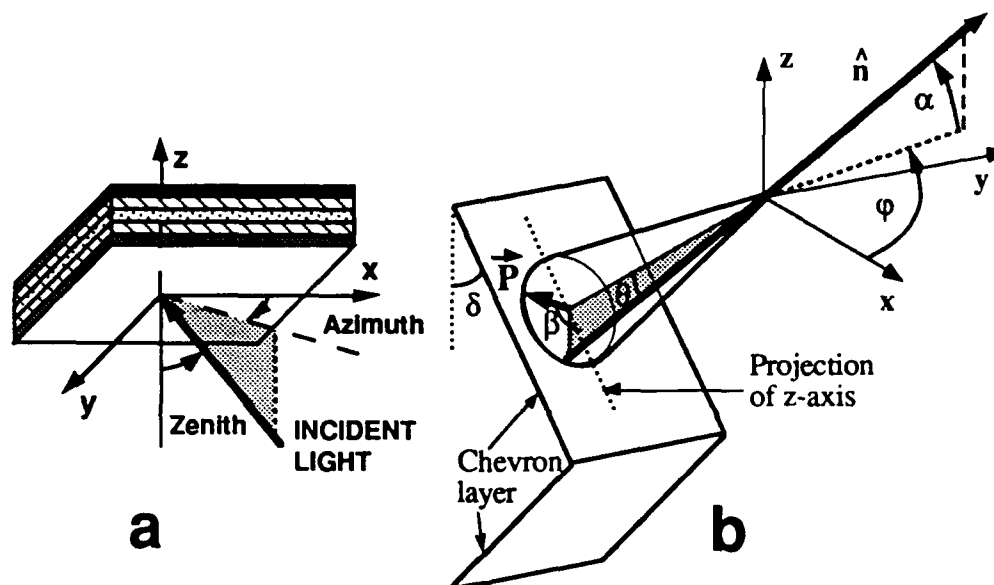


Figure 1. a) Coordinate framework for a display. b) Angles for the geometrical expressions. IPT and OPT are φ and α respectively.

Reference Frame

Figure 1a shows the coordinate system used. The sample is parallel to the x,y plane, normal incidence being along the z-axis. Oblique incidences are characterized by two angles, zenith and azimuth. Unpolarized incident light is simulated by propagating two orthogonal incoherent beams in the required direction.

Figure 1b shows the geometrical parameters of interest in a FLC material. A symmetric chevron case is represented. The homogeneous alignment yields smectic layers parallel to y-axis, forming an angle δ with z-axis. Pretilt angles at the incident surface are taken

positive. The pretilt at the other surface is assumed of the same magnitude unless otherwise stated. However, its sign may be positive or negative depending on whether parallel (-) or antiparallel (+) surface configuration is chosen. The chevron angle, δ , is taken positive when the chevron, taken as an arrow head, points towards the negative x direction ("natural" chevron in our framework).

The director orientation across the cell is described using two angles called in-plane tilt, φ , and out-of-plane tilt, α (IPT and OPT for short). IPT is the angle of the director projection on x-y plane with the x axis. OPT is the angle of the director with the x-y plane.

The OPT and IPT, the angle of the smectic layer (chevron or tilted bookshelf), δ , and the tilt angle of the director on the smectic C cone, θ , are related by the following expression:

$$\cos \theta = \cos \alpha \cos \varphi \cos \delta \pm \sin \delta \sin \alpha \quad (2)$$

where the plus sign applies to the first half of the chevron (incidence side) and the minus sign to the second half.

Director Orientation at the Surfaces

In the chevron case with parallel surface treatment (the most common), either none, one or two geometrical solutions may be found for the IPT director angle at the surface, given a pretilt angle (always positive at the first surface) and a layer angle. The OPT angle at the surface is determined by the pretilt, which depends on surface conditions.

$$\alpha = \alpha_0 \quad (3)$$

No solution for IPT is found when

$$\alpha_0 > |\delta| + \theta \quad (4)$$

If the above condition is avoided, one or two solutions are possible. It can be easily seen that the two solutions case corresponds to two opposite chevrons, with the same angle in magnitude and opposite directions. The range for only one solution to exist is

$$\theta - |\delta| < \alpha_0 \leq \theta + |\delta| \quad (5)$$

And the two solutions coexist when:

$$\alpha_0 \leq \theta - |\delta| \quad (6)$$

These ranges assume $\theta \geq |\delta|$. If $\theta < |\delta|$ only one solution for IPT is possible if $|\delta| - \theta \leq \alpha_0 \leq |\delta| + \theta$, and none exists outside this range. Whenever two solutions coexist, one corresponds to a "natural" chevron and the other to a "antinatural" chevron. The single solution ranges always yield "natural" chevrons.

Bookshelf and tilted bookshelf configurations can be easily derived as particular cases of the above chevron. A tilted bookshelf, under a geometrical point of view, is an asymmetric chevron 100%/0% (i.e. one of the chevron sides is extended over the whole cell thickness and the other is absent). A non-tilted bookshelf is simply a bookshelf where $\delta=0$. It should be noted that parallel or antiparallel glass surface treatment may affect the ranges of the solutions. A tilted bookshelf in a parallel configuration may meet condition (6) at the first surface, and still be not feasible, for (6) is not met at the other surface.

Director Orientation Across the Sample: Non-Splayed Cases.

Equation (2) shows the relationship between chevron, tilt, OPT and IPT angles. The first two angles are conditioned by the material and manufacturing process, and OPT is fixed at the surfaces by the pretilt. It is therefore reasonable to use available data for OPT variations and to derive IPT from them. Alternatively, OPT may be considered to be constant or negligible (low pretilt surface conditioning) and IPT may be assigned to a simple profile.

Several IPT/OPT profiles fairly matching experimental results have been found^{9, 28-30}. In most cases, chevron structures, either symmetric or splayed, are assumed. Symmetric chevron profiles may be roughly classified in two groups (Fig. 2).

- *Triangular Director Profile* (TDP). This simplified model can be used for low pretilt boundary conditions, allowing the use of Jones matrices for the calculations. OPT is neglected and IPT (called twist angle in⁹) is assumed to twist linearly from surface IPT to a

maximum in the middle of the cell and back to surface IPT at the second surface.

- *Boundary Layer Profile* (BLP^{9, 28}). Three regions are defined in this model. Two symmetrical regions at the surfaces linearly twist out IPT from its surface value to the central one. In the central region, IPT is constant.

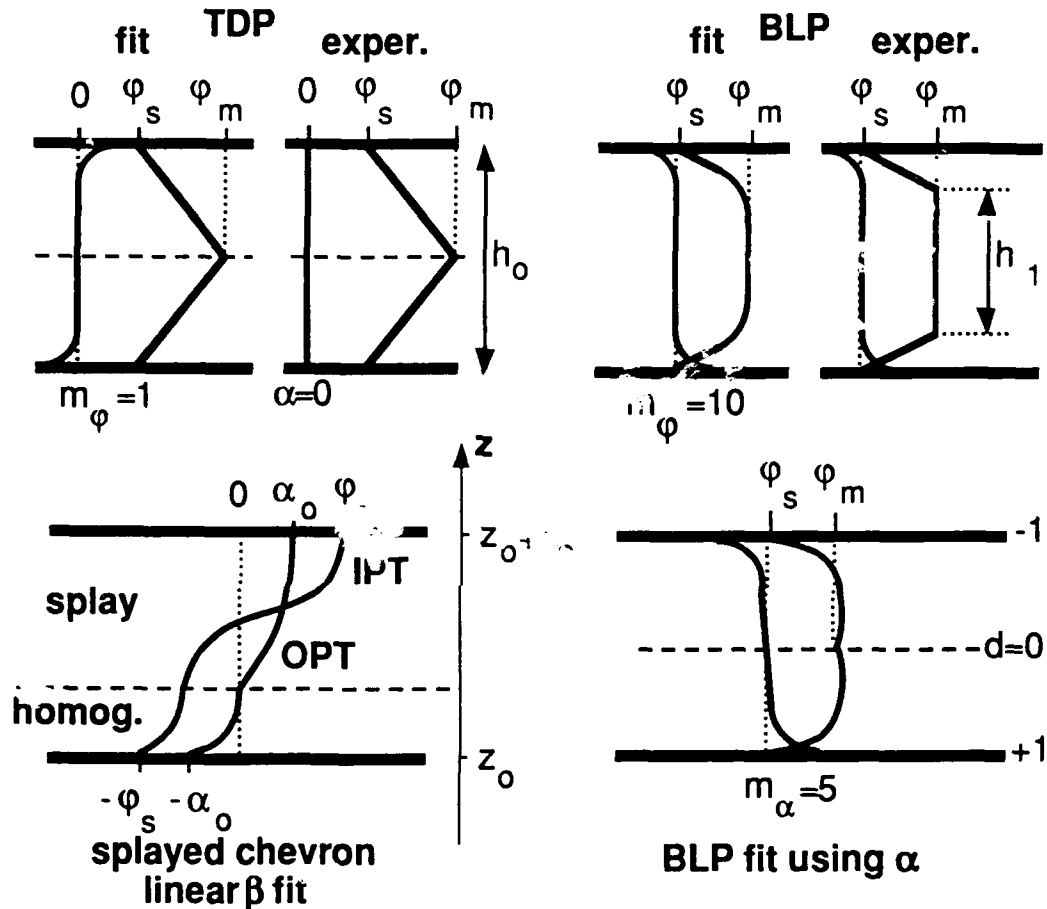


Figure 2. Some director profiles proposed for FLC cells, and polynomial fits using IPT, OPT and β . Note that BLP model uses φ_s as origin of IPT angles.

A simple polynomial fit is proposed to deal with these profiles. The fit may be applied to either IPT or OPT (or both, see below). A TDP configuration may be expressed as:

$$\varphi = \varphi_m + (\varphi_s - \varphi_m) \frac{|z - (z_0 + h_0/2)|}{h_0/2} \quad (7)$$

where φ_s , φ_m are IPT angles at the surfaces and in the middle of the cell, z_0 is the position of the beginning of the slab, and h_0 is the thickness of the slab. Though OPT may be negligible, it may not be zero for flat smectic layers.

A BLP configuration is described as:

$$\varphi = \varphi_m + (\varphi_s - \varphi_m) \frac{|z - (z_0 + h_0/2)| - h_1/2}{(h_0 - h_1)/2} \quad (8)$$

$$\text{for } h_1/2 \leq |z - (z_0 + h_0/2)| \leq h_0/2$$

and

$$\varphi = \varphi_m \quad \text{for } |z - (z_0 + h_0/2)| \leq h_1/2 \quad (9)$$

where h_1 is the thickness of the central region proposed by BLP model. The relative thicknesses of these three regions must be separately established. BLPs may be regarded as TDPs with a constant middle layer.

A normalized distance d is defined to simplify the expressions. The distance (Fig. 2) runs from 0 in the middle of the cell to ± 1 at the surfaces, the plus sign being at the incidence side (the bottom side in our case):

$$d = \frac{z_0 + h_0/2 - z}{h_0/2} \quad (10)$$

Chevron symmetry implies that $\alpha(d) = -\alpha(-d)$ assuming parallel rubbing, and $\varphi(d) = \varphi(-d)$. Moreover, symmetry and equation (2) lead to $\alpha(0) = 0$, whereas α at the surfaces is known (pretilt). Thus, φ_m and φ_s may be found, and a smooth curve may be assigned to the profile variations from the surfaces to the middle. It must be noted, according to Eq.(2), that IPT and OPT cannot be independently assigned, unless non-flat chevron layers and/or variable cone angles are allowed. For example, TDP profile as described above would lead to non-flat chevron layers. Nevertheless, in the low pretilt conditions employed by the authors⁹, the difference is negligible. The

following expressions are used to fit the profiles:

$$\varphi = \varphi_m + (\varphi_s - \varphi_m)d^{m_\varphi} \quad (11)$$

or

$$\alpha = \alpha_0 d^{m_\alpha} \quad (12)$$

The exponents m_α or m_φ control the shape of the profile and the flatness of the middle layer. As mentioned above, *either* m_α *or* m_φ are used. If m_α *and* m_φ fits are jointly used, then a dependence $\delta(d)$ is obtained for a constant θ . This is the case for TDP, where $m_\alpha=0$ and $m_\varphi=1$. BPLs are obtained for high m_φ 's (e.g. $m_\varphi>8$, see Fig. 2). An intermediate constant layer may be added if necessary.

Once the adequate polynomic profile has been chosen, the sample is splitted into slabs for 4×4 matrix calculation. The number of slabs linearly increases running time; therefore the minimum number correctly describing the profile must be used. In our case, the splitting is automatically performed, using a simple algorithm where the thickness of every slab is limited by the angular increment introduced in IPT and OPT. Thus the FLC is divided into strata of different thicknesses, the director in contiguous strata being twisted less than a predetermined angle. An increment of 1° is used; no improvements in transmission calculations have been found below this figure. Most usual FLC configurations are described in this way by 1 - 30 strata.

A final point worth to be mentioned concerns switching. The director might keep the same orientation near the surfaces upon switching, providing strong enough anchoring forces are acting on the FLC molecules. It has been shown³¹, however, that such a non-switchable region, if any, is negligibly thin at least for a standard glass surface conditioning. Hence the models assume the director reorientation occurs in the FLC as a whole.

A different situation may be derived in high pretilt cases (SiO, for example). Here, pretilt angles may be quite close to the tilt angle of the material, forcing the director near the surface to stay in the same position upon switching, the polarization vector of this region being almost parallel to the glass plate. This method is not usually

used in commercial displays. Indeed, it yields highly bistable samples but, unfortunately, switching times are currently high enough to rule out its use at video rates. In addition, manufacturing is not easily implementable. In any case, high pretilt cases may be calculated in the same way as the previous ones, for switching in high pretilts yields almost equivalent director orientations at the surfaces (the same orientation if pretilt matches tilt angle), thus being indistinguishable in optical transmission.

Director Orientation Across the Sample: Splayed Cases.

Splayed structures are often found in test cells and prototypes, though they are not usually desirable in displays. It has been shown that the most usual splayed asymmetric chevrons are not bistable, nor switchable at the surfaces²⁹. In any case, the modelling of such structures may be achieved using similar tools as above.

The sample is described in two parts: the first is a homogeneous layer and the second (usually the thicker) is the splayed layer. This splayed layer may be fitted as a function of IPT and OPT, as above. However, it is easier to define the profile as a function of β , the angle between the polarization vector and the projection of z-axis on the cone base (Fig. 1b). This angle varies linearly for constant rotation steps of the director on the cone surface. The limits of β may be derived respectively from the glass interface conditioning (β_s) and continuity at the boundary with the homogeneous layer (β_m):

$$\tan \beta_s = \frac{\cos \varphi_s \sin \delta - \tan \alpha_0 \cos \delta}{\sin \varphi_s} \quad (13)$$

$$\sin \beta_m = \frac{\tan \delta}{\tan \theta} \quad (14)$$

A linear interpolation from β_s to β_m is then performed. IPT and OPT may be derived from β as:

$$\tan \varphi = \frac{\cos \beta \sin \theta}{\sin \beta \sin \theta \sin \delta - \cos \theta \cos \delta} \quad (15)$$

$$\tan \alpha = \frac{\cos \theta \sin \delta + \sin \beta \sin \theta \cos \delta}{\sqrt{\cos^2 \beta \sin^2 \theta + (\cos \theta \cos \delta - \sin \beta \sin \theta \sin \delta)^2}} \quad (16)$$

Alternatively, an exponential fit as above may be used for the profile. These fits may also be used to simulate so-called banana profiles³⁰.

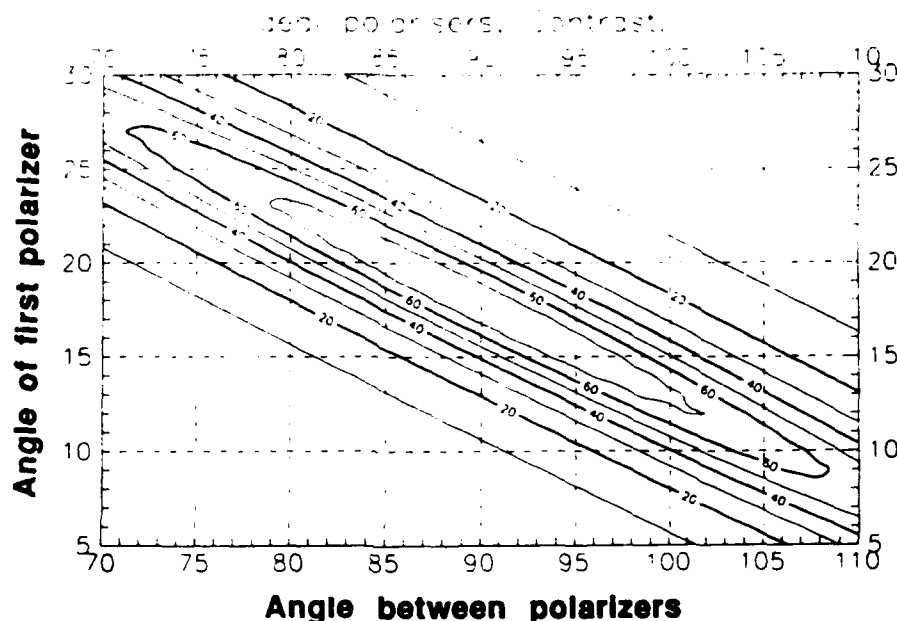


Figure 3. Isocontrast plot of a symmetric chevron case. Numbers inside are contrast ratios. Angles are relative to the projected smectic layer normal. These plots and brightness plots are used together to decide optimum angles of polarizers.

RESULTS AND DISCUSSION

Our current simulation process for a FLC prototype consists of several steps:

- *Structure configuration and director profile.* The director is defined as accurately as possible. When a unique director orientation cannot be decided, the most probable ones are tested in the following steps.
- *Polarizer optimization at normal incidence.* The orientation of polarizers is optimized using brightness and contrast criteria.

When polarizers are rotated brightness variations are usually much smoother than contrast variations. However brightness may be the most demanding parameter, especially in displays with high pixel density. The selection ultimately depends on the user: we usually choose the orientation for maximum contrast providing a fair brightness is obtained (Fig. 3). This step is quite costly in running time. A noticeable cut down is achieved by using ideal polarizers and/or fewer wavelengths for a rough estimation of the polarizer orientations. The angular area of interest is refined afterwards using actual polarizers. Most structures show their best results for crossed or near-crossed polarizers. An exception has been found in splayed structures, where the optimum is usually found for much smaller angles.

- *Temperature range.* Several parameters of the sample are affected by temperature changes. Variations in cone angles and other structural and FLC parameters must be tested within the limits of the expected working range of temperatures. This step may result in a shift of external variables (e.g. polarizer orientations) towards "safer" values.

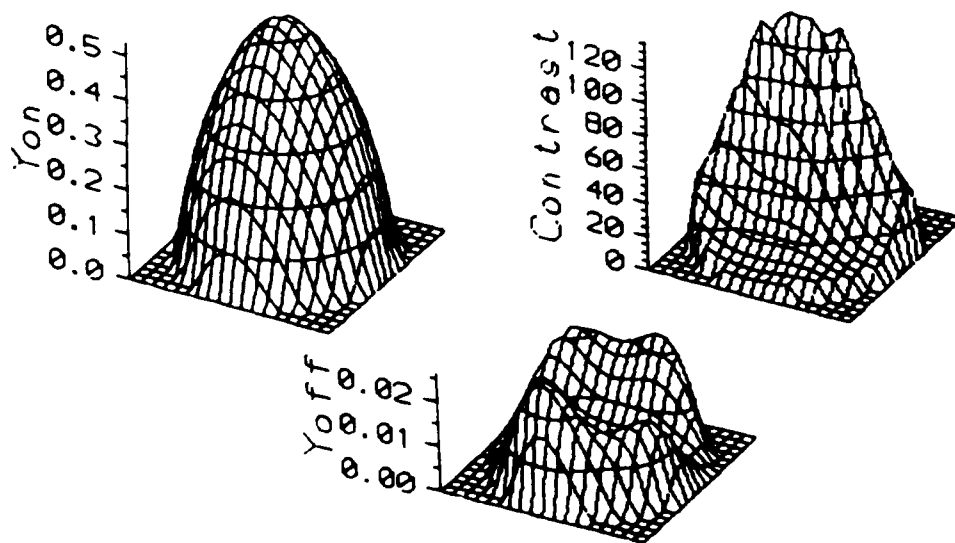


Figure 4. 3-D luminance plots for clear and dark states, and contrast ratio plot, for a symmetric chevron. Normal incidence is at the middle of the plot. Zenith angle increases linearly with radial distance from center.

- *Oblique incidences.* Optimization of normal incidence does not guarantee the performance of the display for oblique incidences. Several viewing angles are tested calculating azimuthal circles of brightness and contrast. Again this step may demonstrate pitfalls in the previously chosen set of parameters.
- *Characterization.* Once the whole cell has been correctly defined, several numerical and graphical data presentations may be solicited, as mentioned below.

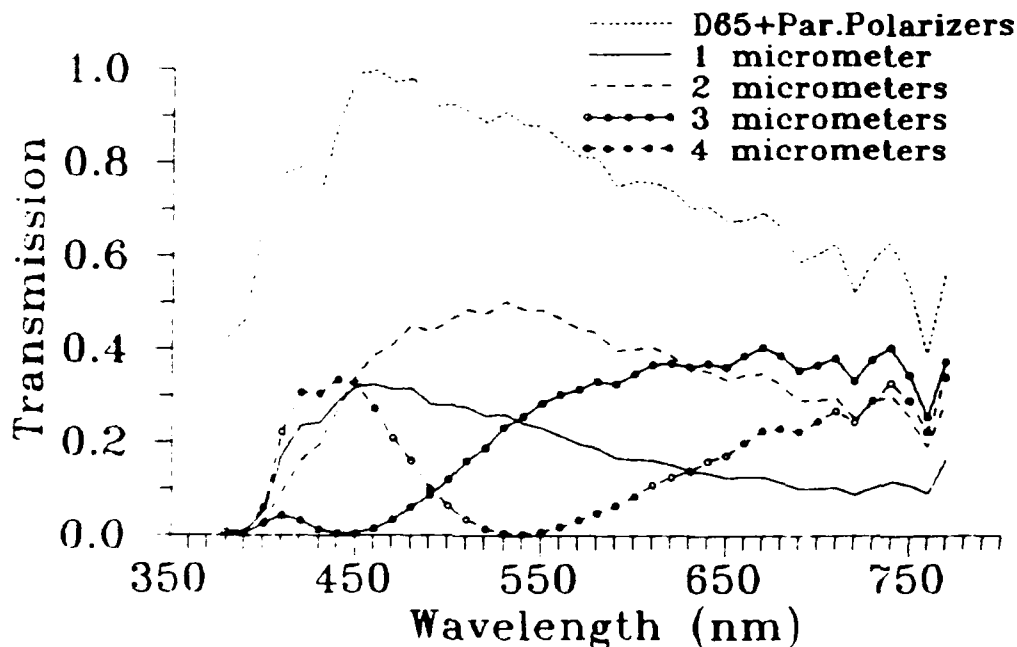


Figure 5. CIE D65 spectral transmissions of some chevron structures

Figures 4 and 5 show angular and spectral results obtained from the simulations. A symmetric chevron structure is calculated. The results may be given as 3-D or topographic plots of angular transmission of clear and dark states or contrast curves, as well as spectral curves or color coordinates for a given angle and backlight.

The design and characterization of FLC display prototypes may take advantage of modelling in several ways. Its results may be compared to actual prototypes to confirm their structures or even to calculate almost any unknown single parameter looking for the best fit of experimental data to computed results. In connection with this, a search for specific experimental setups for independent measuring of relevant variables has been started. The idea is to find setups insensitive to several parameters of the cell whereas other

variables (a single one, if possible) show a marked influence. For example the color coordinates either using white or colored backlight are almost only affected by the sample thickness providing the polarizers are crossed. Moreover, an azimuth round trip transmission plot for a given zenith angle, usually 30° or 45° , yields a curve whose shape may be related to several parameters, including projected tilt angle, which in turn may be eventually related to chevron angle when the tilt angle is known. If the whole cell is rotated, a polar plot of azimuthal transmissions has a typical peanut shape which becomes an oval for lower phase shifts. If a cell is rotated between crossed polarizers, a daisy-shaped curve with eight "petals" is obtained (Fig. 6).

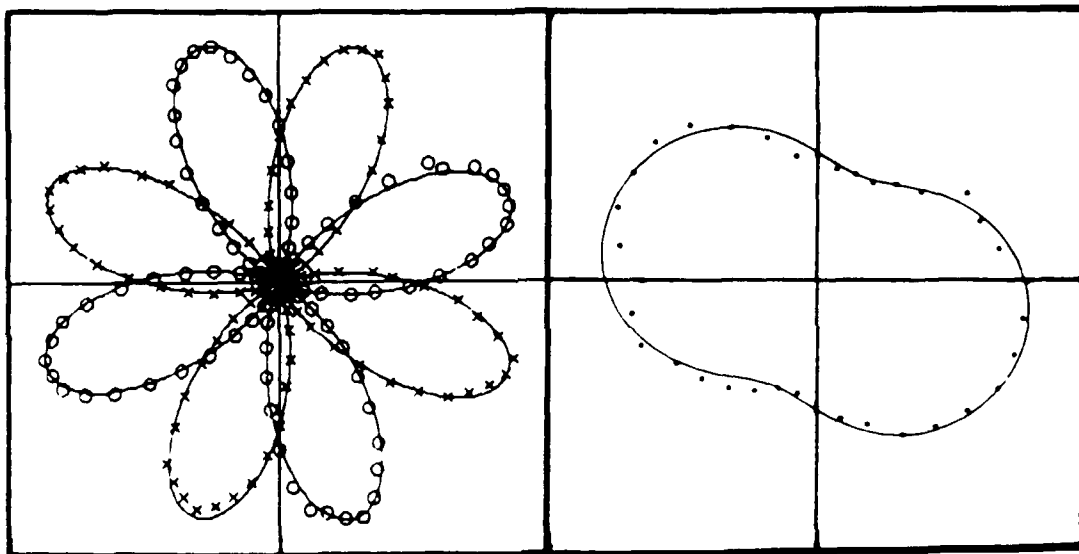


Figure 6. Experimental results and model fitting of daisy- and peanut-shaped polar plots of oblique transmissions for a constant zenith angle. In the daisy curve, four petals (\times points) from one state are interleaved with another four petals (o points) from the other.

On the other hand the models may be used to predict the properties of designed displays before manufacturing the actual prototypes. Considering the inaccuracies of the manufacturing process and the limitations of the models themselves, the usefulness of this predicting power is not based on exact calculations of specific structures, but rather in delimiting dangerous or safe ranges of design parameters.

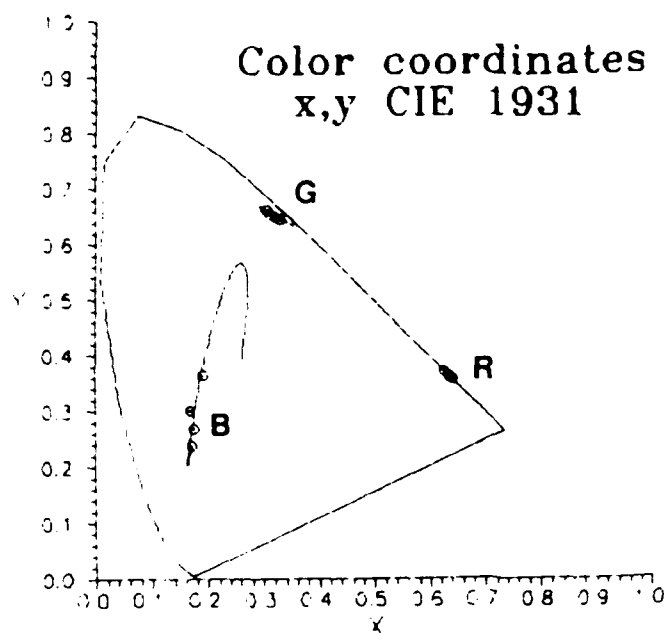


Figure 7. Predicted and experimental color coordinates for increasing sample thicknesses using RGB filters. Experimental points range from 2.1 to 3.8 μm . The B curve beyond the points is the range predicted for 4-7 μm .

For example, a color display based on fluorescent backlight and color filters may be severely impaired if the sample thickness is high (Fig. 7). A plot of color coordinates on a CIE x, y chromaticity diagram shows drastic color changes when thickness is increased. Experimental points were calculated from averages of 50 clear state spectra obtained with the OMA gated at 1 ms.

Monochromatic backlights could obviously be used to overcome this problem, for no color variations may arise in this case (see R and G points, Fig. 7). However, the usual fluorescent backlight/color filter system employed in flat panel displays must use broader filters (B points) to increase brightness. In this case, unless birefringent correction plates are used, color outputs may show high variations for thick samples ($>2.5 \mu\text{m}$ for example), where phase shifts are comparable to visible wavelengths. The same effect is shown in the spectra, as seen in Fig. 5.

ACKNOWLEDGEMENTS

Authors are indebted to all the research groups of FELICITA Project for their continuous assistance, comments and feedback. Special thanks to S.T. Lagerwall and I. Dahl from Chalmers University, and to E.P. Raynes from R.S.R.E. for stimulating discussions. FLC materials kindly supplied by T. Geelhaar (Merck), test cells from B.M. Nicholas (GEC), and color filters from L.G. Banks (Thorn EMI) are also acknowledged. This work has been supported by EC ESPRIT II Project 2360 FELICITA and TIC 89/0171 Project of Spanish Comisión Interministerial de Ciencia y Tecnología (CICyT).

REFERENCES AND NOTES

- [1] N.A. Clark and S.T. Lagerwall *Appl. Phys. Lett.* **36** (11) 899 (1980).
- [2] N.A. Clark and S.T. Lagerwall *Proc. 6th Int. Display Res. Conf.*, Tokyo, Japan (1986) p. 456.
- [3] T.R. Rieker, N.A. Clark, G.S. Smith, D.S. Parmar, E.B. Sirota and C.R. Safinya *Phys. Rev. Lett.* **59** (23) 2658 (1987).
- [4] Y. Ouchi, Ji Lee, H. Takezoe and A. Fukuda *Jpn. J. Appl. Phys.* **27** (5) 725 (1988).
- [5] J. Kanbe, H. Inoue, A. Mizutome, Y. Hanyuu, K. Katagiry and S. Yoshihara *Ferroelectrics* **114** (1-4) 3 (1991).
- [6] P.W.H. Surguy, L.G. Banks, A.N. Carrington, L.K.M. Chan, M.J. Naylor and N.E. Riby *Proc. 10th Intl. Display Res. Conf. EURODISPLAY'90*, Amsterdam (1990) p. 146.
- [7] A. DeVos and C. Reynaerts *J. Appl. Phys.* **65** (7) 2616 (1989).
- [8] A. DeVos *Liq. Cryst.* **6** (3) 373 (1989).
- [9] M.H. Anderson, J.C. Jones, E.P. Raynes and M.J. Towler *J. Phys. D* (in press, 1991).
- [10] See for example: *Display Modelling System. Program Features*. Autronic GmbH (1990).
- [11] N.A. Clark and S.T. Lagerwall *Ferroelectrics* **59**, 25 (1984).
- [12] T. Carlsson and B. Zeks *Liq. Cryst.* **5** (1) 359 (1989).
- [13] M. Nakagawa *Displays* **11** (2) 67 (1990).
- [14] I. Dahl: *On Order, Ferroelectricity and Elasticity in Smectic Liquid Crystals*. Ph. D. Thesis, Chalmers University of Technology, Göteborg, Sweden (1990).
- [15] T. Carlsson, I.W. Stewart and F.M. Leslie *Liq. Cryst.* **9** (5) 661 (1991).
- [16] T. Uchida, M. Hirano and H. Sakai *Liq. Cryst.* **5** (4) 1127 (1989).
- [17] A. Martín and A. Labanda: *Fotometría y Colorimetría*. EUIT Telecomunicación edns., Madrid (1978).
- [18] Experimental measurements of commercial RGB filters used in Thorn EMI have been provided by L.G. Banks.
- [19] Experimental measurements of G1220 polarizers employed by GEC Marconi Research have been provided by M.C.K. Wiltshire.
- [20] Merck's FLC experimental and commercial mixtures, including ZLI-3654, have been provided by T. Geelhaar.
- [21] D.W. Berreman *J. Opt. Soc. Am.* **62** (4) 502 (1972).
- [22] D.W. Berreman *J. Opt. Soc. Am.* **63** (11) 1374 (1973).
- [23] R.C. Jones *J. Opt. Soc. Am.* **31** 483 (1941).
- [24] J.E. Bigelow and R.A. Kashnow *Appl. Opt.* **16** (III) 2090 (1977).
- [25] H.L. Ong *J. Appl. Phys.* **64** (2) 614 (1988).
- [26] H. Wöhler, G. Haas, M. Fritsch and D.A. Mlynski *J. Opt. Soc. Am. A* **5** (9) 1554 (1988).
- [27] K.H. Yang *J. Appl. Phys.* **68** (4) 1550 (1990).
- [28] C.R. Lavers and J.R. Sambles *Liq. Cryst.* **8** (4) 577 (1990).
- [29] J.E. MacLennan, N.A. Clark, M.A. Handschy and M.R. Meadows *Liq. Cryst.* **7** (6) 753 (1990).
- [30] S.J. Elston *Liq. Cryst.* **9** (6) 769 (1991).
- [31] J. Xue, N.A. Clark and M.R. Meadows *Appl. Phys. Lett.* **53** (24) 2397 (1988).

SECTION L
COMMENTS AFTER THE CONFERENCE

Comment after the conference (letter)

SIMPLE PICTURE OF THE ANTIFERROELECTRIC SMECTIC C_A PHASE

INGOLF DAHL

Physics Department, Chalmers University of Technology,
S-412 96 Göteborg, Sweden

Abstract A simple picture of a possible packing of the molecules in the antiferroelectric smectic C_A phase is presented. This picture could give some hints about the physics involved.

The smectic C_A phase was introduced 1989 by Chandini *et al.*¹. There is strong evidence that this phase is a tilted smectic C phase, where the tilt is reversed in every second layer. If the molecules are chiral and possess permanent dipole moments, such an arrangement should be antiferroelectric. It is still an open question why the molecules prefer alignment in this way. There have been speculations about dipole-dipole interactions as a cause, but this explanation maybe becomes a bit too artificial when it is used in the case of a racemate showing C_A phase.

Which forces are important for the geometry of other liquid crystal phases? In the nematic phase, steric interaction and van der Waals forces between elongated molecules to a large extent are responsible for the formation of the phase. The smectic A phase can be explained by nematic forces plus the attraction and alignment of similar parts of the molecules. In the smectic C phase the molecular shape (zig-zag) seems to play an important role. Can we explain the C_A phase in a similar way? Inspired by the bent toothpicks from the conference dinner, I suggest that the molecules are bent at least once. A simple packing arrangement, giving reverse tilt in every second layer, is shown in Figure 1. If we can number the segments between the bends in the

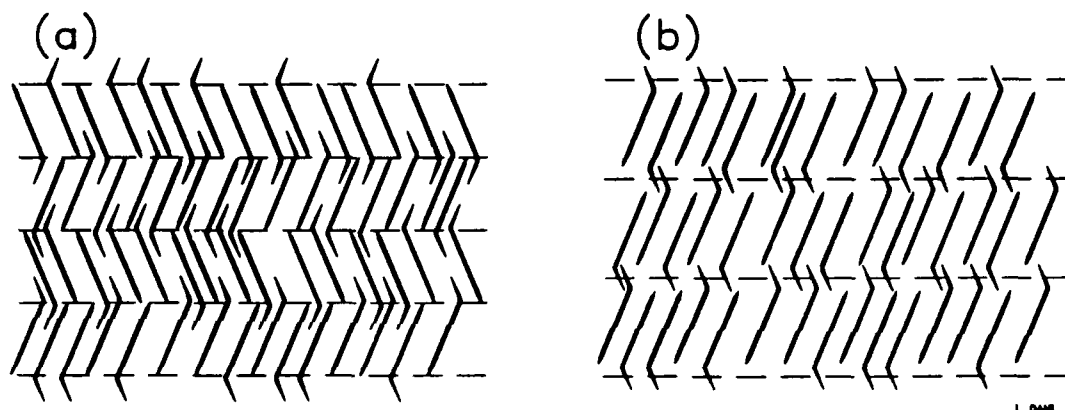


FIGURE 1 In the C_A phase, in (a), the bent ends of the molecules are suggested to penetrate into the next layer, and to align the main part of the molecules there, causing a reversed tilt. In the ordinary smectic C phase, in (b), the layers are spaced wider apart, and the bent ends mainly interact with the bent ends from the next layer.

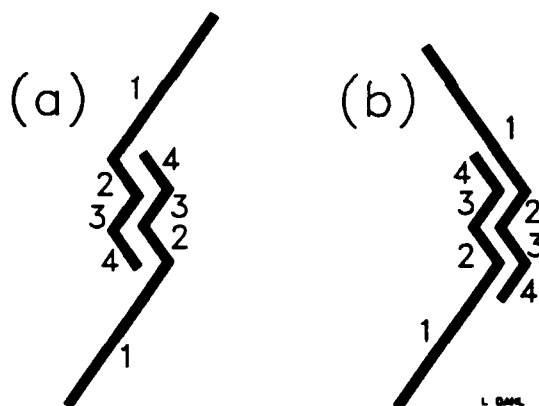


FIGURE 2 Strong even-odd effects could result if bent molecules in different smectic layers align in different ways. We can number the segments of the bent molecules as indicated. If even numbered segments in one layer align with even numbered segments in the next, the molecules will align parallel, as in (a). If even numbered segments instead align with odd numbered segments in the next layer, reversed tilt is favoured, as in (b).

molecule, we can get the reverse tilt if even numbered segments in one layer align with odd segments in the next layer. If even segments in one layer instead align with even segments in the next layer, ordinary smectic C will result (Figure 2). My suggestion is thus that the prime factor, causing the C_A phase, is the shape of the molecules, acting together with intermolecular forces, which cause alignment and attraction between molecular segments.

There is evidence indicating that there is some physical content in the simplified picture given here. There have been reports that odd-even effects are important for the formation of the C_A phase². The smectic layer thickness also in some case shows a marked decrease from the smectic C phase. If the picture is correct, the phase will be found not only in racemates, but also in nonchiral substances. The most obvious candidates are dimers of mesogenic molecules connected end-to-end with a bent link in between.

REFERENCES

1. A. D. L. Chandini, Y. Ouchi, H. Takezoe, A. Fukuda, K. Terashima, K. Furukawa, and A. Kishi, *Jpn. J. Appl. Phys.*, **28**, pp. L1261- L1264 (1989) and
A. D. L. Chandini, E. Gorecka, Y. Ouchi, H. Takezoe, and A. Fukuda, *Jpn. J. Appl. Phys.*, **28**, pp. L1265- L1268 (1989)
2. H. Takezoe in oral contribution O-47 at this conference.

AUTHOR INDEX

Proceedings of The Third International Symposium on Ferroelectric Liquid Crystals

Volumes 121-122

- Anabuki, T. 295
Anderson, M. H. 137
Andersson, G. 481
Armitage, D. 593
Arnett, K. E. 247
Ayliffe, P. J. 417
- Bang, T. 113
Bata, L. 275, 493, 503
Bawa, S. S. 435
Betterton, K. 55
Biradar, A. M. 435
Birch, M. J. 417
Blinc, R. 575
Bone, M. F. 417
Bonvent, J. J. 285
Bose, T. K. 1
Buisine, J. M. 21
- Cambon, P. 443
Čepić, M. 575
Chandra, S. 435
Chandrasekhar, S. 307
Clark, N. A. 127, 143, 147, 247, 567
Coulson, I. 417
Crooker, P. P. 537
Crossland, W. A. 417
- Dahl, I. 665
Daido, K. 259
De Bougrenet De La Tournaye, J. L. 443
De Ley, E. 103
De Meyere, A. 103
Destrade, C. 21, 187, 285
Dohgane, I. 167
- Éber, N. 275, 493
- Fodor-Csorba, K. 275, 503
Fujisawa, K. 167
Fukuda, A. 521
- Ganelina, A. 335
Glogarova, M. 45, 285
Goodby, J. W. 235
Gotou, T. 259
Grüneberg, K. 513
- Haase, W. 55
Handschy, M. A. 147
Hara, M. 521
Hartmann, W. J. A. M. 355
Hashimoto, K. 407
Hauck, G. 607
Heeks, S. K. 381
Higashii, T. 167
Hirai, T. 225
Hiyama, T. 159
Hofmann, A. 13
Holly, S. 503
Hmine, J. 21
Hughes, J. R. 417
- Ikeda, A. 521
Ikegaki, T. 179
Isaert, N. 21, 187
Ishibashi, Y. 531
Itoh, M. 33
Itoh, K. 521
Iwane, H. 521
- Johnson, K. M. 455
Jones, J. C. 91, 137
- Kapitza, H. 481
Kawasaki, K. 407
Kennedy, K. 583
Khened, S. M. 307, 319, 343
Kikuchi, M. 179
Killinger, M. 443
Kimura, M. 33
Kitzerow, H.-S. 537
Kobayashi, S. 33, 113
Koden, M. 205, 295
Koswig, H. D. 607
Kozlovsky, M. V. 503
Kremer, F. 13, 69
Kühnast, K. 513
Kuratate, T. 205
Kusumoto, T. 159
- Lagerwall, S. T. 481
Landreth, B. 455
Legrand, C. 21
- Mao, C. C. 455

- Marcerou, J. P. 285
Maximus, B. 103
Minai, M. 167
Miyazawa, K. 179
Mochizuki, A. 33, 113, 391
Moddel, G. 455
More, K. 219
Morita, Y. 259
Moritake, H. 467
Mosley, A. 381
Motoyoshi, K. 391
- Nabor, M. F. 187
Nakagawa, M. 633
Nakatsuka, M. 391
Neubert, M. E. 235
Nguyen, H. T. 21, 187, 285
Nicholas, B. M. 381
Nozaki, R. 1
- Olarte, F. 647
Orihara, H. 531
Otón, J. M. 647
Ozaki, M. 259, 467
- Parmar, D. S. 551
Parneix, J. P. 21
Pauwels, H. 103
Pavel, J. 45
Pena, J. M. S. 647
Pfeiffer, M. 55
Polashenski, S. 583
Poths, H. 69, 481
Prasad, S. K. 235, 307, 319, 343
- Rabinovich, A. 335
Raja, V. N. 235, 307, 319, 343
Rao, D. S. S. 235, 343
Raynes, E. P. 91, 137
Rego, J. A. 247
Ros, M. B. 143, 247
Ross, P. W. 417
Rundle, P. C. 381
- Sadohara, Y. 259
Saito, S. 179
Sakaguchi, K. 205
Saunders, F. C. 417
Serrano, A. 647
Scherowsky, G. 493, 513
Schiller, P. 615
Schliwa, A. 493
Schlusche, P. 381
Schönfeld, A. 13, 69
- Schwenk, N. 13
Sekine, C. 167
Sekiya, T. 407
Shao, R. F. 127, 247, 567
Sharma, C. P. 435
Shigeno, N. 467
Skiomi, Y. 205
Shivkumar, B. 307, 319
Sierra, T. 247
Skarp, K. 481
Soto, G. 55
Stommels, F. J. 79
Subramaniam, G. 583
Surguy, P. W. H. 417
Szabon, J. 275, 503
- Tagawa, A. 467
Takanishi, Y. 521
Takehara, S. 159
Takezoe, H. 521
Terashima, K. 179
Thoen, J. 1
Thurmes, W. N. 213, 219
Towler, M. J. 91, 137, 417
Twieg, R. 55, 187
- Uchida, S. 407
Uemura, Y. 167
Umemoto, T. 521
Utsumi, M. 259
- Vajda, A. 275
Vallerien, S. U. 13, 69
Velsco, S. P. 247
Verhulst, A. G. H. 79
Vohra, R. T. 213, 219, 247
- Walba, D. M. 143, 213, 219, 247
Wand, M. D. 143, 213, 219, 247
Watanabe, J. 521
Williams, P. A. 143
Willis, P. C. 127
Wrobel, S. 55
- Yang, Y. B. 113
Yokoyama, A. 225
Yoshino, K. 259, 467
Yoshizawa, A. 225
Yuasa, K. 407
- Žekš, B. 575
Zentel, R. 69, 481
Zhuang, Z. 567
Zou, Z. 147

Special Issue on Piezoelectric and Electrostrictive Actuators

A special issue of the international journal *Ferroelectrics* is scheduled for the middle of 1992 on the subject "Piezoelectric and Electrostrictive Actuators."

Recent developments in piezoelectric and electrostrictive ceramics are remarkable, especially in the field of optics and precision machinery. Camera shutters, dot-matrix printers, and air valves have been widely commercialized. Ultrasonic motors will partially replace conventional electromagnetic motors in the future.

This special issue will cover the fundamental studies of ceramic actuators and applications:

1. Ceramic actuator materials — piezoelectrics, electrostrictors, phase transition — related ceramics
2. Fabrication processes — powders, tape casting
3. Micro/macrostructure — grain size dependence, monomorph, electrode configuration
4. Control technique — polarization control, pulse drive method
5. Applications — deformable mirrors, positioners, pulse drive motors
6. Ultrasonic motors

Invited and contributed papers are welcome. All manuscripts will be reviewed. Manuscripts should be prepared according to the instructions on the inside back cover of "Ferroelectrics."

Authors are cordially invited to submit their papers not later than December 31, 1991 to the Guest Editors below:

Professor Kenji Uchino
Department of Physics
Sophia University
Kioi-cho 7-1, Chiyoda-ku
Tokyo 102, Japan

or

Materials Research Laboratory
The Pennsylvania State University
University Park, PA 16802, USA
(July 1-September 30)

Professor L. Eric Cross
Materials Research Laboratory
The Pennsylvania State University
University Park, PA 16802

For further information, please feel free to contact the Guest Editors.

The Eighth INTERNATIONAL MEETING OF FERROELECTRICITY

8-13 August 1993

**National Institute of Standards and Technology
Gaithersburg, Maryland USA**

The scope of the conference will be similar to that of the preceding IMFs. Both invited and contributed papers will be presented on fundamental and applied research on ferroelectrics, including but not limited to:

Phase transitions and critical phenomena
Electronic structure, quantum effects
Lattice dynamics, lattice instabilities, and soft modes
First principles calculations
Low-temperature properties
Superconductivity in oxides
Charge density waves, polarization fluctuations
Structure and crystal growth
X-ray and neutron scattering
Acoustic and ferroelastic properties
Dielectric, piezoelectric, and pyroelectric properties
Optical properties and phase conjugation
Modulated and incommensurate systems

Disordered and glassy systems
Domains, domain boundaries, and imperfections
Raman, Brillouin, IR, and submillimeter spectroscopy
NMR, ESR, PAC, and other types of spectroscopy
Electron microscopy
High-pressure effects
Polymers and liquid crystals
Ceramics and composite materials
Sensors, actuators, and transducers
Thin films and surfaces
Ferroelectric/semiconductor integration

Wallace A. Smith
Office of Naval Research
IMF8 Chairman

L. Eric Cross
Pennsylvania State University
IMF8 Vice Chairman

George W. Taylor
Princeton Resources
IMF8 Vice Chairman

To receive future announcements,
send your name and address to:

Ms. Kathy Kilmer, IMF8 Conference Manager
National Institute of Standards and Technology
Administration Building, Room A917
Gaithersburg, MD 20899
TEL (301) 975-2776; FAX (301) 926-1630

Title and Name	_____
Institution	_____
Department	_____
Street	_____
City/State/Zip	_____
Country	_____
Phone	_____
FAX	_____

- ☐ I will present a paper entitled: _____
- ☐ I will be accompanied by _____ guests.
- ☐ I will attend, but will not present a paper.
- ☐ I will not attend, but would like to be kept informed.

"Arthur von Hippel Special Issue" on Dielectric properties of Ferroelectrics

A special issue of *Ferroelectrics* is planned in honor of Professor Arthur von Hippel's 93rd birthday. Because Professor von Hippel founded the Massachusetts Institute of Technology Laboratory for Insulation Research in 1940 and supervised it until his retirement, we thought a fitting topic for this special issue would be "Dielectric Properties of Ferroelectrics." This is only one of his many areas of interest, and papers on other topics of particular interest to him are welcome.

Papers reporting original research on this topic not published elsewhere are requested. They should be sent to one of the Guest Editors named below, who will arrange for refereeing and publication. Also, we invite submission of review papers, but to avoid duplication, the topic of the review should be discussed with one of the Guest Editors beforehand.

To facilitate correspondence, it is suggested that you work with the Guest Editor in your geographical area as listed below.

Europe (including USSR) and Africa:

Professor Bozena Hilczer
Institute of Molecular Physics
Polish Academy of Sciences
Smoluchowskiego 17/19
60-179 Poznan, Poland

Asia and Australia:

Professor Toshio Mitsui
Department of Physics
School of Science and Technology
Meiji University
1-1-1 Higashimita, Tama-ku
Kawasaki 214, Japan

North and South America:

Professor V. Hugo Schmidt
Department of Physics
Montana State University
Bozeman, MT 59717 USA

We ask that you submit your manuscript by December 31, 1991 to one of the above Guest Editors.

Second USSR/USA Seminar on Ferroelectricity

22-26 June 1992

**A.F. Ioffe Physical Technical Institute
194021 St Petersburg, USSR**

Organizing Committee

A.M. Prokhorov, Honorary President

USSR

**Chairman: K.S. Aleksandrov
Vice-Chairman: L.A. Shuvalov
V.V. Lemanov
O.O. Vendik
Secretary: V.M. Fridkin
N.K. Yushin
Program Chairman: A.K. Tagantsev
Local Arrangements: A.I. Nikkonen**

USA

**Chairman: G.W. Taylor
Vice-Chairman: S.K. Kurtz
Secretary: J.F. Scott
Members: L.E. Cross
A. Bhalla
A. Glass
V.H. Schmidt
N. Clark
G. Samara
K. Lyons
F. Ullman**

For information please contact:

**V.V. Lemanov
A.F. Ioffe Physical Technical Institute
194021 St Petersburg, USSR
Tel. No 007812 515 6660
Telex 121 1453 FTIANSU
Fax No 007812 515 6747**

or

**G.W. Taylor
Princeton Resources
P.O. Box 211
Princeton, NJ 08540 USA
Tel. No. (609) 921-3192
Fax No. (609) 924-9020**

**The seminar will be devoted to the physics of
ferroelectrics and related materials:**

- 1. Optics and Spectroscopy**
- 2. Films and Composites**
- 3. Liquid Crystals and Glasses**
- 4. Superconducting Oxides**
- 5. Structure and Properties of New Crystals and Ceramics**
- 6. Disordered Ferroelectrics**

**"Nakamura Special Issue" on
Structural Phase Transitions in
Ferroelectrics and Related Materials**

A special issue of the international journal *Ferroelectrics* is scheduled for late 1991 on the subject "Structural Phase Transitions in Ferroelectrics and Related Materials."

This special issue will be dedicated to Professor Torutaro Nakamura on the occasion of his sixty-eighth birthday. Professor Nakamura's work is well known internationally. During his eminent scientific career, his seminal contributions are responsible for several milestones in the history of ferroelectricity research.

This special issue will cover the full scope of ferroelectric phenomena discussed in the light of the physics of the structural phase transition.

Invited papers and tributes will make up the bulk of the issue, but contributed papers are welcome as well.

Authors are cordially invited to submit their papers not later than June 30, 1991, to one of the guest editors listed here:

Professor L. Godefroy
Laboratoire de Physique du Solide
Université de Bourgogne
BP 138, F-21004
Dijon Cédex, France

Professor W. Kinase
Department of Physics, School of
Science and Engineering
Waseda University
3-4-1 Okubo, Shinjuku-ku
Tokyo 169, Japan

Professor A.P. Levanyuk
Institute of Crystallography
USSR Academy of Sciences
59 Leninsky Prospekt
117333 Moscow, USSR

Professor F.G. Ullman
Electric Engineering Department
University of Nebraska
Lincoln, NE 68588-0511 USA

Manuscripts should be prepared according to the instructions on the inside back cover of *Ferroelectrics*. All manuscripts will be refereed.

The following Japanese associate guest will assist Professor Kinase: Professor K. Ohi, Professor A. Sawada, Professor M. Takashige, and Dr. S. Kojima.

For further information, please contact any of the guest editors listed above.

**Special Issue on
Ferroelectricity, Structural Instability,
and High-Temperature Superconductivity**

A special issue of the international journal *Ferroelectrics* is scheduled for 1991 on the subject "Ferroelectricity, Structural Instability, and High-Temperature Superconductivity." The aim of this issue is to present a review of the present state of the art (experimental as well as theoretical), on possible interrelations, common features, and outstanding differences of ferroelectric and superconducting oxides. Emphasis is put on their structural instability, which is common to both ferroelectricity and superconductivity. Authors are invited to submit their contributions to one of the Guest Editors, listed below.

A. Bussmann-Holder
Max-Planck Institut für
Festkörperforschung
Heisenbergstraße 1
D-7000 Stuttgart 80
Federal Republic of Germany

S. K. Kurtz
Materials Research Laboratory
Pennsylvania State University
University Park, PA 16802 USA

Eiko Matsushita
Maritime Safety Academy
Kure 737, Japan

N. M. Plakida
Joint Institute for Nuclear Research
141980 Dubna, USSR

J. F. Scott
Physics Department
University of Colorado
Boulder, CO 80309 USA

Manuscript should be prepared according to the instructions on the inside back cover of *Ferroelectrics*. All manuscripts will be refereed. For further information, please contact any of the Guest Editors listed above.

ISAF '92



IEEE International Symposium on the Application of Ferroelectrics

August 31 - September 2, 1992
Hyatt Regency, Greenville, South Carolina

*Sponsored by the Ultrasonics, Ferroelectrics and Frequency Control Society of the IEEE
in Cooperation with the Electronics Division of the American Ceramic Society*

First Call for Papers

Abstract Deadline: February 1, 1992

Meeting Chair:

Prof. Gene Haertling
206 Olin Hall
Clemson University
Clemson, SC 29634-0907
Tel. (803) 656-0180
Fax (803) 656-2698

The next International Symposium on the Application of Ferroelectrics will be held August 31 - September 2, 1992, in Greenville, South Carolina.

This biannual meeting emphasizes the application of ferroelectric materials in the form of single crystals, bulk ceramics, and thick and thin films. Papers are solicited describing original work in the following categories. These categories reflect those properties of the materials which primarily determine their application. Within each category, papers are requested covering **processing; properties; theory and modelling; performance (reliability and failure); and particularly new applications and new materials.**

Technical Program Chair:

Prof. Angus I. Kingon
Materials Research Ctr.
N.C. State University
Centennial Campus
Box 7919
Raleigh, NC 27695-7919
Tel. (919) 737-2867
Fax (919) 737-3419

• Ferroelectric

Materials and applications in which the primary property utilized is polarization reversal (ferroelectric switching) Topics include thin film processing, integrated memories, integration, performance, fatigue, ageing, modelling and new applications.

• Dielectric

Materials and applications in which the primary property utilized is the high permittivity of the ferroelectric materials. Topics include multilayer capacitors; thick film capacitors; thin film integrated static capacitors; packaging; dielectric breakdown and reliability; high frequency dielectrics; PTC materials; boundary layer capacitors; and processing. A new topic will be electrorheological fluids.

• Piezoelectric and Electrostrictive

Materials and applications in which the primary property utilized is piezoelectricity (and the related electrostriction). Applications to include actuators; transducers; micromotors and microactuators; resonators; and sensors. Topics to include processing and modelling, and material categories to include ceramics, ceramic/polymer composites, and polymers.

• Electrooptic, Pyroelectric, etc.

Materials and applications in which the primary properties utilized are the electrooptic effect, pyroelectricity, photorefractive, and related optical properties. This category will include ferroelectric liquid crystals. Applications to include phase modulators, second harmonic generators, displays, optical NDRO devices, optical comparators, digital and analogue image storage, thermal sensors and imagers, detectors, etc.

Accommodations

Accommodations will be available at the Hyatt Regency in downtown Greenville, South Carolina or at several other hotels and motels in the local area. The Hyatt will serve as the conference headquarters. More detailed information will be supplied at a later date.

Location

Greenville, South Carolina is located approximately 150 miles northeast of Atlanta, Georgia along Interstate I-85 connecting Atlanta and Charlotte, North Carolina. International flights are available into Atlanta, GA and Charlotte and Raleigh, NC. Domestic flights are also available into the Greenville-Spartanburg airport located 10 miles from downtown Greenville.

During the symposium, the group will be traveling to Clemson, SC, about 30 miles west of Greenville, for a brief visit to the campus of Clemson University and an evening outdoor social function at Lake Hartwell on the University grounds.

Abstracts

Abstracts are to be submitted according to the accompanying abstract format. The deadline is February 1, 1992. Abstracts to be submitted to the Technical Program Chair, Prof. Angus I. Kingon, at the address given. Abstracts will receive careful evaluation. Evaluation criteria will include; scientific contribution, originality; overall interest to the ferroelectrics (including user) community; and clarity.

Notice of acceptance of abstracts will be mailed in April 1992. Complete manuscripts must be received by August 1, 1992, to ensure timely review. The symposium proceedings will be published shortly after the symposium.

A second call for papers will be issued in September 1991. That announcement will include a list of invited speakers. Program details and lodging information will be mailed in April 1992.

ISAF '92
Preparation of Abstracts

TITLE UPPER CASE ADJUSTED LEFT.

(Space)

A.A. Author One and B.B. Author Two¹

Affiliation and Address

¹Second Affiliation and Address if required.

(Space)

Abstract to fill the remaining space. No references or figures to be included. The complete abstract to fit into this space measuring 13.5 by 18 centimeters. Presenting author underlined, if known. Single spacing (12 pt. Times). This abstract will be printed in this camera-ready form to be available at the symposium.

*Include funding agency acknowledgement if desired.

Please mark the category into which you feel your paper best fits:

☐ Ferroelectric

☐ Dielectric

☐ Piezoelectric and electrostrictive

☐ Electrooptic, pyroelectric, optical, etc.

Name and address of author to whom correspondence should be sent:

Name _____

Address _____

Telephone _____ FAX _____

Check box:

☐ I prefer oral presentation

☐ I prefer poster

☐ I do not have a preference

☐ I plan to bring my spouse/guest

Submit your abstract (by February 1, 1992) to: **Prof. Angus I. Kingon/Ms. Jan Jackson**
Materials Research Center
North Carolina State University, Centennial Campus
Box 7919, Raleigh, NC 27695-7919.

ISAF '92

In order for the organizers to ensure appropriate facilities and lodging, please indicate your interest in the symposium:

☐ I intend to attend and submit a paper by February 1, 1992. A tentative title is _____ (optional).

☐ A second paper will be entitled: _____ (optional).

Category: ☐ Ferroelectric ☐ Dielectric
☐ Piezoelectric and electrostrictive ☐ Electrooptic, pyroelectric, optical, etc.

☐ I will attend, but not present a paper.

☐ I will not be attending. Please remove my name from your mailing list.

Name _____

Address _____

Telephone _____ FAX _____

Return as soon as possible to: **Prof. Gene Haertling**
206 Olin Hall
Clemson University
Clemson, SC 29634-0907

ISAF '92

In order for the organizers to ensure appropriate facilities and lodging, please indicate your interest in the symposium:

☐ I intend to attend and submit a paper by February 1, 1992. A tentative title is _____ (optional).

☐ A second paper will be entitled: _____ (optional).

Category: ☐ Ferroelectric ☐ Dielectric
☐ Piezoelectric and electrostrictive ☐ Electrooptic, pyroelectric, optical, etc.

☐ I will attend, but not present a paper.

☐ I will not be attending. Please remove my name from your mailing list.

Name _____

Address _____

Telephone _____ FAX _____

Return as soon as possible to: **Prof. Gene Haertling**
206 Olin Hall
Clemson University
Clemson, SC 29634-0907

Announcement

ECAPD2/ISIF4
The Second European Conference on
The Applications of Polar Dielectrics
and
The Fourth International Symposium on
Integrated Ferroelectrics

Imperial College of Science, Technology, and Medicine
South Kensington, London, UK

12-15 April 1992

The program will include the following topics:

- **FERROELECTRICS:** fundamental properties, new materials
- **THIN FILMS:** memory devices thin film capacitors, piezoelectric devices
- **PROCESSING:** single crystals, fibers, ceramics, thin films
- **DIELECTRICS:** multilayer capacitors, relaxors, microwave dielectrics
- **PIEZOELECTRICS:** sensors, actuators, motors, polymers, composites
- **PYROELECTRICS:** detectors, imaging

- **INTEGRATED CERAMICS:** smart materials, multi-component structures
- **ELECTROOPTICS:** nonlinear optics, organic materials, devices

To receive further details on ECAPD2/ISIF4, please contact the Conference Secretary:

Ms. K. J. Humphrey
ECAPD2
Alcan International Ltd.
Southam Road
Banbury, Oxfordshire
OX16 7SP, United Kingdom
TEL: +44-295-274348
FAX: +44-295-274210

FERROELECTRICS

and related materials

NOTES FOR CONTRIBUTORS

Manuscripts should be typewritten with double-spacing and submitted in triplicate. Authors are requested to forward their manuscripts to either the Editor:

G. W. Taylor
Princeton Resources,
P.O. Box 211,
Princeton, NJ 08540, USA

or one of the Associate Editors:

Peter Günter
Institut für
Quantenelektronik
ETH
CH 8093 Zürich
Switzerland

Sidney B. Lang
Department of Chemical
Engineering
Ben Gurion University of
the Negev
Beer Sheva 84120, Israel

Koichi Toyoda
Research Institute of
Electronics
Shizuoka University
Hamamatsu 432
Japan

Submission of a paper to *Ferroelectrics* will be taken to imply that it represents original work not previously published, that it is not being considered for publication elsewhere, and that if accepted it will not be published elsewhere in the same form, in any language, without the consent of the editors.

It is a condition of the acceptance by the editor of a typescript for publication that the publishers acquire automatically the copyright in the typescript throughout the world.

Manuscript length: The maximum length preferred is 35 units, where a unit is a double-spaced typewritten page or one figure. Longer papers, or papers not following the prescribed editorial format, cannot be guaranteed prompt publication.

Abstracts and Key Words: Each manuscript should contain a leading abstract of approximately 100–150 words and be accompanied by up to six key words which characterize the contents of the paper.

Figures should be given numbers and captions, and should be referred to in the text. Captions should be collected on a separate sheet. Please label each figure with the figure number and the name of the author. Line drawings of high enough quality for reproduction should be prepared in India ink on white paper or on tracing cloth; coordinate lettering should be included. Figures should be planned so that they reduce to a 64 cm column width. The preferred width of submitted figures is 12 to 15 cm, with lettering 4 mm high, for reduction by one-half. Photographs intended for halftone reproduction should be good, original glossy prints, at roughly twice the desired size. Redrawing, and author's alterations in excess of 10%, will be charged.

Color Plates: Whenever the use of color is an integral part of the research, or where the work is generated in color, the journal will publish the color illustrations without charge to authors. Reprints in color will carry a surcharge. Please write to the Editor for details.

Equations should be typewritten wherever possible, with subscripts and superscripts clearly indicated. It is helpful to identify unusual symbols in the margin.

Units: Acceptable abbreviations will be found in the *Style Manual* of the American Institute of Physics and similar manuals. Metric units are preferred.

References and Notes are indicated in the text by superior numbers; the full list should be collected and types on a separate page at the end of the paper. Listed references are arranged as follows:

1. J. C. Slater, *J. Chem. Phys.* **9**, 16 (1941).
2. F. Jona and G. Shirane, *Ferroelectric Crystals* (Pergamon Press, Oxford, 1962), pp. 186–7.

Proofs: Page proofs, including figures, will be forwarded by air mail to authors for checking.

Reprints: Reprints may be purchased; a reprint order form will be sent with page proofs.

There are no page charges to authors or to institutions.



a

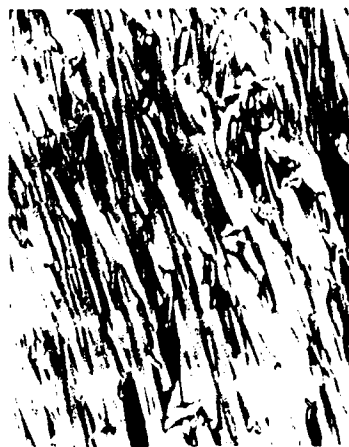


b

COLOR PLATE I

See Herrmann, Figures 2a and b

FERROELECTRICS, Volume 122, 1-4



(a) SmA (90°C)



(b) SmC* (52°C)



(c) Sm1 (25°C)

COLOR PLATE II

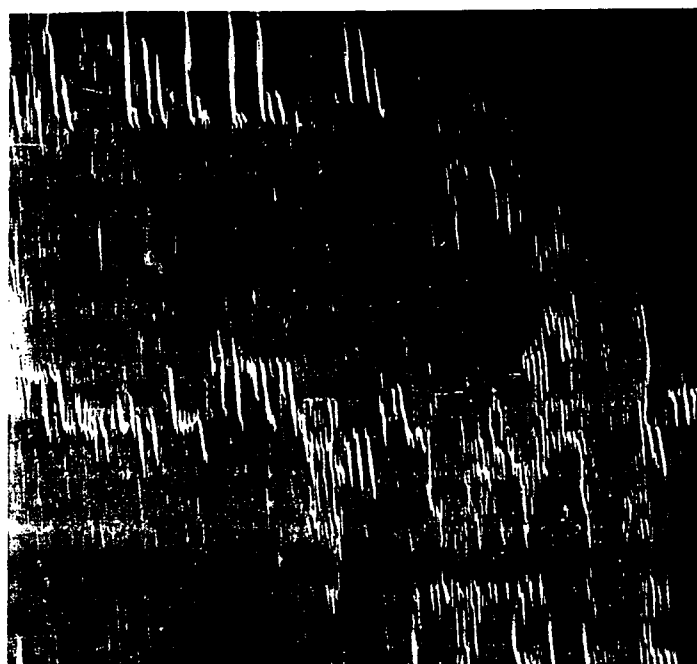
See Yasuda *et al.*, Figures 2a and b

FERROELECTRICS, Volume 122, 1-4

layer normal



+2.5 V



COLOR PLATE III

See Yuasa *et al.*, Figure 7

FERROELECTRICS, Volume 122(1-4)

layer normal



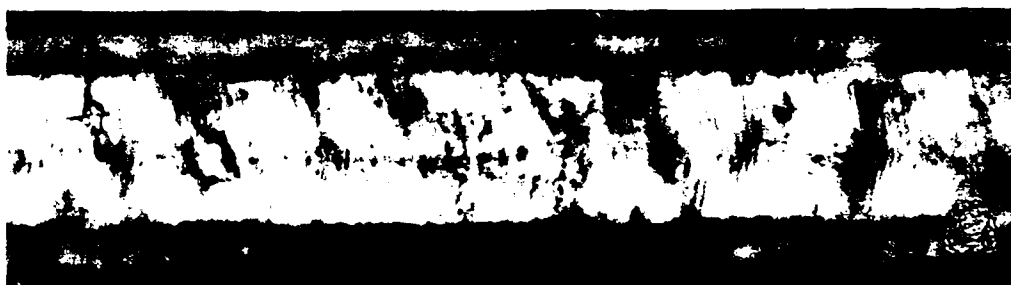
-0.5 V



COLOR PLATE IV

See Yuasa *et al.*, Figure 8

FERROELECTRICS, Volume 122(1-4)



cut direction →

COLOR PLATE V
See Yasui *et al.*, Figure 11
FERROELECTRICS, Volume 122(1-4)

(a) on state



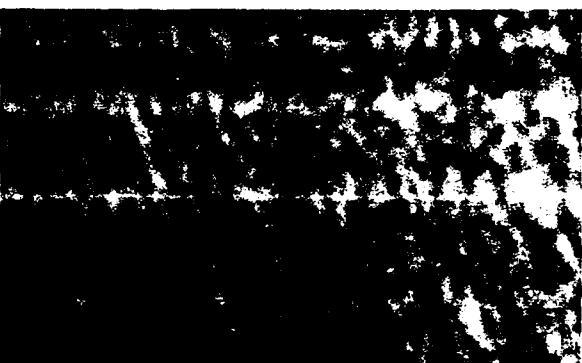
(b) off state



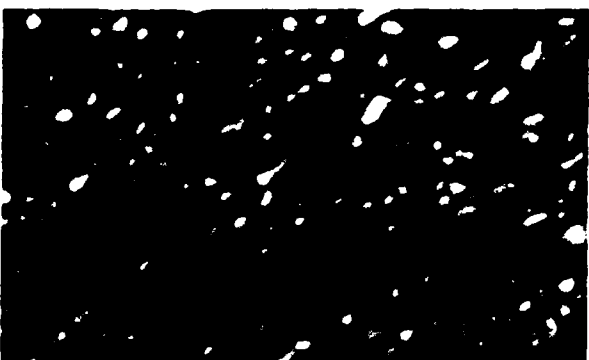
COLOR PLATE VI
See Yasui *et al.*, Figure 12
FERROELECTRICS, Volume 122(1-4)



$U = -90 \text{ V}$



$U = 0 \text{ V}$

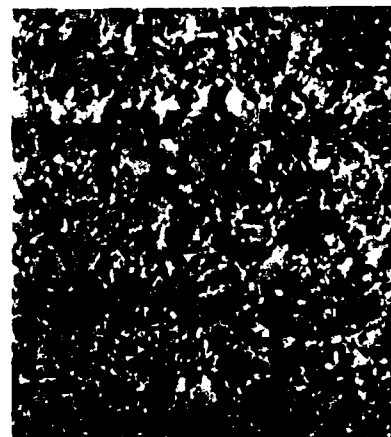


$U = +90 \text{ V}$

COLOR PLATE VII. See Sharp *et al.*, Figure 7c,
FERROELECTRICS, Volume 122(1-4).



antiferro (0 V)
low birefringence



ferro (20 V)
high birefringence

A



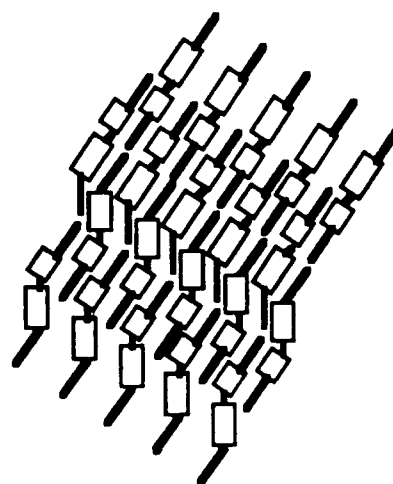
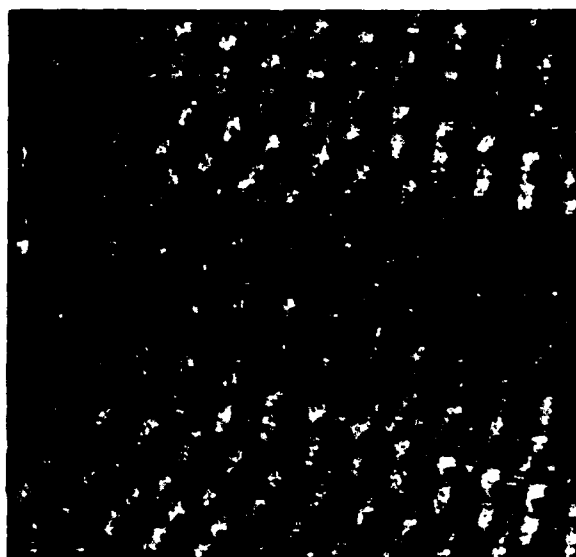
applied voltage = 0 V
low birefringence



applied voltage = 180 V
high birefringence

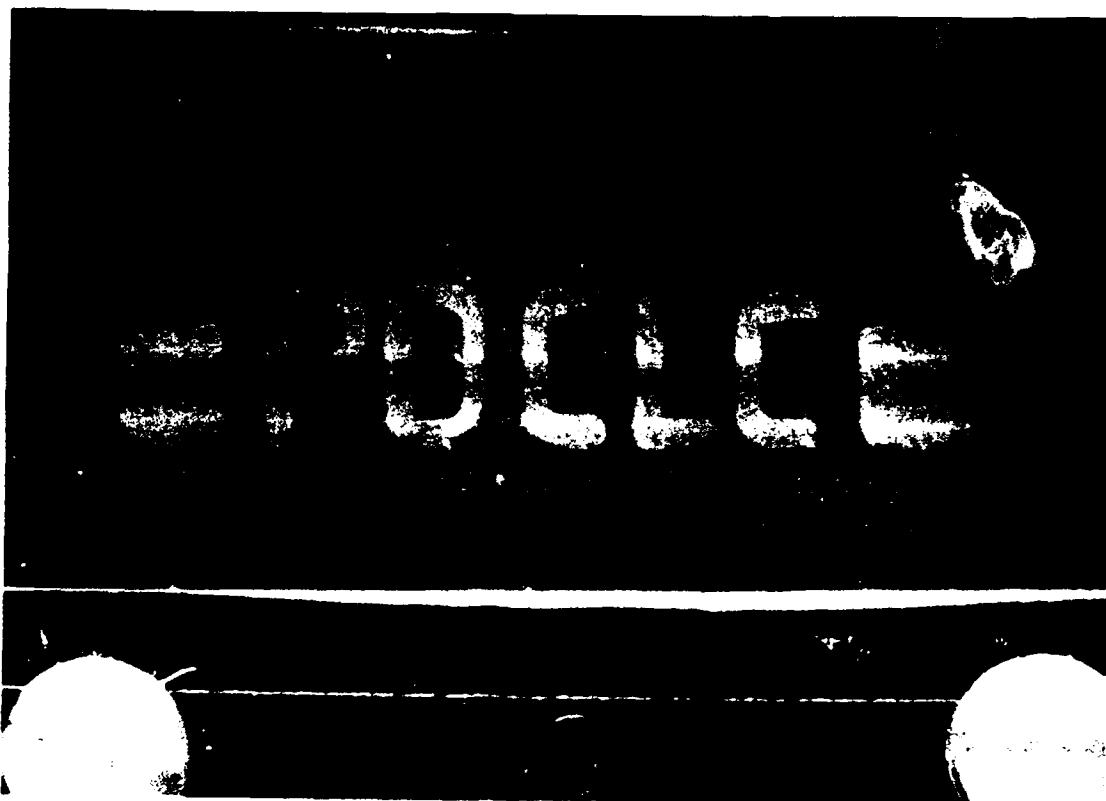
B

COLOR PLATE VIII. See Skarp *et al.*, Figures 8a and b.
FERROELECTRICS, Volume 122(1-4).

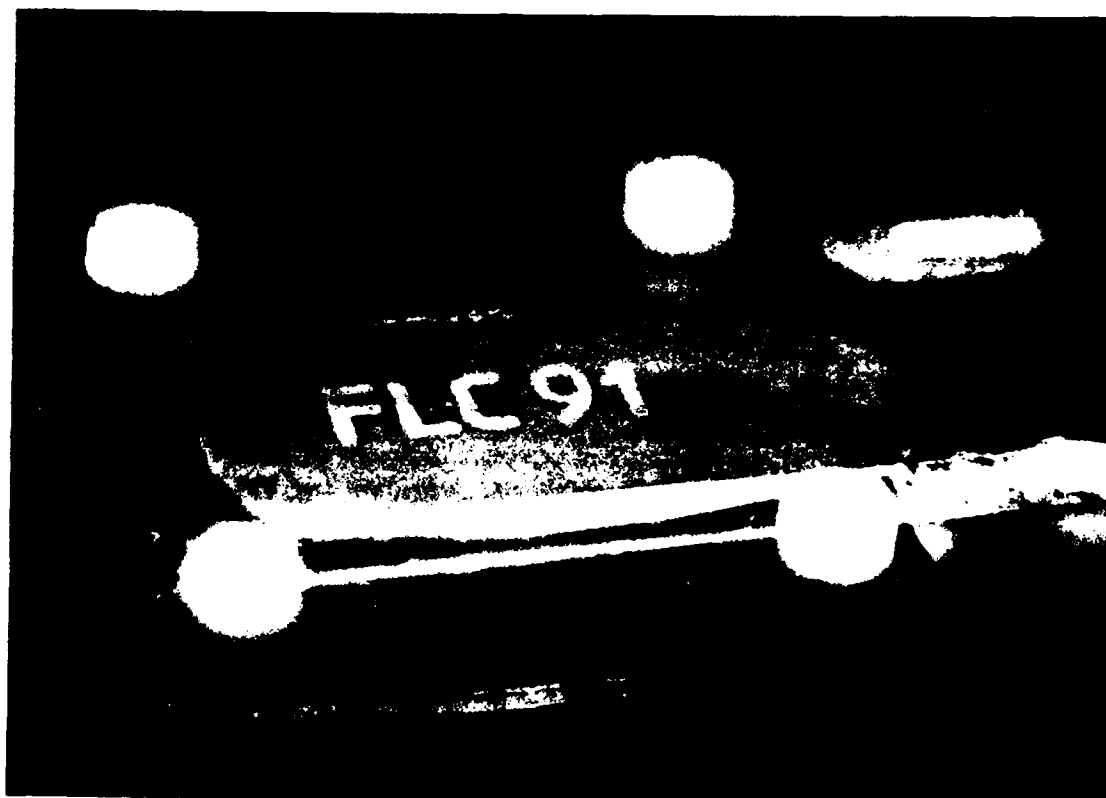


COLOR PLATE IX.
See Takezoe *et al.*, Figure 6.
FERROELECTRICS, Volume 122(1-4).

(a)

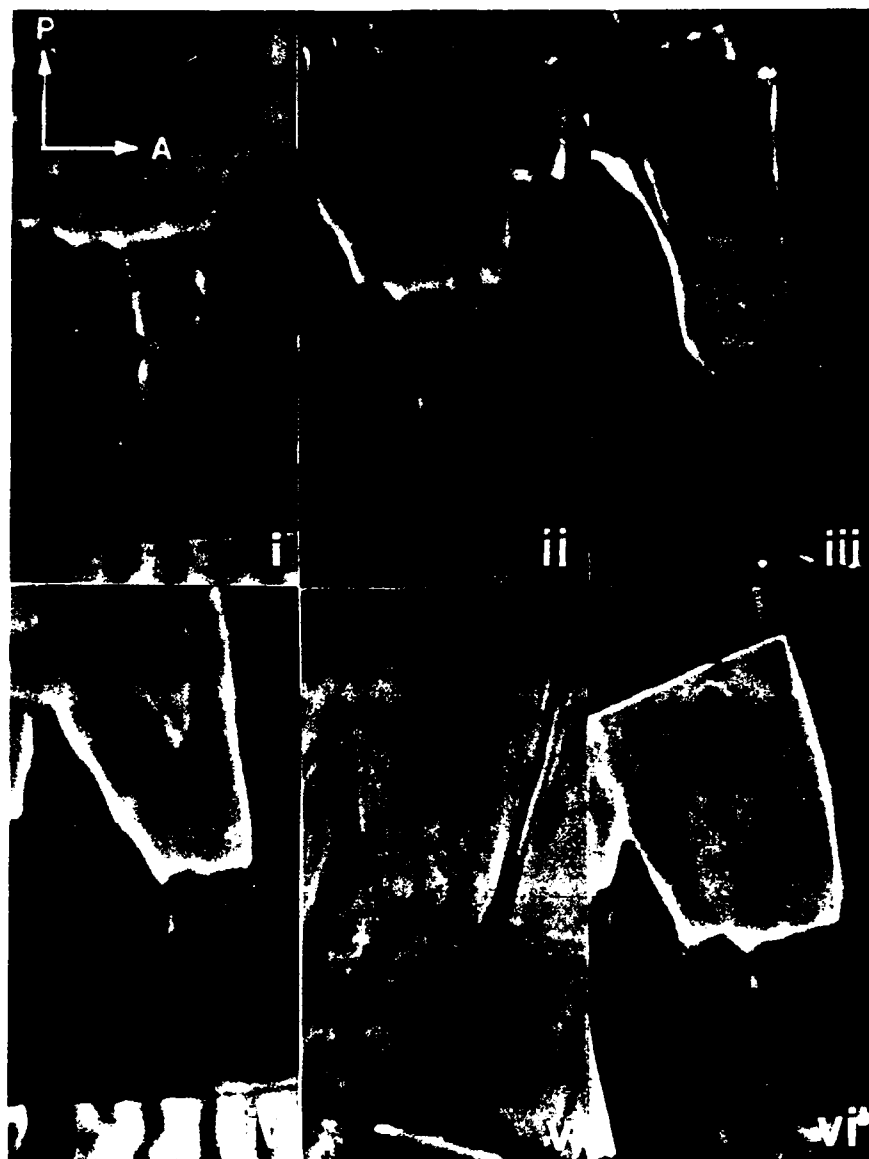


(b)



COLOR PLATE X

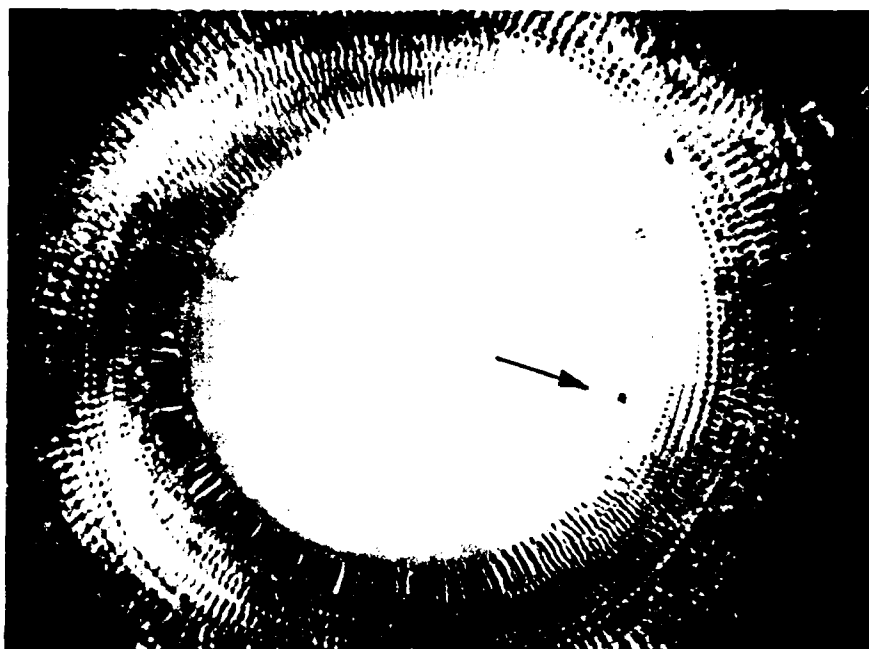
See K-12 for a color photograph of the same
HEROIC CHIEFS X stamp.



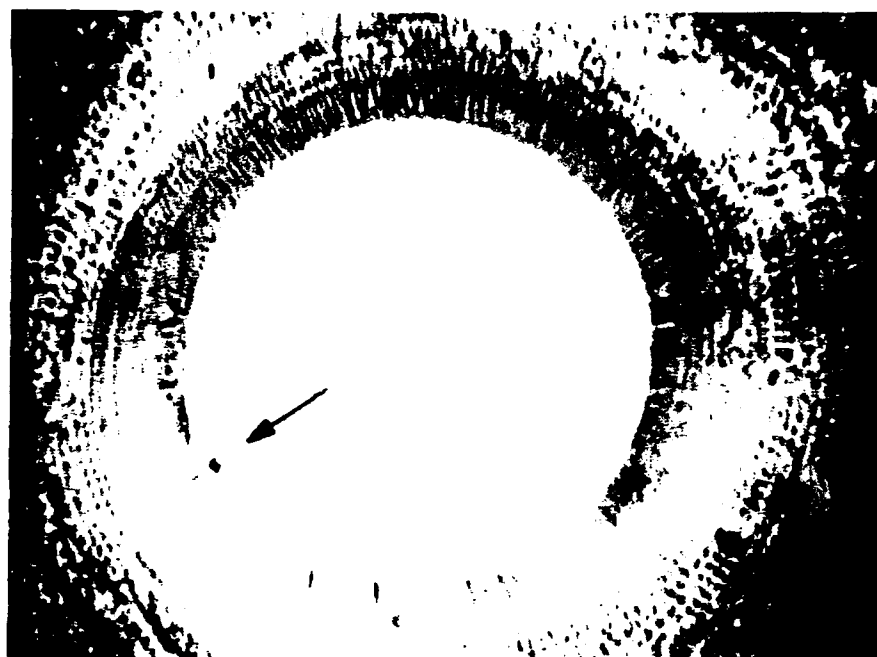
COLOR PLATE XI
 See Shao *et al.*, Figure 1a.
FERROELECTRICS, Volume 122(1-4)



COLOR PLATE XII.
See Shao *et al.*, Figure 2.
FERROELECTRICS, Volume 122(1-4).



(a)



(b)

COLOR PLATE XIII
 See Hauck and Koswig, Figures 3a and b
FERROELECTRICS, Volume 122(1-4)



COLOR PLATE XIV.
See Hauck and Koswig, Figure 4.
FERROELECTRICS, Volume 122(1-4).

(continued from inside front cover)

Ordering Information Published monthly. Subscriptions are renewed on an annual basis. Current Volume Block: 113-124.

Orders may be placed with your usual supplier or directly with Gordon and Breach Science Publishers S.A., % STBS Ltd., P.O. Box 90, Reading, Berkshire RG1 8JL, U.K. Journal subscriptions are sold on a volume basis only; single issues are not available separately. Claims for nonreceipt of issues should be made within three months of publication of the issue or they will not be honored without charge. Subscriptions are available for microform editions. Details will be furnished upon request.

SUBSCRIPTION RATES Base list subscription price per volume, SFr. 521.00. Available only to single users who subscribe directly from the Publisher and who pay by personal check or credit card.

Separate rates exist for different users such as academic and corporate institutions. These rates may also include photocopy licenses and postage and handling charges. Special discounts are also available to continuing subscribers through our Subscriber Incentive Plan (SIP).

For price information in your territory, please contact your local agent or one of the STBS Marketing Departments:

USA

P.O. Box 786, Cooper Station, New York, NY 10276
Telephone: (212) 206-8900
Telex: 236735 GOPUB U'R
Fax: (212) 645-2459

UK and EUROPE

P.O. Box 90, Reading, Berkshire RG1 8JL, U.K.
Telephone: (073) 456-0080
Telex: 849870 SCIPUB G
Fax: (073) 456-8211

JAPAN

Yohan Western Publications Distribution Agency
3-14-9, Okubo, Shinjuku-ku, Tokyo 169
Telephone: (03) 208-0181
Telex: 2324818 YOHAN J
Fax: (03) 209-0288

All issues are dispatched by air mail throughout the world.

ASIA

Kent Ridge, P.O. Box 1180, Singapore 9111
Telephone: (65) 4459663
Telex: RS 24200 TMSR QUOTE TM 4418
Fax: (65) 4458411

AUSTRALIA

Private Bag 8, Camberwell, Victoria 3124
Telephone: (03) 819-6650
Telex: 10723126 (GTFT)
Fax: (03) 819-6651